



# THE UNIVERSITY *of* EDINBURGH

This thesis has been submitted in fulfilment of the requirements for a postgraduate degree (e.g. PhD, MPhil, DClinPsychol) at the University of Edinburgh. Please note the following terms and conditions of use:

This work is protected by copyright and other intellectual property rights, which are retained by the thesis author, unless otherwise stated.

A copy can be downloaded for personal non-commercial research or study, without prior permission or charge.

This thesis cannot be reproduced or quoted extensively from without first obtaining permission in writing from the author.

The content must not be changed in any way or sold commercially in any format or medium without the formal permission of the author.

When referring to this work, full bibliographic details including the author, title, awarding institution and date of the thesis must be given.

# Nonequilibrium steady states from a random-walk perspective

Anthony James Wood



Doctor of Philosophy  
The University of Edinburgh  
November 2019

# Abstract

It is well known that at thermal equilibrium (whereby a system has settled into a steady state with no energy or mass being exchanged with the environment), the microstates of a system are exponentially weighted by their energies, giving a Boltzmann distribution. All macroscopic quantities, such as the free energy and entropy, can be in principle computed given knowledge of the partition function. In a nonequilibrium steady state, on the other hand, the system has settled into a stationary state, but some currents of heat or mass persist. In the presence of these currents, there is no unified approach to solve for the microstate distribution. This motivates the central theme of this work, where I frame and solve problems in nonequilibrium statistical physics in terms of random walk and diffusion problems.

The system that is the focus of Chapters 2, 3, and 4 is the (Totally) Asymmetric Simple Exclusion Process, or (T)ASEP. This is a system of hard-core particles making jumps through an open, one-dimensional lattice. This is a paradigmatic example of a nonequilibrium steady state that exhibits phase transitions. Furthermore, the probability of an arbitrary configuration of particles is exactly calculable, by a matrix product formalism that lends a natural association between the ASEP and a family of random walk problems.

In Chapter 2 I present a unified description of the various combinatorial interpretations and mappings of steady-state configurations of the ASEP. As well as deriving new results, I bring together and unify results and observations that have otherwise been scattered in the combinatorics and physics literature. I show that particular particle configurations of the ASEP have a one-to-many mapping to a set of more abstract paths, which themselves have a one-to-many mapping to permutations of numbers.

One observation from this wider literature has been that this mapped space can be interpreted as a larger set of configurations in some equilibrium system. This naturally gives an interpretation of ASEP configuration probabilities as summations

of Boltzmann weights. The nonequilibrium partition function of the ASEP is then a summation over this equilibrium ensemble, however one encounters difficulties when calculating more detailed measures of this state space, such as the entropy.

This motivates the work in Chapter 3. I calculate a quantity known as the *Rényi entropy*, which is a measure of the partitioning of the state space, and a deformation of the familiar Shannon entropy. The Rényi entropy is simple for an equilibrium system, but has yet to be explored in a classical nonequilibrium steady state. I use insights from Chapter 2 to frame one of these Rényi entropies — requiring the enumeration of the *squares* of configuration weights — in terms of a two-dimensional random walk with absorbing boundaries. I find the appropriate generating function across the full phase diagram of the TASEP by generalising a mathematical technique known as the *obstinate kernel* method. Importantly, this nonequilibrium Rényi entropy has a different structural form to any equilibrium system, highlighting a clear distinction between equilibrium and nonequilibrium distributions.

In Chapter 4 I continue to examine the Rényi entropy of the TASEP, but now performing a time and space continuum limit of the random walk problem in Chapter 3. The resultant problem is a two-dimensional *diffusion* problem with absorbing boundary conditions, which once solved should recover TASEP dynamics about the point in the phase diagram where the three dynamical phases meet. I derive a generating function, sufficiently simple that its singularities can be analysed by hand. This calculation entails a novel generalisation of the obstinate kernel method of Chapter 3: I find a solution by exploiting a symmetry in the Laplace transform of the diffusion equation.

I finish in Chapter 5 by introducing and solving another nonequilibrium system, termed the *many-filament Brownian ratchet*. This comprises an arbitrary number of filaments that stochastically grow and contract, with the net effect of moving a drift-diffusing membrane by purely from thermal fluctuations and steric interactions. These dynamics draw parallels with those of actin filament networks at the leading edge of eukaryotic cells, and this improves on previous ‘pure ratchet’ models by introducing interactions and heterogeneity in the filaments. I find an  $N$ -dimensional diffusion equation for the evolution of the  $N$  filament-membrane displacements. Several parameters can be varied in this system: the drift and diffusion rates of each of the filaments and membrane, the strength of a quadratic interaction between each filament with the membrane, and the strength of a surface tension across the filaments. For several interesting physical cases I find the steady-state distribution exactly, and calculate how the mean velocity of the membrane varies as a function of these parameters.

# Lay summary

Statistical physics endeavours to explain the tangible, collective observables of a system (such as its energy) by looking at how the system behaves on average at a microscopic level. In this thesis, I investigate the statistical physics of systems that have some sort of outside force applied, but have been given a long time to settle, known as *nonequilibrium steady states*. The statistical physics method for completely isolated *equilibrium* systems have been known since the late 1800's. The inclusion of an outside force, however, introduces surprisingly large complexity to the underlying mathematics, and these nonequilibrium steady states are being *solved* — that is, the microscopic details are ascertained — on a case-by-case basis, often with much difficulty.

One such system that forms the basis of a lot of this work is called the “asymmetric simple exclusion process”. This has dynamics not dissimilar to that of vehicles on a single-lane, one-way road: particles enter from one end, move along a line, and leave from the other end. This is nonequilibrium as there is a flow of particles, and is one of few such systems that have been solved. In this work I use the mathematical formalism that solves this traffic-like system to deeper explore the microscopic details, thinking about the system as a representation of some more abstract mathematical structure. Using this structure, I find some new properties of the process, and highlight ways in which this model is fundamentally different to any isolated equilibrium system.

I then look at a second system, called the “many-filament Brownian ratchet”. This model comprises a large number of growing and shrinking rods that act together to displace a *membrane*, not by pushing it, but instead by ratcheting it. This is nonequilibrium because the system as a whole is moving over time, but in this work we show that it is in fact possible to solve this system — and crucially, determine how fast the membrane will move — even when the filaments are interacting with one another. This system draws parallels with cell movement in living organisms, where one observes polymer networks growing and shrinking to move cell membranes, at the microscopic level.

# Declaration

I declare that this thesis was composed by myself, that the work contained herein is my own except where explicitly stated otherwise in the text, and that this work has not been submitted for any other degree or professional qualification except as specified.

Parts of this work have been published in References [1] and [2].

Other parts of this work are being prepared for publication. This is available in preprint form in Reference [3].

*(Anthony James Wood, November 2019)*

# Acknowledgements

I would like to extend my grateful thanks:

to Martin Evans and Richard Blythe, for being fantastic supervisors throughout my time here and helping guide the work presented in this thesis;

to my friends in Edinburgh — in particular the swim group, my office mates and my housemates Jack, Joe and Jana — for making me laugh and putting up with my complaints in equal measure;

to Julia, for being a wonderfully supportive partner and making these four years in Edinburgh a joy;

to Mum, Dad, Claire and Louise for their love and support before, and all the way through this.

# Contents

<b>Abstract</b>	i
<b>Lay summary</b>	iii
<b>Declaration</b>	v
<b>Acknowledgements</b>	vii
<b>Contents</b>	ix
<b>1 Introduction</b>	1
1.1 Overview .....	1
1.2 Nonequilibrium steady states and the master equation .....	5
1.3 The asymmetric simple exclusion process .....	5
1.3.1 Matrix product ansatz.....	6
1.3.2 Explicit matrix representation .....	8
1.3.3 TASEP partition function .....	9
1.3.4 Phase diagram .....	10
1.3.5 The partially asymmetric and symmetric simple exclusion processes.....	12
1.4 Rényi entropy .....	16
1.4.1 Properties of the Rényi entropy.....	17
1.4.2 Rényi entropy at equilibrium.....	18



1.5	Random walks and diffusion processes.....	19
1.5.1	Setting up a random walk .....	21
1.5.2	Boundary conditions.....	22
1.5.3	Continuum limit.....	23
1.6	Generating functions and asymptotic analysis.....	27
1.6.1	Generating function calculation — a simple example.....	28
1.6.2	Generating function of the TASEP partition function.....	29
1.6.3	Asymptotic analysis of a generating function.....	31
1.7	Combinatorics in the ASEP.....	32
1.7.1	Combinatorial factors in $\alpha = \beta = 1$ SSEP and TASEP partition functions.....	32
1.7.2	TASEP partition function in terms of bicoloured Motzkin and Dyck paths.....	34
1.7.3	Ballot numbers and the one-transit walk.....	36
<b>2</b>	<b>Combinatorial mappings of exclusion processes</b>	<b>39</b>
2.1	Orientation.....	39
2.2	$\alpha = \beta = 1$ TASEP .....	40
2.2.1	Mapping to a dominated path problem.....	41
2.2.2	Other representations.....	48
2.3	$\alpha = \beta = 1$ SSEP.....	50
2.3.1	Mapping to a permutation problem .....	51
2.4	Generalised parameter mappings .....	54
2.4.1	$\alpha = \beta = 1$ PASEP and weighted permutations .....	55
2.4.2	Determinant form of TASEP weight with general $\alpha, \beta$ .....	57
2.4.3	$\alpha, \beta$ generalisation of path dominance problem .....	60

2.4.4	Mappings for general $\alpha, \beta, q$ .....	60
2.5	Summary .....	63
<b>3</b>	<b>Rényi entropy of the TASEP</b> .....	<b>65</b>
3.1	Orientation.....	65
3.2	Preliminaries.....	66
3.2.1	Sum of squared weights as a tensor product, generating function .	66
3.3	Mapping to a random walk.....	68
3.3.1	Introductory example: calculation of partition function generat- ing function by a kernel method .....	69
3.3.2	Generating function for the sum of squared weights.....	72
3.3.3	Recurrence relation .....	74
3.3.4	Symmetry and factorisation of the kernel .....	76
3.4	Generating function for the $\alpha = \beta = 1$ weights, $\mathcal{Q}(z; 1, 1)$ .....	77
3.4.1	$y^0$ coefficient extraction .....	79
3.4.2	$x^0$ coefficient extraction, $\mathcal{Q}(z; 1, 1)$ result.....	79
3.4.3	$x^+$ coefficient extraction, obtaining $\mathcal{Q}(z; \alpha, 1)$ .....	81
3.5	Generating function for general $\alpha, \beta$ weights, $\mathcal{Q}(z; \alpha, \beta)$ .....	83
3.5.1	$\mathcal{Q}(z; \alpha, \beta)$ result .....	84
3.6	Asymptotic analysis .....	85
3.6.1	Low density phase $\alpha < 1/2, \alpha < \beta$ .....	85
3.6.2	High density phase $\beta < 1/2, \beta < \alpha$ .....	87
3.6.3	Maximal current phase $\alpha > 1/2, \beta > 1/2$ .....	87
3.6.4	Rényi entropy across the phase diagram.....	89
3.6.5	Bounds on Gibbs-Shannon entropy.....	89

3.7	Discussion .....	90
3.7.1	Rényi entropy of the one-transit walk.....	90
3.7.2	Higher-order Rényi entropies .....	92
3.8	Summary .....	94
<b>4</b>	<b>Rényi entropy of the TASEP in the continuum limit</b>	<b>95</b>
4.1	Orientation.....	95
4.2	Introductory calculation: continuum limit of partition function .....	96
4.2.1	Solution for $\mathcal{Z}_C(z; \alpha, \beta)$ .....	99
4.2.2	Asymptotic analysis .....	101
4.3	Sum of squared weights calculation .....	104
4.3.1	Taking a continuum limit .....	104
4.3.2	Attempt at solution by images.....	107
4.3.3	Solution by a kernel method.....	109
4.3.4	Symmetry and factorisation of the kernel .....	111
4.3.5	$v$ domain extraction .....	113
4.3.6	Two required formulae .....	115
4.3.7	$u > 0$ domain extraction .....	117
4.3.8	Solution for $\mathcal{Q}_C(z; \alpha, \beta)$ .....	119
4.4	Asymptotic analysis .....	119
4.4.1	Low density phase $\alpha < 1/2$ , $\alpha < \beta$ ( $a > 1$ , $a > b$ ) .....	120
4.4.2	High density phase $\beta < 1/2$ , $\beta < \alpha$ ( $b > 1$ , $b > a$ ) .....	121
4.4.3	Maximal current phase $\alpha > 1/2$ , $\beta > 1/2$ ( $a < 1$ , $b < 1$ ) .....	121
4.5	Summary of results .....	122

4.6	On higher-order weight enumerations.....	124
4.6.1	Orbit sums .....	124
4.6.2	Attempt at solving 3D diffusion — sum of cubed weights .....	126
4.6.3	Continuum limit for higher-order weight enumerations .....	127
4.7	Summary .....	128
<b>5</b>	<b>Many-filament diffusive Brownian ratchet</b>	<b>131</b>
5.1	Orientation.....	131
5.2	Model derivation .....	134
5.2.1	Diffusion equation.....	136
5.2.2	Reflecting boundary conditions .....	138
5.2.3	Membrane velocity formula.....	140
5.3	Introductory example: single filament .....	142
5.4	Constant drift solution for many filaments.....	143
5.4.1	Mean membrane velocity.....	144
5.4.2	Steady-state condition.....	145
5.5	Quadratic potential solution .....	147
5.5.1	Restoring force between filaments and the membrane .....	149
5.5.2	Surface tension .....	151
5.6	Link to diffusion problems in exclusion processes .....	155
5.7	Summary .....	156
<b>6</b>	<b>Conclusion</b>	<b>159</b>
<b>A</b>	<b>Demonstration of <math>DE = D + E</math> in path dominance problem</b>	<b>163</b>

<b>B</b>	<b>Details of <math>\mathcal{Q}(z; \alpha, \beta)</math></b>	167
B.1	Extraction of coefficients for obtaining $\mathcal{R}(t; a, a, b, b)$ .....	167
B.1.1	$y^0$ coefficient extraction .....	168
B.1.2	$x^+$ coefficient extraction .....	169
B.2	Residues of $Q(z; \alpha, \beta)$ .....	173
	<b>Bibliography</b>	175

# Chapter 1

## Introduction

### 1.1 Overview

In a physical system, *macrostates* are quantities that can be directly observed. Examples of macrostates include energy and volume, which are measurable using standard laboratory devices. However, knowledge of these observables does not give the observer an understanding about the underlying physics of the system in question. For this, one must investigate the finer details of the system, specifically the system's *microstates*. A microstate, or *configuration*, is an exact description of every individual component of a system, and even a system with modest complexity will have an incomprehensibly large number of accessible microstates. *Statistical mechanics* is the analysis of microstates, in order to explain the measured values of different macroscopic variables.

The process of determining the macroscopic behaviour of an *equilibrium* system is now a standard technique. We begin with the most simple example: a system A in thermal equilibrium with a large heat bath B. On average, no net heat is being transferred between A and B, and the total energy  $E = E_A + E_B$  is constant. The microstates of the combined system AB obey the *principle of equal a priori probability*: at equilibrium, every accessible microstate is equally probable. This leads to a statistical definition of temperature in the full system [4]:

$$T = \frac{\partial E_A}{\partial(k_B \log W_A)} = \frac{\partial E_B}{\partial(k_B \log W_B)} \quad (1.1)$$

with  $k_B = 1.3806 \text{ JK}^{-1}$  the Boltzmann constant, and  $W_A, W_B$  the number of microstates

of A and B with energies  $E_A$ ,  $E_B$  respectively. Suppose we are interested in the state of A only, specifically the probability  $\mathcal{P}$  of finding system A in a particular microstate  $\mathcal{C}$ , with energy  $E(\mathcal{C})$ , taking no interest in the state of the bath. Using our definition of a temperature, one derives the famous result

$$\mathcal{P}(\mathcal{C}) = \frac{1}{Z} \exp\left(-\frac{E(\mathcal{C})}{k_B T}\right) \quad (1.2)$$

where

$$Z = \sum_{\mathcal{C}} \exp\left(-\frac{E(\mathcal{C})}{k_B T}\right) \quad (1.3)$$

is the equilibrium *partition function* [4]. At a glance this is an innocuous normalisation factor, but from the definition of the Gibbs-Shannon entropy [5] it is in fact closely related to the free energy  $F = \langle E \rangle - ST$ :

$$S = -k_B \sum_{\mathcal{C}} \mathcal{P}(\mathcal{C}) \log \mathcal{P}(\mathcal{C}) \quad (1.4)$$

$$= -k_B \sum_{\mathcal{C}} \mathcal{P}(\mathcal{C}) \left( \log \frac{1}{Z} - \frac{E(\mathcal{C})}{k_B T} \right) \quad (1.5)$$

$$= k_B \log Z + \frac{\langle E \rangle}{T} \quad (1.6)$$

$$F = -k_B T \log Z. \quad (1.7)$$

Using Maxwell's relations — the set of equations that relates all macroscopic thermodynamic quantities in terms of partial derivatives of one another — Eq. (1.7) serves as a gateway for which all macroscopic statistics of the system can be derived [4]. While it remains impossible to determine the *exact* microstate at any point in time, the equilibrium statistical mechanics approach gives us a complete understanding of the macroscopic properties of the system.

This formalism was established on the assumption that there was no net transfer of heat or mass between systems A and B. Nature, however, is rarely this accommodating. Real-world systems are often *entirely* characterised by currents of mass or heat, such as the flow of cars in traffic, radiation from a hot object, or self-induced motility in biological systems. These all fall into a larger family of *nonequilibrium* regimes. In general these systems have no notion of a statistical temperature (as we had in Eq. (1.1)), and the principle of equal a priori probability does not hold [6].

Without this standard approach, we are compelled to look at a more general *master equation* formalism for the microstate probabilities  $\mathcal{P}(\mathcal{C})$ . A master equation is not a

closed-form solution for  $\mathcal{P}$ , but rather an expression that describes the time evolution of  $\mathcal{P}$  as a function of the various dynamics in the system. The principle aim, then, is to solve the master equation for  $\mathcal{P}$ . However, this is in general a very challenging problem. A subset of these nonequilibrium systems settle in the long time limit into a *nonequilibrium steady state*. In this state, while currents still persist, the probability distribution has stabilised. This introduces a simplification to the master equation, as we can eliminate any time dependence. The work in this thesis falls within this subset of solvable nonequilibrium steady states.

In this chapter, we take an exploration of the physical and mathematical themes that are central to the work around nonequilibrium steady states, and techniques we will use to learn more about them. Naturally, we begin by formalising the master equation approach to solving nonequilibrium systems in Section 1.2, and highlight the simplification that arises in the steady state.

In Section 1.3, we focus on a specific system called the (totally) asymmetric simple exclusion process, or (T)ASEP [7]. The model comprises a one-dimensional lattice of particles hopping from left to right, and is among the simplest nonequilibrium processes one could devise. What is remarkable, then, is that the solution that this model admits has embedded a deep, intricate mathematical structure that is yet to be fully understood, despite it being known for nearly thirty years. We will introduce this model, and in particular discuss the *matrix product* formalism; this is the mathematical approach that solves the steady-state master equation. Using this formalism we then perform some introductory calculations, including the nonequilibrium partition function.

The partition function is a measure of the probability distribution of the ASEP, explicitly the sum of weights of all possible microstates. Another, more intricate measure of the probability distribution is the entropy. Usually the ‘entropy’ refers to the Gibbs-Shannon entropy that we saw in Eq. (1.4), as a measure of information. In the context of nonequilibrium steady states, however, we are interested in what is known as *Rényi* entropy [8]. This is a generalisation of the Gibbs-Shannon entropy, and we discuss its properties in Section 1.4.

We shall see that a calculation of the Gibbs-Shannon entropy of the ASEP would entail a very complicated enumeration problem (unlike the equivalent problem in an equilibrium system). On the other hand, it turns out the Rényi entropy of the TASEP is more analytically tractable. By a particular interpretation of the matrix product formalism, we can interpret whether a site is occupied or not in terms of the different



directions a random walker can move. This allows us to write the Rényi entropy as a random walk problem, and is an example of a running theme in the thesis as a whole: the solving of statistical physics problems by writing them as enumerations of random walks, and solving those random walks. In order to prepare us for formulating and solving these problems, we describe in Section 1.5 how a random walk problem is written using the master equation formalism, and the procedure of taking *continuum limits* to reduce the walk to a diffusion in continuous time.

As well as in the ASEP, this random walk formulation proves crucial in Chapter 5, where we investigate another system entirely. We call this a *many-filament Brownian ratchet*, and is a network of growing and shrinking filaments, interacting with a constraining fluctuating membrane. Over time, this system exhibits a phenomenon which we term *ratcheting*: the membrane moves at a velocity (and perhaps direction) different to its natural drift, exclusively due to steric interactions with the filaments and thermal fluctuations, with no work being done to push the membrane [9]. Despite being an interacting many-dimensional system, we are able to find cases where the underlying algebra dramatically simplifies and makes the steady state exactly solvable. We find this by writing the steady state as a random walk problem, relating to the separations between the membrane and each of the filaments.

For random walks that can not be obviously solved directly, another common and very successful approach is to use *generating functions*. These are functions that have a desired quantity (e.g. a total number of walks of a certain length) embedded as coefficients of the series expansion in another conjugate variable [10]. We introduce these functions in Section 1.6, as well as the mathematical formalism and notation we use for writing, solving and *inverting* them, as well as using them to perform asymptotic analyses. In later chapters we analyse several physical quantities by calculating and analysing their corresponding generating functions.

We finish this literature review in Section 1.7 by returning to the ASEP, and taking a more detailed look at the matrix product formalism. Specifically, we make three simple observations of the matrix product formalism. These all allude to a deeper, underlying mathematical interpretation, which turns out to be combinatorial in nature. This serves as a preliminary to Chapter 2, where we present and formalise the steady-state distribution in finer detail.



**Figure 1.1** *The TASEP. Particles enter at rate  $\alpha$ , hop right at rate 1, and exit at rate  $\beta$ . The exclusion property means that particles can not overtake each other.*

## 1.2 Nonequilibrium steady states and the master equation

Given a set of configurations  $\mathcal{C}$ , we define the probability of observing a system in a particular  $\mathcal{C}$  at time  $t$  as  $\mathcal{P}(\mathcal{C}, t)$ . This probability obeys a master equation, which describes how the configuration probability changes as a function of time. This equation will depend on the transition rates  $R(\mathcal{C} \rightarrow \mathcal{C}')$  at which the system can change from a given configuration to another [11–13]:

$$\partial_t \mathcal{P}(\mathcal{C}, t) = \sum_{\mathcal{C}' \neq \mathcal{C}} \mathcal{P}(\mathcal{C}', t) R(\mathcal{C}' \rightarrow \mathcal{C}) - \sum_{\mathcal{C}' \neq \mathcal{C}} \mathcal{P}(\mathcal{C}, t) R(\mathcal{C} \rightarrow \mathcal{C}'). \quad (1.8)$$

This equation comprises *gain* terms of the form  $\mathcal{P}(\mathcal{C}', t) R(\mathcal{C}' \rightarrow \mathcal{C})$  — a product of the probability of being in  $\mathcal{C}'$ , and the rate at which the microstate moves into  $\mathcal{C}$  from  $\mathcal{C}'$ . Similarly the *loss* terms  $\mathcal{P}(\mathcal{C}, t) R(\mathcal{C} \rightarrow \mathcal{C}')$  are products of the rate of moving away from  $\mathcal{C}$  to some other  $\mathcal{C}'$ , and the probability of being in  $\mathcal{C}$  to begin with. A *steady-state* distribution is the solution to the master equation in the case  $\partial_t \mathcal{P}(\mathcal{C}, t) = 0$ , assuming the distribution stabilises in the long time limit.

In the master equation (1.8) we have assumed that the space of configurations  $\mathcal{C}$  is discrete. This will indeed be the case for the ASEP (which has  $2^N$  configurations corresponding to binary occupation variables for each of the  $N$  sites), but for the Brownian ratchet which forms the basis of Chapter 5 we find the configuration is specified by a set of displacements, in a continuous space. In turn there is a formalism for writing these gain and loss terms in a continuous system [12], see Section 1.5.3.

## 1.3 The asymmetric simple exclusion process

We now specify the dynamics and important properties of the asymmetric simple exclusion process (ASEP). The ASEP is a stochastic, open 1D system, defined on a lattice of  $N$  sites (Figure 1.1, and later Figure 1.4). This system has consistently attracted interest since the latter half of the 20<sup>th</sup> century as a simple model of driven diffusion [14–16], interface growth [17, 18] and biological transport [6, 15, 19]. In this

work we focus on the single-lane, single-particle variant. This has turned out to be a seminal model upon which a variety of generalisations have been introduced and studied, including models with multiple classes of particle [20–25], lattices with defects [26–29], and generalised update procedures [30–35].

In the ASEP, particles are introduced from a left reservoir at rate  $\alpha$  when the first site of the lattice is available, and make unit hops left and right stochastically, at rates  $q \geq 0$  and 1 respectively. Particles are then absorbed from the right-most site of the lattice by a right reservoir at rate  $\beta$ . The exclusion property forbids particles from overlapping or overtaking.

In the long time limit, this traffic-like system approaches a nonequilibrium steady state. This steady state is characterised by a stabilisation in the time-averaged left-to-right current of particles, which we denote  $J$ , and a density profile  $(\langle\tau_1\rangle, \langle\tau_2\rangle, \dots, \langle\tau_N\rangle)$ , where  $\langle\tau_i\rangle$  is the time-averaged occupation of site  $i$ .

We begin with a detailed analysis of the *totally asymmetric* system (TASEP, Figure 1.1), and later in Section 1.3.5 introduce the *symmetric* ( $q = 1$ ) and *partially asymmetric* ( $0 < q < 1$ ) systems (PASEP, SSEP respectively, Figure 1.4). These three systems are variants of one another, with different particle hopping rates.

### 1.3.1 Matrix product ansatz

A TASEP configuration is written  $\mathcal{C} = (\tau_1, \tau_2, \dots, \tau_N)$ , where  $\tau_i = 1$  if site  $i$  is occupied, and  $\tau_i = 0$  if it is not. In the original work [36], Derrida, Evans, Hakim and Pasquier make the ansatz that the steady-state probability of observing the TASEP in a given configuration  $\mathcal{C}$  is described as an inner product of vectors with an ordered product of matrices:

$$\mathcal{P}(\mathcal{C}) = \frac{\langle W | \prod_{i=1}^N X_i(\tau_i) | V \rangle}{Z_N}, \quad (1.9)$$

where  $X_i(\tau_i)$  is a *matrix representation* of the occupation of site  $i$ . The  $\langle W |$  and  $| V \rangle$  are vectors, that reduce the product to a scalar.  $Z_N$  is the system-size-dependent normalisation factor that we will see can be interpreted as a *nonequilibrium partition function*.

Given this ansatz, what remains is to find appropriate forms of  $X_i$ ,  $\langle W |$ ,  $| V \rangle$ , by analysis of the master equation. It turns out that when occupied sites are given a matrix representation  $X_i(1) = D$ , and vacant sites a representation  $X_i(0) = E$ , the

master equation is satisfied when the matrices obey the following *reduction relations*:

$$D|V\rangle = \frac{1}{\beta}|V\rangle, \quad (1.10)$$

$$\langle W|E = \frac{1}{\alpha}\langle W|, \quad (1.11)$$

$$DE = D + E, \quad (1.12)$$

$$\langle W|V\rangle = 1. \quad (1.13)$$

This is a *quadratic* algebra [37] that is able to reduce any string of  $D$  and  $E$  matrices into a summation of *normal-ordered* terms  $\langle W|E \dots ED \dots D|V\rangle$ , that can be directly evaluated, to find the weight of *any* configuration in the steady state as a function of  $\alpha, \beta$ .

In the original work, the authors demonstrate that probabilities of the matrix product form in Eq. (1.9) give a set of microstates for which  $\partial_t \mathcal{W}(\mathcal{C}) = 0$ , given that the representations  $D, E, \langle W|, |V\rangle$  satisfy the reduction relations (1.10)–(1.13). Note that this does not make all configurations equally *likely*, only their probabilities remain stationary. We omit the full algebraic proof of Eq. (1.9) and the reduction relations (1.10)–(1.13), but present an example of writing the master equation for a particular configuration.

Suppose  $\mathcal{C} = (0, 1, 0, 1, 0)$ . This is a 5-site system with two particles at sites  $i = 2, 4$ . Using the matrix product form of the weights in Eq. (1.9), the steady-state weight of  $\mathcal{C}$  is obtained by using the reduction relations (1.10)–(1.13):

$$\mathcal{W}(01010) = \langle W|EDEDE|V\rangle \quad (1.14)$$

$$= \langle W|(EDED + EDEE)|V\rangle \quad (1.15)$$

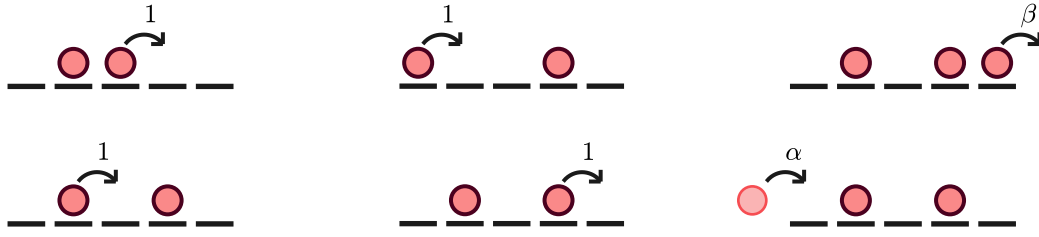
$$= \langle W|(EDD + EED + EDE + EEE)|V\rangle \quad (1.16)$$

$$= \langle W|(EDD + EED + ED + EE + EEE)|V\rangle \quad (1.17)$$

$$= \frac{1}{\alpha\beta^2} + \frac{1}{\alpha^2\beta} + \frac{1}{\alpha\beta} + \frac{1}{\alpha^2} + \frac{1}{\alpha^3}. \quad (1.18)$$

These weights are dependent on  $\alpha, \beta$  only, as they are the only parameters in the system that can be varied.

Configuration  $\mathcal{C}$  evolves in accordance with the master equation (1.8). We make this explicit by writing all out all configurations that are one particle jump away from  $\mathcal{C}$



**Figure 1.2** The six configuration transitions that either enter (top row), or exit (bottom row)  $\mathcal{C} = (0, 1, 0, 1, 0)$ .

(See Figure 1.2):

$$\begin{aligned}
 \partial_t \mathcal{W}(01010) &= \mathcal{W}(01100) + \mathcal{W}(10010) + \beta \mathcal{W}(01011) - \mathcal{W}(01010) - \mathcal{W}(01010) - \alpha \mathcal{W}(01010) \\
 &\quad (1.19)
 \end{aligned}$$

where the rates  $R = \alpha, \beta, 1$  for particles that enter, leave and move through the system respectively. The positive gain terms refer to the configurations that enter  $\mathcal{C}$  with a single jump, and the negative loss terms are from the ways of leaving  $\mathcal{C}$ . Using this, the master equation is given in matrix product form:

$$\begin{aligned}
 \partial_t \mathcal{W}(01010) &= \langle W | EDDEE | V \rangle + \langle W | DEEDE | V \rangle + \beta \langle W | EDEDD | V \rangle \\
 &\quad - \langle W | EDEDE | V \rangle - \langle W | EDEDE | V \rangle - \alpha \langle W | EDEDE | V \rangle. \quad (1.20)
 \end{aligned}$$

Using Eqs. (1.10)–(1.13), one can eventually show this sum of matrix product terms to be zero. The weight is therefore stationary, and the steady-state weight of  $\mathcal{C}$  is indeed given by Eq. (1.18).

### 1.3.2 Explicit matrix representation

We have so far used the reduction relations (1.10)–(1.13) in a formal way to calculate configurational weights — that is, without reference to any *explicit* representation of the matrices  $D$  and  $E$ , and the vectors  $\langle W |$  and  $|V\rangle$ , but simply using how they relate to one another. One can go on to calculate physical observables, such as the current and density profile, in this way [36]. However, it is often helpful to write out  $D$ ,  $E$ ,  $\langle W |$ ,  $|V\rangle$  explicitly. With one trivial exception (see Section 1.3.4), no finite-size matrices obey relations (1.10)–(1.13) and we instead resort to semi-infinite representations, of which

several are known. For our purposes, the most useful representation is [36]

$$D = \begin{pmatrix} 1 & 1 & \cdot & \cdot & \cdots \\ \cdot & 1 & 1 & \cdot & \cdots \\ \cdot & \cdot & 1 & 1 & \cdots \\ \cdot & \cdot & \cdot & 1 & \cdots \\ \vdots & \vdots & \vdots & \vdots & \ddots \end{pmatrix}, \quad E = \begin{pmatrix} 1 & \cdot & \cdot & \cdot & \cdots \\ 1 & 1 & \cdot & \cdot & \cdots \\ \cdot & 1 & 1 & \cdot & \cdots \\ \cdot & \cdot & 1 & 1 & \cdots \\ \vdots & \vdots & \vdots & \vdots & \ddots \end{pmatrix}, \quad (1.21)$$

with the boundary vectors

$$\langle W| = \sqrt{1-ab} (1, b, b^2, b^3, \dots), \quad |V\rangle = \sqrt{1-ab} (1, a, a^2, a^3, \dots)^T. \quad (1.22)$$

Here we have employed the shorthand

$$a = \frac{1-\alpha}{\alpha}, \quad b = \frac{1-\beta}{\beta}. \quad (1.23)$$

Notice that the representations of  $D$  and  $E$  in Eq. (1.21) are reminiscent of quantum mechanical *ladder* operators [38]; these matrices may act on a state ket

$$|n\rangle = (\underbrace{0, \dots, 0}_n, 1, 0, 0, \dots)^T \quad (1.24)$$

to transform it into a superposition of  $|n\rangle$  and  $|n \pm 1\rangle$ :

$$D|n\rangle = |n\rangle + |n-1\rangle, \quad E|n\rangle = |n\rangle + |n+1\rangle. \quad (1.25)$$

This observation is the genesis of several random walk interpretations that we associate to the TASEP in this work.

### 1.3.3 TASEP partition function

The nonequilibrium partition function

$$Z_N = \sum_{\mathcal{C}} \mathcal{W}(\mathcal{C}) \quad (1.26)$$

$$= \langle W|(D+E)^N|V\rangle \quad (1.27)$$

is a sum of the weights of the  $2^N$  TASEP configurations of length  $N$ , as the binomial expansion of  $(D+E)^N$  yields all permutations of  $\{D, E\}^N$ . As well as normalising configuration weights, the analytic properties of the nonequilibrium partition function

are, much like its equilibrium counterpart, indicative of the phase dynamics of the system, and allows us to calculate macroscopic quantities.

For the TASEP,  $Z_N$  is exactly calculable via the matrix product formalism. For now, we quote this result from Ref. [36]:

$$Z_N = \sum_{p=1}^N \sum_{q=0}^p \frac{p(2N-p-1)!}{N!(N-p)!} \left(\frac{1}{\alpha}\right)^q \left(\frac{1}{\beta}\right)^{p-q}. \quad (1.28)$$

See Section 1.6.2 for a full derivation of  $Z_N$ , in the context of *generating functions*.

### 1.3.4 Phase diagram

The formula for  $Z_N$  in Eq. (1.28) is exact, but it is not clear how the function scales for large values of  $N$ . In Section 1.6.3 we discuss how we can derive this via generating functions, but for now we quote the scaling obtained directly from analysis of Eq. (1.28) in Ref. [36]:

$$Z_N \sim \begin{cases} \frac{\beta(1-2\alpha)}{(\beta-\alpha)(1-\alpha)} [(\alpha(1-\alpha))]^{-N} & \text{(i) if } \alpha < 1/2, \alpha < \beta \\ \frac{\alpha(1-2\beta)}{(\alpha-\beta)(1-\beta)} [\beta(1-\beta)]^{-N} & \text{(ii) if } \beta < 1/2, \beta < \alpha \\ \frac{4\alpha\beta(\alpha+\beta-1)}{\sqrt{\pi}(2\alpha-1)^2(2\beta-1)^2} 4^N N^{-\frac{3}{2}} & \text{(iii) if } \alpha, \beta > 1/2. \end{cases} \quad (1.29)$$

We see three different regions in the  $\alpha$ - $\beta$  plane where  $Z_N$  has different asymptotic scaling behaviour. When  $N$  is large, then, we expect the functional form of  $Z_N$  to change sharply when moving across the boundary between two regions. We identify these sharp changes as dynamical *phase transitions*. We term these three phases the (i) *low density* (LD), (ii) *high density* (HD) and (iii) *maximal current* (MC). These phases are characterised by nonanalytic changes in the bulk density profile  $\langle \tau_i \rangle$  and current  $J$ . These phases converge at the *tricritical point*  $\alpha = \beta = 1/2$ .

Let us calculate the steady-state current  $J$ . As  $J$  is constant across every site in the system, we are free to calculate it as the current through site  $N$ . This is a product of the site- $N$  density  $\langle \tau_N \rangle$  and the rate  $\beta$  at which particles leave site  $N$  [36]:

$$J = \frac{\beta \langle W|(D+E)^{N-1}D|V \rangle}{\langle W|(D+E)^N|V \rangle} \quad (1.30)$$

$$= \frac{\langle W|(D+E)^{N-1}|V \rangle}{\langle W|(D+E)^N|V \rangle} \quad (1.31)$$

$$= \frac{Z_{N-1}}{Z_N} \quad (1.32)$$

which is the ratio of two partition functions for TASEPs of size  $(N-1)$ , and  $N$ . Taking the asymptotic forms of  $Z_N$  in Eq. (1.29), we find for  $J$

$$J \sim \begin{cases} \alpha(1-\alpha) & \text{LD} \\ \beta(1-\beta) & \text{HD} \\ 1/4 & \text{MC} . \end{cases} \quad (1.33)$$

We present the *phase diagram* of the TASEP in Figure 1.3, accompanied with typical density profiles  $\langle \tau_i \rangle$ . For any site  $i$ , the average occupation is exactly calculable by the matrix product approach (see Ref. [36] for more details and exact results) as:

$$\langle \tau_i \rangle = \frac{1}{Z_N} \langle W | (D + E)^{i-1} D (D + E)^{N-i} | V \rangle \quad (1.34)$$

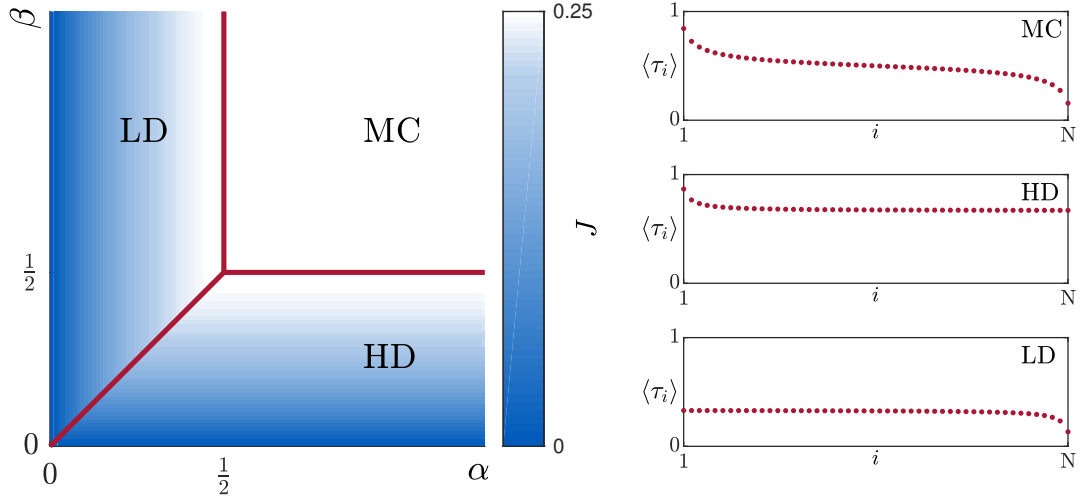
which is a sum of probabilities over all configurations where site  $i$  is occupied. The profile is dependent on  $\alpha$ ,  $\beta$  and the system size  $N$ . It can be shown that the *bulk* densities seen away from the boundaries approaches  $\alpha$ ,  $(1-\beta)$  and  $1/2$  in the LD, HD and MC phases respectively, with the tails of the profiles taking different forms in different phases — see Ref. [7] for a more comprehensive discussion.

We see in the structure of the phase diagram in Figure 1.3 a symmetry along the line  $\alpha = \beta$ . This is a manifestation of a more general *particle-hole* symmetry in this system that equally applies to the PASEP and SSEP: the dynamics of particles moving to the right are identical to the dynamics of holes moving to the left [7]. The system of particles moving left-to-right though the lattice is identical to a system of holes moving from right to left, with an entry rate  $\beta$  and exit rate  $\alpha$ . In this regard, the high density phase is the counterpart, for holes, of the low density phase and the low density phase is the counterpart, for holes, of the high density phase. Evidence of this particle-hole symmetry is in the manifest  $\alpha$ - $\beta$  symmetry in the partition function in Eq. (1.28) and in turn the particle current in Eq. (1.30) (as the current of particles to the right is equal to the current of holes to the left).

We also mention that higher-order correlations can be written using the matrix product formalism as per Eq. (1.34). For example, the second order  $\langle \tau_{i_1} \tau_{i_2} \rangle$  (with  $i_1 > i_2$ ) is given by [39]

$$\langle \tau_{i_1} \tau_{i_2} \rangle = \frac{1}{Z_N} \langle W | (D + E)^{i_1-1} D (D + E)^{i_2-i_1-1} D (D + E)^{N-i_2} | V \rangle . \quad (1.35)$$





**Figure 1.3** *Left: phase diagram of the TASEP with overlay of current. Right: example density profiles.*

### Factorisation line

There is one line in the phase diagram,  $\alpha + \beta = 1$ , where the matrix product algebra simplifies significantly. Along this line, the matrix product of  $\langle W | (DE - ED) | V \rangle$  is [40]

$$\langle W | (DE - ED) | V \rangle = \langle W | (D + E - ED) | V \rangle \quad (1.36)$$

$$= \frac{1}{\beta} + \frac{1}{\alpha} - \frac{1}{\alpha\beta} \quad (1.37)$$

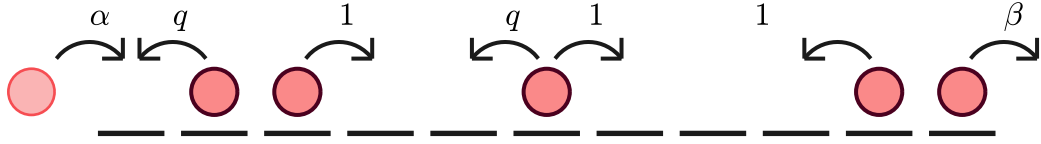
$$= \frac{1}{\alpha\beta} (\alpha + \beta - 1) = 0 \quad (1.38)$$

thus, when between a  $\langle W |$  and  $| V \rangle$ ,  $D$  and  $E$  can be treated as commuting scalars in this specific case. Here, configuration probabilities follow a *Bernoulli* distribution [41], and any calculations involving the matrix product formalism are trivial. We refer to this as the *factorisation line*. The tricritical point  $\alpha = \beta = 1/2$  lies on this line, where every configuration has equal probability. This line will prove useful as a consistency check for later calculations we perform over the whole phase diagram; upon fixing  $\alpha = \beta = 1$ , we should always recover this trivial Bernoulli measure.

### 1.3.5 The partially asymmetric and symmetric simple exclusion processes

We are also interested in two generalisations of the TASEP. These are termed the *partially asymmetric* and *symmetric* simple exclusion processes (PASEP and SSEP respectively).

The PASEP assumes the same dynamics as the TASEP, with the additional feature



**Figure 1.4** *The PASEP.*

that particles may also hop *left* at a rate  $q$ , except at the left-most site (Figure 1.4). Like the TASEP, the steady-state distribution of this system is exactly calculable by a matrix product approach. However, the resultant reduction relations have an additional factor of  $q$  compared to relations (1.10)–(1.13) [36]:

$$D|V\rangle = \frac{1}{\beta}|V\rangle, \quad (1.39)$$

$$\langle W|E = \frac{1}{\alpha}\langle W|, \quad (1.40)$$

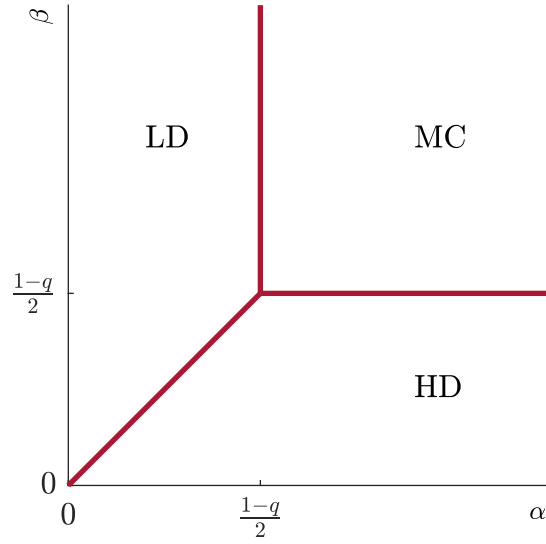
$$DE = qED + D + E, \quad (1.41)$$

$$\langle W|V\rangle = 1. \quad (1.42)$$

This  $q$ -generalisation introduces significant algebraic complexity [42–44], and as a result the partition function of the PASEP is rather complicated (see Ref. [42] for details). However, several macroscopic quantities can still be derived, including the phase diagram (Figure 1.5) [42]. One finds that there are still three main dynamical phases, but now the tricritical point is at  $\alpha = \beta = (1 - q)/2$ . Notice that in the limit of  $q \rightarrow 1$ , the tricritical point moves to  $\alpha = \beta = 0$ , and there are no phase transitions. In this limit — the SSEP — particles have no directional preference when making jumps in the bulk. While the  $q$ -general case is technically challenging, many calculations simplify when  $q = 1$ , as we later see in this section with the partition function.

### Explicit matrix representation

Like our discussion in Section 1.3.2, the reduction relations (1.39)–(1.42) can be used in a formal way to calculate physical quantities in the PASEP. However it is often useful to have an explicit matrix representation of these matrices, of which several are known.



**Figure 1.5** Phase diagram of the PASEP.

The following is a generalisation of the representation in Eqs. (1.21), (1.22) [7, 42, 45]:

$$D = \frac{1}{1-q} \begin{pmatrix} 1 & \sqrt{1-q} & \cdot & \cdot & \cdots \\ \cdot & 1 & \sqrt{1-q^2} & \cdot & \cdots \\ \cdot & \cdot & 1 & \sqrt{1-q^3} & \cdots \\ \cdot & \cdot & \cdot & 1 & \cdots \\ \vdots & \vdots & \vdots & \vdots & \ddots \end{pmatrix}, \quad (1.43)$$

$$E = \frac{1}{1-q} \begin{pmatrix} 1 & \cdot & \cdot & \cdot & \cdots \\ \sqrt{1-q} & 1 & \cdot & \cdot & \cdots \\ \cdot & \sqrt{1-q^2} & 1 & \cdot & \cdots \\ \cdot & \cdot & \sqrt{1-q^3} & 1 & \cdots \\ \vdots & \vdots & \vdots & \vdots & \ddots \end{pmatrix}, \quad (1.44)$$

with the boundary vectors

$$\langle W| = \kappa \left( 1, \frac{a}{\sqrt{1-q}}, \frac{a^2}{\sqrt{(1-q)(1-q^2)}}, \frac{a^3}{\sqrt{(1-q)(1-q^2)(1-q^3)}}, \dots \right), \quad (1.45)$$

$$|V\rangle = \kappa \left( 1, \frac{b}{\sqrt{1-q}}, \frac{b^2}{\sqrt{(1-q)(1-q^2)}}, \frac{b^3}{\sqrt{(1-q)(1-q^2)(1-q^3)}}, \dots \right)^T. \quad (1.46)$$

$\kappa$  is a normalisation factor defined such that  $\langle W|V \rangle = 1$ , and we use the shorthand (a  $q$ -generalisation of Eq. (1.23))

$$a = \frac{1 - q - \alpha}{\alpha}, \quad b = \frac{1 - q - \beta}{\beta}. \quad (1.47)$$

In this representation, recover Eqs. (1.21), (1.22) by setting  $q = 0$ . These individual representations diverge as  $q \rightarrow 1$ , however any scalar product of the form  $\lim_{q \rightarrow 1} \langle W|DEDDE \dots |V \rangle$  is well-defined, and gives the correct SSEP configuration weight. Other representations are possible, see Ref. [7]. Like in Section 1.3.2, one can draw a parallel between this matrix representation and, in this case, the ladder operators for a  $q$ -deformed quantum harmonic oscillator, a fact that was exploited in References [42, 45] to calculate physical properties for the PASEP.

### Partition function of the SSEP

We now calculate the partition function of the SSEP. We present perhaps the most straightforward of several approaches [46–48], following that of Vanicat in Ref. [47]. We first write  $Z_N$

$$Z_N = \langle W|C^N|V \rangle = \langle W|(D + E)C^{N-1}|V \rangle \quad (1.48)$$

where  $C \equiv D + E$ . We now use Eq. (1.41) to derive the following commutation property for  $q = 1$

$$[D, C] = D(D + E) - (E + D)D \quad (1.49)$$

$$= C \quad (1.50)$$

which implies that  $DC = C(D + 1)$ . Repeating this  $(N - 1)$  times gives

$$DC^{N-1} = C^{N-1}(D + N - 1) \quad (1.51)$$

which we insert into Eq. (1.48) and apply the reduction relations (1.39)–(1.42)

$$Z_N = \langle W|C^{N-1}(D + N - 1)|V \rangle + \langle W|EC^{N-1}|V \rangle \quad (1.52)$$

$$= \left( \frac{1}{\alpha} + \frac{1}{\beta} + N - 1 \right) Z_{N-1}. \quad (1.53)$$

Given that  $Z_0 = \langle W|V \rangle = 1$ , this recursion is easily solved to give

$$Z_N = \frac{\Gamma\left(\frac{1}{\alpha} + \frac{1}{\beta} + N\right)}{\Gamma\left(\frac{1}{\alpha} + \frac{1}{\beta}\right)} \quad (1.54)$$

with  $\Gamma(x) = (x-1)!$  the usual gamma function. Using Stirling's approximation [10] we can straightforwardly write the asymptotic expansion of  $Z_N$  as

$$Z_N \sim \frac{\sqrt{2\pi}}{\Gamma\left(\frac{1}{\alpha} + \frac{1}{\beta}\right)} N^{-\frac{1}{2}} \left(\frac{\frac{1}{\alpha} + \frac{1}{\beta} + N}{e}\right)^{\left(\frac{1}{\alpha} + \frac{1}{\beta} + N\right)}. \quad (1.55)$$

The partition function for the SSEP here and the partition function for the TASEP (Eq. (1.28)) measure the size of the state space of the  $2^N$  configurations of particles and holes. In this work we are particularly interested in more intricate measures of the probability distribution, relating to the partitioning of these state spaces. This leads us naturally onto a discussion of one such measure, known as the *Rényi entropy*, which we introduce in a more general manner, away from exclusion processes.

## 1.4 Rényi entropy

Suppose we have a system with a set of  $M$  accessible configurations,  $\{\mathcal{C}\}$ , with associated probabilities  $\{\mathcal{P}(\mathcal{C})\}$ , normalised so that  $\sum_{\mathcal{C}} \mathcal{P}(\mathcal{C}) = 1$ . From this, one can construct the familiar Gibbs-Shannon entropy that we saw in Eq. (1.4) [49]:

$$S = - \sum_{\mathcal{C}} \mathcal{P}(\mathcal{C}) \log \mathcal{P}(\mathcal{C}) ,$$

that specifies the level of microscopic uncertainty implied by the system macrostate. It is easy to show that Eq. (1.4) has several properties that one would postulate a measure of uncertainty to have [50–52]:

1.  $S(p, 1-p)$  is continuous on  $p \in [0, 1]$ ;
2.  $S(p_1, \dots, p_M)$  is symmetric on exchanging any two  $p_i$ ;
3.  $S$  is minimised with a distribution  $\{\mathcal{P}(\mathcal{C})\} = (1, 0, \dots, 0)$ ;
4.  $S$  is maximised with a distribution  $\{\mathcal{P}(\mathcal{C})\} = (1/M, \dots, 1/M)$ ;

5.  $S(p_1, \dots, p_{M-1}, tp_M, (1-t)p_M) = S(p_1, \dots, p_M) + p_M S(t, 1-t)$ , a “grouping” property which implies:

$$(a) \quad S(\mathcal{P}_1 \star \mathcal{P}_2) = S(\mathcal{P}_1) + S(\mathcal{P}_2).$$

This final property is *additivity*: for two independent systems with joint distribution  $\mathcal{P}_1 \star \mathcal{P}_2$ , the total entropy is the sum of the entropies of the two individual systems, isolated. Furthermore, it can be shown that the Gibbs-Shannon entropy is the *only* measure that satisfies all of these properties [8, 53, 54].

This leads us to the *Rényi entropy* [8]. Rényi entropy is a deformation of the Gibbs-Shannon entropy, where a new parameter  $\lambda$  tunes the sensitivity of the function to the details of the probability distribution. It is defined as

$$H_\lambda = \frac{1}{1-\lambda} \log \sum_{\mathcal{C}} \mathcal{P}(\mathcal{C})^\lambda. \quad (1.56)$$

Although valid for any base of logarithm, we use the natural logarithm in this work.

### 1.4.1 Properties of the Rényi entropy

Structurally, Eq. (1.56) is similar to the Gibbs-Shannon entropy: for any positive  $\lambda$  it satisfies Postulates 1–4, and the weaker postulate 5(a) [8]. We can recover the Gibbs-Shannon entropy from Eq. (1.56) in the limit  $\lambda \rightarrow 1$ :

$$\lim_{\lambda \rightarrow 1} H_\lambda = \lim_{\lambda \rightarrow 1} \frac{\log \sum_{\mathcal{C}} \mathcal{P}(\mathcal{C}) e^{(\lambda-1) \log \mathcal{P}(\mathcal{C})}}{1-\lambda} = - \sum_{\mathcal{C}} \mathcal{P}(\mathcal{C}) \log \mathcal{P}(\mathcal{C}) = S. \quad (1.57)$$

The Rényi entropy is a nonincreasing function of  $\lambda$ : for  $\lambda_1 > \lambda_2$ ,  $H_{\lambda_1} \leq H_{\lambda_2}$ . Knowledge of  $H_0$  and any Rényi entropy  $H_{\lambda>1}$  then gives upper and lower bounds on the Gibbs-Shannon entropy [55, 56].

While the Gibbs-Shannon entropy is the only measure that satisfies the full set of postulates, the Rényi entropy is a more general function of how the state space is divided amongst the set of microstates (perhaps more succinctly put as the *partitioning of the partition function*). By increasing  $\lambda$ ,  $H_\lambda$  places more weight on more probable configurations, which is made clear with two extreme cases. First,  $H_0$  is simply the logarithm of the number of configurations with a nonzero probability, and  $H_\infty$  is a measure of only the largest probability in the set  $\{\mathcal{P}(\mathcal{C})\}$  (or probabilities in the presence of degeneracies) [52]. Thus, by knowing  $H_\lambda$  for different values of  $\lambda$ , the Rényi entropy probes finer details of a probability distribution than the Gibbs-Shannon entropy alone.

The exponential of the Rényi entropy is

$$e^{H_\lambda} = \left[ \sum_{\mathcal{C}} \mathcal{P}(\mathcal{C})^\lambda \right]^{\frac{1}{1-\lambda}}. \quad (1.58)$$

To interpret this, consider two extremes of the probability distribution. For a system whereby a single configuration has probability 1,  $e^{H_\lambda} = 1$ . Conversely, for a system with  $M$  equally likely configurations,  $e^{H_\lambda} = M$ . Thus we interpret  $e^{H_\lambda}$  as an *effective number* of configurations or, equivalently, a measure of how localised the system is within its configuration space. In ecology, the effective numbers in Eq. (1.58) are known as *Hill numbers* [57] and give measures of the diversity of a biological community [58, 59].

The  $\lambda = 2$  case of Eq. (1.56) is the focus of Chapters 3 and 4. We therefore make this explicit here:

$$H_2 = -\log \sum_{\mathcal{C}} \mathcal{P}(\mathcal{C})^2. \quad (1.59)$$

This is often referred to in the literature as the *collision entropy* [60], and the corresponding effective number

$$e^{H_2} = \frac{1}{\sum_{\mathcal{C}} \mathcal{P}(\mathcal{C})^2} \quad (1.60)$$

as the *inverse participation ratio* [61, 62] (or in the context of diversity of a biological system, *Simpson's reciprocal index* [63]). This is a commonly used measure of quantum localisation of a wavefunction  $\psi$ , where  $\mathcal{P}(\mathcal{C})^2 = |\psi|^4$  [64, 65].

### 1.4.2 Rényi entropy at equilibrium

For an equilibrium system, we saw in Eq. (1.2) that microstate probabilities are exponentially weighted by their energy, normalised by a partition function  $Z(T)$ , now making the temperature dependence explicit. In this case, the Rényi entropy is readily calculable for all  $\lambda$  as [66]

$$H_\lambda = \frac{1}{1-\lambda} \log \frac{1}{Z(T)^\lambda} \sum_{\mathcal{C}} e^{-\lambda \frac{E(\mathcal{C})}{k_B T}} \quad (1.61)$$

$$= \frac{1}{1-\lambda} \log \frac{Z(\frac{T}{\lambda})}{Z(T)^\lambda}. \quad (1.62)$$

Intriguingly,  $H_\lambda$  involves the ratio of two partition functions  $Z(T)$ ,  $Z(T/\lambda)$  at *different* temperatures. Equivalently, using the definition of equilibrium free energy in Eq. (1.7),

$H_\lambda$  is proportional to the free energy difference between the two temperatures,

$$H_\lambda = \frac{F(T/\lambda) - F(T)}{k_B T(1/\lambda - 1)} . \quad (1.63)$$

We can interpret  $F(T/\lambda) - F(T)$  as the amount of work one can extract from the system between these two temperatures [66].

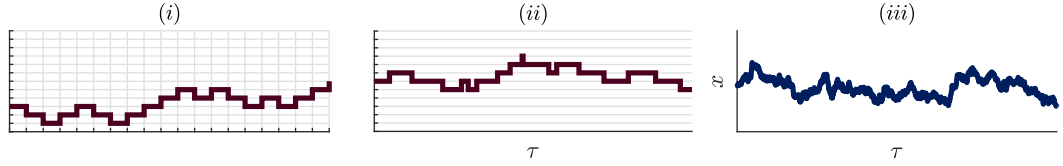
This form of the entropy has consequences for equilibrium systems that exhibit phase transitions. Suppose there is a transition at some temperature  $T = T^*$ . Then, in the thermodynamic limit, there is a nonanalyticity in the partition function  $Z(T^*)$ . Consequently, in Eq. (1.62) we will find not just the usual nonanalyticity at the critical temperature  $T^*$ , but also a secondary transition at  $T = \lambda T^*$ , away from the critical temperature. These particular properties of  $H_\lambda$  rely on the fact that the temperature  $T$  appears as the linear argument of an exponential function in the statistical weights. With any deviation away from such a distribution — as occurs in a nonequilibrium steady state — Eq. (1.62) may no longer apply. As such we consider the equilibrium Rényi entropy as a special case.

Given this particular property, we are interested in how the Rényi entropy manifests in the case of a classical nonequilibrium steady state, where the probability distribution is well-defined but there is no notion of a temperature. This is the motivation behind the work we present in Chapters 3 and 4, where we calculate the Rényi entropy of the TASEP, being a paradigmatic example of such a system. This calculation requires writing the sum of configuration weights in terms of a random walk problem. In preparation for this, we now present a discussion of the formulation of random walk problems.

## 1.5 Random walks and diffusion processes

A random walk is a stochastic process whereby a *walker* (say, a particle) takes steps, where each step is sampled from a distribution of possible steps. Note that the walk can be in an arbitrary number of spatial dimensions. In a given time period, a single manifestation of a walk can not be predicted, but the full ensemble of walks has well-defined statistics. Here, we are interested in how the probability distribution — the probability of finding a random walker at a certain place at a certain time — is expressed as a function of the mechanics of the walk. Given a description of a walk, we will see how to formalise and write master equations that the underlying probability distribution must obey. For the scope of this thesis we may assume Markov-like dynamics, that is





**Figure 1.6** Three types of one-dimensional random walks: (i) Discrete time, discrete space; (ii) Continuous time, discrete space; (iii) Continuous time, continuous space.

the current step is independent of any previous steps.

The random walk is a standard mathematical model of stochastic dynamics, with a scope well beyond what we discuss here. The pedagogical introduction we provide here — including the *continuum limit* of a random walk — echoes those presented in, for example, References [67–71].

A random walk can be specified over continuous or discrete time and distance scales. In this thesis we will encounter three different types of walk:

- *Discrete time, discrete space*: steps are guaranteed to occur at fixed time intervals. At each interval, the step is randomly sampled from a known distribution. These steps move the walker from one lattice site to another;
- *Continuous time, discrete space*: steps occur stochastically at known *rates*. These steps move the walker from one lattice site to another;
- *Continuous time, continuous space*: a diffusion-like process takes place, with infinitesimally small steps — not on a lattice — taken over infinitesimally small time periods. A classic example of this is Brownian motion.

Furthermore, the walker may possibly only be defined within a restricted region of space. If there are regions in space that a walker can not access, one must specify how it behaves when it comes to a *boundary* that separates a valid region from an invalid one. In this thesis we will encounter two types of boundary:

- *Absorbing*: if a walker makes a step that takes it into an invalid region, then the walk terminates at the point it crossed the boundary, and may not return;
- *Reflecting*: on the instant that the walker touches the boundary, the walk dynamics instantaneously change so as to force the walker to move along or away from the boundary.

Although we encounter three different types of walk in this thesis, we will always begin to formulate our master equations from a discrete time, discrete space walk. In order to then obtain equations in continuous space and/or time, we will take what is known as a *continuum limit* of the discrete walk. We introduce a spacing between lattice sites and/or time intervals, and then take the limit of these spacings being small, such that the length and/or time scale can be interpreted as continuous. In this section we will present a comprehensive example of taking a continuum limit in space and time, which we will refer back to in later sections. Our example walker will be in a 2D space, but the principles straightforwardly extend to arbitrary dimension, as we discuss further in Chapter 5.

### 1.5.1 Setting up a random walk

Let us define a 2D random walker in the discrete space  $(i_1, i_2)$ . Suppose that over each of a total of  $N$  discrete intervals, this walker can make any lattice step sampled from the step set  $\{\nearrow, \downarrow, \leftarrow\}$ . This walk that we use as an example is known as a *Kreweras walk* [72]. This step set has an associated probability distribution  $\{p_{\nearrow}, p_{\downarrow}, p_{\leftarrow}\}$  that sums to unity:  $p_{\nearrow} + p_{\downarrow} + p_{\leftarrow} = 1$ . Furthermore, the walker must remain in the *upper-quarter plane* of the space:  $i_1 \geq 0, i_2 \geq 0$ . These dynamics are illustrated in Figure 1.7, left.

We would like to find

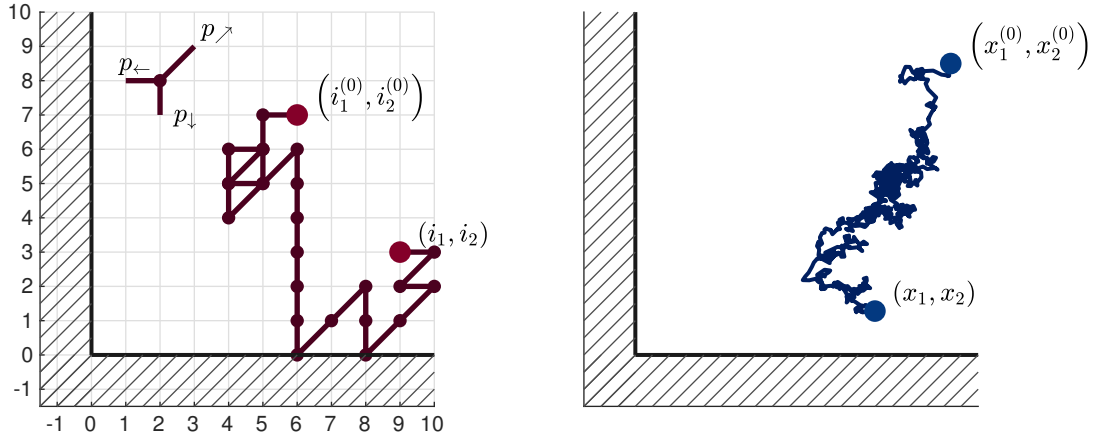
$$\mathcal{P}(i_1, i_2; N) \equiv \mathcal{P}\left(i_1, i_2 \mid i_1^{(0)}, i_2^{(0)}; N\right) \quad (1.64)$$

which we define as the probability of finding the walker at position  $(i_1, i_2)$ , given it started at some initial position  $(i_1^{(0)}, i_2^{(0)})$  and has taken  $N$  steps.

First consider the situation where  $i_1 > 0, i_2 > 0$ , away from the boundaries, which we define as the *bulk*. The master equation that  $\mathcal{P}$  obeys in the bulk is independent of any boundary conditions. The probability of finding the walker at  $(i_1, i_2)$  after  $(N+1)$  steps can be written as a sum of all possible ways of *entering* it, on the  $(N+1)^{\text{th}}$  step:

$$\begin{aligned} \mathcal{P}(i_1, i_2; N+1) = \\ p_{\nearrow} \mathcal{P}(i_1-1, i_2-1; N) + p_{\leftarrow} \mathcal{P}(i_1+1, i_2; N) + p_{\downarrow} \mathcal{P}(i_1, i_2+1; N) . \end{aligned} \quad (1.65)$$

This is a master equation, comprising the probabilities of being at positions one step away from  $(i_1, i_2)$ , multiplied by the probability of making the appropriate step to get to  $(i_1, i_2)$ . It is a recursion relation on the two coordinates  $(i_1, i_2)$  and the step count  $N$ .



**Figure 1.7** The continuum limit of a lattice walk in discrete time (left) yields a diffusion in continuous time and space (right).

### 1.5.2 Boundary conditions

The bulk master equation (1.65) does not apply when the walker is on a boundary. This is because when either of  $i_1$  or  $i_2 = 0$  the master equation would include ill-defined probabilities (specifically  $\mathcal{P}(-1, i_2; N)$ ,  $\mathcal{P}(i_1, -1; N)$ ,  $\mathcal{P}(-1, -1; N)$ ). The equations that describe  $\mathcal{P}$  on the boundary then depend on whether the boundaries are absorbing or reflecting.

#### Absorbing boundary conditions

Let us first consider the case of absorbing boundaries. Here, the walker behaves no differently on the boundaries as it does in the bulk, and can take any step from its original step set. However, if such a step takes it to either  $i_1 = -1$  or  $i_2 = -1$ , then it is *absorbed* and the walk finishes. The boundary conditions are then simply written

$$\mathcal{P}(-1, i_2; N) = \mathcal{P}(i_1, -1; N) = 0 . \quad (1.66)$$

This has the consequence of the ‘loss’ of probability from the valid region over time as walks are absorbed:

$$\sum_{i_1 \geq 0} \sum_{i_2 \geq 0} \mathcal{P}(i_1, i_2; N) \leq 1 . \quad (1.67)$$

## Reflecting boundary conditions

We now take the case where the mechanics of the walk are changed upon reaching a boundary, so as to prevent the walker from crossing it. Unlike the absorbing case, there are a multitude of ways of changing the dynamics to force this [73–76]. In this example, we will change the dynamics such that any step that would take the walker past the boundary is replaced by a *non-movement* step, and instead the walker remains in place. This forces the walker to move either along or away from the boundary, which can be interpreted as reflecting.

For our specific example, this manifests as a non-movement with probability  $p_{\leftarrow}$  on the  $i_1 = 0$  boundary, a non-movement with probability  $p_{\downarrow}$  on the  $i_2 = 0$  boundary, and a non-movement with probability  $(p_{\leftarrow} + p_{\downarrow})$  at  $i_1 = i_2 = 0$ . These three modified dynamics introduce three new equations that the probability distribution must satisfy:

$$\mathcal{P}(0, i_2; N + 1) = p_{\leftarrow} \mathcal{P}(1, i_2; N) + p_{\downarrow} \mathcal{P}(0, i_2 + 1; N) + p_{\leftarrow} \mathcal{P}(0, i_2; N) , \quad (1.68)$$

$$\mathcal{P}(i_1, 0; N + 1) = p_{\leftarrow} \mathcal{P}(i_1 + 1, 0; N) + p_{\downarrow} \mathcal{P}(i_1, 1; N) + p_{\downarrow} \mathcal{P}(i_1, 0; N) , \quad (1.69)$$

$$\mathcal{P}(0, 0; N + 1) = p_{\leftarrow} \mathcal{P}(1, 0; N) + p_{\downarrow} \mathcal{P}(0, 1; N) + (p_{\downarrow} + p_{\leftarrow}) \mathcal{P}(0, 0; N) . \quad (1.70)$$

In this regime, the quadrant probability remains constant:

$$\sum_{i_1 \geq 0} \sum_{i_2 \geq 0} \mathcal{P}(i_1, i_2; N) = 1 , \quad \forall N \quad (1.71)$$

as walks continue indefinitely without being absorbed.

### 1.5.3 Continuum limit

The bulk recursion relation (1.65) is written in terms of a discrete length of walk  $N$  and a discrete lattice  $(i_1, i_2)$ . Over each unit, a step is chosen from the probability distribution  $\{p_{\downarrow}, p_{\leftarrow}, p_{\nearrow}\}$ . Suppose now we want to investigate the random walk where, instead of steps occurring at discrete intervals, steps occur stochastically at prescribed average *rates*. For this, we take the continuum limit of Eq. (1.65) in  $N$ .

#### Time continuum limit

The walk so far has been defined by a number of steps  $N$ . To associate a time-like scaling to this walk, we introduce a continuous spacing  $\lambda$  with dimensions of time, such

that steps occur every time an interval  $\lambda$  has elapsed. We then define  $\tau$  as the total elapsed time after  $N$  steps:

$$\tau = N\lambda . \quad (1.72)$$

We are free to write the probability  $\mathcal{P}$  in terms of this new variable  $\tau$ :

$$\mathcal{P}(i_1, i_2; N) \longrightarrow \mathcal{P}(i_1, i_2; \tau) . \quad (1.73)$$

We now take this time spacing  $\lambda$  to be small. We can write the probability of having taken one more step from  $\tau$  as  $\mathcal{P}(i_1, i_2; \tau + \lambda)$ . If we treat  $\lambda$  as small, we can make the approximation

$$\mathcal{P}(i_1, i_2; \tau + \lambda) \approx \mathcal{P}(i_1, i_2; \tau) + \lambda \partial_\tau \mathcal{P}(i_1, i_2; \tau) + \mathcal{O}(\lambda^2) . \quad (1.74)$$

We can apply this approximation to the bulk equation (1.65) to obtain

$$\begin{aligned} \mathcal{P}(i_1, i_2; \tau) + \lambda \partial_\tau \mathcal{P}(i_1, i_2; \tau) + \mathcal{O}(\lambda^2) = \\ p_{\nearrow} \mathcal{P}(i_1 - 1, i_2 - 1; N) + p_{\leftarrow} \mathcal{P}(i_1 + 1, i_2; N) + p_{\downarrow} \mathcal{P}(i_1, i_2 + 1; N) . \end{aligned} \quad (1.75)$$

Having introduced this spacing  $\lambda$ , we now introduce a new set of variables  $r$ , defined such that

$$p_i = \lambda r_i . \quad (1.76)$$

$r_i$  is interpreted as a rate: if step  $i$  occurs with probability  $p_i$ , then the step is occurring at mean rate  $r_i$ , as the step set is sampled at each time interval  $\lambda$ . In order to prevent these rates from diverging as  $\lambda \rightarrow 0$ , we alter the probabilities such that they no longer sum to unity, and a step does not always occur after every interval. Now, the walker will take one of the three steps with respective probabilities  $\{p_{\downarrow}, p_{\leftarrow}, p_{\nearrow}\} = \{\lambda r_{\nearrow}, \lambda r_{\rightarrow}, \lambda r_{\downarrow}\}$ , but can also *not* move, with probability  $1 - \lambda(r_{\nearrow} + r_{\rightarrow} + r_{\downarrow})$ . With these dynamics, Eq. (1.75) reads

$$\begin{aligned} \mathcal{P}(i_1, i_2; \tau) + \lambda \partial_\tau \mathcal{P}(i_1, i_2; \tau) + \mathcal{O}(\lambda^2) = \\ \lambda r_{\nearrow} \mathcal{P}(i_1 - 1, i_2 - 1; N) + \lambda r_{\leftarrow} \mathcal{P}(i_1 + 1, i_2; \tau) + \lambda r_{\downarrow} \mathcal{P}(i_1, i_2 + 1; \tau) \\ + (1 - \lambda[r_{\nearrow} + r_{\rightarrow} + r_{\downarrow}]) \mathcal{P}(i_1, i_2; \tau) . \end{aligned} \quad (1.77)$$

We find cancellation at  $\mathcal{O}(\lambda^0)$ . Eliminating a common factor of  $\lambda$  and then taking the limit as  $\lambda \rightarrow 0$ , we acquire an equation in continuous time:

$$\begin{aligned} \partial_\tau \mathcal{P}(i_1, i_2; \tau) = & -(r_{\nearrow} + r_{\downarrow} + r_{\leftarrow}) \mathcal{P}(i_1, i_2; \tau) + r_{\nearrow} \mathcal{P}(i_1 - 1, i_2 - 1; \tau) \\ & + r_{\leftarrow} \mathcal{P}(i_1 + 1, i_2; \tau) + r_{\downarrow} \mathcal{P}(i_1, i_2 + 1; \tau) . \end{aligned} \quad (1.78)$$

This continuum equation describes the time evolution of  $\mathcal{P}(i_1, i_2; \tau)$  in terms of the rates at which probability current flows in and out of  $(i_1, i_2)$ . This is precisely the form of Eq. (1.8) with gain and loss terms. This approach is equally applied to equations that describe dynamics on the boundary.

### Space continuum limit

Eq. (1.78) is still defined on a discrete lattice. We now introduce continuous spatial variables to this walk. This follows the same setup as the time limit. We first assume that sites on our 2D lattice are separated by distance  $a$ , where  $a$  is a new variable with dimensions of length. We then define  $(x_1, x_2)$  as spatial variables that describe the displacement of  $(i_1, i_2)$  from the origin, given this lattice spacing:

$$x_1 = i_1 a , \quad x_2 = i_2 a . \quad (1.79)$$

We are free to write the probability in terms of these new coordinates

$$\mathcal{P}(i_1, i_2; \tau) \longrightarrow \mathcal{P}(x_1, x_2; \tau) . \quad (1.80)$$

We rewrite Eq. (1.78) in terms of these new variables

$$\begin{aligned} \partial_\tau \mathcal{P}(x_1, x_2; \tau) = & -(r_{\nearrow} + r_{\downarrow} + r_{\leftarrow}) \mathcal{P}(x_1, x_2; \tau) + r_{\nearrow} \mathcal{P}(x_1 - a, x_2 - a; \tau) \\ & + r_{\leftarrow} \mathcal{P}(x_1 + a, x_2; \tau) + r_{\downarrow} \mathcal{P}(x_1, x_2 + a; \tau) . \end{aligned} \quad (1.81)$$

If we treat this length scale  $a$  to be small, we can make the following Taylor expansions:

$$\mathcal{P}(x_1 \pm a, x_2; \tau) = \left( 1 \pm a \partial_1 + \frac{1}{2} a^2 \partial_1^2 \right) \mathcal{P}(x_1, x_2; \tau) + \mathcal{O}(a^3) , \quad (1.82)$$

$$\mathcal{P}(x_1, x_2 \pm a; \tau) = \left( 1 \pm a \partial_2 + \frac{1}{2} a^2 \partial_2^2 \right) \mathcal{P}(x_1, x_2; \tau) + \mathcal{O}(a^3) . \quad (1.83)$$

After some algebra, we find that, for small  $a$ , Eq. (1.81) may be written

$$\begin{aligned} \partial_\tau \mathcal{P}(x_1, x_2; \tau) &= a [(r_{\leftarrow} - r_{\nearrow}) \partial_1 + (r_{\downarrow} - r_{\nearrow}) \partial_2] \mathcal{P}(x_1, x_2; \tau) \\ &+ \frac{1}{2} a^2 [(r_{\nearrow} + r_{\rightarrow}) \partial_1^2 + (r_{\nearrow} + r_{\downarrow}) \partial_2^2 + 2r_{\nearrow} \partial_1 \partial_2] \mathcal{P}(x_1, x_2; \tau) + \mathcal{O}(a^3) \end{aligned} \quad (1.84)$$

or alternatively as a matrix product

$$\begin{aligned} \partial_\tau \mathcal{P}(x_1, x_2; \tau) &= a \begin{pmatrix} r_{\leftarrow} - r_{\nearrow} & r_{\downarrow} - r_{\nearrow} \end{pmatrix} \begin{pmatrix} \partial_1 \\ \partial_2 \end{pmatrix} \mathcal{P}(x_1, x_2; \tau) \\ &+ \frac{1}{2} a^2 (\partial_1, \partial_2) \begin{pmatrix} r_{\nearrow} + r_{\leftarrow} & r_{\nearrow} \\ r_{\nearrow} & r_{\nearrow} + r_{\downarrow} \end{pmatrix} \begin{pmatrix} \partial_1 \\ \partial_2 \end{pmatrix} \mathcal{P}(x_1, x_2; \tau) + \mathcal{O}(a^3). \end{aligned} \quad (1.85)$$

As in the time continuum limit, we will introduce parameters that are scaled by the spacing  $a$ , then take the limit  $a \rightarrow 0$ . However, this time we are compelled to retain both  $\mathcal{O}(a)$  and  $\mathcal{O}(a^2)$  terms in Eq. (1.85). To see this, consider the case where the step rates are equal:  $r_{\leftarrow} = r_{\nearrow} = r_{\downarrow}$ . Then, the leading order terms on the right-hand side of Eq. (1.84) vanish, and we would be left with  $\partial_\tau \mathcal{P} = \mathcal{O}(a^2)$ . To obtain a well-defined expression for  $\mathcal{P}$  then, we must make the following assumption on the rates [70]:

$$r_{\leftarrow} - r_{\nearrow} = \mathcal{O}(a), \quad (1.86)$$

$$r_{\downarrow} - r_{\nearrow} = \mathcal{O}(a). \quad (1.87)$$

We can then define a set of parameters that scale with the lattice spacing  $a$ :

$$\underline{\mu} = a \begin{pmatrix} r_{\leftarrow} - r_{\nearrow} \\ r_{\downarrow} - r_{\nearrow} \end{pmatrix}, \quad S = \frac{a^2}{2} \begin{pmatrix} r_{\nearrow} + r_{\rightarrow} & r_{\nearrow} \\ r_{\nearrow} & r_{\nearrow} + r_{\downarrow} \end{pmatrix}. \quad (1.88)$$

$\underline{\mu}$  has dimensions of length/time, and can be interpreted as a deterministic drift velocity vector. The stochastic element of the walk is seen in  $S$ : the entries of  $S$  have dimensions of length<sup>2</sup>/time. This is interpreted as a *diffusivity*, or a rate of change of squared displacement. We term  $S$  a *diffusion matrix*.

We incorporate these new parameters into Eq. (1.81) and take the limit  $a \rightarrow 0$  to give

$$\partial_\tau \mathcal{P}(x_1, x_2; \tau) = \left( \underline{\mu} \cdot \underline{\nabla} + \underline{\nabla} \cdot (S \underline{\nabla}) \right) \mathcal{P}(x_1, x_2; \tau). \quad (1.89)$$

To summarise, Eq. (1.89) is a *diffusion equation*, and is the time and space continuum limit of the original master equation (1.65). From the form of the parameters in Eq. (1.88), it is straightforward to see how this method generalises for other step sets

(different entries in  $\underline{\mu}$ ,  $S$ ), and higher dimensionality (for an  $N$ -dimensional walk,  $\underline{\mu}$ ,  $S$  are of size  $(N \times 1)$ ,  $(N \times N)$  respectively). Note that for any dimension, the diffusion equation remains second order — any higher-order terms are suppressed.

This same continuum limit method can be applied to the boundary dynamics, say Eqs. (1.68)–(1.70), to find the appropriate continuum limit boundary conditions. For reflecting boundaries the equations turn out to be only first order in space. We will see an example of this in Chapter 5, Section 5.2.2, where in fact this property of the boundary conditions allows us to exactly solve the steady-state diffusion problem.

Using this formalism we are able to clearly define a set of equations that the probability distribution for a random walk must satisfy. The challenge, however, is in solving the set of equations. One tool that we will use in this thesis is known as the *generating function*. We now discuss the basic principles of these functions, and the formalism we adopt for later analysis.

## 1.6 Generating functions and asymptotic analysis

Take an infinite sequence of terms  $(A_0, A_1, A_2, \dots)$ , where successive  $A_N$  are linked by some relation (e.g.  $A_{N+1} = 2A_N + 3$ ). A common problem one may encounter is as follows: *given we know a recursion relation between different  $A_N$  and a known value to iterate from (e.g.  $A_0 = 1$ ), how do we find a closed-form expression for  $A_N$ ?* We saw an example of this in Eq. (1.65), albeit a recursion in three variables.

These problems can often be tackled by generating functions. Instead of finding  $A_N$  directly, one aims to calculate the (closed-form) function defined by

$$\mathcal{F}(z) = \sum_{N \geq 0} z^N A_N \tag{1.90}$$

$$= A_0 + zA_1 + z^2A_2 + z^3A_3 + \dots \tag{1.91}$$

where the coefficient of  $z^N$  in the formal series expansion of  $\mathcal{F}(z)$  is  $A_N$ . As a trivial example, for the sequence of terms  $(1, 1, 1, \dots)$ , the generating function is  $\mathcal{F}(z) = (1 - z)^{-1} = 1 + z + z^2 + z^3 + \dots$

Two challenges then arise: first, in calculating  $\mathcal{F}(z)$  from the recursion relation (if possible), which we will illustrate by an example. Secondly, the *inversion* of  $\mathcal{F}(z)$  to extract a general expression for the coefficient  $A_N$ , or the *asymptotic analysis* to find the scaling behaviour of  $A_N$  as  $N$  becomes large.



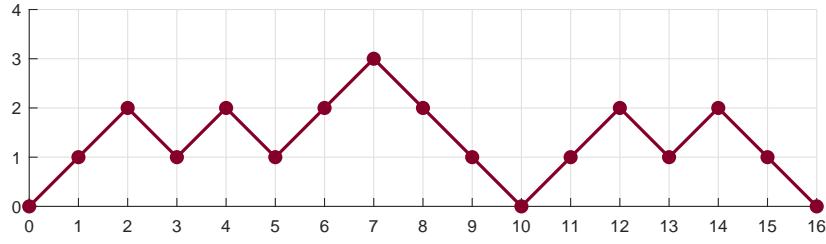


Figure 1.8 A Dyck path.

### 1.6.1 Generating function calculation — a simple example

For this short example we take the opportunity to introduce *Dyck paths*, which turn out to be very closely related to the TASEP (see Section 1.7.2).

A Dyck path is a path comprising an arrangement of  $N$  up steps ( $\nearrow$ ) and  $N$  down steps ( $\searrow$ ), starting and terminating at zero, without crossing below zero. Note that the first step must be an up step, and the final step a down step.

We would like to find  $C_N$ , the number of possible Dyck paths that can be drawn of length  $2N$  (we take  $2N$  as the total number of steps must be even). Let us define the generating function of  $C_N$

$$\mathcal{F}(z) = \sum_{N \geq 0} z^N C_N . \quad (1.92)$$

We can define a recurrence relation for  $C_N$  from a self-similarity property in the structure of a Dyck path: any Dyck path of length  $2(N + 1)$  can be written as an up step, followed by a Dyck path of length  $2k$ , a down step, then a second Dyck path of length  $2(N - k)$ .  $k$  can take values from 0 to  $N$ . This leads to the recursion relation for the number of paths  $C_{N+1}$  [77]:

$$C_{N+1} = \sum_{k=0}^N C_k C_{N-k} . \quad (1.93)$$

We now multiply both sides through by  $z^N$ , sum over all  $N$ , and with some manipulation

of the summation indices obtain

$$\sum_{N \geq 0} C_{N+1} z^N = \sum_{N \geq 0} \sum_{k=0}^N C_k C_{N-k} z^N \quad (1.94)$$

$$\frac{1}{z} \sum_{N \geq 0} C_{N+1} z^{N+1} = \sum_{k \geq 0} \sum_{N \geq k} C_k C_{N-k} z^N \quad (1.95)$$

$$\frac{1}{z} \left( \sum_{N \geq 0} C_N z^N - C_0 \right) = \sum_{k \geq 0} \sum_{N' \geq 0} C_k C_{N'} z^{N'+k} . \quad (1.96)$$

Given that  $C_0 = 1$ , this is written in terms of the generating function

$$\mathcal{F}(z) = z\mathcal{F}^2(z) + 1 \quad (1.97)$$

which is solved to give

$$\mathcal{F}(z) = \frac{1 - \sqrt{1 - 4z}}{2z} . \quad (1.98)$$

We take the negative sign of the square root to ensure  $C_0 = 1$ . The coefficients in the expansion of  $\mathcal{F}(z)$  about zero are the number of Dyck paths that can be drawn of increasing lengths. In this simple example, the coefficients  $C_N$  can be found exactly from the formal expansion of  $\mathcal{F}(z)$ , and turn out to be the familiar *Catalan numbers* [10]

$$\mathcal{F}(z) = 1 + z + 2z^2 + 5z^3 + 14z^4 + \dots \quad (1.99)$$

$$= \sum_{N \geq 0} \frac{1}{N+1} \binom{2N}{N} z^N . \quad (1.100)$$

To summarise this exercise, while the recurrence relation (1.93) did not offer an obvious solution, the generating function obeyed a simple relation in Eq. (1.97) that permitted direct solution.

### 1.6.2 Generating function of the TASEP partition function

With our knowledge of generating functions, we now return to the TASEP and derive the partition function, as we previously stated without calculation in Eq. (1.28). We use a neat approach shown by Depken [78]: first, define the generating function of Eq. (1.27) as  $\mathcal{Z}$ :

$$\mathcal{Z}(z) = \sum_{N \geq 0} \langle W | (D + E)^N | V \rangle z^N . \quad (1.101)$$

Noticing the geometric series in powers of  $z(D + E)$ , we rewrite this as

$$\mathcal{Z}(z) = \langle W | \frac{1}{1 - z(D + E)} | V \rangle. \quad (1.102)$$

Now we use the reduction relation  $DE = D + E$  from Eq. (1.12) to find the relation

$$(1 - \eta D)(1 - \eta E) = 1 - \eta(D + E) + \eta^2 DE \quad (1.103)$$

$$= 1 - \eta(1 - \eta)(D + E). \quad (1.104)$$

Solving  $z = \eta(1 - \eta) \Rightarrow \eta(z) = \frac{1}{2}(1 - \sqrt{1 - 4z})$ ,

$$\mathcal{Z}(z) = \langle W | \frac{1}{1 - \eta(z)E} \frac{1}{1 - \eta(z)D} | V \rangle \quad (1.105)$$

$$= \frac{1}{1 - \frac{\eta(z)}{\alpha}} \frac{1}{1 - \frac{\eta(z)}{\beta}} \quad (1.106)$$

$$= 1 + \left( \frac{1}{\alpha} + \frac{1}{\beta} \right) z + \left( \frac{1}{\alpha} + \frac{1}{\beta} + \frac{1}{\alpha^2} + \frac{1}{\beta^2} + \frac{1}{\alpha\beta} \right) z^2 + \dots \quad (1.107)$$

taking the negative root of  $\eta(z)$  to ensure  $\mathcal{Z}(0) = 1$ . The coefficient of  $z^N$  in the series expansion (1.107) of  $\mathcal{Z}(z)$  is the  $N$ -site TASEP partition function, Eq. (1.28).

### Formal expansion

We must now formally expand  $\mathcal{Z}(z)$ . Let us define  $\{z^N\}\mathcal{F}(z)$  as “the coefficient of  $z^N$  in the Taylor expansion of  $\mathcal{F}(z)$ ”. Taking  $\mathcal{Z}$ , a power series of the denominator of Eq. (1.106) gives

$$\mathcal{Z}(z) = \sum_{q \geq 0} \sum_{q' \geq 0} \left( \frac{1 - \sqrt{1 - 4z}}{2z} \right)^{q' + q} \left( \frac{z}{\alpha} \right)^q \left( \frac{z}{\beta} \right)^{q'}. \quad (1.108)$$

This form allows us to use a known result from the mathematical literature (Eq. (2.5.16) in Ref. [10]), which is derived by a general binomial expansion:

$$\left( \frac{1 - \sqrt{1 - 4z}}{2z} \right)^\zeta = \sum_{k \geq 0} \frac{\zeta(2k + \zeta - 1)!}{k!(\zeta + k)!} z^k \quad (1.109)$$

with  $\zeta = q + q'$  to rewrite

$$\mathcal{Z}(z) = \sum_{q \geq 0} \sum_{q' \geq 0} \sum_{k \geq 0} \frac{(q' + q)(2k + q' + q - 1)!}{k!(q' + q + k)!} z^k \left( \frac{z}{\alpha} \right)^q \left( \frac{z}{\beta} \right)^{q'} \quad (1.110)$$

which is now an explicit power series in  $z$ . To find the coefficient  $\{z^N\}\mathcal{Z}(z)$ , we impose the parameter restriction  $q' + q + k = N$ , fixing  $q' = N - k - q$

$$Z_N = \{z^N\}\mathcal{Z}(z) \quad (1.111)$$

$$= \sum_{k=0}^N \sum_{q=0}^{N-k} \frac{(N-k)(N+k-1)!}{N! k!} \left(\frac{1}{\alpha}\right)^q \left(\frac{1}{\beta}\right)^{N-k-q} . \quad (1.112)$$

Finally, a variable change  $N - k = p$  recovers Eq. (1.28):

$$Z_N = \sum_{p=1}^N \sum_{q=0}^p \frac{p(2N-p-1)!}{N!(N-p)!} \left(\frac{1}{\alpha}\right)^q \left(\frac{1}{\beta}\right)^{p-q} .$$

### 1.6.3 Asymptotic analysis of a generating function

In Chapters 3 and 4 we calculate generating functions that do not admit an obvious formal series expansion. For these, we instead use asymptotic methods to establish how the coefficients  $A_N$  scale as  $N$  grows large. Here we state the outcomes of asymptotic analysis of a generating function, following formalism laid out in Ref. [10].

For a function  $\mathcal{F}(z)$  as defined in Eq. (1.90), the leading-order asymptotic scaling of  $A_N$  is determined by the value of  $z$  closest to the (complex) origin,  $z^*$ , such that  $\mathcal{F}(z^*)$  is nonanalytic [10].

For the case of this being a first order (or *simple*) pole, we perform a series expansion about this pole to acquire

$$\mathcal{F}(z) = \frac{g_{-1}}{z - z^*} + \sum_{j \geq 0} g_j (z - z^*)^j \quad (1.113)$$

where  $g_{-1}$  is the *residue* of the pole, and  $g_j$  are higher-order coefficients in the expansion. This expansion can be shown to imply the following asymptotic scaling of the coefficients  $A_N$ :

$$A_N \sim -\frac{g_{-1}}{z^*} (z^*)^{-N} . \quad (1.114)$$

In the case of a branch point — a discontinuous imaginary contribution — being the first singularity, a series expansion about  $z^*$  yields an imaginary term:

$$\mathcal{F}(z) = i h_k (z - z^*)^k + \sum_{j \geq 0} h_j (z - z^*)^j \quad (1.115)$$

where  $k$  is non-integer and  $h_k$  is real. In this case, the coefficients  $A_N$  scale as

$$A_N \sim \frac{h_k (z^*)^k}{\Gamma(-k)} N^{-(k+1)} (z^*)^{-N} . \quad (1.116)$$

As a short example, let us return to our Catalan number generating function in Eq. (1.98). The first singularity here is a branch point at  $z^* = 1/4$ , about which a series expansion gives

$$\frac{1 - \sqrt{1 - 4z}}{2z} = 2 - 4i(1 - 4z)^{\frac{1}{2}} + \mathcal{O}(1 - 4z) . \quad (1.117)$$

This corresponds to an asymptotic form in Eq. (1.116) with  $k = 1/2$ ,  $h_k = -4$ :

$$C_N \sim \frac{(-4)(1/4)^{\frac{1}{2}}}{\Gamma(-1/2)} N^{-(1/2+1)} (1/4)^{-N} = \frac{4^N}{\sqrt{\pi} N^{3/2}} . \quad (1.118)$$

Similarly, one can perform an asymptotic analysis of the TASEP partition function generating function, Eq. (1.106), to recover the asymptotic scaling stated in Eq. (1.29). In this case (and as we will encounter in Sections 3.6, 4.2.2, and 4.4), there is an additional complication as the dominant singularity *changes* for different values of  $\alpha$ ,  $\beta$ . This in turn leads to the three dynamical phases.

## 1.7 Combinatorics in the ASEP

In Chapter 2 we will show how the ASEP state space has an intricate combinatorial structure arising from the matrix product formalism. Having now introduced the ASEP and the formalism behind random walks, as a preliminary to Chapter 2 we end with some simple observations of the ASEP that allude to a deeper combinatorial structure.

### 1.7.1 Combinatorial factors in $\alpha = \beta = 1$ SSEP and TASEP partition functions

First, in Section 1.3.5, we saw the result in Eq. (1.54) for the partition function of the SSEP:

$$Z_N = \frac{\Gamma\left(\frac{1}{\alpha} + \frac{1}{\beta} + N\right)}{\Gamma\left(\frac{1}{\alpha} + \frac{1}{\beta}\right)} .$$

In the case  $\alpha = \beta = 1$ , this expression reduces to

$$Z_N = (N + 1)! . \quad (1.119)$$

In other words, the sum of (integer) weights of the  $2^N$  SSEP configuration weights is  $(N + 1)!$ . This suggests that the configuration space of the SSEP with  $\alpha = \beta = 1$  can be related to a uniform distribution over the space of permutations. In Section 2.3 we will see that this is the case.

We now turn to the TASEP (the case  $q = 0$ ). Although the underlying ASEP reduction relation  $DE - qED = D + E$  (Eq. (1.41)) simplifies when setting  $q = 0$ , evaluation of the partition function proves more challenging in the case of general  $\alpha$  and  $\beta$ . Nonetheless, we found from a formal expansion of its generating function in Section 1.6.2 the result [7, 78, 79]

$$Z_N = \sum_{p=1}^N \frac{p(2N - p - 1)!}{N!(N - p)!} \sum_{q=0}^p \left(\frac{1}{\alpha}\right)^q \left(\frac{1}{\beta}\right)^{p-q} .$$

This time, setting  $\alpha = \beta = 1$  reduces the partition function to

$$Z_N = \sum_{p=1}^N \frac{p(p + 1)(2N - p - 1)!}{N!(N - p)!} \quad (1.120)$$

$$= \frac{2}{N} \sum_{p=1}^N \binom{p + 1}{2} \binom{2N - p - 1}{N - 1} \quad (1.121)$$

$$= \frac{2}{N} \binom{2N + 1}{N + 2} \quad (1.122)$$

$$= \frac{(2N + 2)!}{(N + 2)!(N + 1)!} \quad (1.123)$$

$$= C_{N+1} \quad (1.124)$$

where we have evaluated the sum using the Chu-Vandermonde identity [80]

$$\sum_{p=-\infty}^{\infty} \binom{p + a}{c} \binom{b - p}{d} = \binom{a + b + 1}{c + d + 1} . \quad (1.125)$$

$C_{N+1}$  is the  $(N + 1)^{\text{th}}$  Catalan number, the number sequence we saw in Section 1.6.1, relating to an enumeration of Dyck paths. These numbers are very well-known in combinatorics in general, solving at least 60 counting problems [81].

We can also obtain this Catalan number result rather directly from the explicit matrix representation, when we write them in terms of ladder operators. First, let us denote a

ladder operator as  $g$ , and state kets  $|n\rangle$  from Eq. (1.24) with the following properties:  $g|n\rangle = |n-1\rangle$ ,  $g^\dagger|n\rangle = |n+1\rangle$ ,  $|-1\rangle = 0$ , and  $\langle n|k\rangle = \delta_{nk}$ . From this, and on setting  $\alpha = \beta = 1$ , the explicit matrix representations of  $D$  and  $E$  detailed in Section 1.3.2, Eq. (1.21) can be written

$$D = 1 + g, \quad E = 1 + g^\dagger. \quad (1.126)$$

Using this, we can then write the following recursion relation for  $C = D + E$  when acting on a state bra  $\langle n|$

$$\langle n|C^N|m\rangle = \langle n-1|C^{N-1}|m\rangle + 2\langle n|C^{N-1}|m\rangle + \langle n+1|C^{N-1}|m\rangle. \quad (1.127)$$

As  $|0\rangle = (1, 0, 0, \dots)^T$  is the ground state, we have the boundary conditions

$$\langle -1|C^N|m\rangle = \langle n|C^N|-1\rangle = 0. \quad (1.128)$$

It is simple to check that this recursion and boundary conditions are satisfied by [36]

$$\langle n|C^N|m\rangle = \binom{2N}{N+n-m} - \binom{2N}{N+2+n+m}. \quad (1.129)$$

Furthermore, for  $\alpha = \beta = 1$  the vectors  $\langle W|$ ,  $|V\rangle$  (Eq. (1.22)) reduce to  $\langle 0|$ ,  $|0\rangle$  respectively. To convert Eq. (1.129) to an expression for the TASEP partition function, then, we set  $n = m = 0$  to arrive at

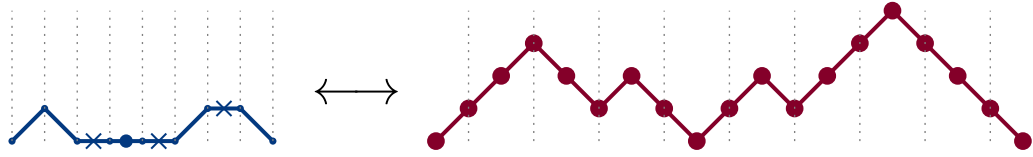
$$Z_N = \langle 0|C^N|0\rangle = \binom{2N}{N} - \binom{2N}{N+2} = C_{N+1}. \quad (1.130)$$

To summarise, for two different variants of the ASEP the results (1.119), (1.124) give two number sequences  $(N+1)! = 1, 2, 6, 24, 120, 720, \dots$  and  $C_{N+1} = 1, 2, 5, 14, 42, 132, \dots$  that are ubiquitous in enumerative combinatorics.

### 1.7.2 TASEP partition function in terms of bicoloured Motzkin and Dyck paths

The second observation is a connection between the TASEP and enumeration problems concerning Dyck paths and what are known as *bicoloured Motzkin paths* [79, 82, 83]. Let us write the partition function in Eq. (1.130) with ladder operators reinstated:

$$Z_N = \langle 0|(2 + g + g^\dagger)^N|0\rangle. \quad (1.131)$$



**Figure 1.9** A bicoloured Motzkin path (left), and its equivalent Dyck path (right).

We can interpret this as an enumeration of paths. Specifically, Eq. (1.131) is the number of walks in the nonnegative plane that start and return to the origin coordinate 0, with  $N$  steps from the set  $\{\nearrow, \searrow, \times, \cdot\}$ :  $\nearrow$  and  $\searrow$  arise from the ladder operators  $g^\dagger$ ,  $g$  respectively, and ‘ $\times$ ’, ‘ $\cdot$ ’ are distinct *non-movement* steps from the ‘2’ term. These are bicoloured Motzkin paths.

To recall, Dyck paths comprise only up and down unit steps, starting and ending at the origin without going below zero. Each Dyck path of length  $2(N + 1)$  is equivalent (that is, maps one-to-one) to a bicoloured Motzkin path of length  $N$  and vice versa. To transform a Motzkin path to a Dyck path we associate to:

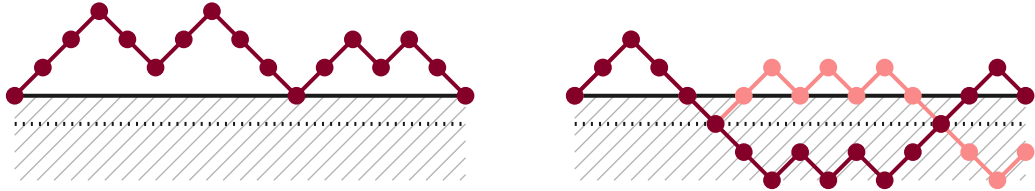
- each  $\times$  an up step followed by a down step ( $\nearrow, \searrow$ );
- each  $\cdot$  a down step followed by an up step ( $\searrow, \nearrow$ );
- each  $\searrow$  two down steps ( $\searrow, \searrow$ );
- each  $\nearrow$  two up steps ( $\nearrow, \nearrow$ );

and finally bookend each walk with an up and down step. See Figure 1.9 for an example.

We have seen that the number of Dyck paths of length  $2N$  is the Catalan number  $C_N$  [81, 84]. To see this directly (that is, without calculating a generating function) note that the total number of paths that start and terminate at zero is  $\binom{2N}{N}$ . The number of *invalid* paths—paths that cross below zero—is counted by reflecting these paths about the axis at the point they first hit  $-1$ . These reflected paths all terminate at  $-2$  (Figure 1.10), and the total number of such paths is  $\binom{2N}{N-1}$ . The number of *valid* paths is then  $\binom{2N}{N} - \binom{2N}{N-1} = \frac{1}{N+1} \binom{2N}{N} = C_N$ .

For the case  $\alpha = \beta = 1$ , each of these paths are equally weighted. Therefore the partition function  $Z_N$  is just an enumeration of all valid paths and is equal to  $C_{N+1}$ , consistent with Eq. (1.124).





**Figure 1.10** *Left: a Dyck path, consisting of equal numbers of up steps and down steps such that the path never goes below 0. Right: a walk that starts and ends at 0, but goes below, and its reflection about the point it first touches  $-1$ , which then terminates at  $-2$ .*

### 1.7.3 Ballot numbers and the one-transit walk

The third observation, staying with the TASEP, is that the partition function in Eq. (1.28) contains the combinatorial factor

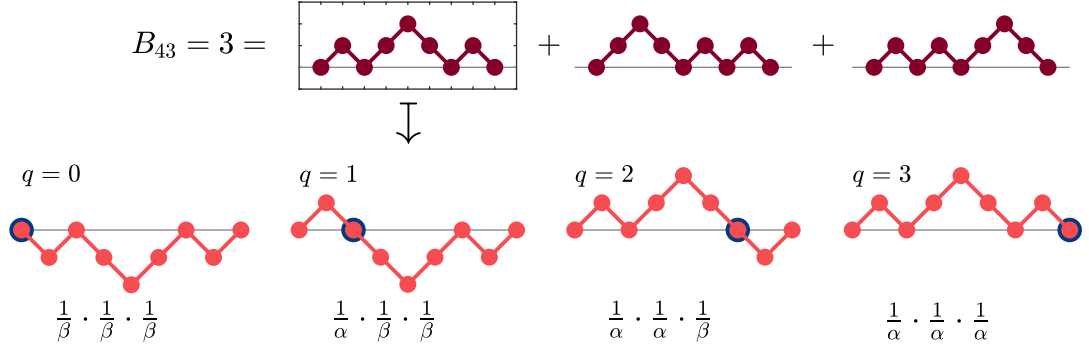
$$B_{N,p} = \frac{p(2N - p - 1)!}{N!(N - p)!}. \quad (1.132)$$

This is sometimes referred to as a *ballot number* [82, 85, 86], and is the solution to the following enumerative problem: the number of Dyck paths that can be drawn of length  $2N$  that return to the origin exactly  $p$  times (including the final return). An example of this is shown in Figure 1.11.

Now, for each of these walks with  $p$  returns, we create a set of  $(p + 1)$  walks whereby the walk is *inverted* about zero at the  $q^{\text{th}}$  return, taking  $q = (0, 1, \dots, p)$ , again see Figure 1.11. Now, finally we associate to each of these new inverted walks a factor of  $(1/\alpha)^q(1/\beta)^{p-q}$ . By this construction, these walks can return to the origin multiple times, and cross it *at most* once. Such walks have been considered in the context of the TASEP in Ref. [82] and is called a *one-transit walk*. A weight  $1/\alpha$  is applied to each return from above, and  $1/\beta$  to each return from below. Summing the weights over all such walks then gives the TASEP partition function in Eq. (1.28) [79, 82].

In this picture, we see very clearly the connection to an equilibrium partition function over an extended configuration space. Recall that in the TASEP, there are  $2^N$  configurations of particles and holes. The corresponding set of one-transit walks contains  $C_{N+1}$  configurations, which exceeds  $2^N$ : this is clearly seen in Eq. (1.118). Each walk has a weight that can be interpreted as a Boltzmann factor; rewriting  $\tilde{\alpha} = \ln \alpha$ ,  $\tilde{\beta} = \ln \beta$ , the weight for a walk with given  $p$  and  $q$  can be written as  $e^{-q\tilde{\alpha} - (p-q)\tilde{\beta}}$ . Summing over multiple such Boltzmann-like weights gives the TASEP partition function, Eq. (1.28).

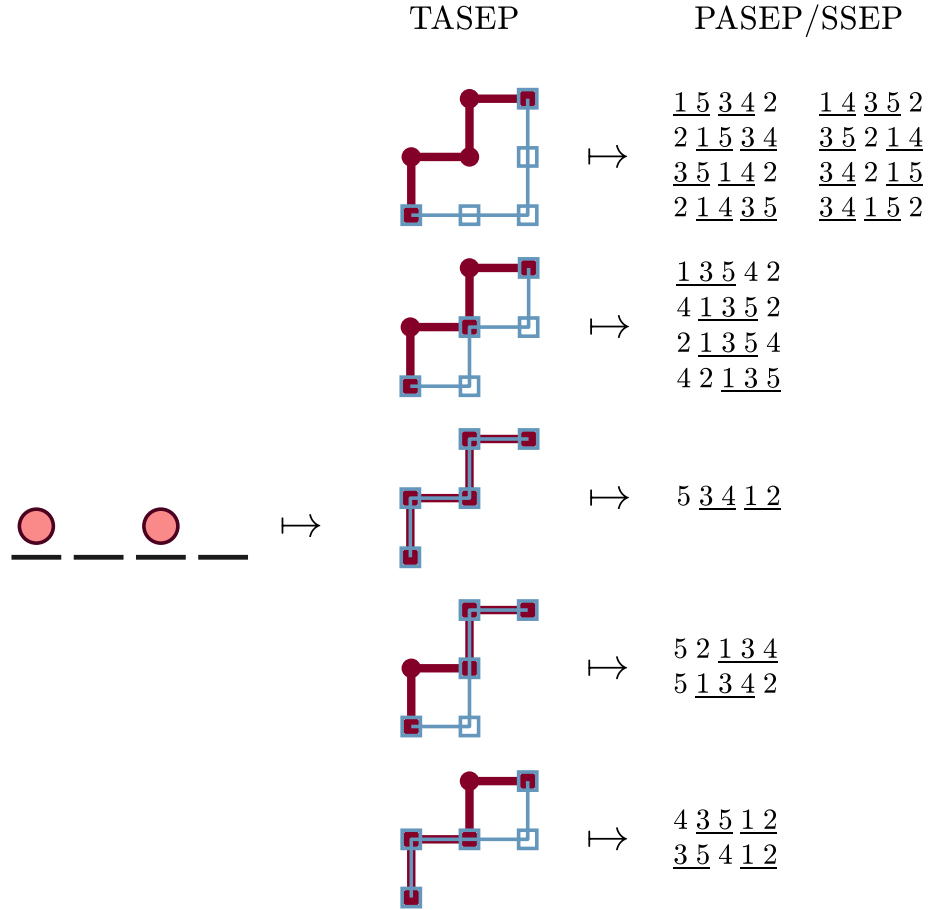
As we further discuss in Section 2.2, the mapping from TASEP configurations to one-



**Figure 1.11** *Dyck paths and one-transit walks. The first row illustrates the three Dyck paths with  $2N = 8$  steps and  $p = 3$  returns. The second row illustrates the four one-transit walks corresponding to the first Dyck path: the Dyck path inverted at each return to make a set of  $p + 1 = 4$  one-transit walks, each with associated weights.*

transit walks and other combinatorial objects is one-to-many. That is, while each walk can be uniquely identified with a TASEP configuration, the converse is not true. Another way to look at this is as the TASEP defining a partitioning of an extended configuration space. The partition function is invariant under this partitioning. Other measures such as entropies, however, are sensitive to it. We investigate this in more detail later in Chapter 3, Section 3.7.1 where we compare the Rényi entropy of the one-transit walk to the TASEP.

The three observations in this section point to a deeper underlying combinatorial structure of the matrix product solution to the ASEP stationary state. Now, we will formalise and develop equivalent combinatorial interpretations of the matrix product weights. See Figure 1.12 for a schematic illustration of the mappings between these interpretations.



**Figure 1.12** Schematic of the combinatorial mappings to be outlined in Chapter 2. An example ASEP configuration (left column) has a one-to-many mapping to certain “dominated paths” (middle column), which themselves appear to have a one-to-many mapping to permutations of numbers that follow certain rules (right column).

## Chapter 2

# Combinatorial mappings of exclusion processes

### 2.1 Orientation

In Chapter 1 we saw how the ASEP admitted exact solution in the steady state by a *matrix product* approach. Upon fixing the parameters  $\alpha = \beta = 1$ , with increasing system size we see the emergence of various number sequences in expressions of the partition function. Some of these we have already seen, and include:

- factorials  $n!$  (which count permutations);
- *Eulerian* numbers  $\langle n_k \rangle$  (which count subsets of permutations [87]);
- Catalan numbers  $C_n$  (which count a variety of objects, including the number Dyck paths);
- ballot numbers  $B_{n,k}$  (which count subsets of Dyck paths);
- *Narayana* numbers  $T(n, k)$  (which count different subsets of Dyck paths to ballot numbers [88]).

These number sequences are ubiquitous within enumerative combinatorics. *Why should so many combinatorial sequences arise in a nonequilibrium physics problem?*

The main contribution of this chapter is a collection and unification of mathematical results that are scattered across the literature, in order to answer this question.

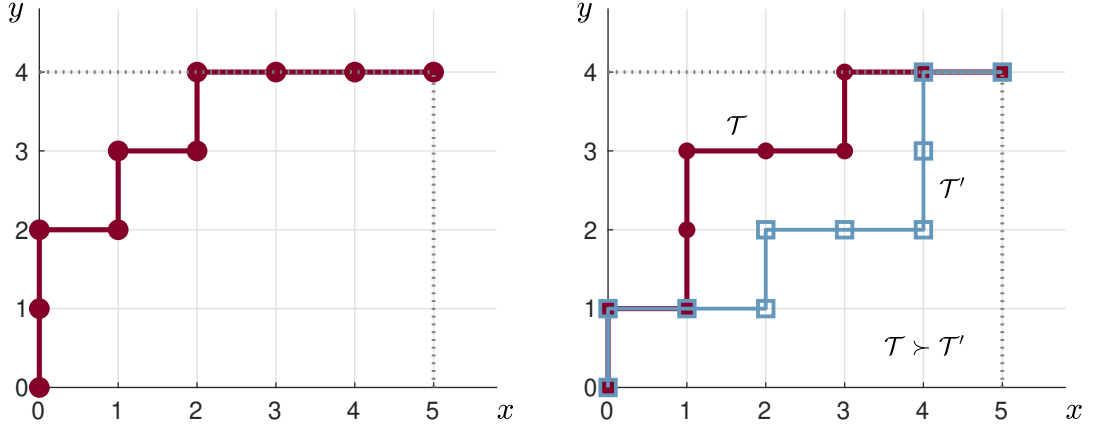
We have already seen in Section 1.7 some features of the ASEP that allude to a combinatorial structure. Here, by an analysis of explicit representations of the matrix product formalism, we will see the existence of one-to-many mappings from arrangements of particles in the ASEP to elements of some larger set of objects (often, but not exclusively, paths on a lattice). The combinatorial factors outlined above then correspond to various ways of counting these objects. Moreover, known results for these counting problems can be used to obtain physical results for the ASEP, sometimes more quickly than within the matrix product formalism. Using these problems we present some novel derivations for quantities in the ASEP, a highlight being the TASEP partition function in the form of a determinant of an  $(N \times N)$  matrix.

An interesting property of the mapping is that the weights associated with the objects in the larger space tend to be rather simple combinations of model parameters and can be interpreted as Boltzmann weights. The weight of an ASEP configuration is obtained by summing over the weights of a subset of objects in the larger space, which yields an interpretation of nonequilibrium weights as sums of equilibrium weights.

As implied in Section 1.7.1, we see the combinatorial structure is at its clearest in the  $\alpha = \beta = 1$  TASEP where Catalan numbers arise. The case  $\alpha = \beta = 1, q = 0$  is the focus of Section 2.2, where we show a mapping between nonequilibrium configurations and path enumeration problems, in particular a *dominated path* interpretation, which is new. In Section 2.3 we discuss a combinatorial problem of *permutations* that the SSEP ( $q = 1$ ) maps to. In Section 2.4 we show how these mappings generalise to the full  $\alpha, \beta, q$  parameter space. One can associate a  $q$ -dependent weight to the permutations of Section 2.3, thus generalising to the PASEP. It then remains to encode the other two parameters  $\alpha, \beta$  into these mappings, which we discuss in Section 2.4.4.

## 2.2 $\alpha = \beta = 1$ TASEP

Of all the different variants of the exclusion process introduced in Chapter 1, the  $\alpha = \beta = 1$  TASEP proves to be the most analytically tractable system as the weights of configurations are integers. We outline a one-to-one mapping between configurations of the TASEP and a class of length- $N$  paths, and introduce a measure of *dominance* [89–91] to find the weight of the configuration. This mapping proves equivalent to several others, including to Motzkin paths which arises naturally from the explicit matrix representation (1.43)–(1.46) in the discussion of Section 1.7.2. We frame the state space in terms of the path dominance mapping, as the translation from TASEP



**Figure 2.1** *Left: the path  $\mathcal{T}$  with the three equivalent specifications (2.2), (2.3) and (2.4). Right: two paths  $\mathcal{T}, \mathcal{T}'$ . Here,  $\mathcal{T}$  dominates  $\mathcal{T}'$ .*

configuration to path is simple in this case and offers an intuitive link between the weight of a configuration and the area its path encloses.

### 2.2.1 Mapping to a dominated path problem

Consider the set of discrete paths  $\mathcal{T} \in \{\uparrow, \rightarrow\}^N$  that begin at  $(0, 0)$ , and end at  $(Q, P)$ , with  $P + Q = N$  steps in total. The total number of paths is

$$\sum_{P=0}^N \binom{N}{P} = 2^N. \quad (2.1)$$

A path  $\mathcal{T}$  can be defined by its set of steps. For example, the path shown in Figure 2.1, left, can be specified as

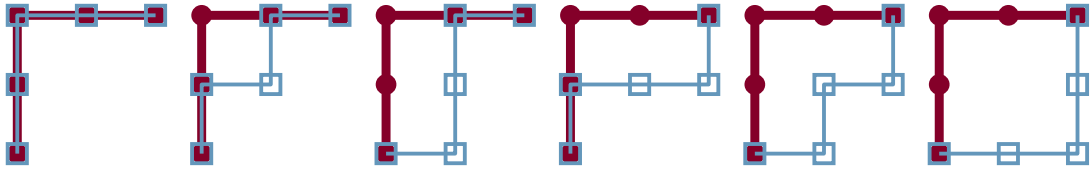
$$\mathcal{T} = (\uparrow, \uparrow, \rightarrow, \uparrow, \rightarrow, \uparrow, \rightarrow, \rightarrow, \rightarrow). \quad (2.2)$$

Alternatively we can specify, for each value of the  $x$ -coordinate  $(0, 1, \dots, Q)$  the maximal  $y$ -coordinate of the path. For the path  $\mathcal{T}$  above, we would have

$$y^{(\mathcal{T})} = (2, 3, 4, 4, 4, 4). \quad (2.3)$$

Equally, we could specify the maximal  $x$ -coordinate for each value of the  $y$ -coordinate  $(0, 1, \dots, P)$ :

$$x^{(\mathcal{T})} = (0, 0, 1, 2, 5). \quad (2.4)$$



**Figure 2.2** The weight of the path  $(\uparrow, \uparrow, \rightarrow, \rightarrow)$  is 6, as 6 distinct paths can be drawn within its perimeter.

With this formalism established, we can now define what is meant by dominance [89–91]. Take two paths  $\mathcal{T}, \mathcal{T}'$  which both terminate at  $(Q, P)$ .  $\mathcal{T}$  *dominates*  $\mathcal{T}'$  (denoted  $\mathcal{T} \succ \mathcal{T}'$ ) if  $\mathcal{T}'$  lies completely on or below  $\mathcal{T}$  (see Figure 2.1, right). In terms of the maximal  $x$  and  $y$ -coordinates,  $\mathcal{T} \succ \mathcal{T}'$  if  $x_i^{(\mathcal{T})} \leq x_i^{(\mathcal{T})}$  for all  $i$ , or, equivalently,  $y_i^{(\mathcal{T})} \geq y_i^{(\mathcal{T})}$  for all  $i$ . By this definition,  $\mathcal{T}$  dominates itself, and it is also possible that for two paths, neither dominates the other; if the paths cross then neither path lies completely under the perimeter of the other. We emphasize that this formalism only applies to paths of the same length that have the same start and end points.

This leads to the following combinatorial problem: *how many paths  $\mathcal{W}(\mathcal{T})$  in total does  $\mathcal{T}$  dominate?*

This quantity can be written out iteratively, accumulating all possible dominated paths as  $\mathcal{T}$  grows step by step. Formally, this is

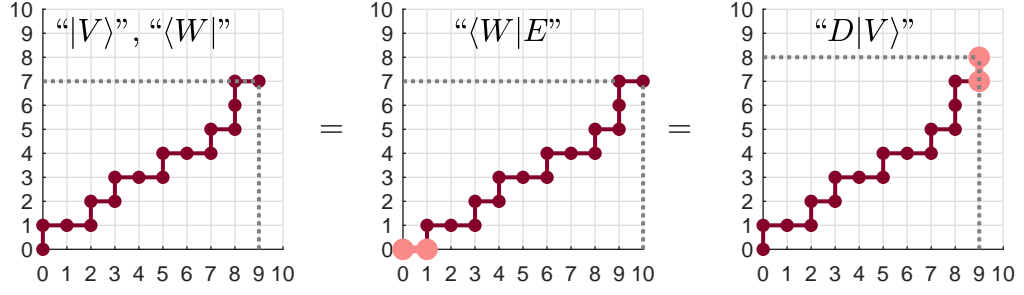
$$\mathcal{W}(\mathcal{T}) = \sum_{n_0=0}^{y_0} \sum_{n_1=n_0}^{y_1} \sum_{n_2=n_1}^{y_2} \cdots \sum_{n_{Q-2}=n_{Q-3}}^{y_{Q-2}} \sum_{n_{Q-1}=n_{Q-2}}^{y_{Q-1}} 1 \quad (2.5)$$

which is a set of  $Q$  nested sums. Take, for example,  $\mathcal{T} = (\uparrow, \uparrow, \rightarrow, \rightarrow)$ ,  $y^{\mathcal{T}} = (2, 2, 2)$ . This has a weight of 6, found by manually drawing all dominated paths (Figure 2.2), or from the summation

$$\mathcal{W}(\mathcal{T}) = \sum_{n_0=0}^2 \sum_{n_1=n_0}^2 1 = \sum_{n_1=0}^2 1 + \sum_{n_1=1}^2 1 + \sum_{n_1=2}^2 1 = 3 + 2 + 1 = 6. \quad (2.6)$$

This problem is of interest to us as each path of length  $N$  maps uniquely to a length- $N$  ASEP configuration. Specifically, an ASEP configuration with occupied sites  $(j_1, j_2, \dots, j_P)$  maps to a path  $\mathcal{T}$  where steps  $(j_1, j_2, \dots, j_P)$  are  $\uparrow$ , and the remaining steps are  $\rightarrow$ . In other words, for a given dominant path  $\mathcal{T}$ , we can read off the TASEP configuration by going along the path and translating each upward step to a particle, and each rightward step to a hole.

The weight of a TASEP configuration then turns out to be given by  $\mathcal{W}(\mathcal{T})$ , the number



**Figure 2.3** Graphical representation of Eqs. (2.11), (2.12). Adding a  $\rightarrow$  to the start or a  $\uparrow$  to the end of a path does not change its weight (i.e., the number of paths it can dominate).

of paths that  $\mathcal{T}$  dominates. For brevity, we will also refer to  $\mathcal{W}(\mathcal{T})$  as the weight of the path. For example, the path in Figure 2.2 maps to  $\mathcal{C} = (1, 1, 0, 0)$ , which indeed has a weight of 6:

$$\langle W | DDEE | V \rangle = \langle W | D(D + E)E | V \rangle \quad (2.7)$$

$$= \langle W | DDE + DEE | V \rangle \quad (2.8)$$

$$= \langle W | (D[D + E] + [D + E]E) | V \rangle \quad (2.9)$$

$$= \langle W | (DD + D + E + D + E + EE) | V \rangle = 6 . \quad (2.10)$$

We can formalise this by showing that the weight of a path in Eq. (2.5) satisfies a set of reduction relations equivalent to Eqs. (1.10)–(1.13). More formally, we require

$$\mathcal{W}(\rightarrow, \mathcal{T}) = \mathcal{W}(\mathcal{T}) , \quad (2.11)$$

$$\mathcal{W}(\mathcal{T}, \uparrow) = \mathcal{W}(\mathcal{T}) , \quad (2.12)$$

$$\mathcal{W}(\mathcal{T}_{(1)}, \uparrow, \rightarrow, \mathcal{T}_{(2)}) = \mathcal{W}(\mathcal{T}_{(1)}, \uparrow, \mathcal{T}_{(2)}) + \mathcal{W}(\mathcal{T}_{(1)}, \rightarrow, \mathcal{T}_{(2)}) , \quad (2.13)$$

where the notation  $\mathcal{W}(\mathcal{T}_{(1)}, \mathcal{T}_{(2)}, \dots)$  denotes concatenation of the path segments  $\mathcal{T}_{(1)}, \mathcal{T}_{(2)}, \dots$ . Eqs. (2.11) and (2.12) are equivalent to  $\langle W | E = \langle W |$  and  $D | V = | V \rangle$  respectively, and are trivial by inspection (Figure 2.3). Relation (2.13) is the equivalent of  $DE = D + E$  (see Figure 2.4) and requires more work, but can be derived directly from the summation formula (2.5), however this is rather complicated and as such we defer this to Appendix A.

We now highlight three results that first originated in the path dominance literature and that we can exploit to give insights into the TASEP without any additional work.



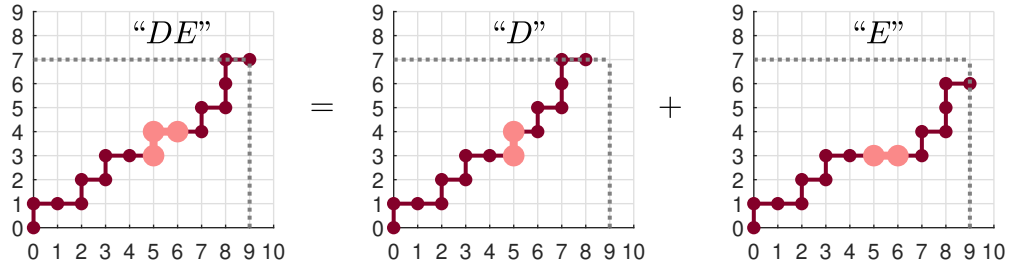


Figure 2.4 Graphical representation of Eq. (2.13).

### Most probable configuration

The first result is a simple observation, and is that for a length- $N$  path with  $P \uparrow$  steps, the most dominant path is  $\mathcal{T}^* = (\uparrow, \dots \uparrow, \rightarrow, \dots \rightarrow)$ , with weight

$$\mathcal{W}(\mathcal{T}^*) = \binom{N}{P} \quad (2.14)$$

as this rectangular path encloses all others. The equivalent TASEP configuration  $\mathcal{C} = (1, \dots, 1, 0, \dots, 0)$  is  $P$  particles stacked to the left, and is the most probable configuration with  $P$  particles. Furthermore, the most probable configuration overall will be  $N/2$  particles followed by  $N/2$  holes (if  $N$  is odd, the  $\lceil N/2 \rceil$  and  $\lfloor N/2 \rfloor$ -particle configurations are equally most probable). In the matrix formalism, this weight corresponds to the decomposition of the string  $\langle W | D^P E^{N-P} | V \rangle$  using the reduction relations (1.10)–(1.13).

At the other extreme, any configuration with  $P$  particles stacked to the right has the minimum weight of 1. This is because the only path that  $\mathcal{T}^* = (\rightarrow, \dots \rightarrow, \uparrow, \dots \uparrow)$  dominates is itself, though in the matrix product formulation this is already trivial given  $\langle W | E \dots E D \dots D | V \rangle = 1$ .

### Weight with fixed particle number and Narayana numbers

Given this mapping, the total weight of configurations  $\mathcal{C}_P$  with  $P$  particles is the *total* weight of *all* paths that terminate at  $(N - P, P)$ . In the path dominance literature this is known [91]:

$$\sum_{\mathcal{C}_P} \mathcal{W}(\mathcal{C}_P) = \frac{N!(N+1)!}{(N-P)!(N-P+1)!P!(P+1)!} \quad (2.15)$$

$$= \binom{N}{P}^2 - \binom{N}{P+1} \binom{N}{P-1} = T(N+1, P+1) \quad (2.16)$$

where  $T(n, k)$  is a *Narayana number* [88] (Table 2.1, sequence A001263 in the OEIS [92]). Consequently  $\sum_{k=1}^n T(n, k) = C_n$ , and we find from Eq. (2.15) that

$$Z_N = \sum_{P=0}^N \left( \sum_{\mathcal{C}_P} \mathcal{W}(\mathcal{C}_P) \right) = \sum_{P=0}^N T(N+1, P+1) = C_{N+1} \quad (2.17)$$

as previously.

We also provide the derivation of this result within the matrix product formalism: first, define  $G(N, P)$  as the sum of all unique orderings of  $P$   $D$ -matrices and  $(N - P)$   $E$ -matrices. Using the ladder operator matrix representation in Eq. (1.126), the following recursion relation holds [93]:

$$\begin{aligned} \langle n | G(N, P) | m \rangle &= \langle n | G(N-1, P-1) | m \rangle + \langle n | G(N-1, P-1) | m \rangle \\ &\quad + \langle n+1 | G(N-1, P-1) | m \rangle + \langle n-1 | G(N-1, P) | m \rangle \end{aligned} \quad (2.18)$$

with boundary conditions

$$\langle -1 | G(N, P) | m \rangle = \langle n | G(N, P) | -1 \rangle = 0. \quad (2.19)$$

The recursion and boundary conditions are solved by

$$\langle n | G(N, P) | m \rangle = \binom{N}{P} \binom{N}{P+n-m} - \binom{N}{P+1+n} \binom{N}{P-1-m}. \quad (2.20)$$

As we did in Section 1.7.1, we set  $n = m = 0$  to find the appropriate expression for the sum of TASEP weights for  $P$  particles, recovering Eq. (2.15):

$$\sum_{\mathcal{C}_P} \mathcal{W}(\mathcal{C}_P) = \langle 0 | G(N, P) | 0 \rangle = \binom{N}{P}^2 - \binom{N}{P+1} \binom{N}{P-1} \quad (2.21)$$

$$= \frac{N!(N+1)!}{P!(P+1)!(N-P)!(N-P+1)!}. \quad (2.22)$$

Summing over all configurations then recovers Eq. (1.130):

$$Z_N = \sum_{P=0}^N \left[ \binom{N}{P}^2 - \binom{N}{P+1} \binom{N}{P-1} \right] \quad (2.23)$$

$$= \binom{2N}{N} - \binom{2N}{N+2} = C_{N+1} \quad (2.24)$$

$n \backslash k$	1	2	3	4	5	6	7	$\Sigma$
1	1							1
2	1	1						2
3	1	3	1					5
4	1	6	6	1				14
5	1	10	20	10	1			42
6	1	15	50	50	15	1		132
7	1	21	105	175	105	21	1	429

**Table 2.1** *The first few Narayana numbers  $T(n, k)$  from Eq. (2.15). Row sums give the Catalan numbers.*

where we have used the Vandermonde identity [94]

$$\sum_{p=-\infty}^{\infty} \binom{a}{c+p} \binom{b}{d-p} = \binom{a+b}{c+d}. \quad (2.25)$$

### Determinant form of configuration weight

The final, and perhaps most significant result is that Narayana [88] (and later Kreweras [90]) has shown in this path dominance problem that the weight of a path can be written as a determinant:

$$\mathcal{W}(\mathcal{T}) = \det M, \quad M_{nm} = \binom{y_{m-1} + 1}{1 + n - m}, \quad n, m = 1, 2, \dots, Q, \quad (2.26)$$

or equivalently (‘turning the path on its side’)

$$\mathcal{W}(\mathcal{T}) = \det M', \quad M'_{nm} = \binom{Q - x_{P-m} + 1}{1 + n - m}, \quad n, m = 1, 2, \dots, P. \quad (2.27)$$

With the mapping from paths, this in turn provides an analytic formula for the weight of any TASEP configuration. Remarkably, however, ten years prior to the matrix product formalism being derived, Shapiro and Zeilberger had derived this same determinant formula for the configuration weight of the  $\alpha = \beta = 1$  TASEP in Ref. [95].

Let us recall the example path from Eq. (2.2), Figure 2.1. Using the first determinant

formula, this has weight from its  $y$ -coordinates in Eq. (2.3)

$$\mathcal{W}(\mathcal{T}) = \det \begin{pmatrix} 3 & 1 & \cdot & \cdot & \cdot \\ 3 & 4 & 1 & \cdot & \cdot \\ 1 & 6 & 5 & 1 & \cdot \\ \cdot & 4 & 10 & 5 & 1 \\ \cdot & 1 & 10 & 10 & 5 \end{pmatrix} = 117 \quad (2.28)$$

and equivalently using its  $x$ -coordinates in Eq. (2.4)

$$\mathcal{W}(\mathcal{T}) = \det \begin{pmatrix} 4 & 1 & \cdot & \cdot \\ 6 & 5 & 1 & \cdot \\ 4 & 10 & 6 & 1 \\ 1 & 10 & 15 & 6 \end{pmatrix} = 117. \quad (2.29)$$

This path  $\mathcal{T}$  maps to the TASEP configuration

$$\mathcal{C} = (1, 1, 0, 1, 0, 1, 0, 0, 0) \quad (2.30)$$

which then implies that the determinants in Eqs. (2.28) and (2.29) are equivalent to the matrix product

$$\mathcal{W}(\mathcal{C}) = \langle W | D D E D E D E E E | V \rangle. \quad (2.31)$$

This reveals a deeper link between the matrix product approach and the reduction relations (1.10)–(1.13) with an elegant determinant structure.

Probing these determinants further, notice from this example that reading down each column reveals the  $(y_{m-1} + 1)^{\text{th}}$  row in Pascal's triangle. It is also 'nearly' a lower-diagonal matrix, and a simple example of a *Hessenberg* matrix [96]. Taking Eq. (2.28), this gives a simplified recursive determinant formula (adapted from Theorem 2.1 of Ref. [97]):

$$\det M = \sum_{r=1}^Q (-)^{Q-r} M_{Qr} \det M_{(r-1)} \quad (2.32)$$

$$= \sum_{r=1}^Q (-)^{Q-r} \binom{y_{r-1} + 1}{Q - r + 1} \det M_{(r-1)} \quad (2.33)$$

where  $M_{(r-1)}$  is the  $(r-1)^{\text{th}}$  minor of  $M$ .

In the context of the TASEP, this determinant formula has since been improved upon

to encode  $\alpha$  and  $\beta$ , see Section 2.4.2 and Ref. [98].

## 2.2.2 Other representations

We refer to an ordered pair of two paths where one dominates the other as a *dominated path*. As previously noted in Section 2.2.1, the total number of dominated paths is given by the Catalan number  $C_{N+1}$ . This set of dominated paths is the extended configuration space. This space can be equivalently expressed in terms of bicoloured Motzkin paths or “complete configurations”, as we now discuss.

### Bicoloured Motzkin paths

From the matrix representation in Eqs. (1.21), (1.22), we have already seen that bicoloured Motzkin paths naturally arise [83, 99]. Here we establish the link between these walks and the dominated path formalism.

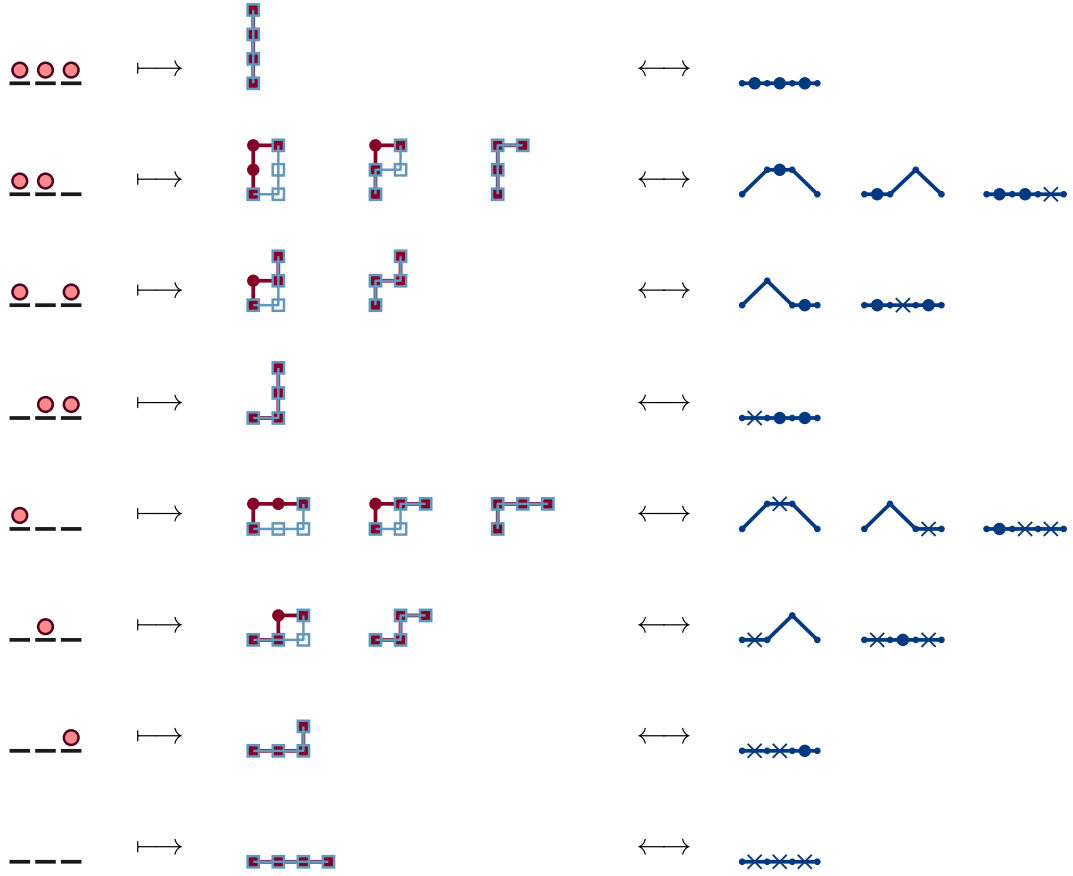
The full partition function  $Z_N$  is the number of unique dominated paths. Consider one such configuration with two paths  $\mathcal{T} \succ \mathcal{T}'$ . Denote the  $i^{\text{th}}$  steps of  $\mathcal{T}, \mathcal{T}'$  as  $\mathcal{T}(i), \mathcal{T}'(i)$  respectively.

Comparing the two paths, on each step we have four possible outcomes, which we track with a height difference  $h \geq 0$ , that must start and end at zero:

- $\mathcal{T}(i) = \uparrow$  and  $\mathcal{T}'(i) = \rightarrow$ . The paths diverge,  $\Delta h = +1$ ;
- $\mathcal{T}(i) = \rightarrow$  and  $\mathcal{T}'(i) = \uparrow$ . The paths converge,  $\Delta h = -1$ ;
- $\mathcal{T}(i) = \mathcal{T}'(i) = \uparrow$ . The paths run parallel vertically,  $\Delta h = 0$ ;
- $\mathcal{T}(i) = \mathcal{T}'(i) = \rightarrow$ . The paths run parallel horizontally,  $\Delta h = 0$ .

Over each step,  $h$  can therefore change by  $\pm 1$ , or zero in two distinct ways (denoted with ‘ $\cdot$ ’ and ‘ $\times$ ’). The partition function is then equivalently the number of paths moving left to right of length  $N$ , from the step set  $\{\nearrow, \searrow, \cdot, \times\}$ , that start and end at zero, without going below zero (as  $\mathcal{T} \succ \mathcal{T}'$ ). This is then an enumeration of bicoloured Motzkin paths.

Extending this, the weight of a length- $N$  configuration  $\mathcal{C}$  with sites  $(j_1, j_2, \dots, j_P)$  occupied is the number of length- $N$  bicoloured Motzkin paths that can be drawn from  $\{\nearrow, \cdot\}$  at steps  $(j_1, j_2, \dots, j_P)$ , and  $\{\searrow, \times\}$  in the remaining steps. This maps each



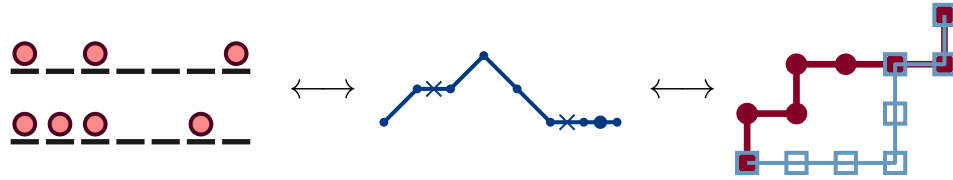
**Figure 2.5** Calculation of the TASEP partition function for  $N = 3$ . For each configuration (left column), we draw all combinations of length- $N$  paths that dominate another (centre column), and their equivalent bicoloured Motzkin path (right column).

Motzkin path one-to-one to a dominated path. See Figure 2.5 for an example, where we write all  $N = 3$  configurations in terms of Motzkin paths.

This Motzkin path interpretation aligns neatly with the ladder operator representation we quote in Eq. (1.126). For other explicit representations, other path interpretations naturally arise. Brak et al. present a comprehensive set of these alternative walks in [99], as well as encoding weights to generalise for  $\alpha, \beta, q$ .

### Markov chain of “complete configurations”

Duchi and Schaeffer [100] express this same space of  $C_{N+1}$  configurations as a set of closed, *two-row* systems, which they term *complete configurations*. Furthermore, they define a Markov process in this space that reproduces ASEP dynamics on the top row of the system.



**Figure 2.6** *Example of a complete configuration in  $[100]$  (left) and its equivalent Motzkin path (centre) and dominated path (right). The top row of the complete configuration shows that these correspond to  $\mathcal{C} = (1, 0, 1, 0, 0, 0, 1)$ .*

Each of these complete configurations comprise  $N$  particles and  $N$  holes (which they refer to as “black” and “white” particles), arranged across two rows of length  $N$ . The particles may be arranged in any way across both rows, given the constraint that there are always at least as many particles as holes in the first  $i$  columns,  $i = 1, 2, \dots, N$  (the “positivity condition”). The top-row configuration is the ASEP state that the complete configuration maps to.

The Markov process that the authors construct is a clockwise flow of these  $N$  particles around both rows, with ASEP-like hopping on the top row, and a set of bottom-row dynamics (involving long-range “sweeps” of clusters of particles or holes) so as to preserve the positivity condition. The top row of these closed configurations replicate open TASEP dynamics. In particular, we note that a feature of a complete configuration is that if the top-left site is empty, the bottom-left row is occupied — otherwise the positivity condition would be violated. This means that a particle can always enter the top row at a rate  $\alpha$ , just as in the TASEP. Similarly, if the top-right site is occupied, the bottom-right site must be empty, allowing particles to exit the top row at rate  $\beta$ , again as in the TASEP.

Here we expand on how each complete configuration in this two-row system maps to a Motzkin path or dominated path. With reference to Figure 2.6, if we assign to each column with  $(\tau_{\text{top}}, \tau_{\text{bottom}})$  entries a  $\nearrow$  for  $(1; 1)$ , a  $\searrow$  for  $(0; 0)$ , a ‘·’ for  $(1; 0)$  and ‘×’ for  $(0; 1)$ , then configurations are once again a set of bicoloured Motzkin paths once the positivity condition is imposed. Corteel and Williams have since introduced a Markov chain that reproduces PASEP dynamics (where the additional parameter  $q$  is introduced), using a larger set of  $(N + 1)!$  configurations [101].

### 2.3 $\alpha = \beta = 1$ SSEP

Our discussion so far has been limited to the TASEP ( $q = 0$ ). We now move from the totally asymmetric case to the totally *symmetric* case where particles can hop either

direction in the bulk at equal rates, by setting  $q = 1$ .

We previously showed that when  $\alpha = \beta = 1$ , the SSEP partition function is  $Z_N = (N+1)!$ , see Eq. (1.119). This combined with the analysis of the TASEP in Section 2.2 suggests that the  $2^N$  configurations of the SSEP may map to an even larger set of  $(N+1)! \geq C_{N+1} \geq 2^N$  configurations. This indeed turns out to be the case; consider the integers  $(1, 2, \dots, N, N+1)$ , of which there are  $(N+1)!$  permutations. The  $2^N$  configurations of the SSEP define a partitioning of these  $(N+1)!$  permutations.

### 2.3.1 Mapping to a permutation problem

The following mapping was first identified and formally proven by Corteel and Williams [101] in the context of a Markov chain of permutations. Here we focus only on the mapping from the SSEP to permutations using a slightly different but equivalent formalism to [101]. We present a more detailed analysis (in the context of the PASEP) in Section 2.4.1.

Consider a permutation of the numbers  $(1, 2, \dots, N, N+1)$ , denoted  $(i_1, i_2, \dots, i_N, i_{N+1})$ . Reading this string of numbers left-to-right, we say that  $i_n$  has been *raised* by  $i_{n+1}$  if  $i_{n+1} > i_n$ . This time, we are interested in the following problem: *how many permutations are there where only a particular set of numbers  $(j_1, j_2, \dots, j_P)$  are raised?*

This proves to be equivalent to the weight of a length- $N$  SSEP configuration with particles at sites  $(j_1, j_2, \dots, j_P)$ . We illustrate this with an example. The SSEP configuration  $\mathcal{C} = (0, 1, 0, 0)$ , has  $N = 4$  sites, and  $P = 1$  particle at position  $j_1 = 2$ . This has a weight of 7, calculated directly with the reduction relations (1.39)–(1.42) for  $q = 1$ :

$$\mathcal{W}(\mathcal{C}) = \langle W | E D E E | V \rangle \quad (2.34)$$

$$= \langle W | E (E D + D + E) E | V \rangle \quad (2.35)$$

$$= \langle W | (E E [E D + D + E] + E [E D + D + E] + E E E) | V \rangle \quad (2.36)$$

$$= 7. \quad (2.37)$$

As anticipated, there are also 7 permutations of  $(1, 2, 3, 4, 5)$  where *only*  $j_1 = 2$  is raised (the underline highlights where a number has been raised):

$$54\underline{2}31, \quad 43\underline{2}\underline{5}1, \quad 4\underline{2}\underline{5}31, \quad 3\underline{2}\underline{5}41, \quad 5\underline{2}\underline{4}31, \quad \underline{2}\underline{5}431, \quad 53\underline{2}\underline{4}1.$$



If the SSEP indeed maps to these permutations, we should expect to find an equivalent set of reduction relations like that of the SSEP in Eqs. (1.39)–(1.42). We show this in Section 2.4.1, in fact for the more general  $DE = qED + D + E$ , where weights as powers of  $q$  are associated with each permutation.

Having established this mapping, we can quickly derive the steady-state density profile and arbitrary-order correlations between sites. We also use a result in the literature on the combinatorics of permutations, which allows us to find the probability of finding  $P$  particles in the system.

### Steady-state density profile

The average steady-state occupation of site  $i$  (Eq. (1.34))

$$\langle \tau_i \rangle = \frac{1}{Z_N} \langle W | (D + E)^{i-1} D (D + E)^{N-i} | V \rangle$$

is equivalently the fraction of permutations of  $(1, 2, \dots, N, N+1)$  where  $i$  is raised. Note that we do not care whether any other integers are raised. One slight complication is that  $i$  can only be raised if it is not at the final position within the permutation. From this interpretation we can very quickly calculate the full density profile. If  $i$  is not in the final position,  $i$  can be raised by any of  $(i+1, i+2, \dots, N, N+1)$  from the  $N$  numbers other than  $i$ , giving a fraction  $(N+1-i)/N$ . We then multiply by the fraction of permutations where  $i$  is not in the final position which is  $N/(N+1)$ . We thus obtain

$$\langle \tau_i \rangle = \frac{N+1-i}{N} \frac{N}{N+1} = 1 - \frac{i}{N+1} \quad (2.38)$$

recovering the known linear density profile [102].

### Arbitrary-order correlation functions

We can extend this approach to calculate higher-order correlations between different sites without having to perform any explicit matrix calculation. First, consider the correlation from Eq. (1.35)

$$\langle \tau_{i_1} \tau_{i_2} \rangle = \frac{1}{Z_N} \langle W | (D + E)^{i_1-1} D (D + E)^{i_2-i_1-1} D (D + E)^{N-i_2} | V \rangle$$

where  $i_2 > i_1$ . This is equivalently the fraction of permutations of  $(1, 2, \dots, N+1)$  where both  $i_1$  and  $i_2$  are raised.

First,  $i_2$  can be raised by any of the  $(N + 1 - i_2)$  numbers from  $(i_2 + 1, \dots, N + 1)$ , and the fraction of suitable permutations is then  $(N + 1 - i_2)/(N + 1)$ . In this subset,  $i_1$  can be raised by any of the  $(N + 1 - i_1)$  numbers from  $(i_1 + 1, \dots, N + 1)$ , *excluding* the number that raised  $i_2$ . The fraction of valid permutations here is then  $(N - i_1)/N$ . Combined, we then recover the result from [46, 102]

$$\langle \tau_{i_1} \tau_{i_2} \rangle = \left( \frac{N + 1 - i_2}{N + 1} \right) \left( \frac{N - i_1}{N} \right) = \left( 1 - \frac{i_2}{N + 1} \right) \left( 1 - \frac{i_1}{N} \right). \quad (2.39)$$

By the same interpretation this can be extended to an arbitrary order correlation between  $K$  different sites  $i_K, i_{K-1}, \dots, i_1$ , where  $i_K > i_{K-1} > \dots > i_1$  [48, 103]:

$$\langle \tau_{i_K} \tau_{i_{K-1}} \dots \tau_{i_2} \tau_{i_1} \rangle = \prod_{k=1}^K \left( \frac{N + 1 + k - K - i_k}{N + 1 + k - K} \right) = \prod_{k=1}^K \left( 1 - \frac{i_k}{N + 1 + k - K} \right). \quad (2.40)$$

### Weight with fixed particle number and Eulerian numbers

The sum of all weights of configurations  $\mathcal{C}_P$  with exactly  $P$  particles is the number of permutations of  $(1, 2, \dots, N, N + 1)$  whereby a *total* of  $P$  numbers are raised. We state the result from the combinatorial literature [104, 105]:

$$\sum_{\mathcal{C}_P} \mathcal{W}(\mathcal{C}_P) = \left\langle \begin{matrix} N + 1 \\ P \end{matrix} \right\rangle \quad (2.41)$$

where

$$\left\langle \begin{matrix} n \\ k \end{matrix} \right\rangle = \sum_{j=0}^{k+1} (-1)^j \binom{n+1}{j} (k+1-j)^n \quad (2.42)$$

is known as an *Eulerian number* (Table 2.2, sequence A008292 in the OEIS [106]), and has several neat properties reminiscent of binomial coefficients, such as the recursion [87]

$$\left\langle \begin{matrix} n+1 \\ k \end{matrix} \right\rangle = (n+1-k) \left\langle \begin{matrix} n \\ k-1 \end{matrix} \right\rangle + (k+1) \left\langle \begin{matrix} n \\ k \end{matrix} \right\rangle. \quad (2.43)$$

$n \backslash k$	0	1	2	3	4	5	6	$\Sigma$
1	1							1
2	1	1						2
3	1	4	1					6
4	1	11	11	1				24
5	1	26	66	26	1			120
6	1	57	302	302	57	1		720
7	1	120	1191	2416	1191	120	1	5040

**Table 2.2** Table of the Eulerian numbers  $\langle n \rangle_k$  from Eq. (2.42). Row sums yield the factorials.

The generating function  $G(t, z)$  of Eq. (2.42) is succinct [87]:

$$G(t, z) = \sum_{N \geq 0} \sum_{P \geq 0} \left\langle \begin{matrix} N+1 \\ P \end{matrix} \right\rangle \frac{t^N z^P}{(N+1)!} \quad (2.44)$$

$$= \frac{1 - e^{t(z-1)}}{t(e^{t(z-1)} - z)} \quad (2.45)$$

$$= 1 + \frac{1}{2!}t(z+1) + \frac{1}{3!}t^2(z^2+4z+1) + \frac{1}{4!}t^3(z^3+11z^2+11z+1) + \dots \quad (2.46)$$

where  $\{t^N z^P\}G(t, z)$  is the probability of finding exactly  $P$  particles in a length- $N$  SSEP. Finally, the summation over Eulerian numbers for fixed  $N$  is equivalent to the  $N$ -site partition function, and gives the factorial [107]

$$\sum_{P=0}^N \left\langle \begin{matrix} N+1 \\ P \end{matrix} \right\rangle = (N+1)! . \quad (2.47)$$

This is trivial in the context of Eulerian numbers, as it is simply the summation of all permutations of  $(N+1)$  integers.

## 2.4 Generalised parameter mappings

Up to now, we have focused on the parameter restriction  $\alpha = \beta = 1$ ,  $q = 0, 1$ . To generalise for  $\alpha, \beta, q$ , we do not need to expand beyond the state spaces of dominated paths and permutations already introduced, however we now associate *weights* in terms of  $\alpha, \beta, q$ , raised to integer powers. The highlight of the following is the nice result that a closed-form formula has been derived for the weight of a general TASEP configuration.

### 2.4.1 $\alpha = \beta = 1$ PASEP and weighted permutations

A closed-form expression for the PASEP partition function is known, see Ref. [42]. We omit the details of the expression here, but this function implies an interpolation between the  $q = 1$  and  $q = 0$  mappings identified so far in Sections 2.2 and 2.3. We therefore first expand on the results of Section 2.3.1 by showing how an arbitrary  $q$  is encoded into the mapping of SSEP configurations to permutations, first shown in [108]. We remain with our slightly different formalism introduced earlier.

Take a permutation  $(i_1, i_2, \dots, i_N, i_{N+1})$  where a set of numbers  $(j_1, j_2, \dots, j_P)$  in the permutation are raised. Reading left-to-right, we now associate to each raise a factor  $q^r$ , where  $r$  is the number of integers to the *right* of  $j_1$  that fall between it and the number that raised it. This ties into a  $q$ -generalisation of Eulerian numbers known as Eulerian *polynomials*, introduced in Ref. [109].

As an example, one (of many) permutations that maps to the configuration  $\mathcal{C} = (0, 1, 1, 1, 0, 0, 0)$  is 2 6 3 8 4 7 5 1, which has three numbers (2, 3, 4) that are raised, corresponding to occupied sites 2, 3 and 4. This has weight  $q^7 = q^3 \cdot q^3 \cdot q$ : 2 could have been raised by (3, 4, 5), 3 could have been raised by (4, 5, 7), and 4 could have been raised by 5.

We show that this weighted permutation problem obeys an equivalent set of reduction relations to that of the PASEP, Eqs. (1.39)–(1.42) (for  $\alpha = \beta = 1$ ). Let us first define

$$\mathcal{W}_{N+1}(\underline{j}) \tag{2.48}$$

as shorthand for the total weight of permutations of  $(1, 2, \dots, N, N+1)$  where the numbers  $\underline{j} = (j_1, j_2, \dots, j_P)$  are raised. The reduction relation (1.40),  $\langle W|E = \langle W|$  has an equivalent form

$$\mathcal{W}_{N+2}(\underline{j} + 1) = \mathcal{W}_{N+1}(\underline{j}) \tag{2.49}$$

which is trivial to show: for each permutation on the LHS, increase every number by 1, then append the whole permutation with a 1. This gives each permutation on the RHS, with all weights unchanged. Similarly for Eq. (1.39),  $D|V\rangle = |V\rangle$ ,

$$\mathcal{W}_{N+2}(\underline{j}) = \mathcal{W}_{N+1}(\underline{j}) \tag{2.50}$$

which can be seen as each permutation on the LHS, prepended with an  $(N+2)$ , corresponds to a permutation on the RHS. Again, all weights are unchanged.

Permutation	$\mathcal{W}$	Consecutive?	New permutation	$\mathcal{W}$
<u>1</u> <u>5</u> <u>3</u> <u>4</u> 2	$q^3$	No	<u>2</u> <u>5</u> <u>3</u> <u>4</u> 1	$q^2$
<u>3</u> <u>5</u> <u>1</u> <u>4</u> 2	$q^2$	No	<u>3</u> <u>5</u> <u>2</u> <u>4</u> 1	$q^1$
<u>5</u> <u>1</u> <u>3</u> <u>4</u> 2	$q^1$	No	<u>5</u> <u>2</u> <u>3</u> <u>4</u> 1	$q^0$
<u>1</u> <u>4</u> <u>3</u> <u>5</u> 2	$q^2$	No	<u>2</u> <u>4</u> <u>3</u> <u>5</u> 1	$q^1$
<u>1</u> <u>3</u> <u>5</u> <u>4</u> 2	$q^2$	No	<u>2</u> <u>3</u> <u>5</u> <u>4</u> 1	$q^1$
<u>4</u> <u>1</u> <u>3</u> <u>5</u> 2	$q^1$	No	<u>4</u> <u>2</u> <u>3</u> <u>5</u> 1	$q^0$
<u>3</u> <u>4</u> <u>1</u> <u>5</u> 2	$q^1$	No	<u>3</u> <u>4</u> <u>2</u> <u>5</u> 1	$q^0$
<u>3</u> <u>4</u> <u>2</u> <u>1</u> <u>5</u>	$q^0$	Yes	<u>2</u> <u>3</u> <u>1</u> <u>4</u>	$q^0$
<u>4</u> <u>3</u> <u>5</u> <u>1</u> <u>2</u>	$q^0$	Yes	<u>3</u> <u>2</u> <u>4</u> 1	$q^0$
<u>5</u> <u>2</u> <u>1</u> <u>3</u> <u>4</u>	$q^0$	Yes	<u>4</u> <u>1</u> <u>2</u> <u>3</u>	$q^0$
<u>4</u> <u>2</u> <u>1</u> <u>3</u> <u>5</u>	$q^0$	Yes	<u>3</u> <u>1</u> <u>2</u> <u>4</u>	$q^0$
<u>3</u> <u>5</u> <u>2</u> <u>1</u> <u>4</u>	$q^1$	Yes	<u>2</u> <u>4</u> <u>1</u> <u>3</u>	$q^1$
<u>2</u> <u>1</u> <u>5</u> <u>3</u> <u>4</u>	$q^2$	Yes	<u>1</u> <u>4</u> <u>2</u> <u>3</u>	$q^2$
<u>3</u> <u>5</u> <u>4</u> <u>1</u> <u>2</u>	$q^1$	Yes	<u>2</u> <u>4</u> <u>3</u> 1	$q^1$
<u>5</u> <u>3</u> <u>4</u> <u>1</u> <u>2</u>	$q^0$	Yes	<u>4</u> <u>2</u> <u>3</u> 1	$q^0$
<u>2</u> <u>1</u> <u>4</u> <u>3</u> <u>5</u>	$q^1$	Yes	<u>1</u> <u>3</u> <u>2</u> <u>4</u>	$q^1$

**Table 2.3** *Demonstration of the reduction relation for the configuration  $\mathcal{C} = (1, 0, 1, 0)$ , by the reduction  $DEDE = qEDDE + DDE + EDE$ .  $\mathcal{W}(1010)$  is the number of permutations of  $(1, 2, 3, 4, 5)$  where 1 and 3 are raised.*

Finally, the reduction relation (1.41),  $DE = qED + D + E$  has an equivalent form

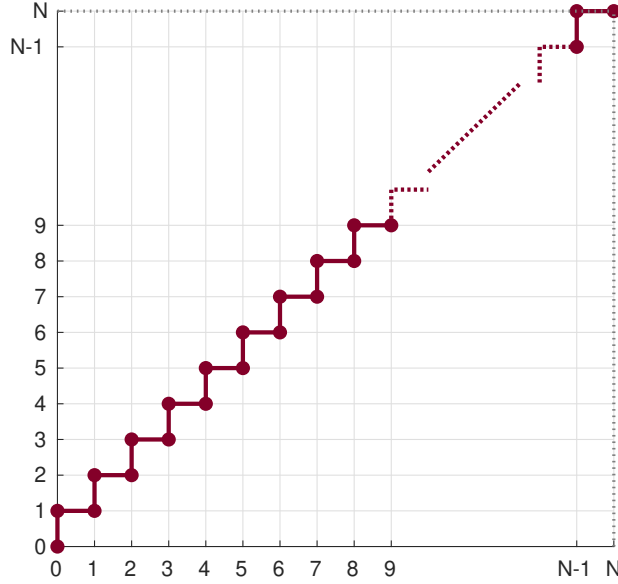
$$\begin{aligned} \mathcal{W}_{N+1}(\underline{j}_1, k, \underline{j}_2) \\ = q\mathcal{W}_{N+1}(\underline{j}_1, k+1, \underline{j}_2) + \mathcal{W}_N(\underline{j}_1, k, \underline{j}_2 - 1) + \mathcal{W}_N(\underline{j}_1, \underline{j}_2 - 1) \end{aligned} \quad (2.51)$$

with all entries of  $\underline{j}_1$  less than  $k$ , and all entries of  $\underline{j}_2$  greater than  $(k+1)$ . Here,  $\mathcal{W}(a, b, c)$  denotes a concatenation of the strings  $a, b, c$ .

We prove this by first identifying all LHS permutations where  $(\underline{j}_1, k, \underline{j}_2)$  are raised (and  $(k+1)$  is not), and  $k, (k+1)$  do *not* appear consecutively. We then switch the positions of  $k, (k+1)$  in each of these. This then yields all permutations where  $(\underline{j}_1, k+1, \underline{j}_2)$  are raised, and  $k$  is not.

From the association of weights that we have already outlined, each of these new permutations has a weight that is a power of  $q$  less than the original permutation. This is the first term of the RHS.

This leaves the permutations on the LHS where  $k$  and  $(k+1)$  *do* appear consecutively. If we take these permutations, remove the  $(k+1)$  entry and reduce all integers greater than  $k$  by one, we are left with a set of permutations of length  $N$  where  $(\underline{j}_1, \underline{j}_2 - 1)$  are raised, and  $k$  may or may not be raised. This is the sum of the final two terms of the RHS. See Table 2.3 for a full example of this decomposition, taking configuration



**Figure 2.7** Partition function  $(D + E)^N$  expressed as a ‘staircase’ path.

$$\mathcal{C} = (1, 0, 1, 0).$$

#### 2.4.2 Determinant form of TASEP weight with general $\alpha, \beta$

Mandelshtam has generalised the determinant form of a TASEP configuration weight in Eq. (2.27) for arbitrary  $\alpha, \beta$  (Corollary 5.2 in [98], modified to be consistent with notation used here):

$$\mathcal{W}(\mathcal{C}) = \frac{\det M}{\alpha^Q \beta^P} \quad (2.52)$$

where the entries of  $M$

$$M_{nm} = \beta^{m-n} \alpha^{-x_{n-1}} \left\{ \alpha^{x_m} \left[ \binom{Q-x_m}{m-n} + \beta \binom{Q-x_m}{m-n+1} \right] + \alpha^{x_{m-1}} \sum_{l=0}^{x_m-x_{m-1}-1} \alpha^l \left[ \binom{Q-x_{m-1}-l}{m-n-1} + \beta \binom{Q-x_{m-1}-l}{m-n} \right] \right\}, \quad (2.53)$$

with  $n, m = 1, \dots, P$ , and the  $x_n, x_m$  are the coordinates associated to an ASEP configuration in Section 2.2.1.

Using this, we find a novel expression for the TASEP partition function, in the form of a determinant.

## Determinantal form of the partition function

Given that

$$(D + E)^N = (DE)^N = \underbrace{(DE) \dots (DE)}_N, \quad (2.54)$$

the partition function is the weight of a single ‘staircase’ path of length  $2N$  (see Figure 2.7). For this path,  $x_m = m$ ,  $\forall m$ , and Eqs. (2.52), (2.53) eventually reduce to

$$Z_N = \det M^{(N)} \quad (2.55)$$

$$M_{nm}^{(N)} = \binom{m-1}{n-m} \left( \frac{1}{\alpha} + \frac{1}{\beta} \right) + \binom{m-1}{n-m-1} \frac{1}{\alpha\beta} + \binom{m-1}{n-m+1}, \quad (2.56)$$

$$= \begin{pmatrix} \left[ \frac{1}{\alpha} + \frac{1}{\beta} \right] & 1 & \cdot & \cdot & \dots \\ \frac{1}{\alpha\beta} & 1 + \left[ \frac{1}{\alpha} + \frac{1}{\beta} \right] & 1 & \cdot & \dots \\ \cdot & \left[ \frac{1}{\alpha} + \frac{1}{\beta} \right] + \frac{1}{\alpha\beta} & 2 + \left[ \frac{1}{\alpha} + \frac{1}{\beta} \right] & 1 & \dots \\ \cdot & \frac{1}{\alpha\beta} & 1 + 2 \left[ \frac{1}{\alpha} + \frac{1}{\beta} \right] + \frac{1}{\alpha\beta} & 3 + \left[ \frac{1}{\alpha} + \frac{1}{\beta} \right] & \dots \\ \cdot & \cdot & \left[ \frac{1}{\alpha} + \frac{1}{\beta} \right] + \frac{2}{\alpha\beta} & 3 + 3 \left[ \frac{1}{\alpha} + \frac{1}{\beta} \right] + \frac{1}{\alpha\beta} & \dots \\ \vdots & \vdots & \vdots & \vdots & \ddots \end{pmatrix}_{N \times N} \quad (2.57)$$

where we see rows of Pascal’s triangle in the coefficients of  $1$ ,  $[1/\alpha + 1/\beta]$ ,  $1/\alpha\beta$  when reading down columns of  $M^{(N)}$ . We now show that Eq. (2.55) and the partition function are equivalent.  $M^{(N)}$  is a Hessenberg matrix [96], which allows its determinant, which we define

$$\det M^{(N)} \equiv Z'_N \quad (2.58)$$

to be expressed in a recursive form using Eq. (2.32), from Theorem 2.1 in [97]

$$Z'_N = \sum_{r=1}^N (-)^{N-r} Z'_{r-1} \left[ \binom{r-1}{N-r-1} \frac{1}{\alpha\beta} + \binom{r-1}{N-r} \left( \frac{1}{\alpha} + \frac{1}{\beta} \right) + \binom{r-1}{N-r+1} \right]. \quad (2.59)$$

We will show that  $Z'_N$  and the TASEP partition function  $Z_N$  in Eq. (1.28) have the same generating function, thus making them equivalent. Define this generating function

in  $\eta$  as  $\mathcal{Z}$

$$\mathcal{Z}(\eta) = \sum_{N \geq 0} Z'_N \eta^N. \quad (2.60)$$

From Eq. (2.59) and knowing  $Z_0 = 1$ ,

$$\mathcal{Z}(\eta) = 1 + \sum_{N \geq 1} \sum_{r=1}^N \eta^N (-)^{N-r} \left[ \binom{r-1}{N-r-1} \frac{1}{\alpha\beta} + \binom{r-1}{N-r} \left( \frac{1}{\alpha} + \frac{1}{\beta} \right) + \binom{r-1}{N-r+1} \right] Z'_{r-1}. \quad (2.61)$$

We switch the order of summation and relabel the dummy index  $M = N - r$ ,

$$\mathcal{Z}(\eta) = 1 + \sum_{r \geq 1} Z'_{r-1} \eta^r \sum_{M \geq 0} (-\eta)^M \left[ \binom{r-1}{M-1} \frac{1}{\alpha\beta} + \binom{r-1}{M} \left( \frac{1}{\alpha} + \frac{1}{\beta} \right) + \binom{r-1}{M+1} \right]. \quad (2.62)$$

Evaluating the summation in  $M$ ,

$$\mathcal{Z}(\eta) = 1 + \sum_{r \geq 1} Z'_{r-1} \eta^r \left[ -\eta(1-\eta)^{r-1} \frac{1}{\alpha\beta} + (1-\eta)^{r-1} \left( \frac{1}{\alpha} + \frac{1}{\beta} \right) + \frac{1}{\eta} (1 - (1-\eta)^{r-1}) \right] \quad (2.63)$$

which we write in terms of the original generating function  $\mathcal{Z}$

$$\mathcal{Z}(\eta) = 1 + \sum_{r \geq 1} Z'_{r-1} (1-\eta)^{r-1} \eta^{r-1} \left[ \eta \left( \frac{1}{\alpha} + \frac{1}{\beta} \right) - \frac{\eta^2}{\alpha\beta} - 1 \right] - \sum_{r \geq 1} Z'_{r-1} \eta^{r-1} \quad (2.64)$$

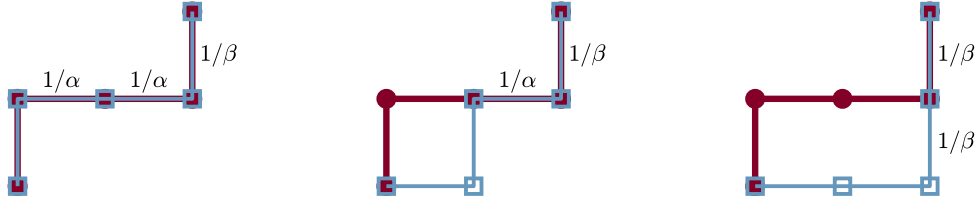
$$= \left[ \eta \left( \frac{1}{\alpha} + \frac{1}{\beta} \right) - \frac{\eta^2}{\alpha\beta} - 1 \right] \mathcal{Z}(\eta(1-\eta)) + \mathcal{Z}(\eta). \quad (2.65)$$

This is factorised to give

$$\mathcal{Z}(\eta(1-\eta)) = \frac{1}{\left(1 - \frac{\eta}{\alpha}\right) \left(1 - \frac{\eta}{\beta}\right)}. \quad (2.66)$$

Substituting  $z = \eta(1-\eta) \Rightarrow \eta(z) = \frac{1}{2} (1 - \sqrt{1-4z})$ , we recover Eq. (1.106), the known generating function for  $Z_N$ . We choose the negative root of  $\eta(z)$  to ensure  $\mathcal{Z}(0) = \langle W|V \rangle = 1$ .





**Figure 2.8** The weight of the path  $\mathcal{T} = (\uparrow, \rightarrow, \rightarrow, \uparrow)$ , corresponding to the TASEP configuration  $\mathcal{C} = (1, 0, 0, 1)$ . Both have weight  $\mathcal{W}(\mathcal{T}) = 1/\alpha^2\beta + 1/\alpha\beta + 1/\beta^2 = \langle W|DEED|V \rangle$ .

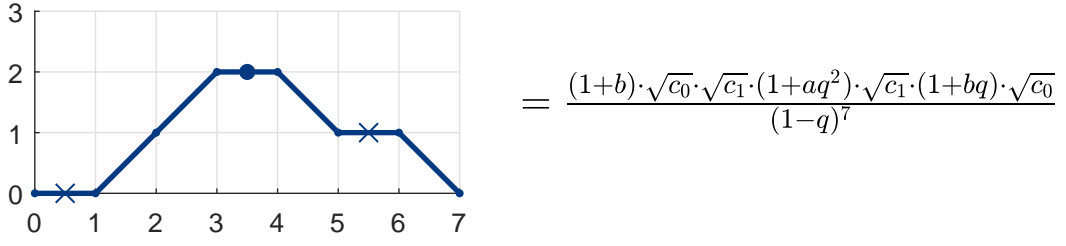
### 2.4.3 $\alpha, \beta$ generalisation of path dominance problem

Following on from the determinant in Eq. (2.52), there is a straightforward generalisation to  $\alpha, \beta$  in the dominated path interpretation of TASEP weights. In the context of the original reference [98] these are referred to as “weighted Catalan paths”, which translate into our formalism as follows: each dominated path has an associated weight  $(1/\alpha)^p(1/\beta)^q$ , where  $p$  is the number of horizontal steps where both paths run together, and  $q$  is the number of up steps the dominated path takes at the end of the walk. See Figure 2.8 for an example.

### 2.4.4 Mappings for general $\alpha, \beta, q$

We have arrived at the most general case of general  $\alpha, \beta, q$ . There is a natural interpretation in terms of bicoloured Motzkin paths that arises from an explicit matrix representation. Otherwise, the most notable progress here has been by Corteel and Williams, who derive a generalised version of the path representation of configurations in Section 2.2.1, termed *permutation tableaux*.

At this level of generality, there are few new physical insights that have been made other than establishment of the mapping.



**Figure 2.9** Weight of the Motzkin path  $(\times, \nearrow, \nearrow, \cdot, \searrow, \times, \searrow)$ . This maps to the configuration  $\mathcal{C} = (0, 1, 1, 1, 0, 0, 0)$ .

### Weighted bicoloured Motzkin paths

In this context, the natural explicit representation to use is [7]

$$D = \frac{1}{1-q} \begin{pmatrix} 1+b & \sqrt{c_0} & \cdot & \cdot & \cdots \\ \cdot & 1+bq & \sqrt{c_1} & \cdot & \cdots \\ \cdot & \cdot & 1+bq^2 & \sqrt{c_2} & \cdots \\ \cdot & \cdot & \cdot & 1+bq^3 & \cdots \\ \vdots & \vdots & \vdots & \vdots & \ddots \end{pmatrix}, \quad (2.67)$$

$$E = \frac{1}{1-q} \begin{pmatrix} 1+a & \cdot & \cdot & \cdot & \cdots \\ \sqrt{c_0} & 1+aq & \cdot & \cdot & \cdots \\ \cdot & \sqrt{c_1} & 1+aq^2 & \cdot & \cdots \\ \cdot & \cdot & \sqrt{c_2} & 1+aq^3 & \cdots \\ \vdots & \vdots & \vdots & \vdots & \ddots \end{pmatrix}, \quad (2.68)$$

$$\langle W| = (1, 0, 0, \cdots), \quad |V\rangle = (1, 0, 0, \cdots)^T, \quad (2.69)$$

with  $a$  and  $b$  defined in Eq. (1.47), and  $c_n = (1 - q^{n+1})(1 - abq^n)$ .  $D$  and  $E$  then operate on a state ket  $|n\rangle$  as

$$D|n\rangle = \frac{1}{1-q} (\sqrt{c_{n-1}}|n-1\rangle + (1+bq^n)|n\rangle), \quad (2.70)$$

$$E|n\rangle = \frac{1}{1-q} (\sqrt{c_{n+1}}|n+1\rangle + (1+aq^n)|n\rangle). \quad (2.71)$$

Note that this representation is distinct from Eqs. (1.43)–(1.46).

This representation associated *weights* to the bicoloured Motzkin paths [43, 99, 110] (or equivalently, dominated paths). In Section 2.2.2 we inferred that the weight of a configuration  $\mathcal{C}$  with sites  $(j_1, j_2, \dots, j_P)$  occupied is an enumeration of bicoloured Motzkin paths of length  $N$ , with steps  $(j_1, j_2, \dots, j_P)$  from  $\{\nearrow, \cdot\}$ , and the remaining

steps from  $\{\searrow, \times\}$ . The same formalism applies here, except for each step we associate weights:

- a  $\nearrow$  from height  $n$  to  $(n+1)$  has weight  $\sqrt{c_n}/(1-q)$ ;
- a  $\searrow$  from height  $(n+1)$  to  $n$  has weight  $\sqrt{c_n}/(1-q)$ ;
- a  $\times$  at height  $n$  has weight  $(1+bq^n)/(1-q)$ ;
- a  $\cdot$  at height  $n$  has weight  $(1+aq^n)/(1-q)$ .


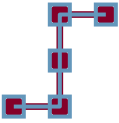
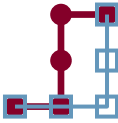
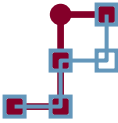



The weight of the path is then the product of these weights. See Figure 2.9 for an example. Note that  $\nearrow$  and  $\searrow$  always appear in pairs, eliminating the square root in factors of  $\sqrt{c_n}$ .

As a final remark, for  $\alpha = \beta = 1$  we conjecture that these Motzkin paths themselves have a one-to-many mapping to the weighted permutations in Section 2.4.1. The weight of a configuration  $\mathcal{C}$  with sites  $(j_1, j_2, \dots, j_P)$  occupied is the total weight of permutations where the numbers  $(j_1, j_2, \dots, j_P)$  are raised. More specifically, the weight of a bicoloured Motzkin path with steps at  $(j_1, j_2, \dots, j_P)$  from  $\{\nearrow, \cdot\}$  and steps at  $(k_1, k_2, \dots, k_P)$  from  $\{\searrow, \cdot\}$  appears to be the weight of permutations where the numbers  $(j_1, j_2, \dots, j_P)$  are *raised by*  $(k_1, k_2, \dots, k_P) + 1$ . See Table 2.4 for an example. This additional partitioning would mean that ASEP configurations have a one-to-many mapping to bicoloured Motzkin paths, which themselves each have a one-to-many mapping to permutations (as was illustrated in Figure 1.12). For each bicoloured Motzkin path, exactly one mapped permutation will have weight  $q^0 = 1$ , and all others a positive power of  $q$ . This would interpolate between the path dominance mapping of the TASEP ( $q \rightarrow 0$ ), and the permutation mapping of the SSEP ( $q \rightarrow 1$ ).

## Permutation and staircase tableaux

For completeness, we mention that Corteel and Williams [108, 111, 112] have mapped the most general case of  $\alpha, \beta, q$  to a problem in an area known as *tableaux combinatorics*. We refer the reader to Ref. [108] for the original work, and Refs. [111, 112] for a more generalised case of *staircase tableaux* that encodes two extra parameters  $\gamma, \delta$  (so particles may also enter from the right, and leave from the left).

The details are beyond the scope of this work, but to sketch their approach the authors take ASEP configurations as paths drawn in Section 2.2.1, and construct a grid across the area the path bounds (a *Young diagram*). Each entry of this grid can take a value

Configuration			
Dominated path			
Motzkin path			
Weight	$\frac{(1+b)(1+a)(1+a)(1+b)}{(1-q)^4}$ $= 1$	$\frac{(1+b)\sqrt{c_0}(1+aq)\sqrt{c_0}}{(1-q)^4}$ $= (1+q)^2$	$\frac{(1+b)(1+a)\sqrt{c_0}\sqrt{c_0}}{(1-q)^4}$ $= 1+q$
Raised	2, 3		
Raised by	3, 4	4, 5	3, 5
Permutations; weights	$\underline{5} \underline{2} \underline{3} \underline{4} 1; 1$	$\underline{3} \underline{4} \underline{2} \underline{5} 1; 1$ $\underline{2} \underline{4} \underline{3} \underline{5} 1; q$ $\underline{3} \underline{5} \underline{2} \underline{4} 1; q$ $\underline{2} \underline{5} \underline{3} \underline{4} 1; q^2$	$\underline{4} \underline{2} \underline{3} \underline{5} 1; 1$ $\underline{2} \underline{3} \underline{5} \underline{4} 1; q$

**Table 2.4** Mapping of the configuration  $C = (0, 1, 1, 0)$  into dominated paths and Motzkin paths, which themselves map to a set of permutations that follow certain rules.

of  $\alpha$ ,  $\beta$ ,  $q$  or 1 (or a generalised hop-right rate  $u$ ), with a set of rules as to which values can go where. The weight of this *permutation tableaux* is then the product of all of the entries. Each ASEP configuration has associated a set of tableaux, and the weight of the configuration is the sum of weights of these tableaux.

## 2.5 Summary

In this chapter we have explored the connection between the stationary weights of configurations in a paradigmatic nonequilibrium statistical mechanical system (the asymmetric simple exclusion process) and combinatorial enumeration problems, such as counting lattice paths. The earliest solutions of the TASEP appealed to recursion relations [40, 113] between configurational weights which can be expressed more powerfully in terms of reduction relations for matrices [36], as described in Section 1.3. Both the application of recursion relations and the reordering of matrices implicitly define some kind of counting problem. However it is not necessarily obvious from the outset what is being counted.

The most straightforward way to relate the matrix product solution to a lattice path enumeration problem is to exploit a representation of the matrices in terms of the identity, and (in general,  $q$ -deformed) raising and lowering operators (Section 1.3.5). A

particular configuration of the ASEP can then be related to a set of Motzkin paths, in which the identity, raising and lowering operators generate steps that are either horizontal, rise upwards, or fall down. Since the matrices are semi-infinite, the paths may not fall below the origin. Thus one set of objects that are being enumerated by the ASEP normalisation is the set of all paths subject to this constraint. This in turn yields a connection to the Catalan numbers, which solve a large number of enumeration problems [81].

Perhaps one of the most appealing representations of a configurational weight in the TASEP (the version of the process in which particles can hop only to the right) is in terms of dominated paths (Section 2.2.1), which is new. Here, a configuration of the TASEP is converted to a path on the square lattice by drawing (in sequence) a vertical step for each particle and a horizontal step for each empty site (hole). The number of paths that fall below this dominant path, and that have the same start and end point, then gives the weight of the TASEP configuration when  $\alpha = \beta = 1$ .

Here we see clearly the general phenomenon whereby a configurational weight in the TASEP is given by a sum over a set of objects with simpler weights that live in a larger space. In the specific case of the dominated paths, the larger space is the set of all lattice paths of a fixed length, and the weights are a power of  $\alpha$  multiplied by a power of  $\beta$ . As discussed in Sections 1.7.3 and 2.4.2, we can think of this as a Boltzmann weight, in which  $\alpha$  and  $\beta$  are the exponential of energetic contributions associated with specific steps along the paths.

From a practical point of view, the mapping to enumeration problems can expedite the calculation of physical quantities. For example, we saw in Sections 2.2 and 2.3 that once the mapping is established, results from enumerative combinatorics can be used to establish certain quantities more easily than deriving them from scratch via the matrix product solution. This leads us naturally to the theme of the next chapter. In Section 1.4 we introduced the *Rényi entropy*, which involves an enumeration of configuration weights raised to a power. For the TASEP, this measure proves very challenging to evaluate using the matrix product formalism directly. However, by building upon the interpretations of the explicit matrix representations discussed here, we are able to solve an equivalent combinatorial problem.

## Chapter 3

# Rényi entropy of the TASEP

### 3.1 Orientation

Having opened with an exploration of the links between the ASEP and a family of combinatorial lattice enumeration problems, in this chapter we present a calculation that capitalises on one of these mappings. We use the random walk interpretation of the matrix product formulation of the TASEP to derive a new measure of the TASEP state space: the  $\lambda = 2$  Rényi entropy, introduced in Eq. (1.59),

$$H_2 = -\log \sum_{\mathcal{C}} \mathcal{P}(\mathcal{C})^2 .$$

This quantity is technically challenging to calculate as it involves raising *each* of the microstate probabilities  $\mathcal{P}(\mathcal{C})$  to a power; in the language of our combinatorial mappings,  $H_2$  is a measure of how the larger set of dominated paths is partitioned amongst the set of TASEP configurations.

The bulk of this chapter is a technical calculation of the generating function  $\mathcal{Q}$  of the sum of squared TASEP weights, which after normalising leads to this particular Rényi entropy. We will use an explicit matrix representation of the TASEP to map this problem to a two-dimensional random walk problem with absorbing boundaries.

Because the generating function of this two-dimensional walk has in turn two counting variables, we will see that there are too many degrees of freedom to solve for  $\mathcal{Q}$  directly from the single recurrence relation. Instead, the solution of this problem entails a generalisation of what is known in the mathematical literature as an *obstinate kernel*

method [72, 114]. We identify a symmetry within the recurrence relation, which we exploit to obtain an additional set of equations for  $\mathcal{Q}$ . Combined, these equations contain enough information to directly solve for the generating function.

Once we have obtained a closed-form solution for the generating function, we use standard asymptotic methods to obtain the  $\lambda = 2$  entropy for all three phases of the TASEP. By the interpretation of the exponential of the Rényi entropy in Eq. (1.58), this provides an effective number of participating configurations in each phase [57]. We find that the leading-order behaviour of this entropy corresponds with that of a Bernoulli measure, and that the form of the leading correction reflects the range of the correlations present in each of the phases.

Finally, we show that the nonequilibrium phase transitions in the TASEP give rise to an analytical structure of the Rényi entropy that distinguishes itself from that seen in equilibrium systems. We will revisit the one-transit walk introduced in Chapter 2. The Rényi entropy is in this case elementary as, despite it sharing a partition function with the TASEP, it is an equilibrium system [66]. Importantly, we find a different form to the Rényi entropy, with the three phases giving rise to *five* different scaling regions in the phase diagram. This draws a clear distinction between equilibrium and nonequilibrium probability distributions.

## 3.2 Preliminaries

### 3.2.1 Sum of squared weights as a tensor product, generating function

The  $\lambda = 2$  Rényi entropy requires the sum of squared weights of all  $N$ -site configurations. In the matrix product formalism, the sum takes the form of a tensor product,

$$\sum_{\mathcal{C}} \mathcal{W}(\mathcal{C})^2 = \langle W | \otimes \langle W | (D \otimes D + E \otimes E)^N | V \rangle \otimes | V \rangle . \quad (3.1)$$

As a familiarisation exercise, we first explicitly calculate this quantity for  $N = 0, 1, 2$  by applying the reduction relations (1.10)–(1.13) directly:

$$\langle W | \otimes \langle W | (D \otimes D + E \otimes E)^0 | V \rangle \otimes | V \rangle = 1 , \quad (3.2)$$

$$\langle W | \otimes \langle W | (D \otimes D + E \otimes E)^1 | V \rangle \otimes | V \rangle = \frac{1}{\beta^2} + \frac{1}{\alpha^2} , \quad (3.3)$$

$$\langle W | \otimes \langle W | (D \otimes D + E \otimes E)^2 | V \rangle \otimes | V \rangle \quad (3.4)$$

$$= \langle W | \otimes \langle W | (DD \otimes DD + EE \otimes EE + ED \otimes ED + DE \otimes DE) | V \rangle \otimes | V \rangle$$

$$= \langle W | \otimes \langle W | (DD \otimes DD + EE \otimes EE + ED \otimes ED \quad (3.5)$$

$$+ D \otimes D + E \otimes E + D \otimes E + E \otimes D) | V \rangle \otimes | V \rangle$$

$$= \frac{1}{\beta^4} + \frac{1}{\alpha^4} + \frac{1}{\alpha^2 \beta^2} + \frac{1}{\beta^2} + \frac{1}{\alpha^2} + \frac{2}{\alpha \beta} . \quad (3.6)$$

We wish to generalise these expressions to arbitrary  $N$ . However, using the reduction relations these rapidly become intractable. We see the additional technical challenge of this problem over the partition function if one makes an attempt to derive a “reduction relation” for the tensors  $D \otimes D$ ,  $E \otimes E$ . The product

$$(D \otimes D)(E \otimes E) = DE \otimes DE \quad (3.7)$$

$$= (D + E) \otimes (D + E) \quad (3.8)$$

$$= D \otimes D + E \otimes E + E \otimes D + D \otimes E . \quad (3.9)$$

In comparison to simple matrix relation  $DE = D + E$  we find no simple reduction in terms, having generated two more irreducible tensors  $(E \otimes D)$ ,  $(D \otimes E)$ .

Instead, then, we define the *generating function* of Eq. (3.1), as  $\mathcal{Q}$ , which is a function of  $\alpha$ ,  $\beta$ , and a counting parameter  $z$  that tracks system size  $N$

$$\mathcal{Q}(z; \alpha, \beta) = \sum_{N \geq 0} \langle W | \otimes \langle W | (D \otimes D + E \otimes E)^N | V \rangle \otimes | V \rangle z^N . \quad (3.10)$$

The generating function  $\mathcal{Q}(z; \alpha, \beta)$  itself is found by interpreting the tensor product expressions in Eqs. (3.1), (3.10) as random walks on a lattice. Before this full calculation, however, we analyse the Rényi entropy along the factorisation line introduced in Section 1.3.4, which proves to be trivial.



### Exact solution along factorisation line

We saw in Section 1.3.4 that along the factorisation line  $\alpha + \beta = 1$ ,  $D$  and  $E$  commute [36]. Configuration probabilities then follow a Bernoulli distribution, and each of the  $N$  sites are independently, individually occupied with probability  $\rho = \alpha = 1 - \beta$ . With this, the sum of configuration weights to an *arbitrary* power  $\lambda$  is an elementary binomial sum

$$\sum_{\mathcal{C}} \mathcal{P}(\mathcal{C})^\lambda = \sum_{P=0}^N \binom{N}{P} [\rho^P (1 - \rho)^{N-P}]^\lambda \quad (3.11)$$

$$= (\rho^\lambda + (1 - \rho)^\lambda)^N \quad (3.12)$$

and we find the full Rényi entropy exactly

$$H_\lambda = \frac{N}{1 - \lambda} \log \left( \rho^\lambda + (1 - \rho)^\lambda \right). \quad (3.13)$$

We note that at the tricritical point  $\alpha = \beta = \rho = 1/2$ ,  $H_\lambda = N \log 2$ , independent of  $\lambda$ . This corresponds to the trivial case where every configuration has probability  $2^{-N}$ .

Along this factorisation line the statistics of the TASEP are mean-field in nature, with no correlations between neighbouring sites. This explains the triviality of these two results. We will use this line as a useful consistency check when deriving more technical results across the full phase diagram later.

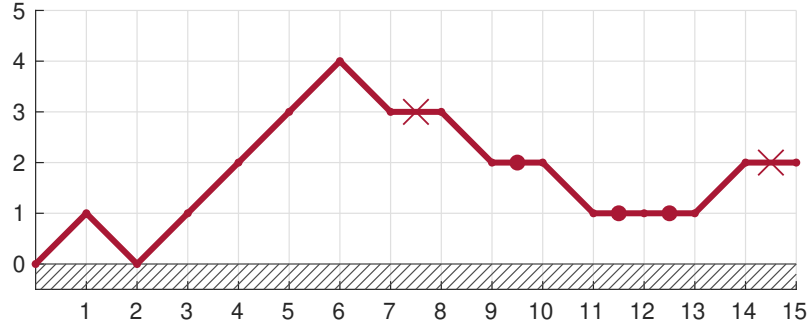
### 3.3 Mapping to a random walk

We now turn to formulating a random walk problem from the explicit ladder operator representations of  $D$ ,  $E$ ,  $\langle W|$ ,  $|V\rangle$  as defined in Eq. (1.21):

$$\begin{aligned} D &= 1 + g, & E &= 1 + g^\dagger, \\ D|k\rangle &= |k\rangle + |k-1\rangle, & E|k\rangle &= |k\rangle + |k+1\rangle, \\ \langle k|D &= \langle k| + \langle k+1|, & \langle k|E &= \langle k| + \langle k-1|. \end{aligned} \quad (3.14)$$

The boundary vectors  $\langle W|$ ,  $|V\rangle$  then contain all  $\alpha$ ,  $\beta$  dependence (Eq. (1.22)).

Before using these ladder interpretations to frame Eq. (3.1) as a random walk, we work through the simpler case of the partition function generating function, which we have already encountered in Section 1.6.2. The intention here is twofold: first, it gives an



**Figure 3.1** *Example of the bicoloured Motzkin path, now with generalised start and end coordinates. This walk begins at  $i = 0$  and terminates at  $k = 2$ . The walk can not move below the boundary at 0 but may touch it.*

opportunity to apply a conventional kernel method [115] to solve a recurrence relation, and in turn helps justify the attribution of the ‘obstinate’ label to the 2D calculation that follows. Secondly, it serves as the 1D case of a more general  $\lambda$ -dimension random walk relevant to higher-order Rényi entropies.

### 3.3.1 Introductory example: calculation of partition function generating function by a kernel method

Using the relations in Eq. (3.14), we write the partition function  $Z_N$  from Eq. (1.27) explicitly as a double summation:

$$Z_N = (1 - ab) \sum_{i \geq 0} \sum_{k \geq 0} a^i b^k \langle i | (g + g^\dagger + 2)^N | k \rangle. \quad (3.15)$$

Using our knowledge of combinatorial properties of the TASEP from Chapter 2, we immediately notice that this is a generalisation of bicoloured Motzkin paths [83]. Specifically, the element  $\langle i | (g + g^\dagger + 2)^N | k \rangle$  that appears in Eq. (3.15) counts the number of paths of length  $N$  from the step set  $\{\uparrow, \downarrow, \times, \cdot\}$  (with  $\times$  and  $\cdot$  distinct non-movement steps) that start at  $i$  and end at  $k$ , remaining in the upper plane. See Figure 3.1 for an example of such a walk. Eq. (3.15) is then a generating function in  $a$  and  $b$  over all possible start and end coordinates.

We take the generating function of the partition function from Eq. (1.101) :

$$\begin{aligned} \mathcal{Z}(z) &\equiv \sum_{N \geq 0} z^N \langle W | (D + E)^N | V \rangle \\ &= \sum_{N \geq 0} z^N (1 - ab) \sum_{i \geq 0} \sum_{k \geq 0} a^i b^k \langle i | (g + g^\dagger + 2)^N | k \rangle \end{aligned} \quad (3.16)$$

which in turn can be calculated using a kernel method (see Ref. [115] for details and further examples), as we now describe.

Define  $\{b^k\}(\mathcal{Z}(z)/(1-ab)) = \mu_k(z; a)$  as:

$$\mu_k(z; a) \equiv \sum_{N \geq 0} z^N \sum_{i \geq 0} a^i \langle i | (g + g^\dagger + 2)^N | k \rangle \quad (3.17)$$

from which we obtain a recursion relation on  $\mu_k$  by applying the operator  $(g + g^\dagger + 2)$  to the bra  $\langle i |$ . Following the relations in Eq. (3.14), we find

$$\mu_k(z; a) = \sum_{i \geq 0} a^i \langle i | k \rangle + \sum_{N \geq 1} z^N \sum_{i \geq 0} a^i (\langle i+1 | + \langle i-1 | + 2\langle i |) (g + g^\dagger + 2)^{N-1} | k \rangle \quad (3.18)$$

$$= a^k + \sum_{N' \geq 0} z^{N'+1} \sum_{i \geq 0} a^i (\langle i+1 | + \langle i-1 | + 2\langle i |) (g + g^\dagger + 2)^{N'} | k \rangle \quad (3.19)$$

$$= a^k + z \sum_{N' \geq 0} z^{N'} \left[ \sum_{i' \geq 1} a^{i'-1} \langle i' | (g + g^\dagger + 2)^{N'} | k \rangle \right. \quad (3.20)$$

$$\left. + \sum_{i'' \geq -1} a^{i''+1} \langle i'' | (g + g^\dagger + 2)^{N'} | k \rangle + 2 \sum_{i \geq 0} a^i \langle i | (g + g^\dagger + 2)^{N'} | k \rangle \right] \\ = a^k + z(2 + a + \bar{a})\mu_k(z; a) - z\bar{a}\mu_k(z; 0) \quad (3.21)$$

where we have introduced the notation  $\bar{a} = 1/a$  that will be used throughout this chapter. Rearranging Eq. (3.21) gives for  $\mu_k(z; a)$

$$\mu_k(z; a) = \frac{z\mu_k(z; 0) - a^{k+1}}{z(2a + a^2 + 1) - a} \quad (3.22)$$

$$= \frac{z\mu_k(z; 0) - a^{k+1}}{z(a - A_-(z))(a - A_+(z))} \quad (3.23)$$

where we have factorised the denominator in  $a$ . We refer to the denominator as the *kernel*. The roots  $A_\pm(z)$  of the kernel are functions of  $z$ :

$$A_\pm(z) = \frac{1 - 2z \pm \sqrt{1 - 4z}}{2z} \quad (3.24)$$

with  $A_-(z)A_+(z) = 1$ . Thus  $\mu_k(z; a)$  exhibits a priori two poles at  $a = A_\pm(z)$ . However, as we now argue, one of these poles must be cancelled by the numerator which furnishes the condition that fixes the undetermined function  $\mu_k(z; 0)$  in Eq. (3.23).

From Eq. (3.17), we see that  $\mu_k(z; a)$  is a series with nonnegative powers of  $z$  and  $a$ .

Looking at the denominator of Eq. (3.23), we see that since  $A_+(z) \rightarrow 1/z$  as  $z \rightarrow 0$ , a Taylor expansion of this factor about  $z = 0$  and  $a = 0$  yields nonnegative powers. However,  $A_-(z) \rightarrow 0$  as  $z \rightarrow 0$ , which generates a spurious  $1/a$  term. Since  $\mu_k(z; 0)$  depends on  $z$  (and not on  $a$ ), the only way to eliminate this divergence is to cancel the pole  $(a - A_-(z))$  when  $a \rightarrow z$ . This condition fixes  $\mu_k(z; 0) = A_-(z)^{k+1}/z$  and gives our closed-form expression for  $\mu_k(z; a)$ :

$$\mu_k(z; a) = \frac{A_-(z)^{k+1} - a^{k+1}}{z(a - A_-(z))(a - A_+(z))} . \quad (3.25)$$

We insert this into the full generating function, Eq. (3.16), and evaluate the geometric sum

$$\mathcal{Z}(z) = (1 - ab) \sum_{k \geq 0} \left( \frac{A_-(z)^{k+1} - a^{k+1}}{z(a - A_-(z))(a - A_+(z))} \right) b^k \quad (3.26)$$

$$= \frac{1}{z(a - A_+(z))(bA_-(z) - 1)} . \quad (3.27)$$

Reintroducing  $\eta(z) = \frac{1}{2}(1 - \sqrt{1 - 4z})$ , we have

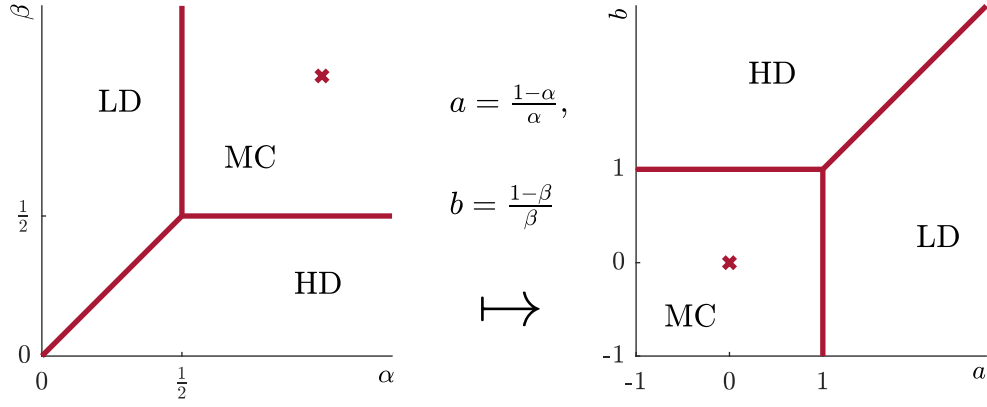
$$z = \eta(1 - \eta) , \quad A_+ = \frac{1 - \eta}{\eta} , \quad A_- = \frac{\eta}{1 - \eta} , \quad (3.28)$$

and Eq. (3.27) can be expressed in a form manifestly symmetric in  $(a, b)$

$$\begin{aligned} \mathcal{Z}(z) &= \frac{1}{[1 - (1 + a)\eta(z)][1 - (1 + b)\eta(z)]} \\ &= \frac{1}{1 - \frac{\eta(z)}{\alpha}} \frac{1}{1 - \frac{\eta(z)}{\beta}} \end{aligned} \quad (3.29)$$

recovering the known expression, Eq. (1.106) from Section 1.3.3. We mention at this point that the geometric series in Eq. (3.27) will have a finite radius of convergence. We perform the calculation assuming we are within this radius of convergence, and extend the domain of the resulting generating function to the full phase diagram (all values of  $a > -1$ ,  $b > -1$  of the TASEP) by analytic continuation.

In fact, for the remainder of this chapter we use the variables  $a$  and  $b$  in place of  $\alpha$ ,  $\beta$  for simplicity. To help visualise this variable space, we have produced the phase diagram in terms of the transformed  $(\alpha, \beta) \mapsto (a, b)$  in Figure 3.2.



**Figure 3.2** The phase diagram of the TASEP in the space  $a = (1-\alpha)/\alpha$ ,  $b = (1-\beta)/\beta$ . The point  $\alpha = \beta = 1$ , marked by a cross, maps to  $a = b = 0$ . The new lower bound of  $-1$  emerges as  $\lim_{\alpha \rightarrow \infty} (1-\alpha)/\alpha = -1$ .

### 3.3.2 Generating function for the sum of squared weights

Building on this simpler example, we now turn to the tensor expression in Eq. (3.10) for the sum of squared weights. Here, the tensors act on  $\langle i| \otimes \langle j|$  as

$$\langle i| \otimes \langle j| (D \otimes D) = \langle i| \otimes \langle j| + \langle i| \otimes \langle j+1| + \langle i+1| \otimes \langle j| + \langle i+1| \otimes \langle j+1|, \quad (3.30)$$

$$\langle i| \otimes \langle j| (E \otimes E) = \langle i| \otimes \langle j| + \langle i| \otimes \langle j-1| + \langle i-1| \otimes \langle j| + \langle i-1| \otimes \langle j-1|. \quad (3.31)$$

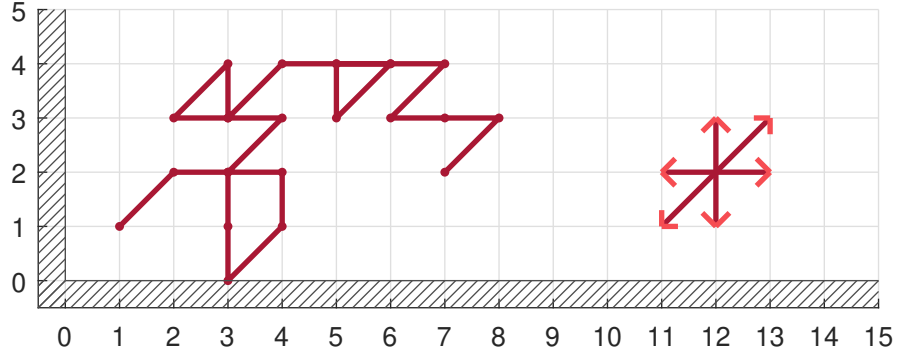
These correspond to possible steps of a walk on a *two*-dimensional lattice spanned by the coordinates  $i$  and  $j$ . We use this explicit representation to write Eq. (3.1)

$$\sum_{\mathcal{C}} \mathcal{W}(\mathcal{C})^2 = (1-ab)^2 \sum_{i \geq 0} \sum_{j \geq 0} \sum_{k \geq 0} \sum_{l \geq 0} a^i a^j b^k b^l \langle i| \otimes \langle j| (\mathcal{V} + 2)^N |k\rangle \otimes |l\rangle \quad (3.32)$$

where  $\mathcal{V}$  denotes the sum over the tensor operators that correspond to the steps  $\{\nearrow, \rightarrow, \uparrow, \swarrow, \leftarrow, \downarrow\}$  on a lattice. This time, the element  $\langle i| \otimes \langle j| (\mathcal{V} + 2)^N |k\rangle \otimes |l\rangle$  is equivalent to the number of distinct length- $N$  paths from the step set  $\mathcal{V} \cup \{\cdot, \times\}$ , where the walk remains in the upper-quarter plane. See Figure 3.3 for an example.

### Variable transformation

It is helpful to make a change of variables that eliminates the two non-movement steps, leaving only the six steps in  $\mathcal{V}$ . To this end, we define a generating function  $\mathcal{R}$  in the variable  $t$ , that counts the number of walks comprising  $N$  steps from the step set



**Figure 3.3** Example of a 2D walk from the step set  $\{\nearrow, \rightarrow, \uparrow, \nwarrow, \leftarrow, \downarrow\}$ . The walk may touch the axes, but not cross them.

$\{\nearrow, \rightarrow, \uparrow, \nwarrow, \leftarrow, \downarrow\}$ , that begin at  $(i, j)$  and end at  $(k, l)$ , remaining in the upper-quarter plane:

$$\mathcal{R}(t; x, y, v, w) = \sum_{N \geq 0} \sum_{i \geq 0} \sum_{j \geq 0} \sum_{k \geq 0} \sum_{l \geq 0} t^N x^i y^j v^k w^l \langle i | \otimes \langle j | \mathcal{V}^N | k \rangle \otimes | l \rangle. \quad (3.33)$$

The five variables  $(t, x, y, v, w)$  track the path length  $N$ , its start coordinates  $(i, j)$  and its end coordinates  $(k, l)$ , respectively. To relate  $\mathcal{Q}$  from Eq. (3.10) to  $\mathcal{R}$ , we use the identity

$$\sum_{N \geq 0} z^N (X + Y)^N = \sum_{N \geq 0} \sum_{P \geq 0} \binom{N}{P} (zX)^P (zY)^{N-P} \quad (3.34)$$

$$= \sum_{P \geq 0} \frac{(zX)^P}{(1 - zY)^{P+1}} \quad (3.35)$$

for commuting objects  $X$  and  $Y$ . Then,

$$\begin{aligned} \mathcal{Q}(z; \alpha, \beta) &= \sum_{N \geq 0} \sum_{i \geq 0} \sum_{j \geq 0} \sum_{k \geq 0} \sum_{l \geq 0} z^N (1 - ab)^2 a^i a^j b^k b^l \langle i | \otimes \langle j | (\mathcal{V} + 2)^N | k \rangle \otimes | l \rangle \\ &= \frac{(1 - ab)^2}{1 - 2z} \sum_{i \geq 0} \sum_{j \geq 0} \sum_{k \geq 0} \sum_{l \geq 0} a^{i+j} b^{k+l} \sum_{P \geq 0} \left( \frac{z}{1 - 2z} \right)^P \langle i | \otimes \langle j | \mathcal{V}^P | k \rangle \otimes | l \rangle \\ &= \frac{(1 - ab)^2}{1 - 2z} \mathcal{R} \left( \frac{z}{1 - 2z}; \frac{1 - \alpha}{\alpha}, \frac{1 - \alpha}{\alpha}, \frac{1 - \beta}{\beta}, \frac{1 - \beta}{\beta} \right). \end{aligned} \quad (3.36)$$

Thus  $\mathcal{R}$  and  $\mathcal{Q}$  are related by the transformation  $t = z/(1 - 2z)$ ,  $z \in [0, \frac{1}{2})$ . We focus on finding an expression for  $\mathcal{R}$ , generalising a result from Bousquet-Mélou, where the end point of this six-step walk was fixed at the origin,  $k = l = 0$  [114].

### 3.3.3 Recurrence relation

We now determine the recurrence relation that  $\mathcal{R}(t; x, y, v, w)$  obeys. We apply the leftmost  $\mathcal{V}$  operator in Eq. (3.33) to  $\langle i | \otimes \langle j |$ ,

$$\begin{aligned} \mathcal{R}(t; x, y, v, w) = & \sum_{i \geq 0} \sum_{j \geq 0} \sum_{k \geq 0} \sum_{l \geq 0} x^i y^j v^k w^l \delta_{ik} \delta_{jl} \\ & + \sum_{i \geq 0} \sum_{j \geq 0} \sum_{k \geq 0} \sum_{l \geq 0} \sum_{N \geq 1} t^N x^i y^j v^k w^l \left[ \langle i+1 | \langle j | + \langle i-1 | \langle j | + \langle i | \langle j+1 | \right. \\ & \left. + \langle i | \langle j-1 | + \langle i+1 | \langle j+1 | + \langle i-1 | \langle j-1 | \right] \mathcal{V}^{(N-1)} |k\rangle |l\rangle \end{aligned} \quad (3.37)$$

where we suppress the tensor product ‘ $\otimes$ ’ symbol to lighten the notation. The first term is the  $N = 0$  contribution, and the second  $N \geq 1$  term makes explicit the six possible steps the walk can take. We rewrite Eq. (3.37) in terms of  $\mathcal{R}$  itself,

$$\begin{aligned} \mathcal{R}(t; x, y, v, w) = & \frac{1}{(1-xv)(1-yw)} + t\bar{x}\bar{y}\mathcal{R}(t; 0, 0, v, w) \\ & - t(\bar{x}\bar{y} + \bar{x})\mathcal{R}(t; 0, y, v, w) - t(\bar{x}\bar{y} + \bar{y})\mathcal{R}(t; x, 0, v, w) \\ & + t(x + \bar{x} + y + \bar{y} + xy + \bar{x}\bar{y})\mathcal{R}(t; x, y, v, w), \end{aligned} \quad (3.38)$$

and we reiterate that we use the notation  $\bar{x} = 1/x$  and  $\bar{y} = 1/y$ . By completing the summations in Eq. (3.37), the we are left with of *counter terms* e.g.  $\mathcal{R}(t; 0, y, v, w)$ . To refer back to our introductory discussion on random walks in Section 1.5, Eq. (3.38) is a master equation for  $\langle i | \otimes \langle j | \mathcal{V}^N |k\rangle \otimes |l\rangle$  in discrete space and path length, with a summation over these three coordinates, with absorbing boundary conditions (e.g.  $\langle i | \otimes \langle j | \mathcal{V}^N |-1\rangle \otimes |l\rangle = 0$ ) enforced.

Moving forward, in a similar way to the 1D example in Section 3.3.1, we define a *kernel*  $K(x, y, t)$  and introduce a shorthand  $K_{xy}$

$$K(x, y, t) \equiv K_{xy} = 1 - t(x + \bar{x} + y + \bar{y} + xy + \bar{x}\bar{y}) \quad (3.39)$$

and Eq. (3.38) becomes

$$\begin{aligned} K_{xy}\mathcal{R}(t; x, y, v, w) = & \frac{1}{(1-xv)(1-yw)} + t\bar{x}\bar{y}\mathcal{R}(t; 0, 0, v, w) \\ & - t(\bar{x}\bar{y} + \bar{x})\mathcal{R}(t; 0, y, v, w) - t(\bar{x}\bar{y} + \bar{y})\mathcal{R}(t; x, 0, v, w). \end{aligned} \quad (3.40)$$

By making the substitution  $(x, y, v, w) \rightarrow (a, a, b, b)$ , we find a simplification using the

symmetry of the walk along the diagonal

$$a^2 K_{aa} \mathcal{R}(t; a, a, b, b) = \frac{a^2}{(1 - ab)^2} + t \mathcal{R}(t; 0, 0, b, b) - 2t(1 + a) \mathcal{R}(t; a, 0, b, b) . \quad (3.41)$$

We see from Eq. (3.41) that an expression for  $\mathcal{R}(t; a, 0, b, b)$  is sufficient to find the more general  $\mathcal{R}(t; a, a, b, b)$ , the generating function for the random walk, and in turn  $\mathcal{Q}(z; \alpha, \beta)$ , the generating function for the TASEP squared weight enumeration with arbitrary  $\alpha, \beta$ . However, therein lies the difficulty in this problem. With the kernel as a function of two variables  $x, y$ , there is insufficient information in this single recurrence relation to fix the right hand side terms of Eq. (3.40) by a pole-cancelling method, as used in the introductory example of the partition function in Section 3.3.1. Instead, we must turn to the more sophisticated method seen in Refs. [72, 114, 116] which exploits a symmetry property of the kernel to solve for  $\mathcal{R}$ .

### Overview of the obstinate kernel method

We first give a brief description of the obstinate kernel method that eventually solves Eq. (3.40) [116]:

1. Identify a set symmetries of the kernel: coordinate transformations of  $x, y$  under which  $K(x, y)$  remains invariant;
2. Exploit this symmetry to eliminate an unknown function in the recurrence relation;
3. Perform a formal series expansion of the simplified recurrence relation in both positive and negative powers of the variable  $y$ ;
4. Read off and extract the coefficient of  $y^0$ , eliminating any dependence on  $y$ ;
5. Perform a formal series expansion of this new relation in positive and negative powers of  $x$ ;
6. Read off and extract either the coefficient of  $x^0$  or the positive powers in  $x$ , depending on the desired generality, to find a closed-form expression for a generating function on the RHS of Eq. (3.40).

With this roadmap, we first analyse the kernel, identifying its roots and symmetry properties.



### 3.3.4 Symmetry and factorisation of the kernel

The kernel in Eq. (3.39) has the following symmetry property:

$$K(x, y, t) = K(x, \bar{x}\bar{y}, t) = K(\bar{x}\bar{y}, y, t) \quad (3.42)$$

where it is easily seen that these two parameter transformations leave the kernel invariant.

We now define the two roots of the kernel  $K$  in the variable  $y$  as  $Y_-(x, t)$ ,  $Y_+(x, t)$  (the choice of  $y$  over  $x$  is arbitrary given the symmetry of the problem) and write it in factorised form

$$K_{xy} = -\frac{t(1+x)}{y} (y - Y_-(x, t)) (y - Y_+(x, t)) , \quad (3.43)$$

$$Y_{\pm}(x, t) = \frac{1 - t(\bar{x} + x) \pm \sqrt{\Delta(x, t)}}{2t(1+x)} , \quad (3.44)$$

$$\Delta(x, t) = 1 - 6t^2 + t^2(x^2 + \bar{x}^2) - 2t(1+2t)(x + \bar{x}) , \quad (3.45)$$

where  $Y_-(x, t)Y_+(x, t) = \bar{x}$ .  $\Delta(x, t)$  is termed the *discriminant*, which can also be factorised: as a product of its roots in  $x$ ,

$$\Delta(x, t) = \Delta_0 \Delta_+(x, t) \Delta_+(\bar{x}, t) , \quad (3.46)$$

$$\Delta_0(t) = \frac{t^2}{X_-(t)X_+(t)} , \quad (3.47)$$

$$\Delta_+(x, t) = (1 - X_-(t)x)(1 - X_+(t)x) . \quad (3.48)$$

The roots  $X_-(t)$ ,  $X_+(t)$  are functions of  $t$  alone

$$X_{\pm}(t) = \frac{2t+1}{2t} \pm \sqrt{\frac{3t+1}{t} - \frac{\sqrt{2t+1}}{2t} \sqrt{1+6t \pm 4\sqrt{t(3t+1)}}} . \quad (3.49)$$

We refer to the kernel  $K$ , the discriminant  $\Delta$  and their respective roots  $Y_{\pm}$ ,  $X_{\pm}$  throughout the proceeding calculation. Knowing these roots, we can rework the reciprocal of the kernel:

$$\frac{1}{K(x, y, t)} = \frac{y}{\sqrt{\Delta(x, t)}} \frac{Y_-(x, t) - Y_+(x, t)}{(y - Y_-(x, t))(y - Y_+(x, t))} \quad (3.50)$$

$$= \frac{y}{\sqrt{\Delta(x, t)}} \left[ \frac{1}{1 - \bar{y}Y_-(x, t)} + \frac{y}{Y_+(x, t) - y} \right] \quad (3.51)$$

$$= \frac{1}{\sqrt{\Delta(x, t)}} \left[ \frac{1}{1 - \bar{y}Y_-(x, t)} + \frac{1}{1 - y\bar{Y}_+(x, t)} - 1 \right] . \quad (3.52)$$

Eq. (3.52) is in a form that permits a straightforward power series expansion in  $y$ .

For later reference we define two more quantities that we use when performing the transformation from  $t$ -space back to  $z$ , re-integrating the two non-movement steps into the random walk, as per Eq. (3.36)

$$\Lambda_{\pm}(z) \equiv 2zX_{\pm} \left( \frac{z}{1-2z} \right) \quad (3.53)$$

$$= 1 \pm 2\sqrt{z(1+z)} - 2\sqrt{z + \frac{1}{4} \pm \sqrt{z(1+z)}} , \quad (3.54)$$

$$\Gamma(\alpha, z) \equiv \Gamma(\alpha) = \Delta_+ \left( \frac{1-\alpha}{\alpha}, \frac{z}{1-2z} \right) \quad (3.55)$$

$$= \left[ 1 - \frac{1-\alpha}{2z\alpha} \Lambda_-(z) \right] \left[ 1 - \frac{1-\alpha}{2z\alpha} \Lambda_+(z) \right] . \quad (3.56)$$

### 3.4 Generating function for the $\alpha = \beta = 1$ weights, $\mathcal{Q}(z; 1, 1)$

We now present a full calculation of the generating function for the case  $\alpha = \beta = 1$ , corresponding to  $\mathcal{Q}(z; 1, 1)$ . With reference to Figure 1.3, this is a point in the maximal current phase. Under this restriction, expressions simplify considerably from the case of general  $\alpha$  and  $\beta$ . By working through this particular case in detail we aim to clearly outline this *obstinate kernel* method, while the algebra remains comparatively simple. We find that with increasing generality of the generating function, the algebra becomes more elaborate, but the principles of the calculation remain the same. In this simpler case, our solution follows closely the method of Ref. [114].

For further brevity, define

$$\mathcal{R}_0(x, y) \equiv \mathcal{R}(t; x, y, 0, 0) \quad (3.57)$$

whereby we now have any functional  $t$  dependence as implicit. Because we have set  $v = w = 0$  (the equivalent of fixing  $\beta = 1$  in the TASEP) the recurrence relation (3.40) reduces to

$$xy\mathcal{R}_0(x, y) = \frac{1}{K_{xy}} [xy - t(1+x)\mathcal{R}_0(x, 0) - t(1+y)\mathcal{R}_0(0, y) + t\mathcal{R}_0(0, 0)] . \quad (3.58)$$

It is at this point we use the symmetry property in Eq. (3.42) of the kernel to obtain

from Eq. (3.58) two transformed expressions

$$\bar{y}\mathcal{R}_0(x, \bar{x}\bar{y}) = \frac{1}{K_{xy}} [\bar{y} - t(1+x)\mathcal{R}_0(x, 0) - t(1+\bar{x}\bar{y})\mathcal{R}_0(0, \bar{x}\bar{y}) + t\mathcal{R}_0(0, 0)] , \quad (3.59)$$

$$\bar{x}\mathcal{R}_0(\bar{x}\bar{y}, y) = \frac{1}{K_{xy}} [\bar{x} - t(1+\bar{x}\bar{y})\mathcal{R}_0(\bar{x}\bar{y}, 0) - t(1+y)\mathcal{R}_0(0, y) + t\mathcal{R}_0(0, 0)] . \quad (3.60)$$

We then take the linear combination of Eqs. (3.58) + (3.59) – (3.60) to give

$$\begin{aligned} xy\mathcal{R}_0(x, y) + \bar{y}\mathcal{R}_0(x, \bar{x}\bar{y}) - \bar{x}\mathcal{R}_0(\bar{x}\bar{y}, y) \\ = \frac{1}{K_{xy}} [t\mathcal{R}_0(0, 0) - 2t(1+x)\mathcal{R}_0(x, 0) + xy + \bar{y} - \bar{x}] . \end{aligned} \quad (3.61)$$

This exploitation of the kernel symmetry is the key step in solving an otherwise insufficient recurrence relation (3.58); by making this combination, we have eliminated  $\mathcal{R}_0(0, y)$  and  $\mathcal{R}_0(0, \bar{x}\bar{y})$ . Crucially, we are now able to find closed-form expressions for the generating functions  $\mathcal{R}_0(0, 0)$ ,  $\mathcal{R}_0(x, 0)$  by extracting coefficients of certain powers of  $x$  and  $y$  from Eq. (3.61). This is because we have used the kernel symmetry to make nearly all  $y$ -dependence in Eq. (3.61) explicit [114].

With this in mind, we rewrite Eq. (3.61), this time using the reciprocal of the kernel in Eq. (3.52)

$$\begin{aligned} xy\mathcal{R}_0(x, y) + \bar{y}\mathcal{R}_0(x, \bar{x}\bar{y}) - \bar{x}\mathcal{R}_0(\bar{x}\bar{y}, y) \\ = \frac{1}{\sqrt{\Delta(x)}} \left[ \frac{1}{1 - \bar{y}Y_-(x)} + \frac{1}{1 - y\bar{Y}_+(x)} - 1 \right] \times \\ [t\mathcal{R}_0(0, 0) - 2t(1+x)\mathcal{R}_0(x, 0) + xy + \bar{y} - \bar{x}] . \end{aligned} \quad (3.62)$$

We are able to now formally write Eq. (3.62) as a power series in  $y$ , anticipating both positive and negative powers of  $y$ .

We first want  $\mathcal{R}_0(0, 0)$ . Knowing that this is a function of  $t$  alone, we need to isolate the  $x^0y^0$  coefficient from Eq. (3.62). Having made most of the  $y$ -dependence explicit, we begin by extracting the  $y^0$  component.

### 3.4.1 $y^0$ coefficient extraction

By making explicit the power series on the LHS of Eq. (3.62)

$$\text{LHS (3.62)} = \sum_{i \geq 0} \sum_{j \geq 0} \sum_{N \geq 0} [x^{i+1}y^{j+1} + x^{i-j}y^{-j-1} - x^{-i-1}y^{j-i}] t^N \langle i | \langle j | \mathcal{V}^N | 0 \rangle | 0 \rangle \quad (3.63)$$

we simply read off the  $y^0$  component as

$$\{y^0\} \text{LHS (3.62)} = -\bar{x} \sum_{i \geq 0} \sum_{N \geq 0} \bar{x}^i t^N \langle i | \langle i | \mathcal{V}^N | 0 \rangle | 0 \rangle \equiv -\bar{x} \mathcal{R}_0^{(d)}(\bar{x}) \quad (3.64)$$

where  $\mathcal{R}_0^{(d)}(x)$  is the generating function for walks comprising steps from  $\mathcal{V} = \{\nearrow, \rightarrow, \uparrow, \swarrow, \leftarrow, \downarrow\}$ , from the origin, remaining in the upper-quarter plane and terminating on the diagonal. We now turn to the RHS of Eq. (3.62), which we also write as a formal power series

$$\begin{aligned} \text{RHS (3.62)} &= \frac{1}{\sqrt{\Delta(x)}} \left[ \sum_{i \geq 0} y^{-i} Y_-(x)^i + \sum_{j \geq 0} y^j Y_+(x)^{-j} - 1 \right] \times \\ &\quad [t\mathcal{R}_0(0,0) - 2t(1+x)\mathcal{R}_0(x,0) + xy + \bar{y} - \bar{x}] \quad (3.65) \end{aligned}$$

and read off the  $y^0$  component to leave

$$-\bar{x} \mathcal{R}_0^{(d)}(\bar{x}) = \frac{1}{\sqrt{\Delta(x)}} [t\mathcal{R}_0(0,0) - 2t(1+x)\mathcal{R}_0(x,0) - \bar{x} + 2xY_-(x)] \quad (3.66)$$

having used  $Y_+(x)Y_-(x) = \bar{x}$ . From Eq. (3.66), and the factorisation of the discriminant in Eq. (3.46) it is a simple matter to determine  $\mathcal{R}_0(0,0)$ .

### 3.4.2 $x^0$ coefficient extraction, $\mathcal{Q}(z; 1, 1)$ result

With the explicit form for the root  $Y_-$  and factorised discriminant (Eqs. (3.44), (3.46) respectively), we can rearrange Eq. (3.66) into the form

$$\begin{aligned} &\sqrt{\Delta_+(\bar{x})} \left[ \frac{x}{t} - (1 + \bar{x}) \mathcal{R}_0^{(d)}(\bar{x}) \right] \\ &= \frac{1}{\sqrt{\Delta_0 \Delta_+(x)}} \left[ (1+x)t\mathcal{R}_0(0,0) - 2t(1+x)^2\mathcal{R}_0(x,0) + \frac{x}{t} - 2 - \bar{x} - x^2 \right] \quad (3.67) \end{aligned}$$

having separated the bulk of  $\bar{x}$  terms to the LHS, and the  $x$  terms to the RHS. We now perform two expansions with the factorised form of the discriminant, Eq. (3.46):

$$\sqrt{\Delta_+(\bar{x})} = 1 - \frac{1}{2}(X_- + X_+)\bar{x} + \mathcal{O}(\bar{x}^2), \quad (3.68)$$

$$\frac{1}{\sqrt{\Delta_+(x)}} = 1 + \frac{1}{2}(X_- + X_+)x + \mathcal{O}(x^2), \quad (3.69)$$

and extract the  $x^0$  component of Eq. (3.67) to find

$$-\frac{1}{2}(X_+ + X_-) - \mathcal{R}_0(0, 0) = \frac{1}{\sqrt{\Delta_0}} \left[ t\mathcal{R}_0(0, 0) - 2t\mathcal{R}_0(0, 0) - 2 + \frac{1}{2}(X_+ + X_-) \right]. \quad (3.70)$$

It is now a matter of simple algebraic manipulation to find for  $\mathcal{R}_0(0, 0)$

$$\mathcal{R}(t; 0, 0, 0, 0) = \mathcal{R}_0(0, 0) \quad (3.71)$$

$$= \frac{1}{2t} \frac{(X_- + X_+) - \sqrt{X_- X_+} (4 + X_- + X_+)}{\sqrt{X_- X_+} - 1} \quad (3.72)$$

$$= 1 + 3t^2 + 4t^3 + 26t^4 + 80t^5 + 387t^6 + \mathcal{O}(t^7) \quad (3.73)$$

in terms of the roots of the discriminant  $X_-(t)$ ,  $X_+(t)$  in Eq. (3.49), recovering the known series expansion in [114]. To recall,  $\mathcal{R}(t; 0, 0, 0, 0)$  generates the numbers of 2D walks of  $N$  steps from the step set  $\{\nearrow, \rightarrow, \uparrow, \swarrow, \leftarrow, \downarrow\}$  in the upper quadrant that start and finish at the origin. To find the corresponding generating function for the sum of squared weights in a TASEP of length  $N$ , we apply the transformation (3.36)

$$\mathcal{Q}(z; 1, 1) = \frac{1}{1-2z} \mathcal{R}\left(\frac{z}{1-2z}; 0, 0, 0, 0\right) \quad (3.74)$$

to acquire a complicated preliminary expression involving square roots of the terms in Eq. (3.54), which we simplify by denesting the square roots. This requires extensive use of the identity

$$\sqrt{2}\sqrt{A+B\sqrt{C}} = \sqrt{A+\sqrt{A^2-B^2C}} + \sqrt{A-\sqrt{A^2-B^2C}} \quad (3.75)$$

which reduces a nested square root into a sum of two square roots, if  $A^2 - B^2C$  is a perfect square. We eventually find Eq. (3.74) in the simplest form to be

$$\mathcal{Q}(z; 1, 1) = \frac{1}{4z^2} \left[ 3\sqrt{2z}\sqrt{1-2z-\sqrt{1-8z}} + \sqrt{2(1+z)}\sqrt{1-2z+\sqrt{1-8z}} - 4z - 2 \right]. \quad (3.76)$$

This generating function is a series in positive powers of  $z$ , as required. Expanding about the origin, we find

$$\mathcal{Q}(z; 1, 1) = 1 + 2z + 7z^2 + 30z^3 + 146z^4 + 772z^5 + 4331z^6 + \mathcal{O}(z^7) . \quad (3.77)$$

Eq. (3.76) is the first key result from this calculation. The coefficients in the power series expansion (3.77) match with the enumerated sums of squared TASEP weights, in the case  $\alpha = \beta = 1$ , for systems of size  $N = (0, 1, 2, 3, \dots)$ .

### Link to path dominance problem

On further investigation, this set of coefficients  $\{q_N\} = \{1, 2, 7, 30, 146, 772, 4331, \dots\}$  matches with those of sequence A196148 in the OEIS [117], which take the form

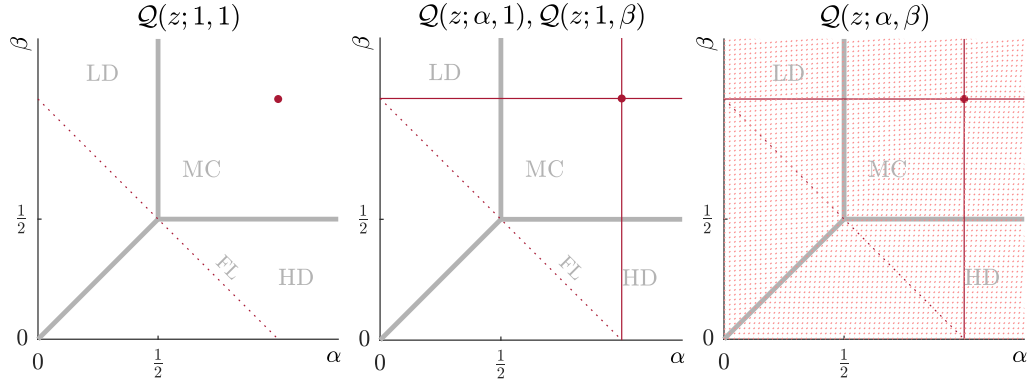
$$q_N = \sum_{P=0}^N \frac{(2N+1)!(N+1)!}{(2P+1)!(2N-2P+1)!(P+1)!(N-P+1)!} . \quad (3.78)$$

From this OEIS reference, we find that expression (3.78) is the known solution to an equivalent problem in the path dominance problem that we discussed in Chapter 2, Section 2.2.1. Specifically, the summand in Eq. (3.78) is the total number of distinct *triples* of paths comprising  $P$  ‘ $\uparrow$ ’ steps and  $(N-P)$  ‘ $\rightarrow$ ’ steps, where one path dominates the two others [89]. Having already proven the equivalence between these two problems, we obtain the more precise result that the summand of Eq. (3.78) is the sum of squared weights for the subset of configurations with  $P$  particles.

With this we return to the main derivation. To summarise so far, we have in Eq. (3.76) a generating function for the sum of squared weights at the point  $\alpha = \beta = 1$  on the phase diagram. With the same method of applying the kernel symmetry in Eq. (3.61) and extracting coefficients, we now extend this approach to find generating functions first for arbitrary  $\alpha$  but  $\beta = 1$ , and subsequently for arbitrary  $\alpha, \beta$  (see Figure 3.4 for the corresponding lines in the phase diagram).

### 3.4.3 $x^+$ coefficient extraction, obtaining $\mathcal{Q}(z; \alpha, 1)$

Having found  $\mathcal{R}(t; 0, 0, 0, 0)$ , we now generalise to  $\mathcal{R}(t; a, a, 0, 0)$ . Once we make a variable transformation, this corresponds to the generating function along the line  $\beta = 1$  which traverses the low density and maximal current phases as  $\alpha$  is varied. Given the recursion relation (3.58), this requires  $\mathcal{R}(t; x, 0, 0, 0)$  (by symmetry,  $\mathcal{R}(t; 0, y, 0, 0)$



**Figure 3.4** The lines and regions in the phase diagram that the generating function covers with increasing generality. The trivial factorisation line (FL) is included.

follows). We return to Eq. (3.62), and obtain an expression for  $\mathcal{R}_0(x, 0)$  by considering the *positive* powers of  $x$ . The LHS is elementary:

$$\{x^+\} \text{ LHS (3.67)} = \frac{x}{t} \quad (3.79)$$

where  $\{x^+\}$  denotes “the positive powers in  $x$  within”. The RHS is more involved, and we explicitly subtract any  $\mathcal{O}(\bar{x})$  terms:

$$\begin{aligned} \{x^+\} \text{ RHS (3.67)} = & \frac{1}{\sqrt{\Delta_0 \Delta_+(x)}} \left[ t(1+x)\mathcal{R}_0(0, 0) - 2t(1+x)^2\mathcal{R}_0(x, 0) - 2 \right. \\ & \left. - x^2 - \bar{x} + \frac{x}{t} \right] + \frac{1}{\sqrt{\Delta_0}} \left[ t\mathcal{R}_0(0, 0) + 2 + \bar{x} + \frac{1}{2}(X_- + X_+) \right]. \quad (3.80) \end{aligned}$$

This gives us an expression for  $\mathcal{R}_0(x, 0)$  in terms of the known  $\mathcal{R}_0(0, 0)$

$$\begin{aligned} \mathcal{R}_0(x, 0) = & -\frac{1}{2t(1+x)^2} \left[ \left( \sqrt{\Delta_0 \Delta_+(x)} - 1 \right) \frac{x}{t} + 2 - t(1+x)\mathcal{R}_0(0, 0) \right. \\ & \left. + x^2 + \bar{x} - \sqrt{\Delta_+(x)} \left( t\mathcal{R}_0(0, 0) + 2 + \bar{x} + \frac{1}{2}(X_- + X_+) \right) \right]. \quad (3.81) \end{aligned}$$

From this, the steps to finding  $\mathcal{Q}(z; \alpha, 1)$  are straightforward. Using Eq. (3.58), we acquire  $\mathcal{R}_0(x, y) = \mathcal{R}(t; x, y, 0, 0)$  from this new result, whereby we find the generating function for the sum of squared weights for the general  $\alpha, \beta = 1$  case after applying

the transformation (3.36). With further algebraic manipulation, we eventually find

$$\mathcal{Q}(z; \alpha, 1) = \frac{1}{1-2z} \mathcal{R} \left( \frac{z}{1-2z}; \frac{1-\alpha}{\alpha}, \frac{1-\alpha}{\alpha}, 0, 0 \right) \quad (3.82)$$

$$= -\frac{\alpha^2}{z(1-\alpha)} - \frac{\sqrt{\Gamma(\alpha)}\alpha^5 \left( 1 + \frac{1}{1-\alpha} + \frac{2\sqrt{\Lambda_-\Lambda_+}}{2z-\sqrt{\Lambda_-\Lambda_+}} - \frac{2z(1-\alpha)}{\sqrt{\Lambda_-\Lambda_+}\alpha} \right)}{\alpha^2(1-\alpha)^2 - z(\alpha^2 + (1-\alpha)^2)} \quad (3.83)$$

$$= 1 + \left( 1 + \frac{1}{\alpha^2} \right) z + \left( 2 + \frac{2}{\alpha} + \frac{2}{\alpha^2} + \frac{1}{\alpha^4} \right) z^2 + \mathcal{O}(z^4) . \quad (3.84)$$

The coefficients of this power series in  $z$  are the sums of squared weights of the TASEP for increasing system size with  $\beta = 1$ , and match with those calculated in Eqs. (3.2), (3.3), (3.6) using the matrix reduction relations.

By the symmetry between  $\alpha$  and  $\beta$ , we also have from Eq. (3.82)  $\mathcal{Q}(z; 1, \beta)$ , whereby  $\alpha$  is fixed and  $\beta$  is variable. This gives us information along two lines in the phase diagram, crossing at  $\alpha = \beta = 1$ .

### 3.5 Generating function for general $\alpha, \beta$ weights, $\mathcal{Q}(z; \alpha, \beta)$

We come at last to the generating function across the full phase diagram,  $\mathcal{Q}(z; \alpha, \beta)$ , for which we require an expression for  $\mathcal{R}(t; a, a, b, b)$ . To attempt to keep the notation concise, we now redefine

$$\mathcal{R}(x, y) \equiv \mathcal{R}(t; x, y, b, b). \quad (3.85)$$

This function obeys the recurrence relation (3.40)

$$K_{xy}\mathcal{R}(x, y) = \frac{1}{(1-bx)(1-by)} + t\bar{x}\bar{y}\mathcal{R}(0, 0) - t(\bar{x}\bar{y} + \bar{x})\mathcal{R}(0, y) - t(\bar{x}\bar{y} + \bar{y})\mathcal{R}(x, 0) . \quad (3.86)$$

This is essentially Eq. (3.58) only for factors of  $b = (1-\beta)/\beta$  in the first term. While this is a more elaborate relation, we are able to employ the same approach to it as in Section 3.4: exploiting the symmetry of the kernel  $K_{xy}$  to obtain a simplified expression, from which we can extract coefficients to obtain a closed form for the generating function. However, compared to the  $\beta = 1$  case of Section 3.4, these additional factors of  $b$  add a surprising degree of algebraic complication to the calculation.



Nonetheless, we use the symmetry property of the kernel in Eq. (3.42) to arrive at

$$\begin{aligned}
& xy\mathcal{R}(x, y) + \bar{y}\mathcal{R}(x, \bar{x}\bar{y}) - \bar{x}\mathcal{R}(\bar{x}\bar{y}, y) \\
&= \frac{1}{\sqrt{\Delta(x)}} \left[ \frac{1}{1 - \bar{y}Y_-(x)} + \frac{1}{1 - y\bar{Y}_+(x)} - 1 \right] \left[ \frac{xy}{(1 - bx)(1 - by)} \right. \\
&\quad \left. + \frac{\bar{y}}{(1 - bx)(1 - b\bar{x}\bar{y})} - \frac{\bar{x}}{(1 - b\bar{x}\bar{y})(1 - by)} + t\mathcal{R}(0, 0) - 2t(1 + x)\mathcal{R}(x, 0) \right] \quad (3.87)
\end{aligned}$$

which recovers Eq. (3.62) in the case  $b = 0$ . We then extract the  $y^0, x^+$  components from Eq. (3.87), to obtain a closed-form expression for  $\mathcal{R}(t; a, a, b, b)$ . This is an algebraically tedious task, however it follows the same method employed in Section 3.4 and as such we defer the details of this coefficient extraction to Appendix B.1.

### 3.5.1 $\mathcal{Q}(z; \alpha, \beta)$ result

Having performed this coefficient extraction, we find an expression for  $\mathcal{R}(t; a, a, b, b)$ , which we quote in Appendix B.1, Eq. (B.31). With further algebraic manipulation, we obtain the full generating function  $\mathcal{Q}(z; \alpha, \beta)$  recalling the transformation (3.36)

$$\mathcal{Q}(z; \alpha, \beta) = \frac{(1 - ab)^2}{1 - 2z} \mathcal{R}\left(\frac{z}{1 - 2z}, \frac{1 - \alpha}{\alpha}, \frac{1 - \alpha}{\alpha}, \frac{1 - \beta}{\beta}, \frac{1 - \beta}{\beta}\right)$$

eventually arriving at

$$\begin{aligned}
\mathcal{Q}(z; \alpha, \beta) = & -\frac{\alpha^2\beta^2}{z(\alpha + \beta - 2\alpha\beta) + (\alpha + \beta - 1 - \alpha\beta)\alpha\beta} + \sqrt{\frac{\Gamma(\alpha)\Gamma(\beta)}{\Lambda_-\Lambda_+}} \times \\
& \left[ \frac{(1 - \alpha - \beta)\alpha\beta z^2 z_0(\alpha) z_0(\beta)}{4(z_0(\alpha) - z)(z_0(\beta) - z)(1 - \alpha)^2(1 - \beta)^2(z[\alpha + \beta - 2\alpha\beta] + \alpha\beta[\alpha + \beta - 1 - \alpha\beta])} \right] \times \\
& \left[ -2\sqrt{1 - 8z}(1 - \alpha - \beta)^2 + 8z(\alpha + \beta - 2\alpha\beta) - 2(\alpha + \beta - 2\alpha\beta - 1)^2 \right. \\
& \quad \left. - (1 - \alpha - \beta)(\sqrt{1 - 8z} + (1 - 2\alpha)(1 - 2\beta))\sqrt{2 + 8z + 2\sqrt{1 - 8z}} \right] \quad (3.88)
\end{aligned}$$

where

$$z_0(\gamma) = \frac{\gamma^2(1 - \gamma)^2}{\gamma^2 + (1 - \gamma)^2} \quad (3.89)$$

and we have also used the definitions in Eqs. (3.54), (3.56). This is the most general result of this chapter. It would be of no surprise if further simplifications to this generating function were found. However, for the purpose of finding the asymptotic

scaling of the power series of  $\mathcal{Q}(z; \alpha, \beta)$ , Eq. (3.88) is sufficient.

Before analysing the full generating function in detail, we notice immediately that upon fixing the function along the factorisation line,  $\beta = 1 - \alpha$ , we recover

$$\mathcal{Q}(z; \alpha, 1 - \alpha) = \frac{1}{1 - z \left( \frac{1}{\alpha^2} + \frac{1}{(1-\alpha)^2} \right)} \quad (3.90)$$

$$= \sum_{N \geq 0} z^N \left( \frac{1}{\alpha^2} + \frac{1}{(1-\alpha)^2} \right)^N \quad (3.91)$$

from the first term in Eq. (3.88); the second term vanishes. This recovers a generating function for the sum of squared weights, for the case discussed in Section 3.2.1 of a Bernoulli distribution, as one would expect given the dynamics along the factorisation line [36]. This serves as one verification of our method. In addition, one can compute the series expansion of  $\mathcal{Q}(z; \alpha, \beta)$  in  $z$ , to verify that its coefficient series is indeed the sums of squared weights for increasing system size, the first few having been directly evaluated in Eqs. (3.2), (3.3), (3.6).

## 3.6 Asymptotic analysis

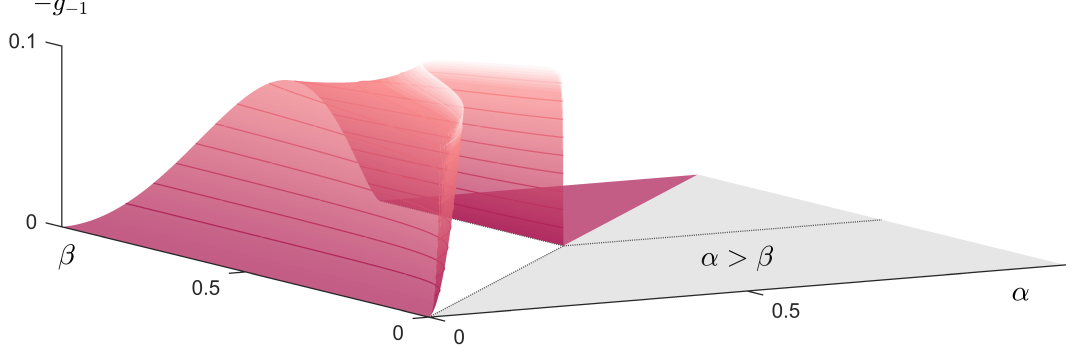
To summarise, we now have in Eq. (3.88) a closed-form expression for the generating function for the sum of squared TASEP weights, Eq. (3.10)

$$\mathcal{Q}(z; \alpha, \beta) = \sum_{N \geq 0} \langle W | \otimes \langle W | (D \otimes D + E \otimes E)^N | V \rangle \otimes | V \rangle z^N.$$

We use this to find the scaling of the sum of squared probabilities, with a view to finding an expression for the  $\lambda = 2$  Rényi entropy from Eq. (1.59). We use standard asymptotic methods, following the formalism outlined in Section 1.6 [10]. Based on the form of  $\mathcal{Q}(z; \alpha, \beta)$  in Eq. (3.88), and  $\mathcal{Q}(z; 1, 1)$  in Eq. (3.76), we expect poles at  $z = z_0(\alpha)$ ,  $z = z_0(\beta)$ , and a branch point at  $z = 1/8$ . Furthermore, we expect the changing of dominant nonanalyticities to coincide with the phase transitions of the TASEP.

### 3.6.1 Low density phase $\alpha < 1/2$ , $\alpha < \beta$

In the low density phase, the first singularity we identify in  $\mathcal{Q}(z; \alpha, \beta)$  is a simple pole, at  $z = z_0(\alpha)$  as defined in Eq. (3.89). We find an elaborate expression for  $g_{-1}$  presented in Appendix B, Eq. (B.32). As there is an  $\alpha$ -dependence in the *location* of the pole



**Figure 3.5** Surface plot of Eq. (B.32), the residue  $g_{-1}$  at  $z = z_0(\alpha)$ . This vanishes moving into the maximal current phase. In the shaded region  $\alpha > \beta$ , a different pole at  $z = z_0(\beta)$  dominates.

$z_0(\alpha)$ , the value of  $\alpha$  affects the Rényi entropy to the leading order.

The vanishing of the residue at  $\alpha = 1/2$ , shown in Figure 3.5, indicates that  $\mathcal{Q}(z; \alpha, \beta)$  is well-behaved at  $z_0(\alpha)$  at this point in the maximal current phase. When probing further we find beyond  $\alpha = 1$ ,  $\beta = 1$  that  $z_0(\alpha)$  again becomes a pole, however not as the singularity closest to the origin.

Focusing on the  $\alpha < 1/2$  region, knowing the position and magnitude of the pole, along with the residue, we use Eq. (1.114) to find the asymptotic scaling of the sum of squared weights

$$\sum_{\mathcal{C}} \mathcal{W}(\mathcal{C})^2 \sim -\frac{g_{-1}}{z_0(\alpha)} \left( \frac{\alpha^2 + (1-\alpha)^2}{\alpha^2(1-\alpha)^2} \right)^N. \quad (3.92)$$

To normalise these squared weights into squared *probabilities*, we divide through Eq. (3.92) by the partition function  $Z_N(\alpha, \beta)$  in Eq. (1.27), squared. Within the low density phase we know the asymptotic form from Eq. (1.29) to be

$$Z_N \sim \frac{\beta(1-2\alpha)}{(\beta-\alpha)(1-\alpha)} \left( \frac{1}{\alpha(1-\alpha)} \right)^N$$

from which we obtain the sum of squared probabilities,

$$\sum_{\mathcal{C}} \mathcal{P}(\mathcal{C})^2 \sim \frac{g_{-1}(1-\alpha)^2(\beta-\alpha)^2}{\beta^2(1-2\alpha)^2} (\alpha^2 + (1-\alpha)^2)^N. \quad (3.93)$$

The  $\lambda = 2$  Rényi entropy  $H_2$  follows, which to leading order is

$$H_2 = -\log \sum_{\mathcal{C}} \mathcal{P}(\mathcal{C})^2 \sim -N \log (\alpha^2 + (1-\alpha)^2) + \mathcal{O}(1) \quad (3.94)$$

and an effective number of configurations with  $e^{H_2}$

$$e^{H_2} \sim \frac{\beta^2(1-2\alpha)^2}{g_{-1}(1-\alpha)^2(\beta-\alpha)^2} \left( \frac{1}{\alpha^2 + (1-\alpha)^2} \right)^N. \quad (3.95)$$

### 3.6.2 High density phase $\beta < 1/2$ , $\beta < \alpha$

By the symmetry of the generating function and of the dynamics of particles and holes in the TASEP, the corresponding results in the high density phase are an  $(\alpha, \beta) \rightarrow (\beta, \alpha)$  mirror of those found in the low density phase.

### 3.6.3 Maximal current phase $\alpha > 1/2$ , $\beta > 1/2$

We find in this phase the dominant singularity to be a branch point, at  $z_1 = 1/8$ . A series expansion of  $\mathcal{Q}(z; \alpha, \beta)$  about this branch point shows the emergence of an imaginary contribution:

$$\mathcal{Q}(z; \alpha, \beta) = ih_{\frac{3}{2}}(\alpha, \beta) \left( z - \frac{1}{8} \right)^{\frac{3}{2}} + \sum_{j \geq 0} h_j \left( z - \frac{1}{8} \right)^j. \quad (3.96)$$

This indicates an algebraic singularity of order  $k = 3/2$ . We find  $h_{\frac{3}{2}}$ , that we quote in Appendix B.2, Eq. (B.33). Using Eq. (1.116), we find the asymptotic scaling of the sum of squared weights

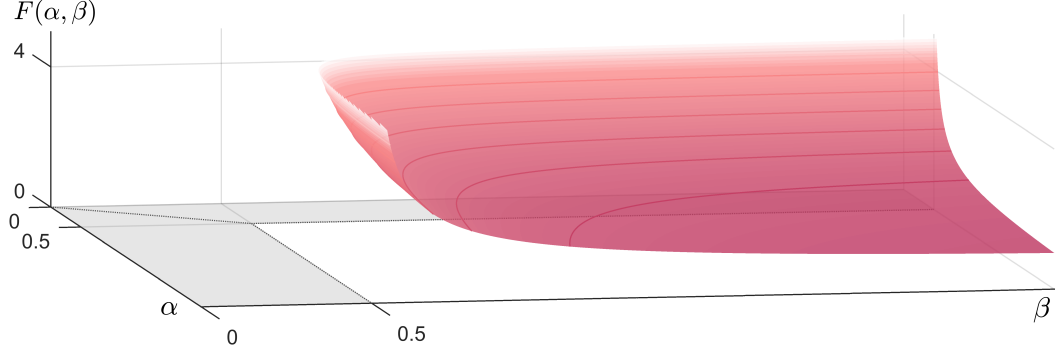
$$\sum_{\mathcal{C}} \mathcal{W}(\mathcal{C})^2 \sim \frac{h_{\frac{3}{2}} \left( \frac{1}{8} \right)^{\frac{3}{2}}}{\Gamma\left(-\frac{3}{2}\right)} \frac{8^N}{N^{\frac{5}{2}}}. \quad (3.97)$$

We normalise this to obtain the sum of squared probabilities using the appropriate asymptotic expression for the partition function from Eq. (1.29)

$$Z_N \sim \frac{4\alpha\beta(\alpha+\beta-1)}{\sqrt{\pi}(2\alpha-1)^2(2\beta-1)^2} \frac{4^N}{N^{\frac{3}{2}}}$$

to obtain a final expression

$$\sum_{\mathcal{C}} \mathcal{P}(\mathcal{C})^2 \sim \frac{1}{F(\alpha, \beta)} \sqrt{\frac{\pi}{2}} \frac{\sqrt{N}}{2^N} \quad (3.98)$$



**Figure 3.6** Surface plot of Eq. (B.34),  $F(\alpha, \beta)$ . Going deeper into the maximal current phase, the effective number of participating configurations  $e^{H_2}$  decreases, towards a constant.  $F$  is divergent on the phase boundaries, however the effective number is well behaved for all  $\alpha, \beta > 1/2$ .

where the prefactor  $F$  (which we quote in the Appendix B.2, Eq. (B.34), see also Figure 3.6) has no dependence on system size  $N$ . Thus the large- $N$  scaling of  $H_2$  is

$$H_2 = -\log \sum_{\mathcal{C}} \mathcal{P}(\mathcal{C})^2 \sim N \log 2 - \frac{1}{2} \log N + \mathcal{O}(1) . \quad (3.99)$$

For large system sizes, the leading contributions to the Rényi entropy become independent of  $\alpha, \beta$ . For the effective number of participating configurations  $e^{H_2}$  [63], however,  $\alpha$  and  $\beta$  arise in the multiplicative factor  $F(\alpha, \beta)$

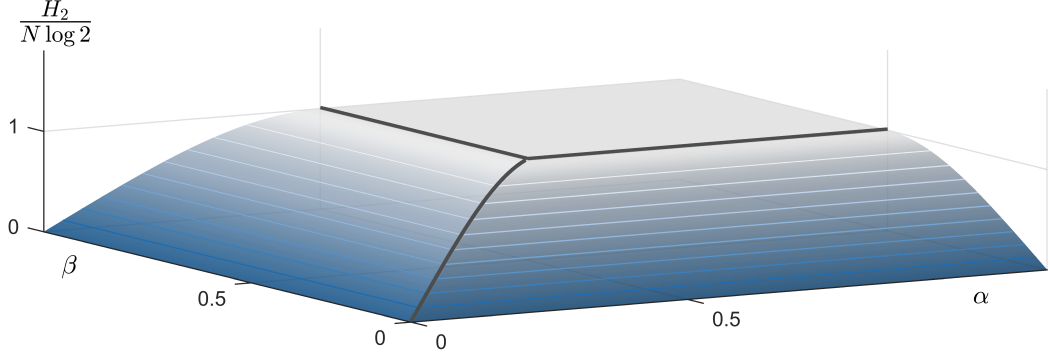
$$e^{H_2} \sim F(\alpha, \beta) \sqrt{\frac{2}{\pi}} \frac{2^N}{\sqrt{N}} . \quad (3.100)$$

To interpret this scaling with system size, recall that the maximal current phase has bulk density  $\rho = 1/2$ . Consider now the asymptotic form of the binomial coefficient [10]

$$\binom{N}{\frac{N}{2}} \sim \sqrt{\frac{2}{\pi}} \frac{2^N}{\sqrt{N}} \quad (3.101)$$

and note the same scaling with  $N$  as the effective number in Eq. (3.100).

Illustrated in Figure 3.6, the prefactor  $F$  is a decreasing function of  $\alpha$  and  $\beta$ , approaching a nonzero constant. In other words as the reservoir parameters increase, the effective number of participating configurations decreases towards a minimum value.



**Figure 3.7** Surface plot of the asymptotic scaling of the Rényi entropy  $H_2$ , across the phase diagram.

For some special cases we obtain neat results for this effective number:

$$e^{H_2}(\alpha, \alpha) \sim \frac{\sqrt{6} (\sqrt{3} + 2\alpha - 1)^2}{2(2\alpha - 1) (\sqrt{3} + 2(2\alpha - 1))} \left[ \sqrt{\frac{2}{\pi}} \frac{2^N}{\sqrt{N}} \right], \quad (3.102)$$

$$e^{H_2}(1, 1) \sim \sqrt{6} \left[ \sqrt{\frac{2}{\pi}} \frac{2^N}{\sqrt{N}} \right], \quad (3.103)$$

$$e^{H_2}(\infty, \infty) \sim \frac{1}{4} \sqrt{6} \left[ \sqrt{\frac{2}{\pi}} \frac{2^N}{\sqrt{N}} \right]. \quad (3.104)$$

### 3.6.4 Rényi entropy across the phase diagram

These results are summarised with a surface plot of  $H_2$  across the phase diagram in Figure 3.7. We find a plateau in this Rényi entropy in the maximal current phase, that arises from the branch point with no  $\alpha$  or  $\beta$  dependence.

### 3.6.5 Bounds on Gibbs-Shannon entropy

The Rényi entropy  $H_\lambda$  is a nonincreasing function of  $\lambda$  [8]. With our results for  $H_2$ , and knowing that  $H_0$  (a trivial measure of the number of accessible TASEP microstates) is  $N \log 2$  across the whole phase diagram, we find bounds on the Gibbs-Shannon entropy (Eq. (1.4)) across the phase diagram:

$$N \log 2 \geq S(\alpha, \beta) \geq -N \log (\alpha^2 + (1 - \alpha)^2) \quad \text{LD}, \quad (3.105)$$

$$N \log 2 \geq S(\alpha, \beta) \geq -N \log (\beta^2 + (1 - \beta)^2) \quad \text{HD}, \quad (3.106)$$

$$N \log 2 \geq S(\alpha, \beta) \geq N \log 2 - \frac{1}{2} \log N \quad \text{MC}. \quad (3.107)$$

### 3.7 Discussion

In Eq. (3.88), we have an elaborate but exact formula for the generating function of the sum of squared weights for the TASEP. In the particular case  $\alpha = \beta = 1$  this simplifies and allows a finite sum expression for the sum of squared weights, Eq. (3.78).

From these expressions we have derived in Eqs. (3.94), (3.99) the large- $N$  behaviour of the  $\lambda = 2$  Rényi entropy. As we shall discuss, the leading order terms in these entropies are what one would obtain from a Bernoulli measure — the system at the same particle density, with correlations absent. While one may anticipate this as the leading order term, the corrections to this order are reflective of correlations in the NESS, which take different forms in the different phases [39]. These in turn give the effective number of participating configurations, Eqs. (3.95), (3.100).

In the high and low density phases, it is known that second-order density correlations (Eq. (1.35)) decay exponentially with distance [39]. In turn, we find the correction to the Bernoulli measure expression to be  $\mathcal{O}(1)$ . In the maximal current phase, however, there is a long-range power law decay: for sites  $i_1$  and  $i_2$  with respective occupations  $\tau_{i_1}$ ,  $\tau_{i_2}$ ,  $\langle (\tau_{i_1} - 1/2)(\tau_{i_2} - 1/2) \rangle \sim |i_1 - i_2|^{-\frac{1}{2}}$  [39]. We in turn find an  $\mathcal{O}(\log N)$  correction in this phase. These corrections represent nonadditive contributions to the Rényi entropy.

It would be interesting to establish how the corrections to the Rényi entropy are intrinsically related to the nature of correlations — specifically, whether one can infer the correction to the Rényi entropy of a system, from the correlations it exhibits.

#### 3.7.1 Rényi entropy of the one-transit walk

One of the motivations of the work in this chapter was how the Rényi entropy manifests in a classical NESS, in comparison with an equilibrium system. We therefore return to the one-transit walk [79], discussed in Chapter 1, Section 1.7.3. To recall, this is an *equilibrium* system of  $C_{N+1}$  configurations, of relevance here because it shares a partition function with the nonequilibrium TASEP (Eq. (1.28)), which we repeat for convenience:

$$Z_N = \sum_{p=1}^N \sum_{q=0}^p \frac{p(2N-p-1)!}{N!(N-p)!} \left(\frac{1}{\alpha}\right)^q \left(\frac{1}{\beta}\right)^{p-q}.$$

We are interested in how the Rényi entropy changes given a different partitioning of the same state space, in particular one with weights that are explicitly Boltzmann-like.

Here, the Rényi entropy is straightforward: using

$$\sum_{\mathcal{C}} \mathcal{W}(\mathcal{C})^\lambda = \sum_{p=1}^N B_{Np} \sum_{q=0}^p \left[ \left( \frac{1}{\alpha} \right)^q \left( \frac{1}{\beta} \right)^{p-q} \right]^\lambda \quad (3.108)$$

$$= Z_N(\alpha^\lambda, \beta^\lambda) \quad (3.109)$$

the entropy of the one-transit walk,

$$H_\lambda = \frac{1}{1-\lambda} \log \frac{Z_N(\alpha^\lambda, \beta^\lambda)}{Z_N(\alpha, \beta)^\lambda} \quad (3.110)$$

is exactly calculable across the full parameter spectrum of  $\alpha, \beta, \lambda$  given knowledge of the partition function (as one expects from an equilibrium system) [66]. However, this alludes to the unique feature of the equilibrium Rényi entropy: in the limit of large  $N$  we find nonanalyticities in  $Z_N$  along the lines

- $\alpha = \beta < 1/2$  (LD  $\leftrightarrow$  HD transition);
- $\alpha = 1/2, \beta > 1/2$  (LD  $\leftrightarrow$  MC);
- $\beta = 1/2, \alpha > 1/2$  (HD  $\leftrightarrow$  MC);

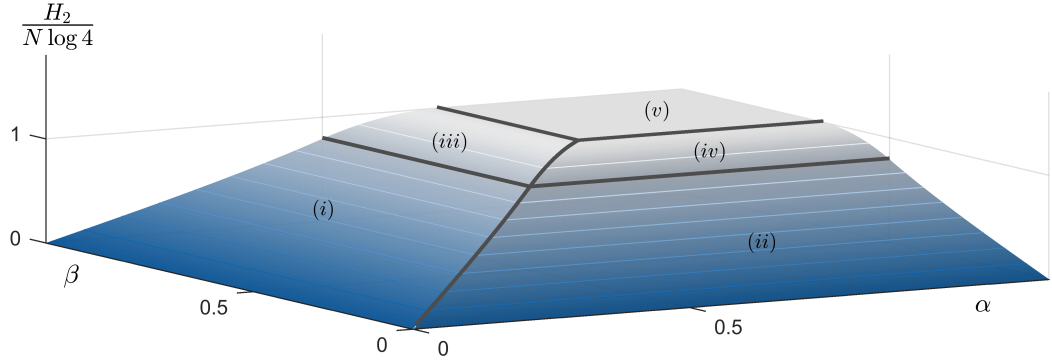
which draw out the phase diagram in Figure 1.3. However, we then anticipate further nonanalyticities from the  $Z_N(\alpha^\lambda, \beta^\lambda)$  term, along

- $\alpha^\lambda = \beta^\lambda < 1/2$ ;
- $\alpha^\lambda = 1/2, \beta^\lambda > 1/2$ ;
- $\beta^\lambda = 1/2, \alpha^\lambda > 1/2$ .

For the case  $\lambda = 2$  we apply the known asymptotic forms of the partition function in Eq. (1.29) to the Rényi entropy formula in Eq. (3.110) to find to leading order in  $N$  (Figure 3.8)

$$H_2 \sim \begin{cases} N \log((1-\alpha^2)/(1-\alpha)^2) & \text{(i) if } \alpha < \beta, \alpha < 1/2 \\ N \log((1-\beta^2)/(1-\beta)^2) & \text{(ii) if } \alpha > \beta, \beta < 1/2 \\ N \log((4\alpha)^2(1-\alpha^2)) & \text{(iii) if } \alpha < \beta, 1/2 < \alpha < 1/\sqrt{2} \\ N \log((4\beta)^2(1-\beta^2)) & \text{(iv) if } \alpha > \beta, 1/2 < \beta < 1/\sqrt{2} \\ N \log 4 & \text{(v) if } \alpha, \beta > 1/\sqrt{2} \end{cases} \quad (3.111)$$





**Figure 3.8** Surface plot of the asymptotic scaling of the Rényi entropy  $H_2$  of the equilibrium one-transit walk, across the phase diagram.

giving *five* different scaling regions in  $H_\lambda$ . As expected from Eq. (1.62), for each phase transition in the partition function, we find *two* nonanalyticities in the Rényi entropy. The *absence* of these secondary lines in the TASEP, then, serves as a verification that the microstate distribution can not be furnished as an equilibrium-like distribution with a temperature-like parameter, otherwise secondary lines would appear in the Rényi entropy.

A question that naturally arises is whether there is a deep underlying reason for this to be the case. The presence of the secondary transition relies on each and every microstate having a Boltzmann weight; a perturbation of a single microstate weight away from this leads to Eq. (3.110) no longer holding. As such, the Rényi entropy may serve as a test as to whether a system is in or out of equilibrium, given its microstate distribution.

### 3.7.2 Higher-order Rényi entropies

This path enumeration approach to sums of TASEP weights can be generalised to arbitrary integer power. Extending the tensor product formalism in Eq. (3.1), the sum of weights to the  $\lambda^{\text{th}}$  power can be written

$$\sum_{\mathcal{C}} \mathcal{W}(\mathcal{C})^\lambda = \langle V |^{\otimes \lambda} (D^{\otimes \lambda} + E^{\otimes \lambda})^N | V \rangle^{\otimes \lambda} \quad (3.112)$$

where  $A^{\otimes \lambda}$  denotes the repeated tensor product

$$A^{\otimes \lambda} = \underbrace{A \otimes \cdots \otimes A}_{\lambda} . \quad (3.113)$$

From the explicit ladder operator representation of  $D$  and  $E$  in Eq. (3.14), this then is equivalent to a problem of enumerating the  $\lambda$ -dimension walks in the upper *orthant*, comprising the  $2^{1+\lambda}$  steps from

$$\prod_{q=1}^{\lambda} (1 + g_q) + \prod_{q=1}^{\lambda} (1 + g_q^{\dagger}) . \quad (3.114)$$

Even in two dimensions, the step set  $\{\uparrow, \downarrow, \rightarrow, \leftarrow, \swarrow, \searrow\}$  has proven one of the more challenging step sets to solve. The enumeration of  $\lambda = 3$  *octant* walks in general is a current area of research [118], but for this particular classification of walk in  $\lambda = 3$  or higher, no analytical techniques are known. Nonetheless, our work on the  $\lambda = 2$  case gives us an insight, and allows us to make some conjectures about these higher-order entropies.

We showed in Section 3.2.1 that along the factorisation line  $\alpha + \beta = 1$  we can write in Eq. (3.13) a simple expression for all Rényi entropies. This is simply the result of a Bernoulli measure for the stationary state. We notice that in the case  $\lambda = 2$  the same expression gives the leading-order term in the exact expressions (3.94), (3.99), when we take  $\rho$  to be the density within the bulk of the system,  $\rho = \alpha, (1 - \beta), 1/2$  in the high density, low density and maximal current phases respectively. We thus conjecture that in the low density and high density phases, the leading scaling with system size  $N$  for all Rényi entropies is given by a Bernoulli measure, Eq. (3.13):

$$\text{LD} \quad H_{\lambda} = \frac{N}{1 - \lambda} \log \left( \alpha^{\lambda} + (1 - \alpha)^{\lambda} \right) + \mathcal{O}(1) , \quad (3.115)$$

$$S = -N (\alpha \log \alpha + (1 - \alpha) \log (1 - \alpha)) + \mathcal{O}(1) , \quad (3.116)$$

$$\text{HD} \quad H_{\lambda} = \frac{N}{1 - \lambda} \log \left( \beta^{\lambda} + (1 - \beta)^{\lambda} \right) + \mathcal{O}(1) , \quad (3.117)$$

$$S = -N (\beta \log \beta + (1 - \beta) \log (1 - \beta)) + \mathcal{O}(1) . \quad (3.118)$$

Within the maximal current phase we conjecture that for *all*  $\lambda \geq 1$ , the leading behaviours are

$$H_{\lambda} \sim N \log 2 - \frac{1}{2} \log N + \mathcal{O}(1) , \quad (3.119)$$

$$e^{H_{\lambda}} \propto \frac{2^N}{\sqrt{N}} , \quad (3.120)$$

so that the leading correction is logarithmic in system size with the prefactor  $1/2$  arising from the square root. To understand this conjecture we note that the behaviour of the effective numbers in Eq. (3.120) would be the asymptotic scaling of the binomial

coefficient  $\binom{N}{N/2}$ . This binomial coefficient gives the number of half-filled configurations, which are the configurations expected to dominate the maximal current phase.

As a check of the conjecture for the high and low density phases in Eqs. (3.115)–(3.118), we consider the  $\lambda \rightarrow \infty$  entropy,  $H_\infty$ . Taking this limit for the case of a Bernoulli measure, Eq. (3.13), we find

$$H_\infty = \lim_{\lambda \rightarrow \infty} \frac{N}{1-\lambda} \log \left( \rho^\lambda + (1-\rho)^\lambda \right) = \begin{cases} -N \log(1-\rho) & \text{if } \rho < \frac{1}{2} \\ -N \log \rho & \text{if } \rho > \frac{1}{2} \end{cases} \quad (3.121)$$

Generally, assuming no degeneracy in the maximum probability  $\max \{P(\mathcal{C})\}$  within the distribution,  $H_\infty$  is equal to  $-\log(\max \{P(\mathcal{C})\})$ . In the low density phase of the TASEP, for large system sizes, the most probable of the  $2^N$  available configurations is an entirely empty system, that has weight  $\mathcal{W} = \langle W|E \cdots E|V \rangle = (1/\alpha)^N$ . By normalising the weight of this empty configuration with Eq. (1.29), we find  $H_\infty$  in this phase to be

$$H_\infty \sim -N \log(1-\alpha) - \log \frac{(1-\alpha)(\beta-\alpha)}{\beta(1-2\alpha)} \quad (3.122)$$

thus the leading-order term is the Bernoulli measure result, Eq. (3.121). The high density result is obtained by similar means, where the most probable configuration is one with every site occupied. Thus the Bernoulli measure result correctly gives the leading-order term for at least the cases  $\lambda = 2, \infty$  (and trivially  $\lambda = 0$ ).

### 3.8 Summary

In this chapter, we have performed a calculation of the  $\lambda = 2$  Rényi entropy of the TASEP for arbitrary entry and exit rates  $\alpha, \beta$ , by deriving the generating function of the sum of squared TASEP weights. Using an explicit matrix representation, we mapped the sum of squared TASEP weights to a two-dimension random walk problem in the upper-quarter plane with absorbing boundaries, which we solved using a generalisation of the obstinate kernel method.

From an asymptotic analysis of the generating function we have found the Rényi entropy to have different scaling for different values of  $\alpha, \beta$ , coinciding as anticipated with the known phase diagram. The leading term of the entropy is consistent with the bulk density across the three phases, with the second order correction indicative of the correlations present. This entropy is structurally distinct to that of any equilibrium system, highlighting a distinction between equilibrium and nonequilibrium probability distributions.

## Chapter 4

# Rényi entropy of the TASEP in the continuum limit

### 4.1 Orientation

In the previous chapter, we found the  $\lambda = 2$  Rényi entropy of the TASEP by using the obstinate kernel method [114]. A drawback of this method was the density of the required algebra; while we eventually found in Eq. (3.88) a closed-form expression for the generating function  $\mathcal{Q}$  for the sum of squared TASEP weights, it was too unwieldy to invert exactly. This is a motivation for the work in this chapter, where we attempt to solve the *continuum limit* of this sum of squared weights problem. We take the discrete walks with absorbing boundaries that we solved in Chapter 3, and investigate their *continuum limit* behaviour. This leads us to diffusion processes.

The primary motivation of taking the continuum limit is that random walk problems often simplify in the continuum limit, as we essentially take an approximation of the random walk [67]. We saw in Section 1.5.3 that, upon associating time and length scales to a discrete walk, the master equation describing the probability distribution can be written as an infinite Taylor series. This involves derivatives with respect to space and time coordinates. In the continuum limit, we take the limit of these length scales approaching zero, upon which all terms higher than the first derivative in time and second derivatives in space vanish. This simplifies the problem, and often allows a closed-form solution to be found. One clear example of this simplification will be seen in Chapter 5.

Following a similar structure to Chapter 3, before presenting the full two-dimensional calculation we first examine the partition function in this continuum limit. From the bicoloured Motzkin path problem in Section 3.3.1, we find the equivalent continuum problem here to be a 1D diffusion with absorbing boundaries, and the probability distribution function is solved directly by a method of images. Extending to the sum of squared weights, we find a 2D diffusion with absorbing boundary conditions, from which we seek the time-dependent probability distribution. This diffusion is anisotropic, in a way that makes it resistant to solution by any image-based approach. Instead, we find the relevant *Laplace transform* by a novel method. This method, like the obstinate kernel method, exploits the symmetry of a *kernel* to simplify a functional relation that otherwise has insufficient information to be solved.

In fact, the steps in this calculation are *analogous* to the obstinate kernel method, but applied to a continuous space. Because of this close relation, we will frequently cross-reference and draw comparison with parts of the calculation in the previous chapter.

After a variable transformation, we find from the resulting Laplace transform a function that approximates the generating function, which we denote  $\mathcal{Q}_C$ , in the vicinity of the tricritical point  $\alpha = \beta = 1/2$  of the TASEP phase diagram, where the three dynamical phases coincide. We will define this as the *scaling region*. In contrast with the discrete case, this continuum result is sufficiently simple that we can simply read off its nonanalyticities. Using this, we recover to second order the known asymptotic behaviour of the sum of squared TASEP weights about the triple point.

We begin with calculation of the TASEP partition function in the continuum limit.

## 4.2 Introductory calculation: continuum limit of partition function

We saw in Section 3.3.1 that from an explicit matrix representation, the generating function of the TASEP partition function can be written out explicitly (introducing a subscript  $D$  to denote “discrete”)

$$\begin{aligned} \mathcal{Z}_D(z) &\equiv \sum_{N \geq 0} Z_N z^N \\ &= (1 - ab) \sum_{N \geq 0} \sum_{i \geq 0} \sum_{k \geq 0} z^N a^i b^k \langle i | (g + g^\dagger + 2)^N | k \rangle . \end{aligned} \tag{4.1}$$

We recall the shorthand  $a = (1 - \alpha)/\alpha$ ,  $b = (1 - \beta)/\beta$ . From Chapters 2 and 3 we know that the summand of Eq. (4.1) is an enumeration of bicoloured Motzkin paths, which we can write in terms of a probability  $\mathcal{P}$ :

$$\mathcal{P}(k|i; N) = \frac{\langle i|(g + g^\dagger + 2)^N|k\rangle}{4^N}. \quad (4.2)$$

$\mathcal{P}(k|i; N)$  is the probability of finding a 1D walker at position  $k$  after taking  $N$  steps from  $i$  from the evenly-weighted step set  $\{\uparrow, \downarrow, \times, \cdot\}$ , with an absorbing boundary  $\mathcal{P}(-1|i; N) = 0$ . The factor  $4^N$  is the number of distinct walks of length  $N$ , in the absence of this absorbing boundary.

With this, we rewrite Eq. (4.1)

$$\mathcal{Z}_D(z) = \frac{\sum_{N \geq 0} \sum_{i \geq 0} \sum_{k \geq 0} z^N a^i b^k 4^N \mathcal{P}(k|i; N)}{\sum_{p \geq 0} (ab)^p}. \quad (4.3)$$

We rewrite  $(1 - ab)$  as  $1/\sum_{p \geq 0} (ab)^p$ .

The probability obeys the master equation

$$\mathcal{P}(k|i; N+1) = \frac{1}{2}\mathcal{P}(k|i; N) + \frac{1}{4}\mathcal{P}(k-1|i; N) + \frac{1}{4}\mathcal{P}(k+1|i; N). \quad (4.4)$$

We now take the time and space continuum limit of this relation. We scale the path length  $N$  to a continuous time-like variable  $\tau$ , and the lattice coordinates  $i, k$  to coordinates  $x, x^{(0)}$  on a continuous space. Using the method outlined in Section 1.5.3 (see also Figure 1.6), we arrive at the diffusion equation

$$\partial_\tau \mathcal{P}(x|x^{(0)}; \tau) = \frac{1}{4} \partial_x^2 \mathcal{P}(x|x^{(0)}; \tau). \quad (4.5)$$

The factor of  $1/4$  arises from the two non-movement steps; every other step on average is a non-movement, which in the continuum limit corresponds to a lower diffusivity.

With this interpretation of  $\mathcal{P}$  in the continuum limit, Eq. (4.1) has a corresponding continuum limit form, found by replacing each summation with an integral spanning the new space, and replacing the probability with the continuous probability density function:

$$\mathcal{Z}_C(z) = \frac{\int_0^\infty d\tau \int_0^\infty dx^{(0)} \int_0^\infty dx z^\tau a^{x^{(0)}} b^x 4^\tau \mathcal{P}(x|x^{(0)}; \tau)}{\int_0^\infty dp (ab)^p}. \quad (4.6)$$

We introduce the subscript  $C$  to denote the continuum limit. Having replaced these discrete summations with integrals over the same space, the numerator of Eq. (4.6)

is now a Laplace transform in disguise. Adopting a more familiar notation, then, we define a new quantity  $G$  as the explicit Laplace transform of the distribution

$$G(s; u, f) \equiv \int_0^\infty d\tau e^{-s\tau} \int_0^\infty dx^{(0)} e^{-fx^{(0)}} \int_0^\infty dx e^{-ux} \mathcal{P}(x|x^{(0)}; \tau) \quad (4.7)$$

which relates to  $\mathcal{Z}_C(z)$  as

$$\mathcal{Z}_C(z) = \frac{G(-\log 4z; -\log b, -\log a)}{\int_0^\infty dp (ab)^p}. \quad (4.8)$$

For a closed-form expression for  $\mathcal{Z}_C(z)$ , we essentially require the Laplace transform in  $x$ ,  $x^{(0)}$  and  $\tau$  of the distribution  $\mathcal{P}(x|x^{(0)}; \tau)$  that obeys Eq. (4.5).

### Scaling region

Before proceeding, we consider when we should expect results from this continuum limit approach to converge to the discrete result. Comparing the continuum limit equation (4.6) to that derived from the matrix product approach in Eq. (4.3), we wish to approximate geometric sums of the form

$$\sum_{k \geq 0} c^k = \frac{1}{1-c}, \quad |c| < 1 \quad (4.9)$$

by integrals

$$\int_0^\infty dk c^k = -\frac{1}{\log c}, \quad 0 < c < 1 \quad (4.10)$$

using the natural logarithm. This result diverges as  $c \rightarrow 1$ , which we see from a series expansion about  $c = 1$ :

$$-\frac{1}{\log c} = \frac{1}{1-c} - \frac{1}{2} - \frac{1}{12}(1-c) + \mathcal{O}(1-c)^2. \quad (4.11)$$

This expansion tells us that Eqs. (4.9) and (4.10) both have poles at  $c = 1$ , with residue 1, thus the continuum integral provides a reasonable approximation to the discrete summation in this *scaling region*. For the integrals in Eq. (4.6), this corresponds to the vicinity of  $a = b = 1$ , or equivalently  $\alpha = \beta = 1/2$  (see Figure 3.2). We therefore expect the following approximations to converge near this region of the phase diagram, where the three dynamical phases converge.

### 4.2.1 Solution for $\mathcal{Z}_C(z; \alpha, \beta)$

We return to the problem of solving this one-dimensional diffusion, specifically, an expression for the Laplace transform  $G$  in Eq. (4.7). We present two different approaches: first, we directly solve the diffusion equation for  $\mathcal{P}$  by a standard method of images [70]. Secondly, we find  $G$  directly, by a method analogous to the kernel method [115], employed in Section 3.3.1. This second method proves a useful introductory exercise for what we later employ to solve the equivalent two-dimensional squared weights problem.

#### Solution by images

As well as satisfying Eq. (4.5), the probability distribution has a delta function initial condition, centred at  $x^{(0)}$

$$\mathcal{P}(x|x^{(0)}; 0) = \delta(x - x^{(0)}) \quad (4.12)$$

and an absorbing boundary at  $x = 0$

$$\mathcal{P}(0|x^{(0)}; \tau) = 0 . \quad (4.13)$$

Eq. (4.5) has the fundamental solution, that is one neglecting the boundary conditions:

$$\mathcal{P}(x|x^{(0)}; \tau) = \frac{1}{\sqrt{\pi\tau}} e^{-(x-x^{(0)})^2/\tau} \quad (4.14)$$

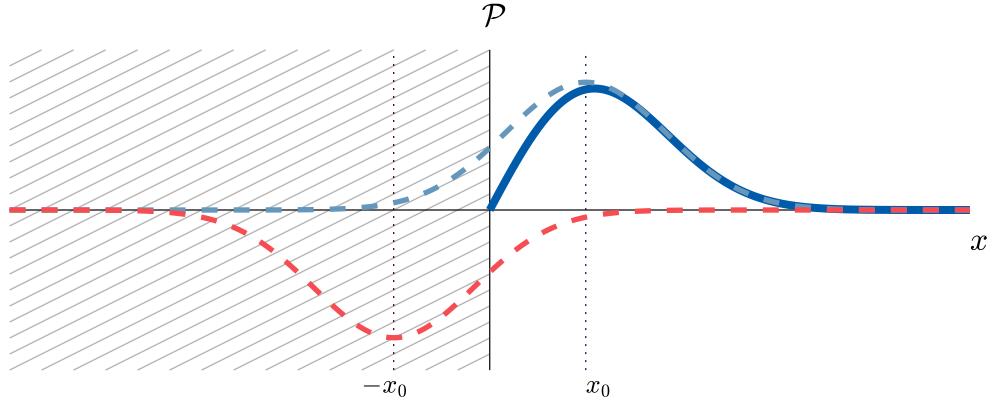
which is easily checked by differentiation. This is of course a normalised Gaussian distribution centred at  $x^{(0)}$ , with a width that grows with time  $\tau$ . We then satisfy the boundary condition (4.13) by placing a negative *image* at  $-x^{(0)}$ , *outside* of the physical region:

$$\mathcal{P}(x|x^{(0)}; \tau) = \frac{1}{\sqrt{\pi\tau}} \left( e^{-(x-x^{(0)})^2/\tau} - e^{-(x+x^{(0)})^2/\tau} \right) , \quad (4.15)$$

see Figure 4.1. At  $x = 0$ , the two terms cancel and the boundary probability is zero at all times. The total area under the physical curve is equal to or less than that of the fundamental curve because, over time, probability is lost at the absorbing boundary.

With this solution for  $\mathcal{P}$ , we would then take Laplace transforms to arrive at an expression for  $G$ , which entails a straightforward set of integrals. However, we will





**Figure 4.1** A physical solution (blue, filled), to the 1D diffusion equation, with a fundamental solution (blue, dashed) combined with an image (red, dashed) beyond the physical region  $x > 0$ .

instead consider our second approach to find  $G$ , which avoids having to solve for  $\mathcal{P}$  directly.

### Solution by a kernel method

We return to the original diffusion equation (4.5), and take Laplace transforms. To lighten the notation, we introduce the shorthand  $\hat{\mathcal{L}}$  for a Laplace transform:

$$\hat{\mathcal{L}}_{\tau}[\cdot] \equiv \int_0^{\infty} d\tau e^{-s\tau}[\cdot], \quad (4.16)$$

$$\hat{\mathcal{L}}_{x^{(0)}}[\cdot] \equiv \int_0^{\infty} dx^{(0)} e^{-fx^{(0)}}[\cdot], \quad (4.17)$$

$$\hat{\mathcal{L}}_x[\cdot] \equiv \int_0^{\infty} dx e^{-ux}[\cdot], \quad (4.18)$$

with a set of conjugate variables  $(s, u, f)$  for  $(\tau, x, x^{(0)})$  respectively. For convenience we quote two well-known Laplace transform identities that will be used (here  $\lambda$  is the conjugate variable of  $c$ ) [119]:

$$\hat{\mathcal{L}}[\partial_c f(c)] = \hat{\mathcal{L}}[f(c)] - f(0), \quad (4.19)$$

$$\hat{\mathcal{L}}[\partial_c^2 f(c)] = \lambda^2 \hat{\mathcal{L}}[f(c)] - \lambda f(0) - [\partial_c f(c)]_{c=0}. \quad (4.20)$$

To begin, then, the Laplace transform of the diffusion equation (4.5) in the variable  $\tau$  is

$$s\hat{\mathcal{L}}_{\tau}\mathcal{P} - \delta(x - x^{(0)}) = \frac{1}{4}\hat{\mathcal{L}}_{\tau}\partial_x^2\mathcal{P} \quad (4.21)$$

having used the initial condition (4.12). We now transform in  $x^{(0)}$ :

$$s\hat{\mathcal{L}}_t\hat{\mathcal{L}}_{x^{(0)}}\mathcal{P} - e^{-fx}\theta(x) = \frac{1}{4}\hat{\mathcal{L}}_t\hat{\mathcal{L}}_{x^{(0)}}\partial_x^2\mathcal{P} , \quad (4.22)$$

and finally in  $x$ :

$$\left(s - \frac{1}{4}u^2\right) G(s; u, f) = \frac{1}{f+u} - \frac{1}{4}\hat{\mathcal{L}}_\tau\hat{\mathcal{L}}_{x^{(0)}} \left[ \partial_{x'}\mathcal{P}(x'|x^{(0)}; \tau) \right]_{x'=0} \quad (4.23)$$

having applied the boundary condition (4.13). This gives the Laplace transform of  $\mathcal{P}$  in terms of the *derivative* of  $\mathcal{P}$  evaluated at the boundary (which is not necessarily zero even though  $\mathcal{P}$  is).

This functional equation (4.23) draws parallels with the relation we saw in the discrete case in Section 3.3.1, Eq. (3.22). There, we employed a pole-cancelling method to fix an unknown quantity. We identify a similar method here.

We notice that  $G(s; u, f)$  exhibits *a priori* two poles in  $s$  at  $s = u^2/4$ . In this case, if we simply set  $u = \sqrt{2s}$  we cancel the LHS:

$$0 = \frac{1}{f+2\sqrt{s}} - \frac{1}{4}\hat{\mathcal{L}}_\tau\hat{\mathcal{L}}_{x^{(0)}} \left[ \partial_{x'}P(x'|x^{(0)}; \tau) \right]_{x'=0} . \quad (4.24)$$

We immediately find the last term in Eq. (4.23), and thus an explicit solution for  $G$ :

$$G(s; u, f) = \frac{1}{s - \frac{1}{4}u^2} \left( \frac{1}{f+u} - \frac{1}{f+2\sqrt{s}} \right) \quad (4.25)$$

$$= \frac{4}{(f+u)(f+2\sqrt{s})(u+2\sqrt{s})} . \quad (4.26)$$

Notice that this is manifestly symmetric in the respective conjugate variables  $u$  and  $f$  for the initial and final coordinates. From this expression, we obtain a simple closed form for  $\mathcal{Z}_C(z; \alpha, \beta)$  with a set of variable changes as for Eq. (4.8)

$$\mathcal{Z}_C(z; \alpha, \beta) = \frac{G(-\log 4z; -\log b, -\log a)}{\int_0^\infty dp (ab)^p} \quad (4.27)$$

$$= \frac{4}{(\log b - 2\sqrt{-\log 4z})(\log a - 2\sqrt{-\log 4z})} . \quad (4.28)$$

#### 4.2.2 Asymptotic analysis

We now analyse  $\mathcal{Z}_C$  to obtain the asymptotic scaling of the partition function  $Z_N$ , treating  $\mathcal{Z}_C$  as if it were an approximation to the exact generating function  $\mathcal{Z}_D$ . We

expect to recover physical properties of the TASEP close to the triple point  $\alpha = \beta = 1/2$ . As usual for the asymptotic analysis we use formalism established in Section 1.6.3.

Before proceeding with the detail, we can read off from Eq. (4.28) the nonanalyticities we expect to see: there are two potential zeros in  $(\log b - 2\sqrt{-\log 4z})$ ,  $(\log a - 2\sqrt{-\log 4z})$ , and a branch point at  $z = 1/4$ . By showing which of these are present and/or dominant for different  $\alpha, \beta$ , we will recover the TASEP phase diagram.

### Low density phase $\alpha < 1/2, \alpha < \beta$ ( $a > 1, a > b$ )

We begin in the low density phase. Within this region, the dominant singularity in  $\mathcal{Z}_C(z)$  is a simple pole, at the point

$$\log a - 2\sqrt{-\log 4z} = 0. \quad (4.29)$$

If  $a < 1$  (beyond the LD phase),  $\log a < 0$  and this has no solution. Within the LD phase  $a > 1$ , we find

$$z^* = \frac{1}{4} \exp\left(-\frac{1}{4} \log^2 a\right). \quad (4.30)$$

This is a monotonically decreasing function of  $a$ . If both  $a, b$  are greater than 1, then, the dominant pole is from whichever of  $a$  or  $b$  is largest. A Taylor series of  $\mathcal{Z}_C$  about this pole yields

$$\mathcal{Z}_C(z) = \frac{2z^* \log a}{\log(b/a)} \frac{1}{(z - z^*)} + \mathcal{O}((z - z^*)^0) \quad (4.31)$$

which gives the asymptotic scaling of the partition function in this phase

$$Z_N \sim \frac{2 \log a}{\log(a/b)} \left[ 4 \exp\left(\frac{1}{4} \log^2 a\right) \right]^N. \quad (4.32)$$

Given this, we obtain an expression for the current from the ratio  $J = Z_{N-1}/Z_N$

$$J_C = \frac{1}{4} \exp\left[-\frac{1}{4} \log^2\left(\frac{1-\alpha}{\alpha}\right)\right] \quad (4.33)$$

$$= \frac{1}{4} - \left(\alpha - \frac{1}{2}\right)^2 - \frac{2}{3} \left(\alpha - \frac{1}{2}\right)^4 + \mathcal{O}\left(\left(\alpha - \frac{1}{2}\right)^6\right). \quad (4.34)$$

To clarify,  $J_C$  is an *estimation* of the asymptotic scaling of the current for large system sizes. However, we already know the *exact* asymptotic scaling from analysis of the

partition function (Eq. (1.33)):

$$J_D \sim \frac{1}{4} - \left( \alpha - \frac{1}{2} \right)^2. \quad (4.35)$$

To second order about  $\alpha = 1/2$ , then, we recover the appropriate scaling of the current (see Figure 4.2).

### High density phase $\beta < \alpha$ , $\beta < 1/2$

Using the  $\alpha \leftrightarrow \beta$  symmetry in the TASEP, the result in the high density phase is an  $(\alpha, \beta) \rightarrow (\beta, \alpha)$  mirror of the low density phase.

### Maximal current phase $\alpha > 1/2$ , $\beta > 1/2$ ( $-1 < a < 1$ , $-1 < b < 1$ )

In this phase, neither of the two aforementioned poles exist, and instead the dominant singularity is a branch point at  $z^* = 1/4$  at order  $k = 1/2$ . A Taylor expansion about this point yields

$$\mathcal{Z}_C(z) = \frac{4}{\log a \log b} + \frac{16 \log ab}{(\log a \log b)^2} i(z - z^*)^{\frac{1}{2}} + \mathcal{O}(z - z^*) \quad (4.36)$$

thus in this phase, the partition function scales as

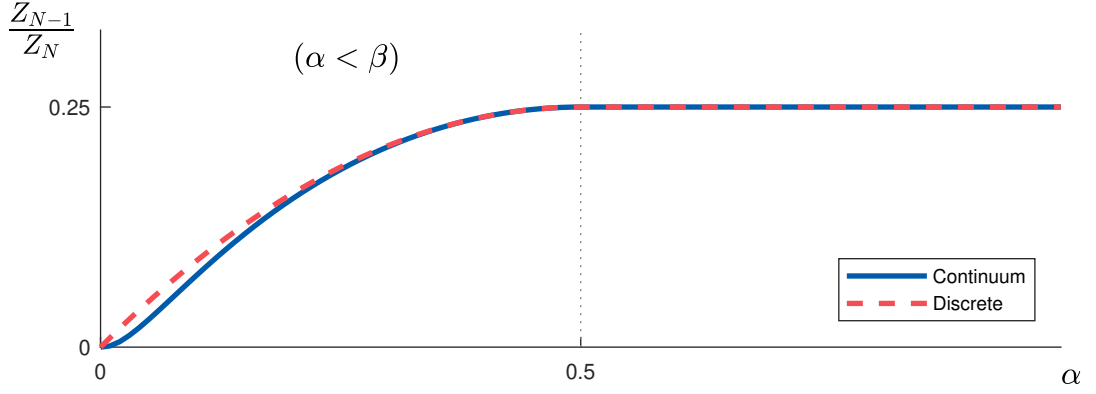
$$Z_N \sim -\frac{4}{\sqrt{\pi}} \frac{\log ab}{(\log a \log b)^2} \frac{4^N}{N^{\frac{3}{2}}}. \quad (4.37)$$

This scaling law  $Z_N \propto 4^N N^{-\frac{3}{2}}$  is the same as we calculated in the discrete case, Eq. (1.29). This time the current  $J$  is simply

$$J_C \sim \frac{1}{4} \quad (4.38)$$

which is the known asymptotic limit in the maximal current phase.

To summarise this exercise, we have calculated a continuum limit approximation of the partition function generating function by a rescaling of the original bicoloured Motzkin paths from Section 3.3.1 to a one-dimensional diffusion. By either solving the diffusion directly or using a kernel ‘trick’, we have found a very simple result for  $\mathcal{Z}_C$  in Eq. (4.28), where the asymptotic scaling of  $Z_N$  is clear by inspection. This approximation of the generating function recovers the phase diagram and current scaling (Figure 4.2) around  $\alpha = \beta = 1/2$ .



**Figure 4.2** Asymptotic form of the current  $J = Z_{N-1}/Z_N$ , across the LD-MC phase transition (with  $\beta > 1/2$ ). The dotted grey line indicates the LD-MC phase transition.

This calculation was straightforward as the underlying diffusion was one dimensional, with a single absorbing boundary. We will now see how the equivalent generating function for the sum of squared weights of the TASEP entails a much more elaborate calculation.

### 4.3 Sum of squared weights calculation

We seek the continuum limit generating function for the sum of squared weights of the TASEP. To make progress, we employ a novel method analogous to the obstinate kernel method that was the focus of Chapter 3, and successfully find a closed-form solution for the generating function.

#### 4.3.1 Taking a continuum limit

To recall, the sum of squared TASEP weights  $Q_N = \sum_C \mathcal{W}(C)^2$  has a corresponding generating function that can be written explicitly (Eq. (3.32))

$$\begin{aligned}
 Q_D(z) &= \sum_{N \geq 0} Q_N z^N \\
 &= \frac{\sum_{N \geq 0} \sum_{i \geq 0} \sum_{j \geq 0} \sum_{k \geq 0} \sum_{l \geq 0} z^N a^{i+j} b^{k+l} \langle i | \langle j | (\mathcal{V} + 2)^N | k \rangle | l \rangle}{\left( \sum_{p \geq 0} (ab)^p \right)^2} \quad (4.39)
 \end{aligned}$$

where  $\langle i|\langle j|(\mathcal{V}+2)^N|k\rangle|l\rangle$  is an enumeration of 2D paths. Like the 1D case, we define a probability

$$\mathcal{P}(k, l|i, j; N) = \frac{\langle i|\langle j|(\mathcal{V}+2)^N|k\rangle|l\rangle}{8^N}. \quad (4.40)$$

$\mathcal{P}(k, l|i, j; N)$  is the probability of finding a walker at  $(k, l)$ , after  $N$  steps from the evenly-weighted step set  $\{\nearrow, \rightarrow, \uparrow, \swarrow, \leftarrow, \downarrow, \times, \cdot\}$ , having started at  $(i, j)$ , in the upper-quarter plane with absorbing boundaries. This probability obeys the master equation

$$\begin{aligned} \mathcal{P}(k, l|i, j; N+1) = & \frac{1}{4}\mathcal{P}(k, l|i, j; N) + \frac{1}{8}\mathcal{P}(k-1, l|i, j; N) + \frac{1}{8}\mathcal{P}(k, l-1|i, j; N) \\ & + \frac{1}{8}\mathcal{P}(k+1, l+1|i, j; N) + \frac{1}{8}\mathcal{P}(k-1, l-1|i, j; N) \\ & + \frac{1}{8}\mathcal{P}(k+1, l|i, j; N) + \frac{1}{8}\mathcal{P}(k, l+1|i, j; N) \end{aligned} \quad (4.41)$$

as well as two absorbing boundaries

$$\mathcal{P}(-1, l|i, j; N) = \mathcal{P}(k, -1|i, j; N) = 0. \quad (4.42)$$

We rewrite  $\mathcal{Q}_D(z)$  in terms of this probability

$$\mathcal{Q}_D(z; \alpha, \beta) = \frac{\sum_{N \geq 0} \sum_{i \geq 0} \sum_{j \geq 0} \sum_{k \geq 0} \sum_{l \geq 0} z^N a^{i+j} b^{k+l} 8^N \mathcal{P}(k, l|i, j; N)}{\left(\sum_{p \geq 0} (ab)^p\right)^2} \quad (4.43)$$

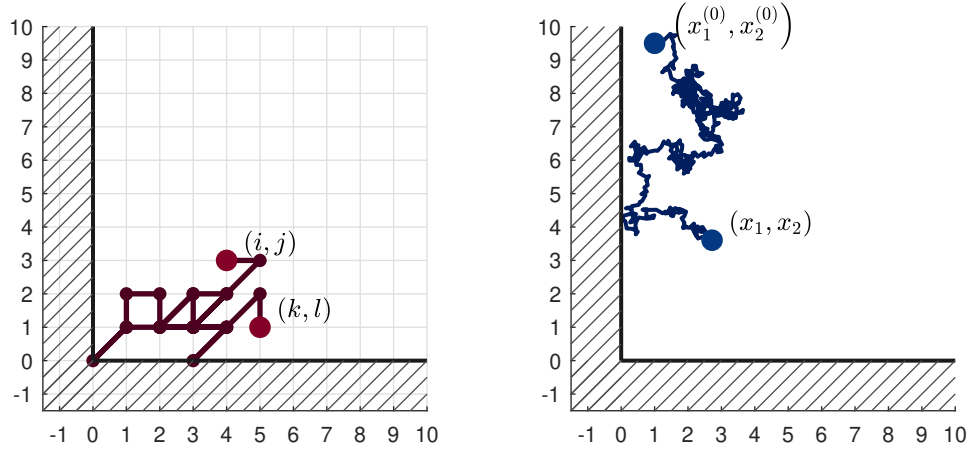
from which we wish to take a continuum limit. Taking the master equation (4.41), we define rescaled coordinates  $(x_1, x_2)$ ,  $(x_1^{(0)}, x_2^{(0)})$  from  $(k, l)$   $(i, j)$ , and a time-like variable  $\tau$  from the walk length  $N$ . Following the method in Section 1.5.3, upon taking the continuum limit in these five variables we arrive at the diffusion equation

$$\partial_\tau \mathcal{P}(x_1, x_2|x_1^{(0)}, x_2^{(0)}; \tau) = \frac{1}{4} (\partial_1^2 + \partial_2^2 + \partial_1 \partial_2) \mathcal{P}(x_1, x_2|x_1^{(0)}, x_2^{(0)}; \tau) \quad (4.44)$$

using the shorthand  $\partial_i = \partial/\partial x_i$ . We lighten the notation and suppress the initial condition:  $\mathcal{P}(x_1, x_2|x_1^{(0)}, x_2^{(0)}; \tau) \equiv \mathcal{P}(x_1, x_2; \tau)$ . In the continuum limit, Eq. (4.44) represents 2D diffusion in the upper-quarter plane with an induced anisotropy from the  $\partial_1 \partial_2$  term (Figure 4.3).  $\mathcal{P}$  has initial condition centred at  $(x_1^{(0)}, x_2^{(0)})$ :

$$\mathcal{P}(x_1, x_2; 0) = \delta(x_1 - x_1^{(0)}) \delta(x_2 - x_2^{(0)}) \quad (4.45)$$

and absorbing boundary conditions on the two axes:



**Figure 4.3** *Reducing the 2D random walk to a continuous diffusion problem, with bias along the diagonal. We now have two boundary conditions that bound the walk to the upper-quarter plane.*

$$\mathcal{P}(0, x_2; \tau) = \mathcal{P}(x_1, 0; \tau) = 0. \quad (4.46)$$

We now find the continuum expression for  $\mathcal{Q}_D(z)$  in terms of this diffusion by replacing each summation in Eq. (4.43) with an integral spanning the new space, and the random walk probability with a continuous distribution:

$$\mathcal{Q}_C(z) \equiv \frac{\int_0^\infty d\tau \int_0^\infty dx_1^{(0)} \int_0^\infty dx_2^{(0)} \int_0^\infty dx_1 \int_0^\infty dx_2 (8z)^\tau a^{x_1^{(0)}+x_2^{(0)}} b^{x_1+x_2} \mathcal{P}(x_1, x_2; \tau)}{(\int_0^\infty dp (ab)^p)^2}. \quad (4.47)$$

Like the 1D case, this has a more natural interpretation in terms of Laplace transforms, and we define

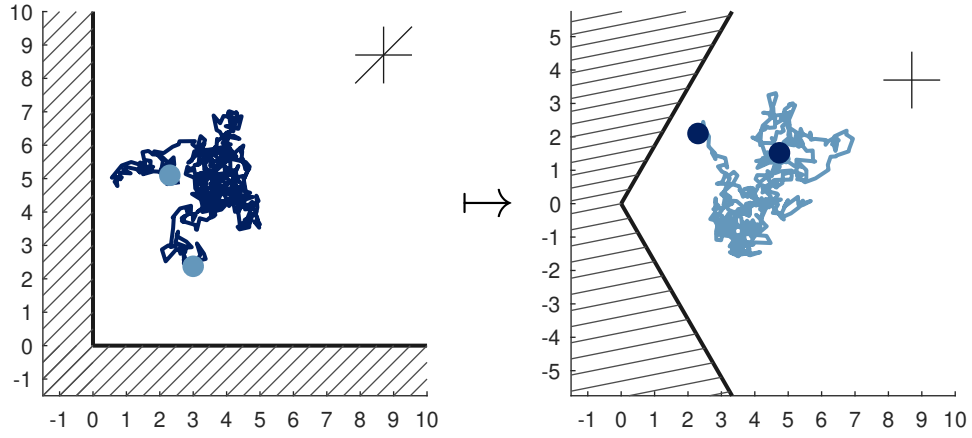
$$\begin{aligned} G(s; u, v, f) &\equiv G(s; u, v) \\ &= \int_0^\infty d\tau \int_0^\infty dx_1 \int_0^\infty dx_2 \int_0^\infty dx_1^{(0)} \int_0^\infty dx_2^{(0)} e^{-s\tau - f(x_1^{(0)}+x_2^{(0)}) - ux_1 - vx_2} \mathcal{P}(x_1, x_2; \tau) \end{aligned} \quad (4.48)$$

relating back to  $\mathcal{Q}_C$  via the transformation

$$\mathcal{Q}_C(z) = \frac{G(-\log 8z; -\log b, -\log b, -\log a)}{(\int_0^\infty dp (ab)^p)^2}. \quad (4.49)$$

The aim of the following calculation is to find an explicit expression for this function  $G$ . We use the shorthand  $G(s; u, v)$ , dropping the explicit dependence on  $f$  as it is not manipulated in the proceeding calculation.

We have now set up the problem. To find an expression for the continuum limit approximation to the sum of squared weights generating function, we are required



**Figure 4.4** Mapping the anisotropic diffusion in the upper-quarter plane to isotropic diffusion in a wedge, with opening angle  $2\pi/3$ .

to find the Laplace transform of the pdf that satisfies the diffusion equation (4.44), initial condition (4.45) and boundary conditions (4.46). A natural first attempt to solve this diffusion equation is by a method of images, as we did for the 1D problem in Section 4.2.1. We show however that in this instance one is forced to place images in the physical region, and the method proves ineffective.

### 4.3.2 Attempt at solution by images

Eq. (4.44) is anisotropic diffusion. We are free to make a coordinate transformation to new coordinates  $(X_1, X_2)$  under which diffusion is isotropic:

$$\begin{aligned} x_1 &= \frac{1}{2} \left( \sqrt{3}X_1 + X_2 \right) , & X_1 &= \frac{1}{\sqrt{3}}(x_1 + x_2) , \\ x_2 &= \frac{1}{2} \left( \sqrt{3}X_1 - X_2 \right) , & X_2 &= x_1 - x_2 . \end{aligned} \quad (4.50)$$

In this space, Eqs. (4.44)–(4.46) become

$$\partial_\tau \mathcal{P}(X_1, X_2; \tau) = (\partial_1^2 + \partial_2^2) \mathcal{P}(X_1, X_2; \tau) , \quad (4.51)$$

$$\mathcal{P}(X_1, X_2; 0) = \delta(X_1 - X_1^{(0)})\delta(X_2 - X_2^{(0)}) , \quad (4.52)$$

$$\mathcal{P}(X_1, -\sqrt{3}X_1; \tau) = \mathcal{P}(X_1, \sqrt{3}X_1; \tau) = 0 . \quad (4.53)$$

Here,  $\partial_i = \partial/\partial X_i$ . This forcing of isotropy has a consequence of transformed boundaries:  $x_1 = 0$  maps to the line  $X_2 = -\sqrt{3}X_1$ , and  $x_2 = 0$  maps to the line  $X_2 = \sqrt{3}X_1$ . Illustrated in Figure 4.4, the domain of this new problem is a wedge of opening angle  $2\pi/3$ .



As this is isotropic diffusion, we can easily write the fundamental solution  $\mathcal{P}^*$

$$\mathcal{P}^*(X_1, X_2; \tau) = \frac{1}{4\pi\tau} e^{-\frac{1}{4\tau}([X_1 - X_1^{(0)}]^2 + [X_2 - X_2^{(0)}]^2)} \quad (4.54)$$

where differentiating shows this satisfies the diffusion equation (4.51) and initial condition (4.53). To also satisfy the boundary conditions (4.52), we systematically insert images so as to cancel probability on both boundaries [120]. For convenience, we rewrite  $(X_1, X_2)$  in a polar basis  $(r, \theta)$

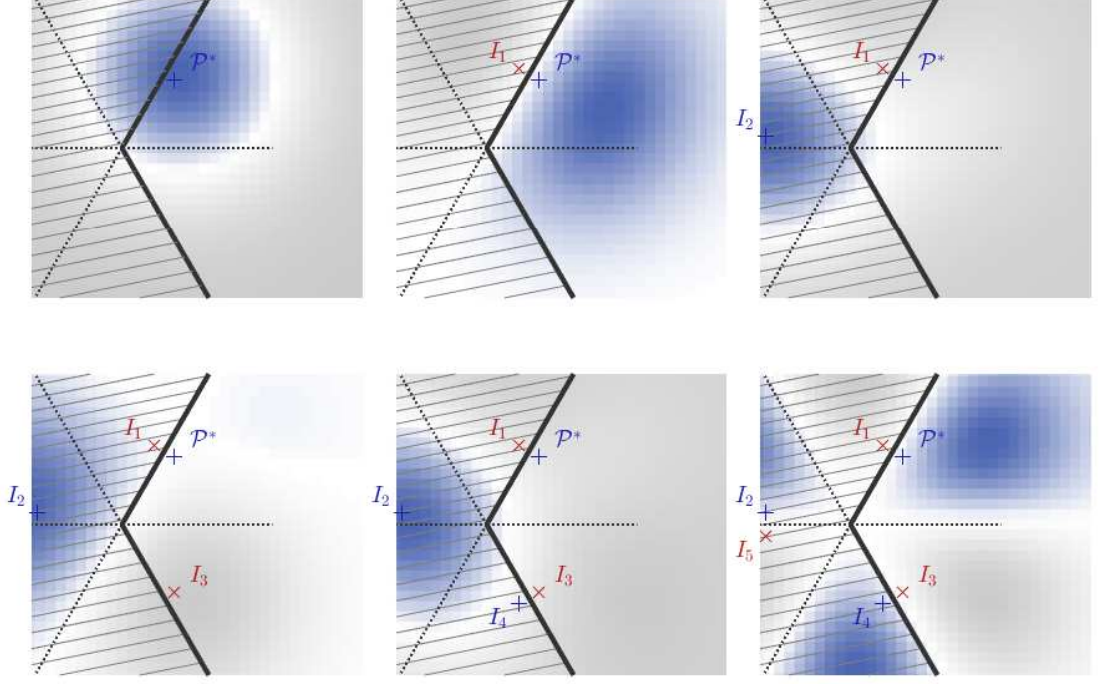
$$X_1 = r \cos \theta, \quad X_2 = r \sin \theta. \quad (4.55)$$

From a fundamental solution centred at  $(X_1^{(0)}, X_2^{(0)}) = (r_0 \cos \theta_0, r_0 \sin \theta_0)$ , we place images at radius  $r_0$  from the origin:

- To satisfy the boundary condition at  $\theta = \pi/3$ , we place a negative image  $I_1$  at  $\theta = 2\pi/3 - \theta_0$ ;
- To cancel  $I_1$  on the  $\theta = -\pi/3$ , boundary, place a positive image  $I_2$  at  $\theta = 2\pi/3 + \theta_0$ ;
- To cancel  $I_2$  on the  $\theta = \pi/3$  boundary, place a negative image  $I_3$  at  $\theta = -\theta_0$ ;
- To cancel  $I_3$  on the  $\theta = -\pi/3$  boundary, place a positive image  $I_4$  at  $\theta = -2\pi/3 + \theta_0$ ;
- To cancel  $I_4$  on the  $\theta = \pi/3$  boundary, place a negative image  $I_5$  at  $\theta = -2\pi/3 - \theta_0$ .

This final image  $I_5$  then cancels the fundamental solution on the  $\theta = -\pi/3$  boundary. The combination of the fundamental solution and the five images satisfies the diffusion equation and boundary conditions. However, the method of images fails in this instance as the image  $I_3$  is in the *physical* region  $|\theta| < \pi/3$ , thus violating the initial condition and introducing negative probability in the physical region. This is illustrated in Figure 4.5, and is a known problem for wedge domains with an opening angle  $m\pi/n$  for  $m$  and  $n$  coprime [120].

Instead of solving for the pdf  $\mathcal{P}$  directly, we turn to solving for a Laplace transform.



**Figure 4.5** By systematically applying images to satisfy the boundary conditions, one resorts to placing a negative image  $I_3$  inside the physical region.

### 4.3.3 Solution by a kernel method

We return to the original diffusion equation (4.44) and take Laplace transforms. Ahead of this, we associate to our five variables five conjugate variables:

$$(\tau, s), \quad (x_1, u), \quad (x_2, v), \quad (x_1^{(0)}, f), \quad (x_2^{(0)}, f). \quad (4.56)$$

We also introduce the following shorthand for Laplace transforms:

$$\hat{\mathcal{L}}_\tau[\cdot] \equiv \int_0^\infty d\tau e^{-s\tau}[\cdot], \quad (4.57)$$

$$\hat{\mathcal{L}}_{x_1}[\cdot] \equiv \int_0^\infty dx_1 e^{-ux_1}[\cdot], \quad (4.58)$$

$$\hat{\mathcal{L}}_{x_2}[\cdot] \equiv \int_0^\infty dx_2 e^{-vx_2}[\cdot], \quad (4.59)$$

$$\hat{\mathcal{L}}_{x_1^{(0)}}[\cdot] \equiv \int_0^\infty dx_1^{(0)} e^{-fx_1^{(0)}}[\cdot], \quad (4.60)$$

$$\hat{\mathcal{L}}_{x_2^{(0)}}[\cdot] \equiv \int_0^\infty dx_2^{(0)} e^{-fx_2^{(0)}}[\cdot]. \quad (4.61)$$

Notice that we use the same conjugate variable in the Laplace transforms in  $x_2^{(0)}$  and  $x_1^{(0)}$  as they both relate to the variable  $a$  in the expression for  $\mathcal{Q}_C(z)$ , see Eq. (4.47). We begin with a Laplace transform of Eq. (4.44) in  $\tau$ :

$$s\hat{\mathcal{L}}_\tau\mathcal{P} - \delta(x_1 - x_1^{(0)})\delta(x_2 - x_2^{(0)}) = \frac{1}{4}(\partial_1^2 + \partial_2^2 + \partial_1\partial_2)\hat{\mathcal{L}}_\tau\mathcal{P} \quad (4.62)$$

having used the initial condition (4.45). Following this, we perform a Laplace transform in  $x_1$ :

$$\begin{aligned} s\hat{\mathcal{L}}_\tau\hat{\mathcal{L}}_{x_1}\mathcal{P} - e^{-ux_1^{(0)}}\delta(x_2 - x_2^{(0)}) \\ = \frac{1}{4}(u^2 + u\partial_2 + \partial_2^2)\hat{\mathcal{L}}_\tau\hat{\mathcal{L}}_{x_1}\mathcal{P} - \frac{1}{4}\left[\partial_1\hat{\mathcal{L}}_\tau\mathcal{P}\right]_{x_1=0} - \frac{1}{4}\left[\partial_2\hat{\mathcal{L}}_\tau\mathcal{P}\right]_{x_1=0} \end{aligned} \quad (4.63)$$

using the  $x_1 = 0$  absorbing boundary condition (4.46). Next, a transform in  $x_2$

$$\begin{aligned} \left(s - \frac{1}{4}[u^2 + v^2 + uv]\right)\hat{\mathcal{L}}_\tau\hat{\mathcal{L}}_{x_1}\hat{\mathcal{L}}_{x_2}\mathcal{P} \\ = e^{-ux_1^{(0)}-vx_2^{(0)}} - \frac{1}{4}\hat{\mathcal{L}}_\tau\hat{\mathcal{L}}_{x_2}\left[\partial_1\mathcal{P}\right]_{x_1=0} - \frac{1}{4}\hat{\mathcal{L}}_\tau\hat{\mathcal{L}}_{x_1}\left[\partial_2\mathcal{P}\right]_{x_2=0} \end{aligned} \quad (4.64)$$

using the  $x_2 = 0$  boundary condition. Finally, we perform transforms over  $x_1^{(0)}$ ,  $x_2^{(0)}$ , using the same conjugate variable  $f$  for both transforms, to finally arrive at

$$K(u, v)G(s; u, v) = \frac{1}{(u + f)(v + f)} - F(u) - F(v) \quad (4.65)$$

having defined the *kernel*

$$K(u, v) \equiv s - \frac{1}{4}(u^2 + v^2 + uv) \quad (4.66)$$

and the unknown functions

$$F(\lambda) \equiv \frac{1}{4}\hat{\mathcal{L}}_\tau\hat{\mathcal{L}}_{x_1^{(0)}}\hat{\mathcal{L}}_{x_2^{(0)}}\int_0^\infty dx_2 e^{-\lambda x_2}\left[\partial_{x_1'}\mathcal{P}(x_1', x_2; \tau)\right]_{x_1'=0} \quad (4.67)$$

$$= \frac{1}{4}\hat{\mathcal{L}}_\tau\hat{\mathcal{L}}_{x_1^{(0)}}\hat{\mathcal{L}}_{x_2^{(0)}}\int_0^\infty dx_1 e^{-\lambda x_1}\left[\partial_{x_2'}\mathcal{P}(x_1, x_2'; \tau)\right]_{x_2'=0}, \quad (4.68)$$

with equivalence arising knowing the symmetry of the diffusion along the diagonal. On the LHS of Eq. (4.64) we have the desired function  $G(s; u, v)$  and a quadratic  $K(u, v)$ . There is also a second unknown function  $F$  involving the derivative of  $\mathcal{P}$  on the boundary. We can draw a parallel between this and Eq. (3.40) that we saw in the previous chapter — the main recursion relation that describes the generating function in the discrete case.

We solved Eq. 3.40 by the obstinate kernel technique, and for Eq. (4.65) we use a novel, related method. In this case, we find the algebra to be less elaborate, and the final result for  $G$  more concise.

### Outline of calculation

As we did in Chapter 3, we provide a roadmap of the calculation to follow:

1. Factorise and identify a set of symmetries in the kernel; transformations in the  $(u, v)$  variables under which the kernel remains invariant;
2. Use this kernel symmetry in order to obtain from Eq. (4.65) two more relations involving the functions  $G(s; u, v)$ ,  $F(u)$ , and  $F(v)$ ;
3. Combine these three equations to eliminate  $F(v)$ ;
4. Write the simplified relation in terms of an integral over the space of  $x_2$ ;
5. Isolate the domain of the integral so as to eliminate any  $v$ -dependence;
6. Write the relation in terms of an integral over the space of  $x_1$ ;
7. Isolate the domain of the integral that is convergent for  $u > 0$ , to find a closed-form expression for  $F(u)$ , and also  $F(v)$  by symmetry;
8. Substitute  $F(u)$  and  $F(v)$  into Eq. (4.65) to find a closed-form expression for  $G(s; u, v)$ .

We begin by analysing the kernel.

#### 4.3.4 Symmetry and factorisation of the kernel

The kernel in Eq. (4.66) is a quadratic in the variables  $u$  and  $v$ , in contrast with the discrete case (Eq. (3.39)), where the kernel was a quartic. We factorise in the variable  $v$  to find two simple roots  $\omega_+(u)$ ,  $\omega_-(u)$ :

$$K(u, v) = [v - \omega_-(u)] [v - \omega_+(u)] , \quad (4.69)$$

$$\omega_{\pm}(u) = -\frac{1}{2}u \pm \sqrt{4s - \frac{3}{4}u^2} \quad (4.70)$$

$$\equiv -\frac{1}{2}u \pm \sqrt{\Delta_u} . \quad (4.71)$$

We have defined the *discriminant*

$$\Delta_u = 4s - \frac{3}{4}u^2 \quad (4.72)$$

which also has a trivial factorisation:

$$\Delta_u = \frac{3}{4} \left( \sqrt{\frac{16s}{3}} + u \right) \left( \sqrt{\frac{16s}{3}} - u \right) \quad (4.73)$$

$$\equiv \Delta^0 \Delta_u^+ \Delta_u^- \quad (4.74)$$

where

$$\Delta^0 = \frac{3}{4}, \quad \Delta_u^+ = \sqrt{\frac{16s}{3}} + u, \quad \Delta_u^- = \sqrt{\frac{16s}{3}} - u. \quad (4.75)$$

Comparing these formulae to the factorisation in the discrete case (Section 3.3.4), we anticipate a less algebraically complicated calculation to follow.

We find a three-fold symmetry in the kernel:

$$K(u, v) = K(-u - v, v) = K(-u - v, u). \quad (4.76)$$

These are a set of variable transformations that leave the kernel invariant. We can then write two more expressions from Eq. (4.65):

$$K(u, v)G(s; u, -u - v) = \frac{1}{(f + u)(f - u - v)} - F(u) - F(-u - v), \quad (4.77a)$$

$$K(u, v)G(s; -u - v, v) = \frac{1}{(f - u - v)(f + v)} - F(-u - v) - F(v). \quad (4.77b)$$

Now, the combination of Eqs. (4.65) + (4.77a) - (4.77b) yields

$$\begin{aligned} G(s; u, v) + G(s; u, -u - v) - G(s; -u - v, v) \\ = \frac{1}{K(u, v)} \left[ \frac{f - 2u}{(f + u)(f + v)(f - u - v)} - 2F(u) \right] \end{aligned} \quad (4.78)$$

eliminates the unknown functions  $F(v)$ ,  $F(-u - v)$ . Aside from the  $G$  functions, all dependence on  $v$  is now explicit. This simplification draws parallels with the combination of terms in Eq. (3.61). We will now perform a procedure analogous to extracting positive power series, except now we are operating in a continuum limit. We term this *domain extraction*.

In the original relation (4.65), we implicitly assumed that  $G(s; u, v)$  had a well-defined

integral representation within the domains  $s, v, u, f \geq 0$  (Eq. (4.48)). It follows that every term of Eq. (4.65) should also have a well-defined integral form in the same domain. However, the variable transformations in Eqs. (4.77a), (4.77b) have introduced new terms with different domains of convergence:

- Eq. (4.65): well-defined integral form for  $u \geq 0, v \geq 0$ ;
- Eq. (4.77a): variable change  $(u, v) \rightarrow (u, -u - v)$ : well-defined integral form for  $u \geq 0, -u - v \geq 0 \implies v \leq 0$ ;
- Eq. (4.77b): variable change  $(u, v) \rightarrow (-u - v, v)$ : well-defined integral form for  $v \geq 0, -u - v \geq 0 \implies u \leq 0$ .

The combination of expressions in Eq. (4.78) eliminates  $F(v)$ , but mixes three different sets of domains. We then write Eq. (4.78) entirely in an integral form, then extract from this the part that lies within the required domain. We seek an expression for  $F(u)$ , which is well-defined for  $u > 0$ , and has no  $v$ -dependence.

### 4.3.5 $v$ domain extraction

We first obtain the component of Eq. (4.78) that is *independent* of  $v$ . This is in analogy with the  $\{y^0\}$  extraction in Section 3.4.1.

We explicitly write the LHS of Eq. (4.78) as the integral

$$\begin{aligned} \text{LHS (4.78)} &= \int_0^\infty d\tau \int_0^\infty dx_1^{(0)} \int_0^\infty dx_2^{(0)} \int_0^\infty dx_1 \int_0^\infty dx_2 e^{-s\tau - f(x_1^{(0)} + x_2^{(0)})} \\ &\quad \times \left[ e^{-ux_1 - vx_2} + e^{-ux_1 - (-u-v)x_2} - e^{-(-u-v)x_1 - vx_2} \right] \mathcal{P}(x_1, x_2; \tau) . \end{aligned} \quad (4.79)$$

We isolate regions of integration so as to eliminate  $v$ . For the first two terms, this occurs for  $x_2 = 0$ . However, the boundary condition  $P(x_1, 0; \tau) = 0$  allows us to drop these terms entirely. For the final term, we eliminate  $v$  by choosing  $x_1 = x_2$ . We are then left with (where ‘ $\rightarrow$ ’ denotes this isolation)

$$\begin{aligned} \text{LHS (4.78)} &\rightarrow - \int_0^\infty d\tau \int_0^\infty dx_1^{(0)} \int_0^\infty dx_2^{(0)} \int_0^\infty dx^{(0)} e^{-s\tau - f(x_1^{(0)} + x_2^{(0)}) + u(x_1 + x_2)} \mathcal{P}(x_1, x_1; \tau) \\ &\quad (4.80) \end{aligned}$$

$$\equiv - G^{(d)}(-u) . \quad (4.81)$$

$G^{(d)}$  is a function of the probability distribution (the superscript ‘ $(d)$ ’ denotes the diagonal). As it has a well-defined integral form within the domain  $u \leq 0$ , we anticipate

it will be discounted when isolating the  $u > 0$  domain later, so we will not consider its details here.

We now move to the RHS of Eq. (4.78)

$$\text{RHS (4.78)} = \frac{1}{K(u, v)} \left( \frac{f - 2u}{(f + u)(f - u - v)(f + v)} - 2F(u) \right) \quad (4.82)$$

which we also wish to write as an integral. For this, we write  $1/K(u, v)$  as a partial fraction decomposition in the variable  $v$

$$K(u, v) = \frac{1}{2\sqrt{\Delta_u}} \left( \frac{1}{v - \omega_-(u)} + \frac{1}{\omega_+(u) - v} \right) \quad (4.83)$$

which as an integral is written

$$\frac{1}{K(u, v)} = \frac{1}{2\sqrt{\Delta_u}} \int_0^\infty d\lambda \left[ e^{-(v - \omega_-)\lambda} + e^{-(\omega_+ - v)\lambda} \right]. \quad (4.84)$$

For  $u > 0$ , the two roots of the kernel  $\omega_+(u)$ ,  $\omega_-(u)$  are positive and negative respectively (and both zero at  $u = 0$ ), thus  $\omega_+(u) - v \geq 0$  within the domain  $v \leq 0$ , and  $v - \omega_-(u) \geq 0$  within the domain  $v \geq 0$ .

This partial fraction decomposition has yielded two integrals that are convergent under different domains of  $v$ . We again draw analogy to the discrete case: the series expansion of the kernel in Eq. (3.65) was in both powers of  $y$  and  $1/y$ , which will be well-defined in different radii of convergence. From this, we now extract the part of Eq. (4.84) that is independent of  $v$ , simply fixing  $\lambda = 0$ :

$$\frac{1}{K(u, v)} \rightarrow \frac{1}{2\sqrt{\Delta_u}} [1 + 1] = \frac{1}{\sqrt{\Delta_u}}. \quad (4.85)$$

We apply this same method throughout the RHS of Eq. (4.78): with some algebra, this is written as a partial fraction decomposition in  $v$ :

$$\begin{aligned} \text{RHS (4.78)} = & \frac{(f - 2u)}{2\sqrt{\Delta_u}(f + u)K(u, -f)} \left( \frac{2\sqrt{\Delta_u}}{2f - u} \left[ \frac{1}{f + v} + \frac{1}{f - u - v} \right] \right. \\ & \left. - \frac{1}{v - \omega_-(s, u)} - \frac{1}{\omega_+(s, u) - v} \right) - \frac{1}{\sqrt{\Delta_u}} \left( \frac{1}{v - \omega_-(u)} + \frac{1}{\omega_+(u) - v} \right) F(u). \end{aligned} \quad (4.86)$$

Writing this in an integral representation in the variable  $v$  and extracting the part

independent of  $v$ , we get

$$\text{RHS (4.78)} \rightarrow \frac{(f-2u)}{2\sqrt{\Delta_u}(f+u)K(u,-f)} \left( \frac{2\sqrt{\Delta_u}}{2f-u} [1+1] - 1 - 1 \right) - \frac{1}{\sqrt{\Delta_u}} (1+1) F(u) \quad (4.87)$$

$$= \frac{(f-2u)}{(f+u)K(u,-f)} \left( \frac{2}{2f-u} - \frac{1}{\sqrt{\Delta_u}} \right) - \frac{2}{\sqrt{\Delta_u}} F(u) . \quad (4.88)$$

This has eliminated any  $v$ -dependence from Eq. (4.78), leaving us with

$$-G^{(d)}(-u) = \frac{(f-2u)}{(f+u)K(u,-f)} \left( \frac{2}{2f-u} - \frac{1}{\sqrt{\Delta_u}} \right) - \frac{2}{\sqrt{\Delta_u}} F(u) . \quad (4.89)$$

We are nearly at a closed-form expression for  $F(u)$ , but for the matter of eliminating the unknown  $G^{(d)}(-u)$ ; this is well-defined for  $u \leq 0$ , so we can eliminate it by extracting the parts of Eq. (4.89) that are well-defined for  $u > 0$ . This step of the calculation is in analogy with the  $\{x^+\}$  extraction in the discrete case (Section 3.4.3), and much like the discrete case this proves to be a more involved step.

We see from Eq. (4.89) that  $u$ -terms are buried in the square root of the discriminant  $\sqrt{\Delta_u} = \sqrt{4s - 3u^2/4}$ . This term is not straightforwardly written as an integral, so we instead derive a pair of formulae that allows us to proceed without having to write any explicit integral for the discriminant.

### 4.3.6 Two required formulae

First, define a general function  $g(-u)$ , written so as to emphasise that it is convergent in the domain  $u \leq 0$ . Suppose this has some integral representation

$$g(-u) = \int_0^\infty d\lambda_1 e^{u\lambda_1} \mathcal{W}(\lambda_1) \quad (4.90)$$

with an unspecified weight function  $\mathcal{W}$ . We now multiply by a second function  $1/(c+u)$ ,  $c \geq 0$ , that has a well-defined integral representation for  $c \geq 0$ ,  $u > 0$ :

$$\frac{g(-u)}{c+u} = \int_0^\infty d\lambda_1 e^{u\lambda_1} \mathcal{W}(\lambda_1) \int_0^\infty d\lambda_2 e^{-(c+u)\lambda_2} . \quad (4.91)$$

Here we have mixed two different domains in  $u$ . The challenge now is to extract the part of Eq. (4.91) that is well-defined in the domain  $u > 0$ . We isolate values of  $\lambda_1$ ,  $\lambda_2$



that keeps the prefactor of  $u$  nonpositive. Here, this is  $\lambda_1 < \lambda_2$ :

$$\frac{g(-u)}{c+u} \xrightarrow{u>0} \int_0^\infty d\lambda_1 \left[ \int_{\lambda_1}^\infty d\lambda_2 e^{-(c+u)\lambda_2} \right] e^{u\lambda_1} \mathcal{W}(\lambda_1) \quad (4.92)$$

$$= \int_0^\infty d\lambda_1 \left[ \frac{e^{-(c+u)\lambda_1}}{c+u} \right] e^{u\lambda_1} \mathcal{W}(\lambda_1) \quad (4.93)$$

$$= \frac{1}{c+u} \int_0^\infty d\lambda_1 e^{-c\lambda_1} \mathcal{W}(\lambda_1) \quad (4.94)$$

$$= \frac{g(c)}{c+u} . \quad (4.95)$$

We use the notation  $\xrightarrow{u>0}$  to denote “isolating the ( $u > 0$ )-convergent part”. In practice, this function  $g(-u)$  is the root of the discriminant  $\sqrt{\Delta_u^-} = (\sqrt{16s/3} - u)^{1/2}$ , Eq. (4.75). Importantly, we did not specify any details about the weight function  $\mathcal{W}$ . We can therefore apply this identity taking  $g(-u) = \sqrt{\Delta_u^-}$ , without considering how  $\sqrt{\Delta_u^-}$  could be written as an integral.

The second formula relates to functions of the form  $h(u)$  within the  $u > 0$  domain, with some representation

$$h(u) = \int_0^\infty d\lambda_1 e^{-u\lambda_1} \mathcal{W}(\lambda_1) \quad (4.96)$$

again with an unspecified weight  $\mathcal{W}$ . We multiply  $h(u)$  with  $1/(c-u)$ ,  $c \geq 0$ , which has a well-defined integral representation in the  $u \leq 0$  domain:

$$\frac{h(u)}{c-u} = \int_0^\infty d\lambda_1 e^{-u\lambda_1} \mathcal{W}(\lambda_1) \int_0^\infty d\lambda_2 e^{-(c-u)\lambda_2} . \quad (4.97)$$

Isolating the  $u > 0$  domain demands  $\lambda_1 > \lambda_2$ :

$$\frac{h(u)}{c-u} \xrightarrow{u>0} \int_0^\infty d\lambda_1 e^{-u\lambda_1} \mathcal{W}(\lambda_1) \left[ \int_0^{\lambda_1} d\lambda_2 e^{-(c-u)\lambda_2} \right] \quad (4.98)$$

$$= \int_0^\infty d\lambda_1 e^{-u\lambda_1} \mathcal{W}(\lambda_1) \left[ \frac{1 - e^{-(c-u)\lambda_1}}{c-u} \right] \quad (4.99)$$

$$= \frac{1}{c-u} \int_0^\infty d\lambda_1 \left[ e^{-u\lambda_1} \mathcal{W}(\lambda_1) - e^{-c\lambda_1} \mathcal{W}(\lambda_1) \right] \quad (4.100)$$

$$\frac{h(u)}{c-u} \xrightarrow{u>0} \frac{1}{c-u} [h(u) - h(c)] \quad (4.101)$$

recovering the original function, minus a counter term  $h(c)$ . Once again, we did not have to specify any details of the weight function  $\mathcal{W}$  of  $h(u)$ , and in practice this function will correspond to  $1/\sqrt{\Delta_u^+}$ .

Equipped with the two formulae (4.95), (4.101) we are ready to isolate the  $u > 0$

component of our main relation.

### 4.3.7 $u > 0$ domain extraction

We return to Eq. (4.89). First, we multiply through by a factor of  $\sqrt{\Delta_u^-}$  to obtain

$$-\sqrt{\Delta_u^-} G^{(d)}(-u) = \frac{(f-2u)}{(f+u)K(u,-f)} \left( \frac{2\sqrt{\Delta_u^-}}{2f-u} - \frac{1}{\sqrt{\Delta^0 \Delta_u^+}} \right) - \frac{2}{\sqrt{\Delta^0 \Delta_u^+}} F(u) . \quad (4.102)$$

Importantly, the LHS is entirely well-defined within the  $u \leq 0$  domain; if we were to then extract the  $u > 0$  domain of this equation, we would eliminate the unknown  $G^{(d)}(-u)$ . We rewrite Eq. (4.102) as a partial fraction decomposition in  $u$ , to allow us to apply our two formulae (4.95), (4.101). With elaborate but straightforward algebra we eventually find

$$\begin{aligned} & -\sqrt{\Delta_u^-} G^{(d)}(-u) = \quad (4.103) \\ & -\frac{2}{\sqrt{\Delta^0 \Delta_u^+}} F(u) - \frac{2}{K(f,f)} \left[ \frac{\sqrt{\Delta_u^-}}{2f+(-u)} \right] + \frac{2}{K(f,f)} \left[ \frac{\sqrt{\Delta_u^-}}{f+u} \right] \\ & -\frac{3f}{\sqrt{\Delta^0} K(f,f)} \left[ \frac{1}{\sqrt{\Delta_u^+}(f+u)} \right] - \frac{f+2\omega_-(f)}{\sqrt{\Delta_f} K(f,f)} \left[ \frac{\sqrt{\Delta_u^-}}{-\omega_-(f)+(-u)} \right] \\ & + \frac{(2f+\omega_-(f))(f+2\omega_-(f))}{2\sqrt{\Delta_f} K(f,f)\sqrt{\Delta^0}} \left[ \frac{1}{\sqrt{\Delta_u^+}(-\omega_-(f)+(-u))} \right] \\ & + \frac{(2f+\omega_+(f))(f+2\omega_+(f))}{2\sqrt{\Delta_f} K(f,f)\sqrt{\Delta_0}} \left[ \frac{1}{\sqrt{\Delta_u^+}(\omega_+(f)+u)} \right] - \frac{f+2\omega_+(f)}{K(f,f)\sqrt{\Delta_f}} \left[ \frac{\sqrt{\Delta_u^-}}{u+\omega_+(f)} \right] . \end{aligned}$$

We use square brackets to highlight terms with a dependence on  $u$ . The LHS is trivial, and we find

$$\text{LHS (4.103)} \xrightarrow{u>0} 0 . \quad (4.104)$$

For the RHS we use our identities (4.95), (4.101), to find term-by-term

$$\begin{aligned}
\text{RHS(4.103)} &\xrightarrow{u \geq 0} -\frac{2}{\sqrt{\Delta^0 \Delta_u^+}} F(u) - 0 + \frac{2}{K(f, f)} \frac{\sqrt{\Delta_{-f}^-}}{(f+u)} - \frac{3f}{\sqrt{\Delta^0} K(f, f)} \frac{1}{\sqrt{\Delta_u^+} (f+u)} \\
&+ 0 + \frac{(2f + \omega_-(f))(f + 2\omega_-(f))}{2\sqrt{\Delta_f} K(f, f) \sqrt{\Delta_0}} \frac{1}{-\omega_-(f) - u} \left[ \frac{1}{\sqrt{\Delta_u^+}} - \frac{1}{\sqrt{\Delta_{(-\omega_-(f))}^+}} \right] \\
&+ \frac{(2f + \omega_+(f))(f + 2\omega_+(f))}{2\sqrt{\Delta_f} K(f, f) \sqrt{\Delta_0}} \frac{1}{\sqrt{\Delta_u^+} (u + \omega_+(f))} \\
&- \frac{f + 2\omega_+(f)}{K(f, f) \sqrt{\Delta_f}} \frac{\sqrt{\Delta_{(-\omega_+(f))}^-}}{u + \omega_+(f)} \tag{4.105}
\end{aligned}$$

where we recall that for  $f > 0$ ,  $\omega_-(f) < 0$ ,  $\omega_+(f) > 0$ . With further algebraic manipulation and denesting of square roots, this expression simplifies to

$$F(u) = \frac{\sqrt{3} \sqrt{\Delta_f^+} \sqrt{\Delta_u^+} (\sqrt{4s} - \sqrt{3}u)}{2K(u, -f)(f+u) (\sqrt{4s} + \sqrt{3}f)} - \frac{f - 2u}{2(f+u)K(u, -f)} \tag{4.106}$$

which is finally an explicit expression for  $F(u)$ . We can now return to the central problem, and write an explicit form for the full Laplace transform  $G$ . We use Eq. (4.65) to find

$$G(s; u, u, f) = \frac{1}{K(u, u)} \left( \frac{1}{(f+u)^2} - 2F(u) \right) \tag{4.107}$$

$$\begin{aligned}
&= \frac{1}{(4s - f^2 - u^2 + fu)(f+u)^2} \\
&\quad - \frac{\sqrt{f + \sqrt{\frac{16s}{3}}} \sqrt{u + \sqrt{\frac{16s}{3}}}}{\sqrt{3} (4s - f^2 - u^2 + fu)(f+u) \left( \sqrt{\frac{4s}{3}} + f \right) \left( \sqrt{\frac{4s}{3}} + u \right)}. \tag{4.108}
\end{aligned}$$

We now take this Laplace transform derived from the diffusion equation, and make the appropriate variable transformation to acquire the continuum limit generating function  $\mathcal{Q}_C(z)$  for the sum of squared TASEP weights.

Eq. (4.108) is manifestly symmetric in  $(u, f)$ , which implies we will recover  $(\alpha, \beta)$  symmetry, which serves as one check that this method has been successful.

### 4.3.8 Solution for $\mathcal{Q}_C(z; \alpha, \beta)$

With the expression for  $G$  in Eq. (4.108), we recall how this relates to the continuum limit TASEP generating function  $\mathcal{Q}_C(z)$  from Eq. (4.49):

$$\mathcal{Q}_C(z) = \frac{G(-\log 8z; -\log b, -\log b, -\log a)}{(\int_0^\infty dp (ab)^p)^2}.$$

Under this variable change we find

$$\mathcal{Q}_C(z) = \frac{1 - \frac{\log^2 ab \sqrt{3} \sqrt{3 \log a - \sqrt{-48 \log 8z}} \sqrt{3 \log b - \sqrt{-48 \log 8z}}}{(3 \log a - \sqrt{-12 \log 8z})(3 \log b - \sqrt{-12 \log 8z})}}{\log a \log b - \log^2 a - \log^2 b - 4 \log 8z}. \quad (4.109)$$

This is the main result of this chapter. In comparison to the calculation in Chapter 3, we have a much more analytically tractable function from a less involved calculation. We treat  $\mathcal{Q}_C(z)$  as an approximation to the exact discrete generating function  $\mathcal{Q}_D(z)$  in Eq. (3.88), and perform an asymptotic analysis to find the asymptotic scaling of  $\sum_C \mathcal{W}(C)^2$ . Pleasingly, the simplicity of Eq. (4.109) allows us to identify by inspection how the three phases of the TASEP will emerge.

As in Section 4.2.2 for the partition function, we expect to recover asymptotic TASEP dynamics in a scaling region around  $\alpha = \beta = 1/2$ .

## 4.4 Asymptotic analysis

For the asymptotic analysis, we again use notation established in Section 1.6.3. Before formally expanding, we take advantage of the simple form of  $\mathcal{Q}_C(z)$  to identify where and how we expect different singularities to arise.

The dominant singularities of Eq. (4.109) are contained in the term

$$\frac{1}{(3 \log a - \sqrt{-12 \log 8z})(3 \log b - \sqrt{-12 \log 8z})}. \quad (4.110)$$

There are also additional poles from the denominator of  $\mathcal{Q}_C(z)$ , but these are not dominant. Eq. (4.110) has a pole situated at  $z^*(\alpha)$  for

$$3 \log \left( \frac{1 - \alpha}{\alpha} \right) - \sqrt{-12 \log (8z^*(\alpha))} = 0 \quad (4.111)$$

and an equivalent  $z^*(\beta)$ . This has solution for  $0 < \alpha < 1/2$  only, as  $\log([1 - \alpha]/\alpha)$  is

negative for  $1/2 < \alpha < 1$ . In this case, the solution

$$z^*(\alpha) = \frac{1}{8} \exp \left[ -\frac{3}{4} \log^2 \left( \frac{1-\alpha}{\alpha} \right) \right], \quad 0 < z^* < 1/8. \quad (4.112)$$

The pole associated with  $\beta$  has identical properties. As  $z^*$  is a monotonically increasing function of  $\alpha$ ,  $\beta$ , the dominant pole is associated with the smallest of  $\alpha$  or  $\beta$ .

The second singularity in Eq. (4.110) is a branch point;  $\sqrt{-12 \log 8z}$  is purely imaginary for  $z > 1/8$ . Here, then, the poles vanish, and this branch point is the dominant singularity.

This gives three different regions:

- $\alpha < 1/2, \alpha < \beta$ : dominant pole is  $z^*(\alpha)$ ;
- $\beta < 1/2, \beta < \alpha$ : dominant pole is  $z^*(\beta)$ ;
- $\alpha, \beta > 1/2$ : branch point at  $1/8$ ;

which of course correspond to the LD, HD and MC phases. We now probe these in detail.

#### 4.4.1 Low density phase $\alpha < 1/2, \alpha < \beta$ ( $a > 1, a > b$ )

In this region, the simple pole at  $z^*(\alpha)$  (Eq. (4.112)) is dominant, about which a series expansion yields

$$\mathcal{Q}_C(z) = \frac{\sqrt{3} z^* \log^2(ab) (\log a)^{\frac{3}{2}} \sqrt{\log(a^2/b)}}{2 \log(a/b) [2 \log^2(a) + \log(b) \log(a/b)]} \frac{1}{(z - z^*(\alpha))} + \mathcal{O}((z - z^*(\alpha))^0). \quad (4.113)$$

This corresponds to the asymptotic scaling

$$\sum_C \mathcal{W}(C)^2 \sim \frac{\sqrt{3} \log^2(ab) (\log a)^{\frac{3}{2}} \sqrt{\log(a^2/b)}}{2 \log(b/a) [2 \log^2(a) + \log(b) \log(a/b)]} \left[ 8 \exp \left( \frac{3}{4} \log^2 a \right) \right]^N. \quad (4.114)$$

From the sum of squared weights as  $Q_N = \sum_C \mathcal{W}(C)^2$ , we define the ratio

$$L \equiv \frac{Q_{N-1}}{Q_N} \quad (4.115)$$

which indicates how the sum of squared weights scales with increasing system size. We know the exact asymptotic scaling from the discrete case (subscript ‘D’), using Eq. (3.92):

$$L_D \sim \frac{\alpha^2(1-\alpha)^2}{\alpha^2 + (1-\alpha)^2} \quad (4.116)$$

$$= \frac{1}{8} - \frac{3}{2} \left( \alpha - \frac{1}{2} \right)^2 + 5 \left( \alpha - \frac{1}{2} \right)^4 + \mathcal{O} \left( \left( \alpha - \frac{1}{2} \right)^4 \right). \quad (4.117)$$

In comparison, we find from our continuum limit calculation (subscript ‘C’)

$$L_C \sim \frac{1}{8} \exp \left[ -\frac{3}{4} \log^2 \left( \frac{1-\alpha}{\alpha} \right) \right] \quad (4.118)$$

$$= \frac{1}{8} - \frac{3}{2} \left( \alpha - \frac{1}{2} \right)^2 + 8 \left( \alpha - \frac{1}{2} \right)^4 + \mathcal{O} \left( \left( \alpha - \frac{1}{2} \right)^4 \right). \quad (4.119)$$

We therefore recover this ratio to second order, about  $\alpha = 1/2$ , as we did for the asymptotic scaling of the current (Section 4.2.2).

#### 4.4.2 High density phase $\beta < 1/2$ , $\beta < \alpha$ ( $b > 1$ , $b > a$ )

Once again, the symmetry of  $\alpha$  and  $\beta$  in this problem allows us to write the high density result as the  $(\alpha, \beta) \rightarrow (\beta, \alpha)$  mirror of the low density phase.

#### 4.4.3 Maximal current phase $\alpha > 1/2$ , $\beta > 1/2$ ( $a < 1$ , $b < 1$ )

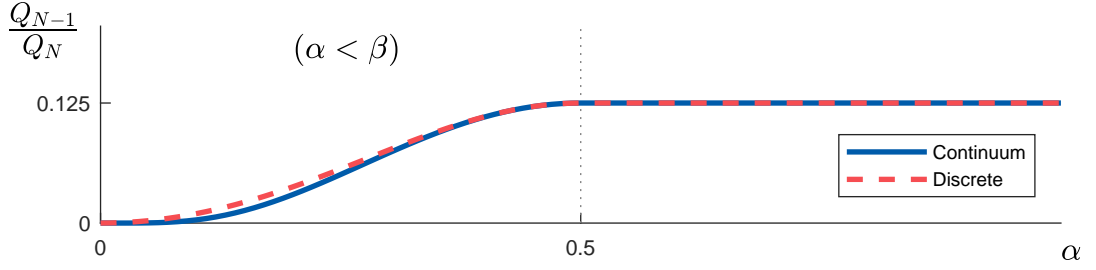
In this region, the dominant singularity is a branch point at  $z^* = 1/8$ . A series expansion of  $\mathcal{Q}_C(z)$  around this point yields

$$\mathcal{Q}_C(z) = A_0 + A_1 (z - z^*) - \frac{128\sqrt{2}\log^3(ab)}{9(\log a \log b)^{7/2}} i (z - z^*)^{3/2} + \mathcal{O}(z - z^*)^2 \quad (4.120)$$

with real coefficients  $A_{0,1}$  and an imaginary contribution at order  $k = 3/2$ . This expansion implies the asymptotic behaviour

$$\sum_c \mathcal{W}(C)^2 \sim -\frac{2\log^3 ab}{3\sqrt{\pi}(\log a \log b)^{7/2}} N^{-5/2} 8^N. \quad (4.121)$$

This is the same scaling with system size as found in the discrete case, Eq. (3.97). The ratio  $L$  is simply  $1/8$  in both instances.



**Figure 4.6** Asymptotic form of the ratio  $Q_{N-1}/Q_N$ . The LD-MC transition occurs at the dotted line.

## 4.5 Summary of results

We summarise by listing the asymptotic scaling for the quantities  $Z_N$ ,  $J = Z_{N-1}/Z_N$ ,  $Q_N$ ,  $L = Q_{N-1}/Q_N$ , and finally the Rényi entropy  $H_2$ , predicted by both the exact and continuum generating functions:

- Sum of weights  $Z_N = \sum_C \mathcal{W}(C)$

$$Z_{N,D} \propto \begin{cases} \left( \frac{1}{\alpha(1-\alpha)} \right)^N & (\text{LD}) \\ \frac{4^N}{N^{3/2}} & (\text{MC}) \end{cases}, \quad (4.122)$$

$$Z_{N,C} \propto \begin{cases} \left( 4 \exp \left[ \frac{1}{4} \log^2 \left( \frac{1-\alpha}{\alpha} \right) \right] \right)^N & (\text{LD}) \\ \frac{4^N}{N^{3/2}} & (\text{MC}) \end{cases}; \quad (4.123)$$

- Ratio  $J = Z_{N-1}/Z_N$  (current)

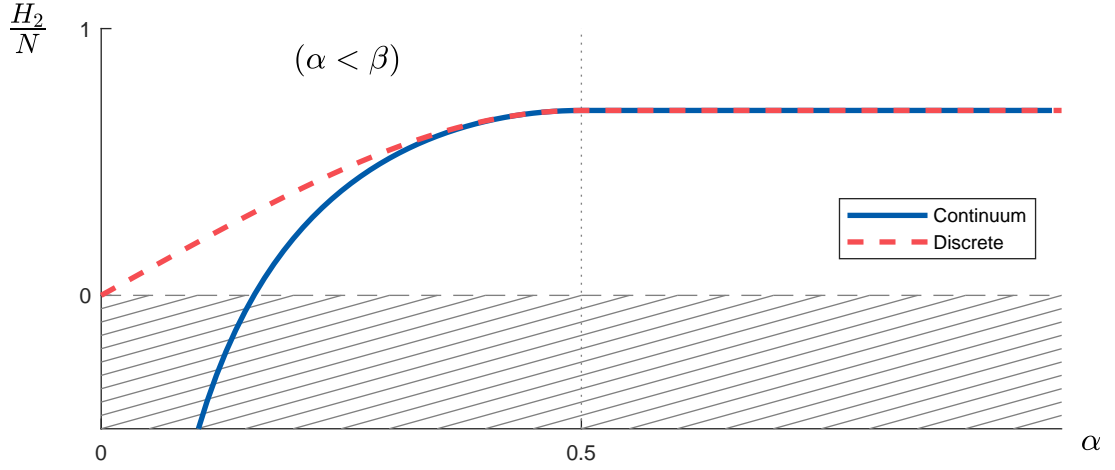
$$J_D \sim \begin{cases} \alpha(1-\alpha) & (\text{LD}) \\ \frac{1}{4} & (\text{MC}) \end{cases}, \quad (4.124)$$

$$J_C \sim \begin{cases} \frac{1}{4} \exp \left[ -\frac{1}{4} \log^2 \left( \frac{1-\alpha}{\alpha} \right) \right] & (\text{LD}) \\ \frac{1}{4} & (\text{MC}) \end{cases}; \quad (4.125)$$

- Sum of squared weights  $Q_N = \sum_C \mathcal{W}(C)^2$

$$Q_{N,D} \propto \begin{cases} \left( \frac{\alpha^2(1-\alpha)^2}{\alpha^2+(1-\alpha)^2} \right)^N & (\text{LD}) \\ \frac{8^N}{N^{5/2}} & (\text{MC}) \end{cases}, \quad (4.126)$$

$$Q_{N,C} \propto \begin{cases} \left( 8 \exp \left[ \frac{3}{4} \log^2 \left( \frac{1-\alpha}{\alpha} \right) \right] \right)^N & (\text{LD}) \\ \frac{8^N}{N^{5/2}} & (\text{MC}) \end{cases}; \quad (4.127)$$



**Figure 4.7** Asymptotic form of the Rényi entropy  $H_2$ . The LD-MC phase transition occurs at the dotted line.

- Ratio  $L = Q_{N-1}/Q_N$

$$L_D \sim \begin{cases} \frac{\alpha^2 + (1-\alpha)^2}{\alpha^2(1-\alpha)^2} & \text{(LD)} \\ \frac{1}{8} & \text{(MC)} \end{cases}, \quad (4.128)$$

$$L_C \sim \begin{cases} \frac{1}{8} \exp \left[ -\frac{3}{4} \log^2 \left( \frac{1-\alpha}{\alpha} \right) \right] & \text{(LD)} \\ \frac{1}{8} & \text{(MC)} \end{cases}. \quad (4.129)$$

For both  $J = Z_{N-1}/Z_N$ ,  $L = Q_{N-1}/Q_N$ , (Figures 4.2, 4.6) the continuum results converge to the known result around  $\alpha = 1/2$ , and have characteristically similar curves within the LD phase.

We can also calculate the Rényi entropy from Eq. (1.59),  $H_2 = -\log(Q_N/Z_N^2)$  (Figure 4.7):

$$H_{2,D} \sim \begin{cases} N \log(\alpha^2 + (1-\alpha)^2)^{-1} + \mathcal{O}(1) & \text{(LD)} \\ N \log 2 - \frac{1}{2} \log N + \mathcal{O}(1) & \text{(MC)} \end{cases}, \quad (4.130)$$

$$H_{2,C} \sim \begin{cases} N \left( \log 2 - \frac{1}{4} \log^2 \left( \frac{1-\alpha}{\alpha} \right) \right) + \mathcal{O}(1) & \text{(MC)} \\ N \log 2 - \frac{1}{2} \log N + \mathcal{O}(1) & \text{(LD)} \end{cases}. \quad (4.131)$$

Taking Figure 4.7 at a glance, the Rényi entropy is troubling: Figure 4.7 shows that the continuum and discrete entropies converge at  $\alpha = 1/2$  as expected. However, the continuum limit result suggests an entropy that rapidly becomes *negative* deeper into the LD phase. We identify this as an artefact of the loss of discretisation of the TASEP configurations;  $H_2$  can be interpreted as the logarithm of an effective number, therefore



a negative entropy implies an effective number between 0 and 1. In the exact (discrete) case, the lowest possible effective number is 1, and the minimum entropy is zero. In the continuum limit, however, the probability density is free to approach zero, and the logarithm of this effective number therefore diverges. More generally, there is a concept of *differential entropy* [121, 122] and even differential *Rényi* entropy [123, 124] for dealing with continuous probability distributions.

## 4.6 On higher-order weight enumerations

The advantage of this continuum approach over the exact approach of Chapter 3 is that the equations involved are far more analytically tractable, whilst still recovering TASEP phase dynamics. For this reason, one may ask how this continuum approach could extend to calculating higher-order weight sums. By kernel methods, the partition function proved simple and the sum of squared weights was also calculable. However, these kernel methods do not appear to extend to any higher dimension. In this section we give a more general discussion about these higher weight sums in the context of kernel methods and *orbit sums* [114]. We do this in the context of the previous continuum calculation, but the principles originated from, and equally apply to, work on discrete walks [114, 125, 126].

### 4.6.1 Orbit sums

Let us return to the equation for the Laplace transform  $G(s; u, v)$  that we solved in the two-dimensional case in Eq. (4.65):

$$K(u, v)G(s; u, v) = \frac{1}{(f+u)(f+v)} - F(u) - F(v) ,$$

$$K(u, v) = s - \frac{1}{4} (u^2 - v^2 - uv) .$$

We solved this by exploiting the symmetry property in Eq. (4.76):

$$K(u, v) = K(-u - v, v) = K(u, -u - v) .$$

This symmetry can be stated more formally in the context of variable mappings. Specifically, there are two mappings  $M_1$ ,  $M_2$  of the variables  $u$  and  $v$  that leave the

kernel invariant:

$$M_1 : \quad (u, v) \mapsto (u, -u - v) , \quad (4.132)$$

$$M_2 : \quad (u, v) \mapsto (-u - v, v) . \quad (4.133)$$

Furthermore, *successive* applications of  $M_1$  and  $M_2$  will also leave the kernel invariant.

We then successively apply  $M_1$   $M_2$  alternatively to  $(u, v)$ :

$$(u, v) \xrightarrow{M_1} (u, -u - v) \xrightarrow{M_2} (v, -u - v) \xrightarrow{M_1} (v, u) \xrightarrow{M_2} (-u - v, v) \xrightarrow{M_1} (-u - v, u) \xrightarrow{M_2} (u, v) \quad (4.134)$$

arriving back at  $(u, v)$ . This sequence of mappings is known in the literature as an *orbit*, and as we have returned to  $(u, v)$  this is a *finite* orbit. For each of these variable transformations, we are free to write a new equation from Eq. (4.65):

$$K(u, v)G(u, v) = \frac{1}{(f+u)(f+v)} - F(u) - F(v) , \quad (4.135a)$$

$$K(u, v)G(u, -u - v) = \frac{1}{(f+u)(f-u-v)} - F(u) - F(-u - v) , \quad (4.135b)$$

$$K(u, v)G(v, -u - v) = \frac{1}{(f+v)(f-u-v)} - F(v) - F(-u - v) , \quad (4.135c)$$

$$K(u, v)G(v, u) = \frac{1}{(f+v)(f+u)} - F(v) - F(u) , \quad (4.135d)$$

$$K(u, v)G(-u - v, v) = \frac{1}{(f-u-v)(f+v)} - F(-u - v) - F(v) , \quad (4.135e)$$

$$K(u, v)G(-u - v, u) = \frac{1}{(f-u-v)(f+u)} - F(-u - v) - F(u) . \quad (4.135f)$$

The *orbit sum* is then defined in the literature as the alternating sum of these six equations [114]:

$$(4.135a) + (4.135b) - (4.135c) + (4.135d) - (4.135e) + (4.135f) . \quad (4.136)$$

For the majority of these types of problem that form a finite orbit, this orbit sum cancels *all* terms involving  $F$ , leaving on several functions of  $G$  over different domains, from which  $G(u, v)$  is extracted. However, the orbit sum for our particular diffusion completely cancels on both sides. This problem is then referred to as an *obstinate* kernel. In this case we have instead taken a *half-orbit* sum

$$(4.135a) + (4.135b) - (4.135c)$$

to yield Eq. (4.78), a slight but not full simplification that yields, with more work, a closed form for  $F(u)$  and therefore  $G(u, v)$ .

With this notion of an orbit sum established, we give a qualitative discussion on the calculation of the sum of *cubed* weights.

#### 4.6.2 Attempt at solving 3D diffusion — sum of cubed weights

We have seen that the continuum limit partition function has the underlying diffusion equation (4.5)

$$\partial_\tau \mathcal{P} = \frac{1}{4} \partial_1^2 \mathcal{P}$$

which arises from the continuum limit of the recursion relation describing Eq. (1.27)

$$\sum_c \mathcal{W}(C) = \langle W | (D + E)^N | V \rangle .$$

Similarly, there is an underlying two-dimensional diffusion equation (4.44) for the sum of squared weights

$$\partial_\tau \mathcal{P} = \frac{1}{4} (\partial_1^2 + \partial_2^2 + \partial_1 \partial_2) \mathcal{P}$$

which arises from the continuum limit of the recursion relation describing Eq. (3.1)

$$\sum_c \mathcal{W}(C)^2 = \langle W | \otimes \langle W | (D \otimes D + E \otimes E)^N | V \rangle \otimes | V \rangle .$$

Following this, one can show that the *three*-dimensional diffusion

$$\partial_\tau \mathcal{P} = \frac{1}{4} (\partial_1^2 + \partial_2^2 + \partial_3^2 + \partial_1 \partial_2 + \partial_1 \partial_3 + \partial_2 \partial_3) \mathcal{P} \quad (4.137)$$

emerges upon taking the continuum limit of the recursion relation describing the sum of *cubed* weights

$$\sum_c \mathcal{W}(C)^3 = \langle W | \otimes \langle W | \otimes \langle W | (D \otimes D \otimes D + E \otimes E \otimes E)^N | V \rangle \otimes | V \rangle \otimes | V \rangle . \quad (4.138)$$

Like the one and two-dimensional cases, this has a delta function initial condition centred at  $(x_1^{(0)}, x_2^{(0)}, x_3^{(0)})$ , and absorbing boundaries on  $x_1, x_2, x_3 = 0$ . This is diffusion in 3D space, with anisotropy introduced from the  $\partial_1 \partial_2$ ,  $\partial_2 \partial_3$ ,  $\partial_1 \partial_3$  terms. Taking a set of Laplace transforms over six initial and final coordinates and the time  $\tau$ , one arrives

at an equation of characteristic form

$$K(u, v, w)G(s; u, v, w) = \frac{1}{(f+u)(f+v)(f+w)} - F(u, v) - F(v, w) - F(u, w) \quad (4.139)$$

where  $(\tau; x_1, x_2, x_3)$  have conjugate variables  $(s; u, v, w)$ , and the initial coordinates all have conjugate variable  $f$ . Like in the 2D case of Eq. (4.65),  $G$  is the time and space Laplace transform of  $\mathcal{P}$ , and  $F$  is a function of the *derivative* of  $\mathcal{P}$  evaluated on one of the three axes. This time, the kernel

$$K(u, v, w) = s - \frac{1}{4} (u^2 + v^2 + w^2 + uv + uw + vw) \quad (4.140)$$

is a quadratic in  $u, v$  and now additionally  $w$ . Considering the symmetry of this new kernel in the context of orbits, we find three mappings  $M_1, M_2, M_3$  that leave the kernel invariant:

$$M_1 : \quad (u, v, w) \xrightarrow{M_1} (u, v, -u - v - w) , \quad (4.141)$$

$$M_2 : \quad (u, v, w) \xrightarrow{M_2} (u, -u - v - w, w) , \quad (4.142)$$

$$M_3 : \quad (u, v, w) \xrightarrow{M_3} (-u - v - w, v, w) . \quad (4.143)$$

These mappings, when applied successively, yield an orbit of length 12:

$$\begin{aligned} (u, v, w) &\xrightarrow{M_1} (u, v, \Gamma) \xrightarrow{M_2} (u, w, \Gamma) \xrightarrow{M_3} (v, w, \Gamma) \xrightarrow{M_1} (v, w, u) \\ &\xrightarrow{M_2} (v, \Gamma, u) \xrightarrow{M_3} (w, \Gamma, u) \xrightarrow{M_1} (w, \Gamma, v) \xrightarrow{M_2} (w, u, v) \\ &\xrightarrow{M_3} (\Gamma, u, v) \xrightarrow{M_1} (\Gamma, v, w) \xrightarrow{M_2} (\Gamma, v, w) \xrightarrow{M_3} (u, v, w) \end{aligned} \quad (4.144)$$

(with  $\Gamma = -u - v - w$ ), from which we would acquire 12 different equations from the original relation (4.139). The orbit sum of these terms is again zero. Furthermore, with the introduction of a third variable we are not able to find any partial orbit sum (or any combination of these equations for that matter) which provide a simplification what would allow us to isolate domains. On the discrete side, these 3D problems are a current area of research [118, 126].

### 4.6.3 Continuum limit for higher-order weight enumerations

The main advantage of working in a continuous space over the exact discrete random walks in Chapter 3 is the relative simplicity of the algebra; the continuum limit generating function in Eq. (4.109) is written in one line, and we can identify the various phases of the TASEP by inspection. This difference stems from the kernels

in both instances: in the discrete case (Eq. (3.39)) it is a quartic function, whereas the continuum kernel (Eq. (4.66)) is only quadratic, giving a simpler factorisation.

This may then be a more attractive starting point for calculating higher-order Rényi entropies. We saw in Section 3.7.2 that the sum of TASEP weights to arbitrary integer power,  $\sum_{\mathcal{C}} \mathcal{W}(\mathcal{C})^\lambda$ , is an enumeration of walks in the upper  $\lambda$ -dimensional *orthant*, comprising the  $2^{1+\lambda}$  steps from the operators

$$\prod_{q=1}^{\lambda} (1 + g_q) + \prod_{q=1}^{\lambda} (1 + g_q^\dagger)$$

which emerge from the explicit representation from Eq. (1.21),  $D = 1 + g$ ,  $E = 1 + g^\dagger$ . This has products of up to  $\lambda$  different ladder operators along different axes. Alternatively, one can show in the continuum limit that this reduces to the following diffusion equation

$$\partial_\tau \mathcal{P} = \frac{1}{8} \sum_{n=1}^{\lambda} \sum_{m=1}^{\lambda} (1 + \delta_{nm}) \partial_n \partial_m \mathcal{P} \quad (4.145)$$

$$= \frac{1}{8} (\partial_1 \ \partial_2 \ \partial_3 \ \dots \ \partial_\lambda) \begin{pmatrix} 2 & 1 & 1 & \dots & 1 \\ 1 & 2 & 1 & \dots & 1 \\ 1 & 1 & 2 & \dots & 1 \\ \vdots & \vdots & \vdots & \ddots & \vdots \\ 1 & 1 & 1 & \dots & 2 \end{pmatrix} \begin{pmatrix} \partial_1 \\ \partial_2 \\ \partial_3 \\ \vdots \\ \partial_\lambda \end{pmatrix} \mathcal{P} \quad (4.146)$$

where products of more than two differential operators have vanished in the continuum limit. Although the kernel method does not seem to extend beyond  $\lambda = 2$ , the behaviour of this diffusion with increasing dimensionality may be an interesting problem to investigate by other methods.

## 4.7 Summary

From the random-walk interpretation of the matrix product formalism, the enumeration of TASEP weights can be written in terms of random walk problems. We have shown in this chapter that we recover physical features of the TASEP when instead considering the time and space *continuum limits* of these random walks.

The partition function is an enumeration of bicoloured Motzkin paths. In the continuum limit, these become a simple 1D diffusion with a single absorbing boundary. This is straightforward to solve by images or otherwise. An asymptotic analysis of the Laplace

transform of the time-dependent pdf recovers the three dynamical phases of the TASEP, and correctly predicts the particle current to second order.

The sum of squared weights is an enumeration of 2D paths from the step set  $\{\nearrow, \rightarrow, \uparrow, \swarrow, \leftarrow, \downarrow, \times, \cdot\}$ . In the continuum limit, we found this walk reduced to *anisotropic* diffusion in the upper-quarter plane, with absorbing boundaries along the two axes. This diffusion problem proves stubborn to any image-based method, and we instead solve for a Laplace transform of the probability distribution, by a novel method that draws parallels with the obstinate kernel method of Chapter 3. This involves a mixing of different functions that converge within different domains, then extracting the part of the expression that is convergent within a certain domain. We are still to hone in on the precise analytic details of this new technique, but we are confident that we have the correct answer; first, we recover a nontrivial  $\alpha$ - $\beta$  symmetry that was broken earlier in the problem, and secondly the predicted asymptotic scaling of  $\sum_{\mathcal{C}} \mathcal{W}(\mathcal{C})^2$  matches the result from Chapter 3 to second order. In contrast with the discrete case, this continuum function is much simpler to analyse, and can be done by hand.

We finished with a discussion about the enumeration of the sum of *cubed* weights in the continuum limit, and how this problem would require solution of a 3D anisotropic diffusion. This problem would demand a new technique; our kernel method does not appear to extend to higher dimensions. However, when considering higher integer power weight enumerations in general, the resultant  $\lambda$ -dimensional diffusion problem appears promising to investigate further, even if by techniques away from the kernel methods discussed here.

We showed in Section 4.2 that the scaling region of this continuum limit is in the vicinity of  $\alpha = \beta = 1/2$ . Although this allows us to predict the phase behaviour of the TASEP, the coincidence of this scaling region with the triple point is not obvious, and opens up some more general questions concerning the physical significance of these diffusion processes. The taking of a continuum limit of a random walk to acquire a diffusion process is a standard technique. The random walks seen here, however, stem from representations of *physical phenomena* — namely, whether a particle is on a site or not.

The lattice on which the random walk is defined stems from the array of numbers in the matrix representations, which are labelled with discrete indices. By introducing a lattice spacing and taking that spacing to zero, we depart from any ‘matrix’ in the usual sense as these indices are no longer discrete. Furthermore, the walk length arises from the product of a finite number of matrices which each represent a site on

the TASEP. The introduction of a continuous time eliminates any notion of a finite product, and in turn of any discrete sites. In this chapter we have performed particular calculations in the limit, but it would be interesting to look more fundamentally at the physical implications of this limit. With the loss of discreteness, we speculate that the approximate analysis in this chapter of the partition function and sum of squared weights in Eq. (4.28) could be an exact analysis, for some other related driven continuum system.

## Chapter 5

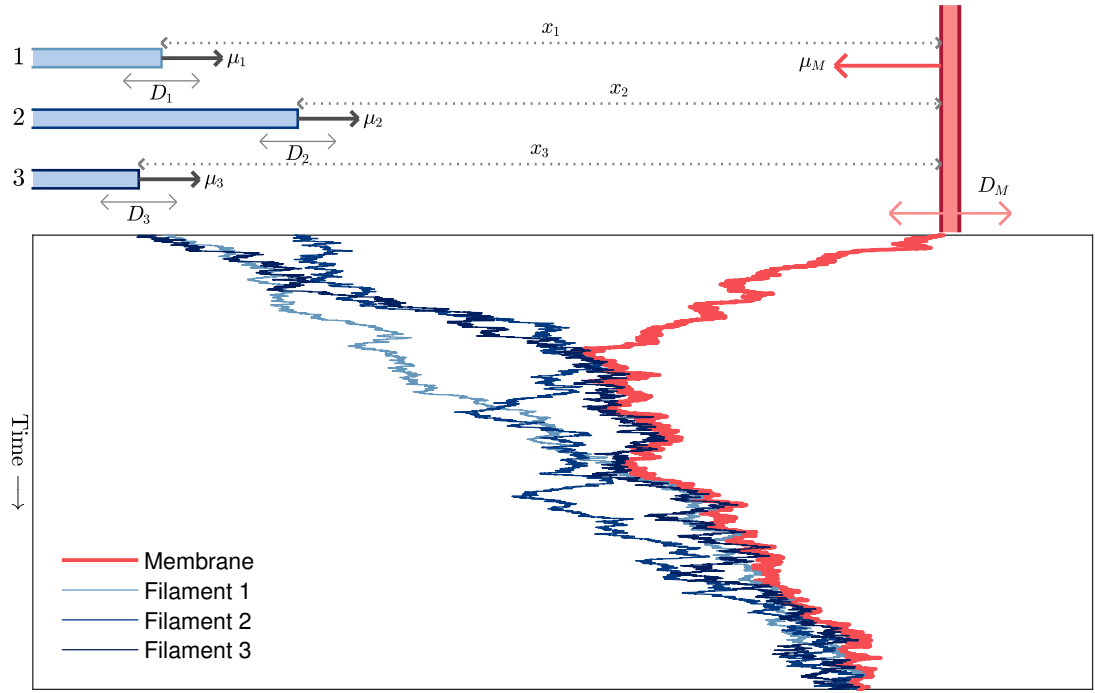
# Many-filament diffusive Brownian ratchet

### 5.1 Orientation

In this chapter, we depart from the exclusion processes that have formed the bulk of the work presented so far. We shift focus to a different system entirely; one that pertains to the movement of a drift-diffusing membrane by a network of stochastically growing and shrinking filaments. The exclusion interactions involved lead us to term this system a *diffusive Brownian ratchet*. Our interest in this model originated from an observation; when writing the dynamics of the Brownian ratchet, one can interpret its evolution in time as a diffusion, with similar dynamics to the two-dimensional diffusion we saw in Chapter 4. The major difference here is that the boundaries are *reflecting*, and we will see that with this boundary condition we can solve the steady-state diffusion with much greater generality, and in turn the Brownian ratchet as a whole.

Broadly, a Brownian ratchet comprises a ratchet-and-pawl device in a surrounding medium [127, 128]. Its theoretical interest stems from it providing a mechanism to move a fluctuating object without directly exerting any forces on it. Instead, it is thermal fluctuations and steric interactions that generate the motion [129, 130] in a manner that is consistent with the second law of thermodynamics. In mathematical terms, the standard Brownian ratchet may be formulated as a drift-diffusive problem for the single spatial coordinate of the ratchet-pawl separation [9]. More recently many-filament systems involving several spatial coordinates have been introduced and studied [131–143].





**Figure 5.1** *Visualisation and simulation of a continuum ratchet system with  $N = 3$  filaments. Top: diagram of a three-filament system. Each filament (blue, thin) may have a different diffusion constant  $D_n$  and drift  $\mu_n$ . Bottom: realisation of the system over time, with the time axis running vertically downwards. The membrane (red, thick) naturally drifts left, but the entire system moves right in the steady state, as a result of thermal fluctuations and steric interactions between the three filaments (blue, thin) and the membrane.*

One possible manifestation of a such a many-component ratchet system in nature may be at the boundaries of eukaryotic cells. On the  $\sim \mu\text{m}$  length scale, one observes filaments of joined protein monomers known as *actins*, arranged in a spatially-extended network. These filaments grow and contract in order to move and morph the leading edge of cells [144–146]. The rate of growth of the network is moderated by, among other factors, surrounding monomer concentration [147–149]. One end of the actin filament (the *barbed* end) elongates at a much higher rate than the other (the *pointed* end), associating a directionality to the growth [150, 151]. Consequently, the network appears to “treadmill” in one direction with monomers dissociating on the trailing edge [152]. For the bulk movement of a leading edge (*lamellipodia*), this network tends to be crosslinked, improving the rigidity of the network [144, 153, 154]. There are also individual “spikes” out of the cell (*filopodia*), in which the interior actin filaments form a parallel bundle [155, 156].

The model that we will introduce and solve here is shown in Figures 5.1 and 5.3. We have an array of  $N$  filaments that grow and shrink in a continuous space, constrained by a rigid drift-diffusing membrane. Our model incorporates three major extensions to

previous continuum models [131, 133]:

1. Each filament is characterised by its own polymerisation velocity and variance;
2. The filaments move under an effective potential with respect to the membrane;
3. The filaments have lateral interactions with neighbouring filaments.

The interactions in this model are generally attractive; the filaments are attracted to the membrane and/or to each other. Importantly, in the steady state we find this high-dimensional model to be exactly solvable, for many physically relevant parameter choices. As we will discuss in detail, the essence of this solution is that for these parameter choices, the second-order steady-state equation can be reduced to a set of directly integrable first-order equations.

This model falls into a class that we refer to as *pure* ratchets [139]. The defining property of these systems is that the membrane moves under thermal fluctuations, and the network grows quickly to occupy any space left vacant [9, 131–134]. The key phenomenon that can arise from these pure ratchets, then, is that a membrane that has a natural drift in one direction, may have a net movement in the opposite direction, arising exclusively from steric interactions and thermal fluctuations. This is to be distinguished from other models where filaments directly exert forces, and do work to move the membrane [135–143].

The microscopic dynamics of a real filament network, involving for example tread-milling, crosslinking and heterogeneity, is very complex [144, 145, 147, 156–160]. We emphasize that we are not attempting to model these specific dynamics in detail but instead consider generic heterogeneous filaments, along with interaction potentials to effectively encapsulate this dynamical complexity. The interactions here are attractive, but do not contribute directly to the membrane motion itself. This is a coarse-grained, effective description of more complicated biological, microscopic effects which may force the filament network to evolve within the locality of the membrane, allowing us to interpret the system as a nonequilibrium steady state.

In all of the studies discussed so far, a key observable of interest is the steady-state velocity of the membrane. With the model we introduce here, we gain exact insight into how the various physical properties of the filaments affect the ability of the overall network to move the fluctuating membrane. We show, with analytical expressions, how the membrane velocity increases with an increasing harmonic attraction of filaments to the membrane, but decreases on introducing a surface tension that pulls neighbouring

filaments towards one another. The velocity also increases on increasing the diffusion constant of the membrane.

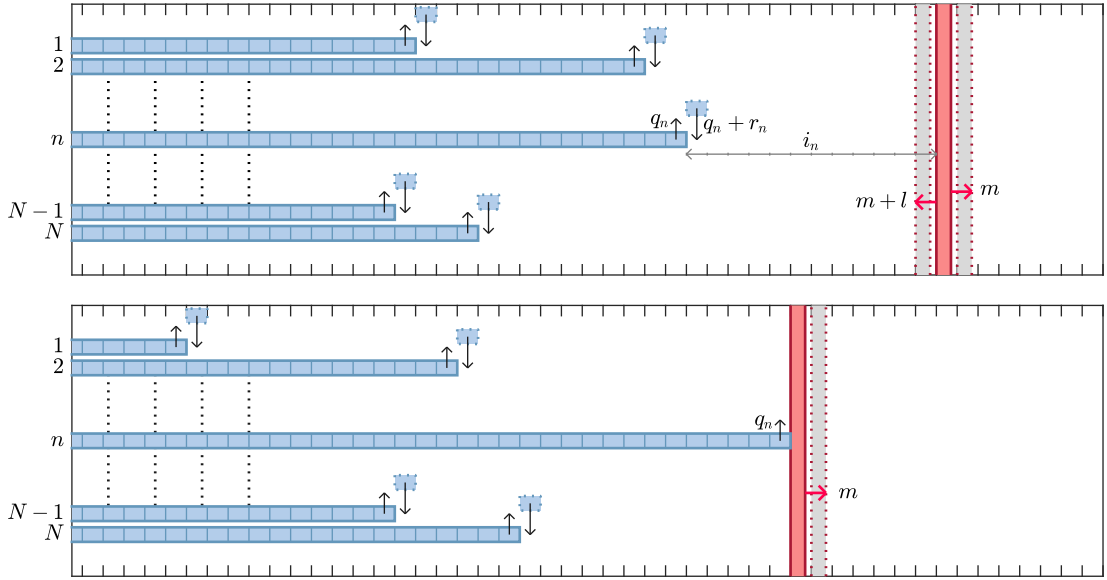
This chapter is organised as follows. In Section 5.2, we introduce and motivate our system by taking the continuum limit of a *lattice* Brownian ratchet [9, 137]. This leads us to a differential equation for the pdf over the displacements between the membrane and each of the filaments. We solve this pdf and derive the membrane velocity, first in Section 5.3 for a single filament, then in Section 5.4 for the case where  $N$  filaments have a constant drift, and finally in Section 5.5 for  $N$  filaments and additional quadratic interactions. In particular in Section 5.5.1 we consider a restoring force towards the membrane and in Section 5.5.2 we consider surface tension across the filament bundle leading edge. We show in Section 5.6 how these diffusion problems can be related back to the ASEP, and finally we summarise in Section 5.7.

## 5.2 Model derivation

Our starting point is a lattice model of a Brownian ratchet in continuous time, where the discrete lattice represents discretised monomers of the filament. We start from a lattice model, as the boundary conditions arising from the exclusion interaction between the filaments and the membrane arise more naturally within the discrete formulation than if one uses a continuum description at the outset.

The dynamics of this lattice model are as seen in Figure 5.2: the rigid membrane makes unit steps to the left and right at rates defined as  $(m+l)$  and  $m$  respectively. Similarly, filament  $n$  ( $n = 1, \dots, N$ ) shrinks (depolymerises) and grows (polymerises) across unit steps at rates  $q_n$  and  $(q_n + r_n)$  respectively. The steps are only permitted when a hard-core exclusion interaction is satisfied: the membrane must stay to the right of the right-most filament(s). Thus, the system exhibits ratcheting, where the membrane moves at a velocity different to its inherent drift — perhaps in the opposite direction entirely — as a result of thermal fluctuations and steric interactions. The polymer filaments do not exert a force on contact with the membrane, or vice versa. The rate  $r_n$  represents the speed of the filament growth and may depend upon the displacement of the filament from the membrane.

Assume now that the system has settled into a steady state, in which the displacements between the filaments and the membrane have stationary distributions. We define  $\underline{i} = (i_1, i_2, \dots, i_N)$ ,  $i_n \geq 0$  as a vector of integer displacements between each of the  $N$  filaments and the membrane. From here on we treat these displacements  $\underline{i}$  as the system



**Figure 5.2** The lattice Brownian ratchet model, which is the starting point of the continuum model we solve in this chapter. On a lattice, each of the  $N$  filaments (blue) polymerise and depolymerise, at the rates shown. The membrane (red) also makes jumps left and right.  $i_n \geq 0$  is the integer displacement between filament  $n$  and the membrane. In the event of a filament touching the membrane (bottom), the membrane may only move right at the usual rate, and the filament in contact may only contract at its usual rate. The dynamics of the other filaments are unaffected.

configuration, although the whole system will in general have a net velocity (unless it is in a *stalled* state). Define  $\mathcal{P}_{\underline{i}}$  as the stationary probability of observing the system with displacements  $\underline{i}$  under the steady-state condition  $\partial_t \mathcal{P}_{\underline{i}} = 0$ . Assume now we are in a *bulk* configuration:  $i_n > 0, \forall n$ , so no filaments are in contact with the membrane. By considering all possible ways the system can enter and leave configuration  $\underline{i}$ , the stationary solution obeys a master equation of the form in Eq. (1.8)

$$0 = - \left[ 2m + l + \sum_{n=1}^N (2q_n + r_n) \right] \mathcal{P}_{\underline{i}} + m \mathcal{P}_{\underline{i}-\underline{1}} + (m+l) \mathcal{P}_{\underline{i}+\underline{1}} + \sum_{n=1}^N [q_n \mathcal{P}_{\underline{i}-\underline{\hat{n}}} + (q_n + r_n) \mathcal{P}_{\underline{i}+\underline{\hat{n}}}] . \quad (5.1)$$

Here  $\underline{\hat{n}}$  is defined as the unit vector along component  $n$ , and  $\underline{1} \equiv \sum_{n=1}^N \underline{\hat{n}}$ .

We now consider the case where filament  $k$  makes contact with the membrane and  $i_k = 0, i_{n \neq k} > 0$ . The membrane can now only move to the right, and filament  $k$  can only move to the left. In this case, the master equation has fewer terms as fewer moves

are possible, and reads

$$0 = - \left[ m + q_k + \sum_{\substack{n=1 \\ n \neq k}}^N (2q_n + r_n) \right] \mathcal{P}_{\underline{i}} + (m + l) \mathcal{P}_{\underline{i}+\underline{1}} \\ + \sum_{\substack{n=1 \\ n \neq k}}^N q_n \mathcal{P}_{\underline{i}-\underline{\hat{n}}} + \sum_{n=1}^N (q_n + r_n) \mathcal{P}_{\underline{i}+\underline{\hat{n}}} \quad (5.2)$$

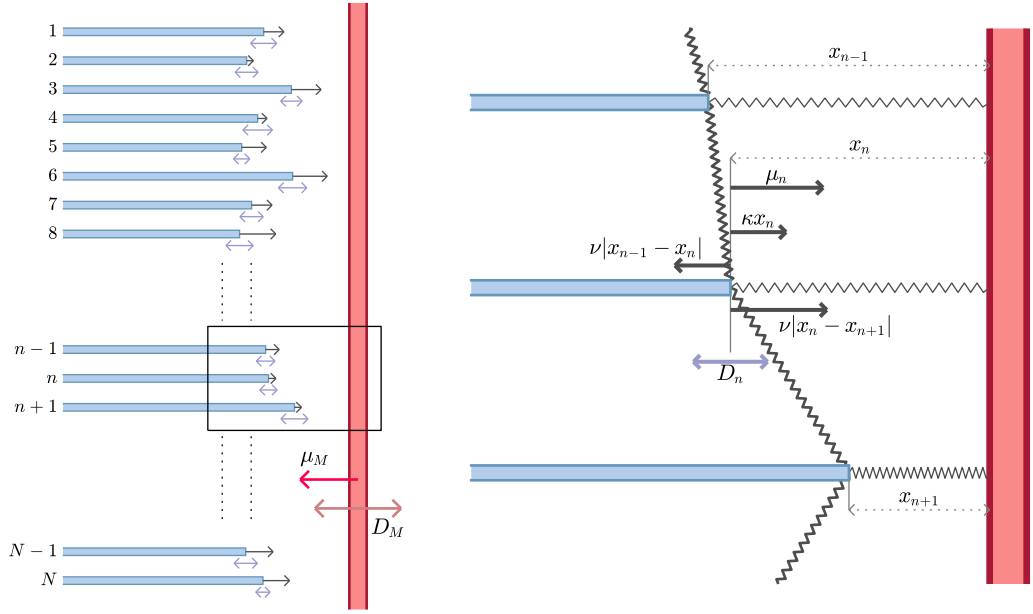
for any  $k = 1, 2, \dots, N$ . It is the continuum limit of this equation that furnishes the appropriate boundary condition for the differential equation we now derive.

We take the limit in which the length of each filament, as well as the position of the membrane, is treated as a continuous random variable. Note that it is in the direction perpendicular to the membrane that the continuum limit is taken; the number of filaments remains discrete (and fixed). We introduce an explicit lattice spacing  $a$  such that  $\underline{x} = (x_1, x_2, \dots, x_N) = a\underline{i}$ . The continuum limit equations then arise following the convention laid out in Section 1.5: taking  $a$  to be small, and performing a series expansion of the master equation for small  $a$ . From Eq. (5.1) we obtain a drift-diffusion equation and from Eq. (5.2) a set of  $N$  boundary conditions. In this limit, the probability approaches a continuous distribution in  $\underline{x}$ , that we denote  $\mathcal{P}(\underline{x})$ . The resulting continuous space system is illustrated in Figure 5.3.

### 5.2.1 Diffusion equation

Beginning with the bulk relation, the master equation (5.1) is written in terms of  $\underline{x} = (x_1, x_2, \dots, x_N) = a\underline{i}$  as

$$0 = - \left[ 2m + l + \sum_{n=1}^N (2q_n + r_n(x_n)) \right] \mathcal{P}(\underline{x}) + m \mathcal{P}(\underline{x} - a\underline{1}) + (m + l) \mathcal{P}(\underline{x} + a\underline{1}) \\ + \sum_{n=1}^N q_n \mathcal{P}(\underline{x} - a\underline{\hat{n}}) + \sum_{n=1}^N [q_n + r_n(x_n + a)] \mathcal{P}(\underline{x} + a\underline{\hat{n}}) . \quad (5.3)$$



**Figure 5.3** *The complete continuum Brownian ratchet system that we address. Each of the filaments (blue) are growing and shrinking by a diffusion process with coefficient  $D_n$ , and drift  $\mu_n$ . The membrane (red) moves with diffusion coefficient  $D_M$  and drift  $\mu_M$  towards the filaments.  $x_n$  is the displacement between filament  $n$  and the membrane. Filament  $n$  may then also be attracted to the membrane by a spring force with strength  $\kappa$ , and also may have a surface tension-like interaction with neighbouring filaments with strength  $\nu$ .*

In the limit of a small lattice spacing  $a$ , we now perform a Taylor expansion of  $\mathcal{P}$  to second order in  $a$ , over each of the  $N$  degrees of freedom. This expansion is written

$$\begin{aligned}
0 \approx & - \left[ 2m + l + \sum_{n=1}^N (2q_n + r_n(x_n)) \right] \mathcal{P}(\underline{x}) + m \left( 1 - a \sum_{n=1}^N \partial_n + \frac{1}{2} a^2 \sum_{n=1}^N \sum_{k=1}^N \partial_n \partial_k \right) \mathcal{P}(\underline{x}) \\
& + (m+l) \left( 1 + a \sum_{n=1}^N \partial_n + \frac{1}{2} a^2 \sum_{n=1}^N \sum_{k=1}^N \partial_n \partial_k \right) \mathcal{P}(\underline{x}) + \sum_{n=1}^N q_n \left( 1 - a \partial_n + \frac{1}{2} a^2 \partial_n^2 \right) \mathcal{P}(\underline{x}) \\
& + \sum_{n=1}^N \left( q_n + \left[ 1 + a \partial_n + \frac{1}{2} a^2 \partial_n^2 \right] r_n(x_n) \right) \left( 1 + a \partial_n + \frac{1}{2} a^2 \partial_n^2 \right) \mathcal{P}(\underline{x}) \quad (5.4)
\end{aligned}$$

using the shorthand  $\partial_n \equiv \partial/\partial x_n$ . All  $\mathcal{O}(a^0)$  terms cancel, and we collect terms in powers of  $a^1$  and  $a^2$  to give

$$\begin{aligned}
0 \approx & a \left( \sum_{n=1}^N [\partial_n r_n(x_n) + (r_n(x_n) + l) \partial_n] \mathcal{P}(\underline{x}) \right) \\
& + a^2 \left( \left[ m + \frac{1}{2} l \right] \sum_{n=1}^N \sum_{k=1}^N \partial_n \partial_k \mathcal{P}(\underline{x}) + \sum_{n=1}^N \left[ \left( q_n + \frac{1}{2} r_n(x_n) \right) \partial_n^2 + \frac{1}{2} \partial_n^2 r_n(x_n) \right] \mathcal{P}(\underline{x}) \right). \quad (5.5)
\end{aligned}$$

As laid out in Section 1.5.3, we now define a set of *diffusion* and *drift* rates, first for

the membrane (subscript ‘ $M$ ’)

$$\mu_M = al, \quad \underline{\mu}_M \equiv \sum_{n=1}^N \mu_M \hat{n}, \quad D_M = a^2 m. \quad (5.6)$$

For the filaments, define

$$\partial_n V(\underline{x}) = ar_n, \quad D_n = a^2 q_n. \quad (5.7)$$

In Eqs. (5.6) and (5.7),  $\partial_n \equiv \partial/\partial x_n$  and the biases (or drifts)  $r_n$  derive from a potential  $V(\underline{x})$ . Note that, as discussed in Section 1.5.3 with Eq. (1.88), the drift coefficients scale with the lattice spacing, and the diffusion coefficients  $D_M$ ,  $D_n$  with the lattice spacing squared [70].

With these definitions, we rewrite Eq. (5.5) with leading-order terms only to obtain our diffusion equation:

$$0 = \sum_{n=1}^N \partial_n \left( \partial_n V(\underline{x}) + \mu_M + D_M \sum_{k=1}^N \partial_k + D_n \partial_n \right) \mathcal{P}(\underline{x}). \quad (5.8)$$

### 5.2.2 Reflecting boundary conditions

Starting from Eq. (5.2), that applies when a filament is in contact with the membrane, we can follow a similar procedure to obtain a boundary condition on the diffusion equation. This time we do not get full cancellation at  $\mathcal{O}(a^0)$ , so we need only expand to first order to obtain:

$$\begin{aligned} 0 \approx & \left[ - \left( m + q_k + \sum_{\substack{n=1 \\ n \neq k}}^N (2q_n + r_n(x_n)) \right) \mathcal{P}(\underline{x}) + (m + l) \left( 1 + a \sum_{n=1}^N \partial_n \right) \mathcal{P}(\underline{x}) \right. \\ & \left. + \sum_{\substack{n=1 \\ n \neq k}}^N q_n (1 - a \partial_n) \mathcal{P}(\underline{x}) + \sum_{n=1}^N (q_n + [1 + a \partial_n] r_n(x_n)) (1 + a \partial_n) \mathcal{P}(\underline{x}) \right]_{x_k=0} \end{aligned} \quad (5.9)$$

which simplifies to

$$0 \approx \left[ (l + r_k(x_k)) \mathcal{P}(\underline{x}) + a \left( q_k \partial_k + \sum_{n=1}^N [\partial_n r(x_n) + (m + l + r_n(x_n)) \partial_n] \right) \mathcal{P}(\underline{x}) \right]_{x_k=0}. \quad (5.10)$$

Now using the definitions in Eqs. (5.6) and (5.7) of the drift and diffusion rates, we ultimately find

$$0 = \left[ \left( \mu_M + \partial_k V_k(x_k) + D_k \partial_k + \sum_{n=1}^N D_M \partial_n \right) \mathcal{P}(\underline{x}) \right]_{x_k=0} \quad (5.11)$$

which, for all  $k = 1, 2, \dots, N$  is the set of reflecting boundary conditions (5.11). These boundary conditions combined with the bulk equation (5.8) fully determine the stationary distribution of filament displacements in our model. Let us express these in a vector-matrix form as we saw in the example in Eq. (1.89): Eq. (5.8) is equivalently written

$$\underline{\nabla} \cdot \left( \underline{\nabla} V(\underline{x}) + \underline{\mu}_M + S \underline{\nabla} \right) \mathcal{P}(\underline{x}) = 0 \quad (5.12)$$

where  $\underline{\mu}_M$  is specified in Eq. (5.7) and

$$S = \begin{pmatrix} D_M + D_1 & D_M & \dots & D_M \\ D_M & D_M + D_2 & \dots & D_M \\ \vdots & \vdots & \ddots & \vdots \\ D_M & D_M & \dots & D_M + D_N \end{pmatrix} \quad (5.13)$$

is the diffusion matrix of the system. From this we see the diffusion of the membrane couples the different  $x_n$ , as indicated with nonzero off-diagonal entries in  $S$ . We then have a spatially-dependent drift  $-\underline{\nabla} V(\underline{x}) - \underline{\mu}_M$ . The sign indicates a negative drift, towards the origin i.e. the filaments and the membrane drift towards one another.

We can also rewrite the set of  $N$  zero-current conditions (5.11) as one equation

$$\left[ \left( \underline{\nabla} V(\underline{x}) + \underline{\mu}_M + S \underline{\nabla} \right) \mathcal{P}(\underline{x}) \right]_{\underline{x}=(0, \dots, 0)} = (0, \dots, 0) . \quad (5.14)$$

We refer to this set of  $N$  equations as *zero-current* boundary conditions, because the equation fixes the probability current at the boundaries to be zero. To see this, note that the stationary diffusion equation (5.12) can be written as  $0 = \underline{\nabla} \cdot \underline{J}$  where  $\underline{J}$  is the  $N$ -component probability current vector and the  $n^{\text{th}}$  component of the operator  $\underline{\nabla}$  is  $\partial_n$ . Then Eq. (5.14) is the condition that the  $n^{\text{th}}$  component of the current  $J_n$  is zero at the boundary  $x_n = 0, \forall n$ .

We now highlight the key property of the steady-state equations (5.12) and (5.14), that makes this system exactly solvable under certain conditions. The boundary condition (5.14) for filament  $n$  holds at  $x_n = 0$ . However, if Eq. (5.14) were to hold not



just at the boundary but also into the bulk, that is

$$\left(\underline{\nabla}V(\underline{x}) + \underline{\mu}_M + S\underline{\nabla}\right) \mathcal{P}(\underline{x}) = (0, \dots, 0) \quad (5.15)$$

then the bulk equation (5.12) would also be satisfied. In scenarios where this occurs, we can reduce the problem to a set of first-order equations that satisfies both equations. We note that for the more general problem of *reflected Brownian motion* with general boundary interactions, solutions can not generally be found in closed-form, at least in two dimensions [75, 161]. Therefore the assumption that Eq. (5.12) holds in the bulk  $x_n \geq 0$ , that is that the stationary solution has a zero probability current everywhere, should be thought of as an ansatz. In a one-filament system this is necessarily the case, however in a higher-dimensional system it is possible to have solutions that only have zero current at the boundaries. We will therefore find certain restrictions on model parameters that are consistent with the zero-current ansatz. The fact that some particular parameter combinations satisfy this ansatz and some do not is interesting; the systems that do not satisfy this ansatz must contain circulatory currents of probability through the bulk, which one would expect yields a more complex steady-state distribution.

### 5.2.3 Membrane velocity formula

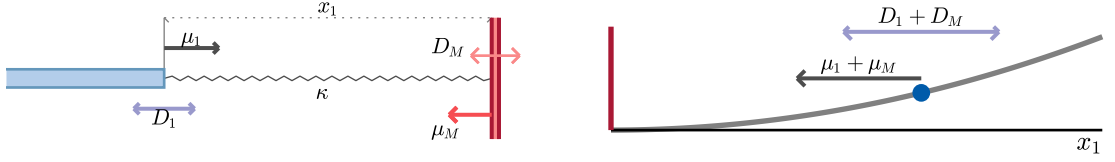
We are particularly interested in obtaining expressions for the mean membrane velocity  $v_M$  as a function of the various parameters in the system. In the continuum limit, it is not obvious what a formula for the membrane velocity would look like as a function of  $\mathcal{P}(\underline{x})$ . We can however write a simple expression for the velocity in the discrete case, so we take a continuum limit of this.

In the discrete system, the membrane will move at an average velocity  $-l$  when no filaments are in contact with it, and at velocity  $+m$  in any configuration  $\underline{i}^{(c)}$  where one or more filaments are in contact (see Figure 5.2):

$$v_M = -l(1 - \mathcal{P}_{\text{contact}}) + m\mathcal{P}_{\text{contact}} \quad (5.16)$$

$$= -l + (m + l) \sum_{\underline{i}^{(c)}} \mathcal{P}_{\underline{i}}. \quad (5.17)$$

By convention,  $v_M$  is positive if the membrane is moving to the right. Here,  $\mathcal{P}_{\text{contact}}$  is the total probability of the membrane being in contact with any filament i.e. a sum over all configurations  $\underline{i}^{(c)}$  where one or more filament contacts the membrane. In the continuum limit, however, we can neglect configurations with more than one contact as



**Figure 5.4** (Left) the single filament we solve in Section 5.3. (Right) the equivalent Brownian motion — a drift-diffusing 1D particle in a harmonic potential with a reflecting boundary at zero.

the probability that two filaments end at exactly the same point in continuous space is vanishingly small. With this simplification and the parameters in Eq. (5.7), we obtain from Eq. (5.17) in the continuum limit

$$v_M = -l(1 - \mathcal{P}_{\text{contact}}) + m\mathcal{P}_{\text{contact}} \quad (5.18)$$

$$\approx -l + (m + l) \sum_{n=1}^N \left[ \prod_{\substack{m=1 \\ m \neq n}}^N \left( \sum_{m \geq 0} \right) \mathcal{P}(\underline{i}|_{i_n=0}) \right] \quad (5.19)$$

$$\approx -\mu_M + \left( \frac{D_M}{a} + \mu_M \right) \sum_{n=1}^N \left[ \prod_{\substack{m=1 \\ m \neq n}}^N \left( \int_0^\infty \frac{dx_m}{a} \right) a^N \mathcal{P}(\underline{x}|_{x_n=0}) \right], \quad (5.20)$$

where  $\mathcal{P}(\underline{x}|_{x_n=0})$  is the pdf evaluated at  $x_n = 0$ . Taking this to leading order in  $a$  we then find

$$v_M = -\mu_M + D_M \sum_{n=1}^N \left[ \prod_{\substack{m=1 \\ m \neq n}}^N \left( \int_0^\infty dx_m \right) \mathcal{P}(\underline{x}|_{x_n=0}) \right]. \quad (5.21)$$

This equation has an intuitive form: the membrane tends to move left at speed  $\mu_M$  (as indicated by the first term), but is then biased right by an amount that increases with increasing contact between the membrane and filaments (as indicated by the boundary integrals in the second term). We note that  $v_M$  can take either sign: the membrane can move in either direction. If  $v_M = 0$  the system has *stalled*.

Before solving the general  $N$ -filament case, as a familiarisation exercise we first solve the ratchet system in the case of a single filament, and calculate the membrane velocity, which even for a single filament turns out to be surprisingly complex.

### 5.3 Introductory example: single filament

Take a single filament that grows and contracts stochastically, with a constant drift  $\mu_1$  towards the membrane along with a restoring force  $\kappa x_1$  and diffusion constant  $D_1$ . The membrane has a diffusion constant  $D_M$ , and a drift  $\mu_M$  towards the filament. We stress that there is an asymmetry in this interaction: the restoring force  $\kappa x_1$  attracts the filament to the membrane, but not vice versa. This is equivalent to a one-dimensional drift-diffusion, in a harmonic potential and a reflecting boundary at zero [162, 163], see Figure 5.4.

Here, the zero-current boundary condition implies that Eq. (5.14) must hold for all  $x_1$ , which in this 1D case reads

$$0 = [\kappa x_1 + \mu_1 + \mu_M + (D_1 + D_M)\partial_1] \mathcal{P}(x_1) . \quad (5.22)$$

This is straightforwardly integrated to give

$$\mathcal{P}(x_1) = \mathcal{A}^{-1} \exp \left( -\frac{\frac{1}{2}\kappa x_1^2 + (\mu_1 + \mu_M)x_1}{D_1 + D_M} \right) . \quad (5.23)$$

The normalisation  $\mathcal{A}$  is fixed by the condition  $\int_0^\infty dx_1 \mathcal{P}(x_1) = 1$  which yields

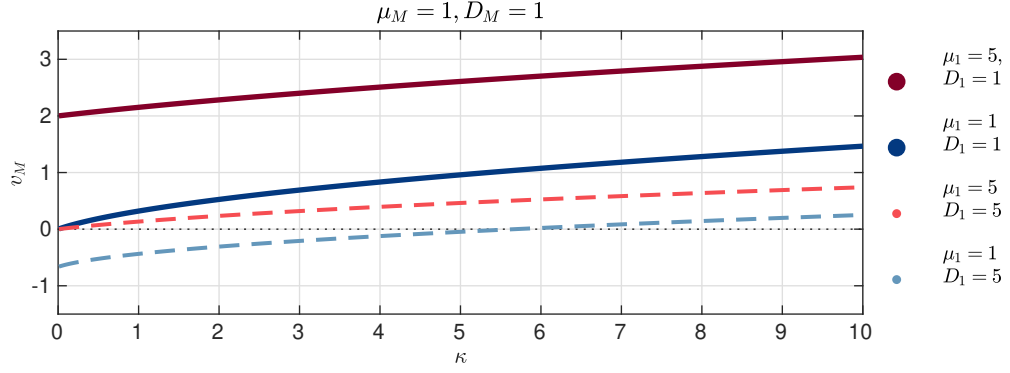
$$\mathcal{A} = \sqrt{\pi} \sqrt{\frac{D_1 + D_M}{2\kappa}} e^{c^2} \operatorname{erfc}(c) \quad (5.24)$$

where  $\operatorname{erfc}(\alpha) = 2/\sqrt{\pi} \int_\alpha^\infty dt e^{-t^2}$  is the complimentary error function, and  $c = (\mu_1 + \mu_M)/\sqrt{2\kappa(D_1 + D_M)}$ . With this, we use Eq. (5.21) to find the membrane velocity

$$v_M = -\mu_M + D_M \mathcal{P}(0) \quad (5.25)$$

$$= -\mu_M + \frac{D_M \sqrt{\frac{2\kappa}{D_1 + D_M}} \exp \left( -\frac{(\mu_1 + \mu_M)^2}{2\kappa(D_1 + D_M)} \right)}{\sqrt{\pi} \operatorname{erfc} \left( \frac{\mu_1 + \mu_M}{\sqrt{2\kappa(D_1 + D_M)}} \right)} . \quad (5.26)$$

We plot  $v_M$  for various filaments in Figure 5.5.  $v_M$  is a monotonically increasing function of  $\kappa$ . For the example  $\mu_1 = 1$ ,  $D_1 = 5$  (red, dashed), we see that the membrane can have a positive, negative or zero velocity depending on the value of  $\kappa$ . Thus a large enough restoring force will always lead to a positive velocity. In the case  $\mu_M + \mu_1 = 0$ , for which the filament and membrane drift towards each other only due to the linear



**Figure 5.5** *Analytic membrane velocity  $v_M$  (5.26) for a single filament system, for four different filaments.  $v_M$  is a monotonically increasing function of the restoring force constant  $\kappa$ . Against the same membrane ( $\mu_M = 1$ ,  $D_M = 1$ ), we see that a less diffusive (filled vs. dashed), higher drift (blue vs. red) filament is the most effective at moving the membrane.*

restoring  $\kappa x_1$ , Eq. (5.26) reduces to

$$v_M = -\mu_M + \frac{D_M}{\sqrt{\pi}} \sqrt{\frac{2\kappa}{D_1 + D_M}} \quad (5.27)$$

and the velocity deviates from the free velocity  $-\mu_M$  as the square root of the force constant  $\kappa$ . This scaling law is in fact general for  $N$  filaments, which we show in Section 5.5.1.

The membrane velocity in Eq. (5.26) is surprisingly elaborate given the simplicity of the system, and we will later see it becomes increasingly difficult to analytically normalise the pdf and calculate  $v_M$  with increasing numbers of filaments. This is not the case, however, in the absence of restoring forces ( $\kappa = \nu = 0$ ), as we now show.

## 5.4 Constant drift solution for many filaments

We now solve the system for  $N$  filaments, in the case of a linear potential  $V(\underline{x})$ , implying constant drifts for each filament:

$$V(\underline{x}) = \underline{\mu}_F \cdot \underline{x}, \quad \underline{\mu}_F \equiv \sum_{n=1}^N \mu_n \hat{n}, \quad (5.28)$$

with the subscript ‘ $F$ ’ denoting the filaments. The zero-current condition (5.15) now reads

$$\left( \underline{\mu}_M + \underline{\mu}_F + S \underline{\nabla} \right) \mathcal{P}(\underline{x}) = 0. \quad (5.29)$$

To solve this, let us trial the normalised distribution

$$\mathcal{P}(\underline{x}) = \left( \prod_{n=1}^N \lambda_n \right) e^{-\underline{\lambda} \cdot \underline{x}} \quad (5.30)$$

with an undetermined  $\underline{\lambda} = (\lambda_1, \dots, \lambda_N)$ . This solution has exponential decay of the filament-membrane separations with decay constants  $\lambda_n$  and the distributions for individual filaments are decoupled, despite the fluctuating membrane coupling the  $x_n$  to one another. Substituting this trial solution into Eq. (5.29) leads to the condition on  $\underline{\lambda}$

$$\underline{\mu}_M + \underline{\mu}_F - S\underline{\lambda} = 0 \quad (5.31)$$

which in turn implies

$$\underline{\lambda} = S^{-1} \left( \underline{\mu}_M + \underline{\mu}_F \right) . \quad (5.32)$$

This gives exact expressions for the  $(\lambda_1, \dots, \lambda_N)$  in terms of the drifts, and diffusion constants embedded within  $S$ . Furthermore, the entries of  $S^{-1}$  are explicitly calculable for any  $N$  via the Sherman-Morrison formula [164]:

$$(S^{-1})_{nk} = D_n^{-1} \left( \delta_{nk} - \frac{D_k^{-1}}{D_M^{-1} + \sum_{n'=1}^N D_{n'}^{-1}} \right) . \quad (5.33)$$

With further algebra, the components of  $\underline{\lambda}$  reduce to

$$\lambda_n = D_n^{-1} \left( \mu_n + \frac{\mu_M D_M^{-1} - \sum_{n'=1}^N \mu_{n'} D_{n'}^{-1}}{D_M^{-1} + \sum_{n''=1}^N D_{n''}^{-1}} \right) \quad (5.34)$$

giving an explicit solution for  $\mathcal{P}(\underline{x})$  as a function of the diffusion and drift parameters of the system. We see that  $\lambda_n$ , the exponential decay constant for the separation, increases with drift  $\mu_n$  but decreases with diffusion constant  $D_n$ . However the dependence on the drift and diffusion constants of the other filaments appears rather complicated. We shall see that these interdependencies are best understood when we consider the membrane velocity.

### 5.4.1 Mean membrane velocity

We initially assume that all  $\lambda_n > 0$  (see Section 5.4.2 for discussion of when this does not hold). With the decoupled exponential form in Eq. (5.30) of  $\mathcal{P}(\underline{x})$ , the membrane

velocity from Eq. (5.21) is straightforward to calculate as

$$v_M = -\mu_M + D_M \sum_{n=1}^N \left[ \prod_{\substack{m=1 \\ m \neq n}}^N \left( \int_0^\infty dx_m \right) \left( \prod_{n'=1}^N \lambda_{n'} \right) e^{-\underline{\lambda} \cdot \underline{x}} \Big|_{x_n=0} \right] \quad (5.35)$$

$$= -\mu_M + D_M \sum_{n=1}^N \lambda_n \quad (5.36)$$

$$= \frac{-\mu_M D_M^{-1} + \sum_{n=1}^N \mu_n D_n^{-1}}{D_M^{-1} + \sum_{n=1}^N D_n^{-1}}. \quad (5.37)$$

Eq. (5.37) is the central result of this section and gives the membrane velocity in terms of all the constituent filament and membrane parameters  $(\mu_1, \dots, \mu_N)$ ,  $(D_1, \dots, D_N)$ ,  $\mu_M$ ,  $D_M$ .

The exponential decay constants  $\lambda_n$  in Eq. (5.34) can then be written

$$\lambda_n = \frac{\mu_n - v_M}{D_n} \quad (5.38)$$

with the numerator of  $\lambda_n$  being the difference between the drift of filament  $n$  and the net velocity of the membrane determined by the whole system. As this difference decreases, the average separation  $\langle x_n \rangle = \lambda_n^{-1}$  naturally increases.

The membrane stalling drift  $\mu_M^*$  is defined as the drift for which  $v_M = 0$ :

$$\mu_M^* = D_M \sum_{n=1}^N \frac{\mu_n}{D_n}. \quad (5.39)$$

This can be interpreted in terms of the ratcheting mechanism.  $\mu_M^*$  increases as the drift of each filament  $\mu_n$  increases. Thus the membrane must have large drift to the left to stall the ratchet mechanism arising from more strongly polymerising filaments. However  $\mu_M^*$  decreases as each  $D_n$  increases. Thus greater variability of the polymerisation process reduces any ratcheting effect. On the other hand, increasing the membrane diffusion constant  $D_M$  increases  $v_M$  and thus requires an increase in membrane drift to stall the ratchet mechanism. This is because the fluctuations in membrane position due to a large  $D_M$  afford more opportunity for polymerisation near the membrane.

### 5.4.2 Steady-state condition

A property of the membrane-filament system is that it may not reach a steady state. If at least one of the  $\lambda_n$  is negative, then  $\mathcal{P}(\underline{x})$  is not normalisable, indicating the absence

of a steady state. Physically, this arises from one or more of the filaments drifting away from the membrane in perpetuity. Thus the requirement for a steady state in which the filaments travel with the membrane is that  $\lambda_n > 0$  for all  $n = 1, \dots, N$ .

To determine when this requirement holds, note that the sign of each  $\lambda_n$  in Eq. (5.34) is dependent on each and every other filament. Given these interdependencies, we then need to determine whether the full system forms a steady state.

Let us label the filaments  $1, \dots, N$  in order of decreasing drift, such that  $\mu_1 \geq \mu_2 \geq \dots \geq \mu_N$ . We first check if the filament with the highest drift, filament 1, would form a steady state with the membrane, if it were the only filament in the system. From the form of  $\lambda_n$  in Eq. (5.34) for  $N = 1$ , this gives the trivial condition  $\mu_1 + \mu_M > 0$ . If this is satisfied, filament 1 participates in the steady state because it moves towards the membrane. If it does not, the membrane and the filament drift apart, and no steady state is formed. Furthermore, as  $\mu_1 \geq \mu_2 \geq \dots \geq \mu_N$ , *none* of the filaments settle into a steady state.

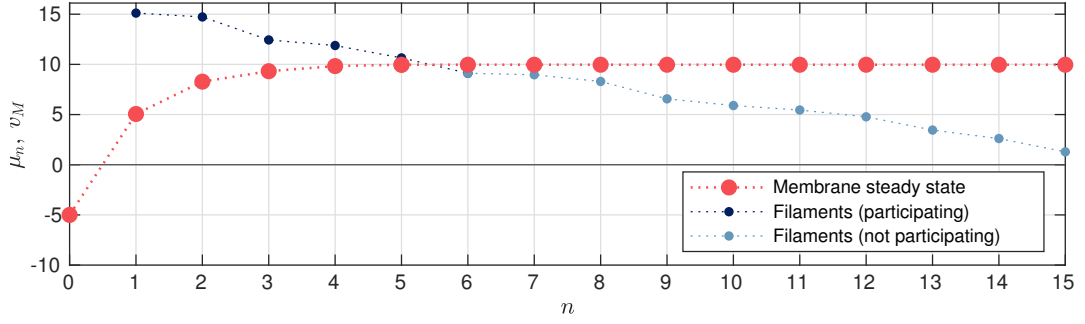
We now add filament 2. We check if  $\lambda_2 > 0$ . From the form of  $\lambda_n$  for  $N = 2$ , this gives the condition  $\mu_2 > (-\mu_M D_M^{-1} + \mu_1 D_1^{-1}) / (D_1^{-1} + D_M^{-1})$ . If this is satisfied, filament 2 also participates in the steady state. If it is not, the single filament-membrane system runs away from filament 2, and also the remaining filaments.

We repeat this process sequentially, and assuming that the condition has been satisfied by all filaments up to  $(n - 1)$ , we add filament  $n$ . The requirement for  $\lambda_n > 0$  is

$$\mu_n > \frac{-\mu_M D_M^{-1} + \sum_{n'=1}^{n-1} \mu_{n'} D_{n'}^{-1}}{D_M^{-1} + \sum_{n''=1}^{n-1} D_{n''}^{-1}}. \quad (5.40)$$

We find a result that, in retrospect, is self-consistent and physically intuitive: filament  $n$  will participate in the steady state if  $\mu_n$  is greater than the steady state membrane velocity in Eq. (5.37) from the system of the  $(n - 1)$  faster filaments. This is independent of  $D_n$ ; the diffusivity of a filament does not affect whether it can ‘catch up’ with a system in the long term.

Each additional participating filament contributes to increasing  $v_M$ . We must then sequentially add filaments by decreasing drift, until a filament is found that is slower than  $v_M$  up to that point. Then, that filament and all lower-velocity filaments do not participate in the steady state, and the pdf  $\mathcal{P}(\underline{x})$  is constructed from the participating filaments only. This procedure is illustrated in Figure 5.6, where filaments are sequentially added, and a new  $v_M$  is calculated on the addition of each filament.



**Figure 5.6** *Sequentially adding filaments to a system with a membrane with  $\mu_M = 5$ , by decreasing velocity. All diffusion parameters are set to 1 for simplicity. In this example, filament 6 is slower than the membrane when it is added, so filaments 1–5 form a steady state and other filaments fall away.*

In the case of a large number of *identical* filaments  $D_1, \dots, D_N = D_F$ ,  $\mu_1, \dots, \mu_N = \mu_F$ , we find

$$v_M = \frac{-\mu_M D_M^{-1} + N \mu_F D_F^{-1}}{D_M^{-1} + N D_F^{-1}} \quad (5.41)$$

$$\approx \mu_F - \frac{1}{N} \frac{D_F}{D_M} (\mu_M + \mu_F) . \quad (5.42)$$

We see that the membrane velocity converges to the filament drift  $\mu_F$  as the number of filaments  $N \rightarrow \infty$ , and all filaments participate. This specific case has been previously derived in Refs. [131, 133].

This ends our discussion of the constant drift case, having derived the pdf and membrane velocity in Eqs. (5.30) and (5.37) respectively, along with steady state conditions. We now go on to add restoring forces to the system.

## 5.5 Quadratic potential solution

We now introduce interactions between components of the system that take the form of linear restoring forces, deriving from quadratic potentials. As we now show, this system is also exactly solvable within the zero-current ansatz for several parameter combinations.

We add a second term to the potential  $V(\underline{x})$ :

$$V(\underline{x}) = \underline{\mu}_F \cdot \underline{x} + \frac{1}{2} \underline{x}^T \Gamma \underline{x} \quad (5.43)$$

$$= \sum_{n=1}^N \mu_n x_n + \sum_{n=1}^N \sum_{m=1}^N \frac{1}{2} \Gamma_{nm} x_n x_m . \quad (5.44)$$



$\Gamma$  is a symmetric matrix that describes interactions at quadratic order. Each diagonal element of the quadratic term represents a harmonic potential for the separation between a filament and the membrane. The off-diagonal terms represent couplings between the different filaments.

Under this potential, Eq. (5.15) reads

$$\left(\underline{\mu}_M + \underline{\mu}_F + \Gamma \underline{x} + S \underline{\nabla}\right) \mathcal{P}(\underline{x}) = 0 . \quad (5.45)$$

Given this new form of the potential, we choose as a trial solution the pdf

$$\mathcal{P}(\underline{x}) = \mathcal{A}^{-1} e^{-\underline{\lambda} \cdot \underline{x} - \frac{1}{2} \underline{x}^T G \underline{x}} . \quad (5.46)$$

The exponent contains all possible linear and quadratic combinations of the  $x_n$ .  $\mathcal{A}$  is a normalising constant and  $G$  is a to-be-determined symmetric matrix. Inserting this trial solution in to Eq. (5.45) yields

$$\underline{\mu}_M + \underline{\mu}_F + \Gamma \underline{x} - S (\underline{\lambda} + G \underline{x}) = 0 . \quad (5.47)$$

This implies a solution for  $\underline{\lambda}$

$$\underline{\lambda} = S^{-1} \left( \underline{\mu}_M + \underline{\mu}_F \right)$$

which is the same as Eq. (5.32), in the constant drift case. The solution for  $G$  is given as

$$G = S^{-1} \Gamma . \quad (5.48)$$

As  $G$  is symmetric, for Eq. (5.46) to be a valid solution, the matrix product  $S^{-1} \Gamma$  must be symmetric. This is not the case for an arbitrary interaction matrix  $\Gamma$ , which suggests that for several filaments the  $x_n = 0$  zero-current conditions (5.15) do *not* extend into the bulk generally. There may be additional currents in the bulk, and the filament-membrane displacements evolve as a more complex nonequilibrium steady state, which does not admit an exponential probability distribution.

In light of this, we seek particular potentials for which  $G = S^{-1} \Gamma$  is symmetric. With reference to the forces illustrated in Figure 5.3, we address two cases. First in Section 5.5.1, a system where the filaments are attracted to the membrane by a restoring spring-like force with strength  $\kappa$ . Then in Section 5.5.2 we introduce an additional surface tension with strength  $\nu$ .

As an aside, with these additional interactions Eq. (5.46) becomes a *multivariate normal distribution* [165]. If the pdf was defined over all space, one could straightforwardly normalise these functions via Gaussian integrals. However, for the ratchet system the domain of  $\mathcal{P}(\underline{x})$  is restricted to the upper *orthant*  $x_n \geq 0$ , and the normalisation factors  $\int_0^\infty dx_1 \dots \int_0^\infty dx_N \mathcal{P}(\underline{x})$  are far more challenging to evaluate than the usual integral over all space [165]. Regardless of this we can still analyse  $\mathcal{P}(\underline{x})$  and in particular find scaling laws for  $v_M$ .

### 5.5.1 Restoring force between filaments and the membrane

We can incorporate a harmonic potential with strength  $\kappa > 0$ . This is by design an asymmetric interaction which attracts each filament to the membrane, but not vice versa. We hope to encapsulate the features of a larger membrane moving in a viscous medium, and a rapidly-evolving network of actins with a variable rate of association and dissociation [145].

This interaction is incorporated with the diagonal matrix

$$\Gamma = \begin{pmatrix} \kappa & \cdot & \cdot & \cdots & \cdot & \cdot \\ \cdot & \kappa & \cdot & \cdots & \cdot & \cdot \\ \cdot & \cdot & \kappa & \cdots & \cdot & \cdot \\ \vdots & \vdots & \vdots & \ddots & & \\ \cdot & \cdot & \cdot & & \kappa & \cdot \\ \cdot & \cdot & \cdot & & \cdot & \kappa \end{pmatrix}. \quad (5.49)$$

With this simple interaction matrix, the matrix  $G$  in Eq. (5.46) is simply  $G = \kappa S^{-1}$ , which is symmetric as  $S^{-1}$  is symmetric (see Eq. (5.33)). Then with the form of  $\underline{\lambda}$  in Eq. (5.32), we can write the full solution  $\mathcal{P}(\underline{x})$  from Eq. (5.46) as

$$\mathcal{P}(\underline{x}) = \mathcal{A}^{-1} e^{-\frac{1}{2} \underline{b}^T S^{-1} \underline{b}} \quad (5.50)$$

where

$$\underline{b} = \kappa^{\frac{1}{2}} \underline{x} + \kappa^{-\frac{1}{2}} \left( \underline{\mu}_M + \underline{\mu}_F \right). \quad (5.51)$$

As each of the filaments is now in a harmonic trap with respect to the membrane, all filaments will participate in the steady state i.e. none lag behind. Mathematically this is seen as the pdf approaches zero as any of the  $x_n \rightarrow \infty$ , given  $\kappa > 0$ . Finally, note that unlike the linear drift case in Eq. (5.30), these quadratic potential systems contain

combinations of the form  $x_n x_m$  in the pdf, implying that the distribution does not decouple over filaments.

Although these multivariate normal distributions are challenging to normalise exactly for large  $N$ , we are still able to extract the leading-order scaling for the membrane velocity, as a function of  $\kappa$ .

### Velocity scaling law

We now argue that the introduction of a harmonic interaction introduces a  $\sqrt{\kappa}$  enhancement to the membrane velocity. For the steady-state pdf in Eq. (5.50), the normalisation constant  $\mathcal{A}$  is found by requiring

$$\prod_{n=1}^N \left( \int_0^\infty dx_n \right) \mathcal{P}(\underline{x}) = 1 . \quad (5.52)$$

We now perform two variable changes. First taking  $\underline{x}' = \kappa^{\frac{1}{2}} \underline{x}$ ,

$$\mathcal{A} = \prod_{n=1}^N \left( \kappa^{-\frac{1}{2}} \int_0^\infty dx'_n \right) e^{-\left( \underline{x}' + \kappa^{-\frac{1}{2}} [\underline{\mu}_M + \underline{\mu}_F] \right)^T S^{-1} \left( \underline{x}' + \kappa^{-\frac{1}{2}} [\underline{\mu}_M + \underline{\mu}_F] \right)} \quad (5.53)$$

and then  $\underline{x}'' = \underline{x}' + \kappa^{-\frac{1}{2}} (\underline{\mu}_M + \underline{\mu}_F)$ ,

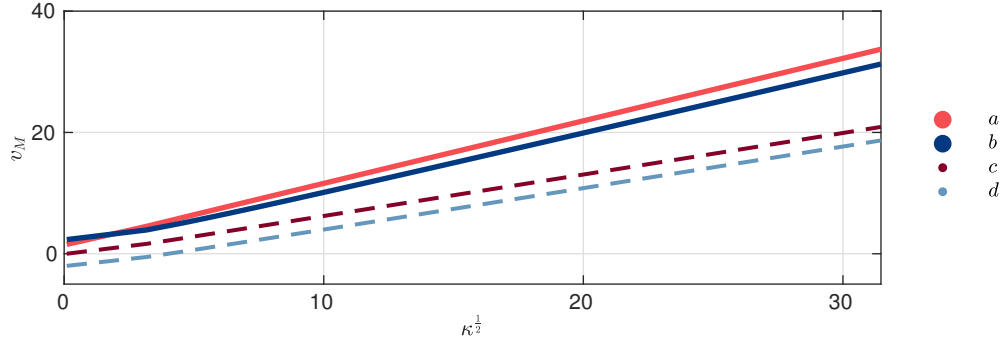
$$\mathcal{A} = \kappa^{-\frac{N}{2}} \prod_{n=1}^N \left( \int_{\kappa^{-\frac{1}{2}} (\underline{\mu}_M + \underline{\mu}_F)}^\infty dx''_n \right) e^{-\underline{x}''^T S^{-1} \underline{x}''} . \quad (5.54)$$

When  $\kappa$  is large, we can approximate the lower bound of each of the  $N$  integrals to extract the dominant  $\kappa$ -dependence

$$\mathcal{A} \approx \kappa^{-\frac{N}{2}} \prod_{n=1}^N \left( \int_0^\infty dx''_n \right) e^{-\frac{1}{2} \underline{x}''^T S^{-1} \underline{x}''} \quad (5.55)$$

$$\equiv \mathcal{B} \kappa^{-\frac{N}{2}} . \quad (5.56)$$

We define  $\mathcal{B}$  as a constant, independent of  $\kappa$ . Similarly, the membrane velocity formula (Eq. (5.21)) is a set of  $(N-1)$ -dimensional integrals. We can then use a similar argument



**Figure 5.7** Numerically-integrated membrane velocity as a function of  $\sqrt{\kappa}$  for four different  $N = 3$  filament systems (a)–(d). For each of these parameter sets, the straight lines indicate a  $v_M \propto \sqrt{\kappa}$  scaling relationship for large  $\kappa$ .  
(a)  $D_M = 1$ ,  $\mu_M = -1$ ,  $D_F = 1$ ,  $\underline{\mu}_F = (1, 3, 1)$ ,  $\nu = 2$ ;  
(b)  $D_M = 1$ ,  $\mu_M = 3$ ,  $D_1 = 2$ ,  $D_2 = 1/2$ ,  $D_3 = 3$ ,  $\underline{\mu}_F = (-2, 5, 2)$ ,  $\nu = 0$ ;  
(c)  $D_M = 1/2$ ,  $\mu_M = 2$ ,  $D_1 = 1/2$ ,  $D_2 = 2$ ,  $D_3 = 1$ ,  $\underline{\mu}_F = (1, 2, 1)$ ,  $\nu = 0$ ;  
(d)  $D_M = 1/2$ ,  $\mu_M = 5$ ,  $D_F = 1$ ,  $\underline{\mu}_F = (2, -1, -1)$ ,  $\nu = 1$ .

to find an overall scaling for the membrane velocity

$$v_M = -\mu_M + D_M \sum_{n=1}^N \left[ \prod_{\substack{m=1 \\ m \neq n}}^N \left( \int_0^\infty dx_m \right) \mathcal{P}(\underline{x}|x_n=0) \right] \quad (5.57)$$

$$\approx -\mu_M + \mathcal{C}\sqrt{\kappa}. \quad (5.58)$$

$\mathcal{C}$  is another  $\kappa$ -independent constant. We expect the correction to the normalisation in Eq. (5.56) to be of order  $\kappa^{-(N+1)/2}$ , corresponding to an  $\mathcal{O}(\kappa^0)$  correction to the velocity. To support this, we present in Figure 5.7 the numerically-integrated membrane velocities against  $\sqrt{\kappa}$  for four  $N = 3$  filament systems, each with different sets of diffusion and drift parameters. In all four cases we observe a linear scaling with  $\sqrt{\kappa}$  for large  $\kappa$ . In the case  $-\mu_M = \mu_1 = \mu_2 = \dots = \mu_N$ , the lower bounds of the integrals in Eq. (5.54) are precisely zero, and the approximations in Eqs. (5.56), (5.58) become exact, an example of which we saw in Eq. (5.27).

### 5.5.2 Surface tension

We now add an attractive harmonic interaction *between* neighbouring filaments. This serves to equalise the length of neighbouring filaments, and thus models a surface tension in the filament bundle.

This additional interaction leads to a new term in the potential  $V(\underline{x})$ :

$$V(\underline{x}) = \underline{\mu}_F \cdot \underline{x} + \frac{1}{2}\kappa \sum_{n=1}^N x_n^2 + \frac{1}{2}\nu \sum_{n=1}^{N-1} (x_{n+1} - x_n)^2, \quad (5.59)$$

where the parameter  $\nu$  specifies the strength of the surface tension. The interaction matrix is then

$$\Gamma = \begin{pmatrix} \kappa + \nu & -\nu & \cdot & \cdots & \cdot & \cdot \\ -\nu & \kappa + 2\nu & -\nu & \cdots & \cdot & \cdot \\ \cdot & -\nu & \kappa + 2\nu & \cdots & \cdot & \cdot \\ \vdots & \vdots & \vdots & \ddots & & \\ \cdot & \cdot & \cdot & & \kappa + 2\nu & -\nu \\ \cdot & \cdot & \cdot & & -\nu & \kappa + \nu \end{pmatrix}. \quad (5.60)$$

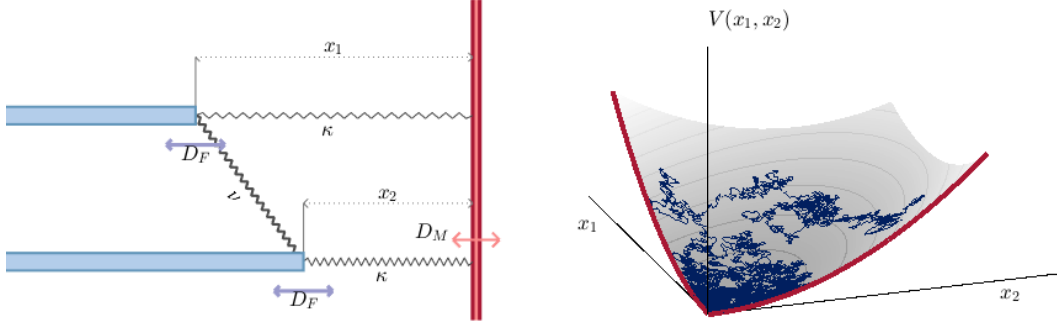
With these interactions, the matrix  $G = S^{-1}\Gamma$  that appears in the stationary solution (5.46) is symmetric only if the  $N$  filament diffusivities each take the same value, which we denote  $D_F$ . This implies any more general diffusivities fall outside of the zero-current ansatz and do not admit a solution of the form in Eq. (5.46). Taking this case of all filament diffusivities being equal, then, we find the entries for  $G$

$$G_{nm} = \kappa D_F^{-1} \left( \delta_{nm} - \frac{D_F^{-1}}{D_M^{-1} + N D_F^{-1}} \right) + \nu D_F^{-1} (2\delta_{nm} - \delta_{n,m-1} - \delta_{n,m+1} - \delta_{n1}\delta_{m1} - \delta_{nN}\delta_{mN}) . \quad (5.61)$$

Taking this form of  $G$  (and  $\underline{\lambda}$  in Eq. (5.32)), we have in Eq. (5.46) the pdf for a ratchet system with inhomogeneous drift terms, a restoring force to the membrane, and a surface tension. Note that we have assumed that filaments 1 and  $N$  are each only coupled to one neighbour, but one can couple them together by adding entries of  $-\nu$  into the top-right and bottom-left entries of  $\Gamma$ . This system can also be shown to have a symmetric form of  $G = S^{-1}\Gamma$  and satisfies the zero-current ansatz.

### Example: two filaments with quadratic interactions

To illustrate the effect of a surface tension on the system, we exactly normalise the pdf, and calculate the membrane velocity for the  $N = 2$  filament case, with both quadratic interactions included. For two filaments with  $\mu_M = \mu_1 = \mu_2 = 0$ , Eq. (5.46) is explicitly



**Figure 5.8** (Left) the interacting two-filament system that we address. (Right) the equivalent Brownian motion — a diffusion in a quadratic potential dependent on  $\nu$  and  $\kappa$ , with reflecting boundaries along the two axes.

$$\mathcal{P}(\underline{x}) = \mathcal{A}^{-1} \exp \left( -\nu \frac{(x_1 - x_2)^2}{2D_F} - \kappa \frac{(x_1^2 + x_2^2)(D_F + D_M) - 2D_M x_1 x_2}{2D_F(D_F + 2D_M)} \right). \quad (5.62)$$

Here, the filaments move towards the membrane by the restoring force only and the evolution may be modelled as a zero-drift Brownian motion in a quadratic potential, see Figure 5.8. In this case, the normalisation constant  $\mathcal{A}$ , obtained by integrating over all  $x_1, x_2 > 0$ , has the exact form

$$\mathcal{A} = \sqrt{\frac{D_F(D_F + 2D_M)}{\kappa(\kappa + 2\nu)}} \left[ \tan^{-1} \left( \frac{D_F\nu + D_M(\kappa + 2\nu)}{\sqrt{\kappa(\kappa + 2\nu)D_F(D_F + 2D_M)}} \right) + \frac{\pi}{2} \right] \quad (5.63)$$

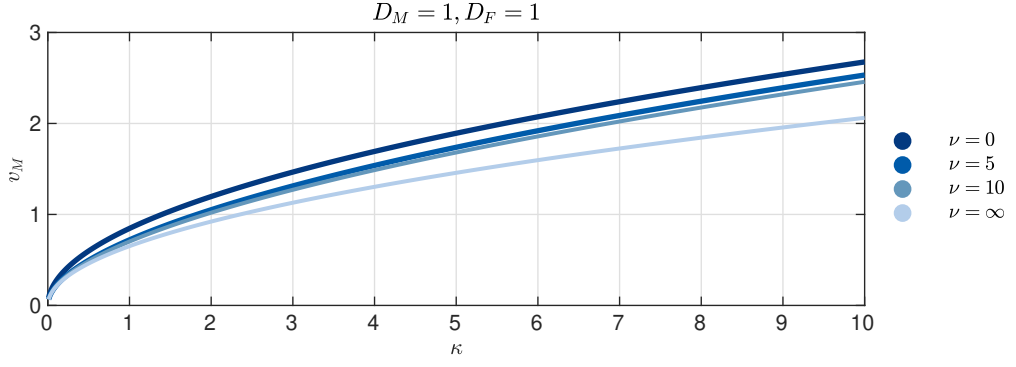
where we have used Eq. (4.3.2) in Ref. [166] to evaluate the integral. Then, the membrane velocity follows using Eq. (5.21):

$$v_M = \frac{\sqrt{2\pi} D_M \sqrt{\frac{\kappa(\kappa + 2\nu)}{D_F(\kappa + \nu) + D_M(\kappa + 2\nu)}}}{\tan^{-1} \left( \frac{D_F\nu + D_M(\kappa + 2\nu)}{\sqrt{\kappa(\kappa + 2\nu)D_F(D_F + 2D_M)}} \right) + \frac{\pi}{2}}. \quad (5.64)$$

This function is plotted in Figure 5.9. For a fixed  $\kappa$ , the membrane velocity *decreases* as the surface tension strength increases. The limit of  $v_M$  as  $\nu \rightarrow \infty$  is

$$\lim_{\nu \rightarrow \infty} v_M = \frac{D_M}{\sqrt{\pi}} \sqrt{\frac{2\kappa}{D_F/2 + D_M}}. \quad (5.65)$$

In this limit the two filaments are tightly bound and resemble a single filament



**Figure 5.9** *Analytic membrane velocity as a function of  $\kappa$ , for a two-filament system at four different surface tension strengths  $\nu$ . On increasing  $\nu$  the filaments become less effective at moving the membrane, with the limiting case  $\nu \rightarrow \infty$  effectively a one-filament system, see Eq. (5.65).*

(Eq. (5.27)), with diffusion constant  $D_F/2$ .

Finally, for the case  $\nu = 0$  (i.e. where there is no surface tension), the velocity reduces to

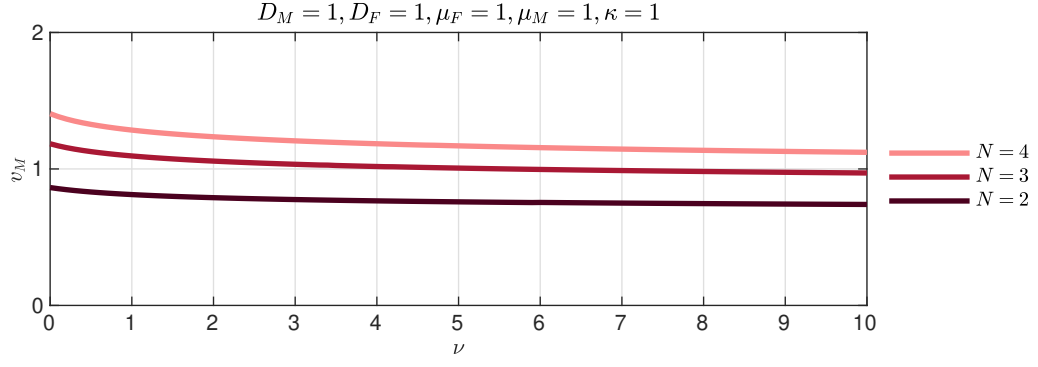
$$v_M = \frac{2\sqrt{2\pi}D_M\sqrt{\frac{1}{D_F+D_M}}}{\tan^{-1}\left(\frac{D_M}{\sqrt{D_F(D_F+2D_M)}}\right) + \frac{\pi}{2}}\sqrt{\kappa} \quad (5.66)$$

which is proportional to  $\sqrt{\kappa}$ , as claimed in Section 5.5.1.

### More than two filaments

In the case of more than two filaments, it is difficult to calculate the normalisation constant  $\mathcal{A}$  in (5.46) in a closed form. Therefore, to investigate this case, we turn to numerical evaluation of both the normalising integral and the integrals that appear in Eq. (5.21) for the membrane velocity. We plot the membrane velocity as a function of surface tension strength for fixed drift and diffusion rates in Figure 5.10. For all  $N = 2, 3, 4$ , we find that the membrane velocity decreases with surface tension, asymptotically approaching a constant.

There is a simple physical interpretation of this result. The ratcheting mechanism means that only a single filament need be in contact with the membrane in order to force it to move right. By introducing a surface tension, there will always be a force on the closest filament from its neighbours that pulls it *away* from the membrane, making the filament network as a whole less efficient at ratcheting the membrane.



**Figure 5.10** *Membrane velocity as a function of surface tension strength  $\nu$  for up to  $N = 4$  filaments, calculated by numerical integration of the pdf in Eq. (5.46). While increasing  $N$  increases  $v_M$ , the velocity decreases with  $\nu$  for all three systems as they become less effective at moving the membrane.*

## 5.6 Link to diffusion problems in exclusion processes

As a short aside, we make an observation that links the diffusion problems discussed here, and those encountered before in the context of the TASEP in Chapter 4. If we return to our bulk ratchet diffusion equation (5.12) and set  $D_M = D_1 = \dots = D_N = 1/8$ , the  $(N \times N)$  diffusion matrix (Eq. (5.13)) reads

$$S = \frac{1}{8} \begin{pmatrix} 2 & 1 & 1 & \cdots & 1 \\ 1 & 2 & 1 & \cdots & 1 \\ 1 & 1 & 2 & \cdots & 1 \\ \vdots & \vdots & \vdots & \ddots & \vdots \\ 1 & 1 & 1 & \cdots & 2 \end{pmatrix}. \quad (5.67)$$

What is interesting is that this is the same matrix that characterises the diffusion in Section 4.6.3, Eq. (4.146), pertaining to the continuum limit generating function for the sum of TASEP weights raised to the  $N^{\text{th}}$  power (note a clash in notation: here,  $N$  denotes the power the weights are raised to and *not* the length of a TASEP). In other words, the underlying diffusion dynamics are the same for both problems. The differences between the two are that the TASEP diffusion process is time-dependent with absorbing boundaries, and the ratchet diffusion is in the steady state, with reflecting boundaries and a negative drift.



## 5.7 Summary

In this chapter we have derived the steady-state distribution of a pure continuum ratcheting system of  $N$  heterogeneous filaments, constricted by a membrane. This model exhibits ratcheting, whereby a membrane moves at a velocity different to its inherent drift, solely due to thermal fluctuations and steric interactions between it and the filaments. This provides a more comprehensive, general formalism than earlier continuum models [131, 133]. We have shown that the  $N$  filament-membrane displacements evolve by an  $N$ -dimensional drift-diffusion process, and derived the corresponding steady-state differential equation with a set of zero-current boundary conditions.

We then identified a number of these ratchet systems whereby the second-order differential equation reduces to a set of first-order equations, which can be directly integrated. In these systems, the zero-current boundary conditions holds at the boundary (equivalently, when a filament makes contact with the membrane), but also extends into the bulk of the system. This zero-current condition holds for a variety of systems including physically relevant cases of fixed filament drift (linear filament-membrane interaction potentials), quadratic filament-membrane and quadratic filament-filament interaction potentials.

For these cases, we have found explicit expressions for the probability distribution of filament displacements (e.g. Eqs. (5.30) and (5.34) for the constant drift case) and from these one can derive expressions for the membrane velocity. In the case of an arbitrary number  $N$  of heterogeneous filaments, each with its own fixed drift and diffusion constant, we have obtained in Eq. (5.37) an explicit and transparent expression for the membrane velocity  $v_M$ , and in Eq. (5.58) a scaling law for when the filaments are also attracted to the membrane by a restoring force. Eq. (5.37) reveals, among other things, how the ratcheting mechanism is enhanced by greater membrane diffusion.

For the case of constant-drift filaments, the probability distribution (Eq. (5.30)) decouples among each of the  $N$  filaments. However, a subtlety arises in that it is not obvious as to whether a collection of filaments will actually form a steady state. A new filament will only participate if its growth velocity is greater than the prior membrane velocity. Conversely, one new high-velocity filament can disrupt a pre-existing steady state, by pulling the system away from other lower velocity filaments. Which filaments participate is a collective outcome of the set of filaments, and may be determined by carefully considering the filaments in decreasing order of drift velocity (Figure 5.6).

For the case of a quadratic interaction potential, all filaments will participate in the steady state. While it is a challenge to normalise the multivariate normal distribution in Eq. (5.46) for large  $N$  we find in Eq. (5.58) that a harmonic attraction to the membrane increases the velocity by an amount proportional to the square root of the force constant  $\kappa$ , to leading order. It is physically intuitive that the velocity would increase as the attractive force increases, however the specific scaling with  $\sqrt{\kappa}$  is less obvious.

Finally, we have introduced a surface tension element between neighbouring filaments, and shown that  $v_M$  decreases as a result. Intuitively, a surface tension will always pull the right-most filament away from the membrane, giving the membrane more space to freely move left. This suggests that the filament network most efficiently moves the membrane when each filament moves independently of one another.

An interesting problem that arises from this work is that some particular parameter combinations have zero probability current in the bulk, and some do not. In these non-ansatz-satisfying systems, one might expect circulatory — perhaps oscillatory — flows of probability current in the bulk. A natural progression from the work presented here would be to further probe these more complex systems, and how the tuning of these parameters gives rise to additional bulk currents.

This system is exactly solvable and the expressions for the membrane velocity  $v_M$  are analytic, for an arbitrary number of filaments. In contrast, the discrete ratchet system in Figure 5.2 does not admit a separable solution. To more closely resemble the dynamics of real actin networks, and to extend beyond the pure ratchet model considered here, it would be desirable to encode some type of direct *contact force* between the filaments and membrane beyond hard-core exclusion [167]. The challenge is that for any non-instantaneous contact (such as *tethering* filaments to the membrane [135]), the zero-current boundary conditions no longer hold. More generally, the zero-current condition is characteristic of a nonequilibrium steady state, that is, one that is maintained through a constant input and subsequent dissipation of energy and for which a general theoretical formalism remains elusive [168].

## Chapter 6

# Conclusion

In this thesis we have presented and solved several statistical mechanics problems, of systems that settle into a nonequilibrium steady state. We have solved these problems by writing them in terms of random walks, and in turn solving those random walks.

The first system we investigated was the asymmetric simple exclusion process. This paradigmatic nonequilibrium system is very simply posed, but has a surprisingly intricate steady-state solution which offers a natural extension to random walk problems. In Chapter 2 we gave a comprehensive discussion of the links between the steady-state distribution obtained via the matrix product approach, and a more general family of combinatorial problems. We saw that the state space of the  $2^N$  configurations of particles and holes can be expressed as a partitioning of a set of  $\frac{1}{N+2} \binom{2N+2}{N+1} \geq 2^N$  more abstract mathematical objects, be it *dominated paths*, *bicoloured Motzkin paths* or *complete configurations*. We observed that these appear to further map to a space of  $(N+1)! \geq \frac{1}{N+2} \binom{2N+2}{N+1} \geq 2^N$  number permutations. Many of these mappings and observations had been scattered in earlier mathematics and physics literature. In this chapter we brought these mappings together under a unified mathematical structure. In addition, we introduced a new representation of the TASEP stationary state space, in terms of *dominated paths*. We write a TASEP configuration as a path, with a sequence of up and right steps in accordance with the sequence of particles and holes. Then, we proved that the weight of that configuration is the number of distinct paths that could be drawn under its perimeter. Under this mapping it is very clear how combinatorial numbers such as the Catalan and Narayana sequences emerge. This, combined with work in the combinatorial literature, allowed us to derive some new results, a highlight being a novel determinantal expression for the partition function.

One clear outcome of Chapter 2 was that the nonequilibrium steady-state distribution of the ASEP could not be fashioned into any sort of equilibrium probability distribution — that is, exponentially weighted with a temperature-like exponent. This rendered any conventional statistical mechanics methods ineffectual when calculating measures such as the Gibbs-Shannon entropy. However, building on what we learned in Chapter 2, we derived in Chapter 3 the  $\lambda = 2$  *Rényi entropy* of the totally asymmetric variant of the ASEP, the TASEP. The main technical challenge here was an enumeration of  $2^N$  *squared* TASEP configuration weights. From the ladder operator interpretation of the matrix product formalism, we expressed this enumeration as a two-dimensional random walk problem with absorbing boundaries. We solved the generating function (counting over starting coordinates, final coordinates and walk length) of this two-dimensional walk. This entailed a generalisation of a mathematical technique known as the *obstinate kernel* method, and we solved the generating function by exploiting a symmetry in the underlying recurrence relation.

The  $\lambda = 2$  Rényi entropy calculation was quite technical and the final generating function could not be obviously inverted by hand. We showed in Chapter 4 that the space and time *continuum limit* of the 2D random walk was also solvable, by a novel method that appeared step-by-step to be analogous with the obstinate kernel method of Chapter 3. The resultant *Laplace transform* in this case was concise and intuitive, and further analysis yielded predictions of properties of the TASEP such as phase dynamics and current, that converged to the physical case within a scaling region where the three dynamical phases coincided. We discussed how this could be a more analytically tractable method for the matter of evaluating higher-order Rényi entropies.

In Chapter 5 we investigated another system entirely, in the many-filament continuum Brownian ratchet. This system comprised a network of stochastically growing and shrinking filaments and a constricting drift-diffusing membrane. We saw the phenomenon of the membrane moving in a direction opposite to its natural drift by a ratcheting mechanism, induced by thermal fluctuations and steric interactions only. Such a system may be observed in reality, at the leading edge of eukaryotic cells, where a network of actins grows and shrinks to move and morph the cell membrane. We modelled the ratchet in the steady state as an  $N$ -dimensional Brownian motion with reflecting boundary conditions, by treating the system as a time evolution of the vector of  $N$  displacements between the membrane and filaments. This diffusion has similar dynamics to the diffusion we saw when calculating the Rényi entropy of the TASEP in the continuum limit, except with different boundary conditions. The diffusion problem here reduced to a set of first-order equations which could be directly integrated, for

a variety of nontrivial sets of parameters, including couplings between neighbouring filaments, and the filaments to the membrane, by quadratic potentials.

The work presented here shows that many problems in paradigmatic nonequilibrium steady states can be expressed in terms of random walk (and more generally, combinatorial) problems, some of which have been solved here. However, many more are still to be explored. For example, we showed how the sum of TASEP weights to arbitrary integer power  $\lambda$  could be formulated as a random walk problem in  $\lambda$  dimensions (or a  $\lambda$ -dimension diffusion in the continuum limit). These higher-dimension walks have not been investigated in detail, but would in turn give higher-order Rényi entropies, and would tell us more about the steady state distribution. More generally, having defined the TASEP, PASEP and SSEP state spaces as partitionings of larger state spaces in accordance with certain mathematical constructs, we can write problems concerning these systems (e.g. Rényi entropies and correlation functions) as well-defined combinatorial problems. Elsewhere, in the continuum Brownian ratchet problem, we found a family of parameter combinations where the underlying diffusion problem reduced to first order. Naturally, our attention turns to the other cases, where the zero-current boundary conditions do not extend into the bulk of the system and we can not directly integrate the diffusion equation. This indicates a more complex steady state, however the work presented here allows us to write the diffusion equation and reflecting boundary conditions for these more complicated systems. The main challenge now the matter of solving them. It would be interesting to learn why some ratchet systems form simple steady states, and the nature of those that do not.

Even more generally, we made the relatively simple observation that for an equilibrium system, a phase transition corresponds to a *pair* of discontinuities in the Rényi entropy, with respect to temperature, or a temperature-like variable. In a nonequilibrium system, however, each phase transition yields just a single discontinuity. Given a system with a phase transition, then, knowledge of its probability distribution is alone enough to determine whether it is in or out of equilibrium, by computing the Rényi entropy. Obviously, for our case the ASEP is nonequilibrium by construction. However, perhaps there are systems where one can observe and construct a probability distribution, and see sharp transitions in macroscopic observables when tuning certain parameters, but not actually know the underlying mechanics of the system. The Rényi entropy could at least indicate whether the dynamics are equilibrium or nonequilibrium.

## Appendix A

# Demonstration of $DE = D + E$ in path dominance problem

We saw in Section 2.2.1 that an ASEP configuration  $\mathcal{C}$  can be uniquely defined by the set of  $x$  or  $y$ -coordinates  $(x_0, x_1, \dots, x_P)$ ,  $(y_0, y_1, \dots, y_Q)$  that its equivalent path  $\mathcal{T}$  traces. We now show that the weight of a path  $\mathcal{W}(\mathcal{T})$ , defined as the number of paths it dominates, has an equivalent property to the matrix reduction relation in Eq. (1.12),  $DE = D + E$ . This, combined with Eqs. (2.11) and (2.12), would then show that the weight of the TASEP configuration is the weight of its equivalent path,  $\mathcal{W}(\mathcal{C}) = \mathcal{W}(\mathcal{T})$ .

Let us split the path  $\mathcal{T}$  into  $\mathcal{T} = (\mathcal{T}_{(1)}, \uparrow, \rightarrow, \mathcal{T}_{(2)})$ . From this, we must show

$$\mathcal{W}(\mathcal{T}) = \mathcal{W}(\mathcal{T}_{(1)}, \uparrow, \mathcal{T}_{(2)}) + \mathcal{W}(\mathcal{T}_{(1)}, \rightarrow, \mathcal{T}_{(2)}) .$$

This is Eq. (2.13) (illustrated in Figure 2.4), and is equivalent to the matrix relation  $DE = D + E$ .

If  $\mathcal{T}$  has a set of  $y$ -coordinates  $(y_0, y_1, y_2, \dots, y_{i-1}, y_i, y_{i+1}, \dots, y_{Q-1}, y_Q)$ , Eq. (2.13) is equivalently

$$\begin{aligned} & \mathcal{W}(y_0, y_1, y_2, \dots, y_{i-1}, y_i, y_{i+1}, \dots, y_{Q-1}, y_Q) \\ &= \mathcal{W}(y_0, y_1, y_2, \dots, y_{i-1}, y_{i+1}, \dots, y_{Q-1}, y_Q) \\ & \quad + \mathcal{W}(y_0, y_1, y_2, \dots, y_{i-1}, y_i - 1, y_{i+1} - 1, \dots, y_{Q-1} - 1, y_Q - 1) . \end{aligned} \quad (\text{A.1})$$

We first write  $\mathcal{W}(\mathcal{T}_{(1)}, \rightarrow, \mathcal{T}_{(2)})$  using the summation formula (2.5)

$$\mathcal{W}(\mathcal{T}_{(1)}, \rightarrow, \mathcal{T}_{(2)}) = \sum_{n_0=0}^{y_0} \sum_{n_1=n_0}^{y_1} \cdots \sum_{n_{i-1}=n_{i-2}}^{y_{i-1}} \sum_{n_i=n_{i-1}}^{y_i-1} \sum_{n_{i+1}=n_i}^{y_{i+1}-1} \sum_{n_{i+2}=n_{i+1}}^{y_{i+2}-1} \cdots \sum_{n_{Q-1}=n_{Q-2}}^{y_{Q-1}-1} 1 \quad (\text{A.2})$$

and rework this expression so to ‘complete’ each of the  $n_i, n_{i+1}, \dots, n_{Q-1}$  summations sequentially:

$$\begin{aligned} \mathcal{W}(\mathcal{T}_{(1)}, \rightarrow, \mathcal{T}_{(2)}) &= \sum_{n_0=0}^{y_0} \sum_{n_1=n_0}^{y_1} \cdots \sum_{n_{i-1}=n_{i-2}}^{y_{i-1}} \sum_{n_i=n_{i-1}}^{y_i} \sum_{n_{i+1}=n_i}^{y_{i+1}-1} \sum_{n_{i+2}=n_{i+1}}^{y_{i+2}-1} \cdots \sum_{n_{Q-1}=n_{Q-2}}^{y_{Q-1}-1} 1 \\ &\quad - \sum_{n_0=0}^{y_0} \sum_{n_1=n_0}^{y_1} \cdots \sum_{n_{i-1}=n_{i-2}}^{y_{i-1}} \left( \sum_{n_{i+1}=n_i}^{y_{i+1}-1} \sum_{n_{i+2}=n_{i+1}}^{y_{i+2}-1} \cdots \sum_{n_{Q-1}=n_{Q-2}}^{y_{Q-1}-1} 1 \right) \end{aligned} \quad (\text{A.3})$$

$$\begin{aligned} &= \sum_{n_0=0}^{y_0} \sum_{n_1=n_0}^{y_1} \cdots \sum_{n_{i-1}=n_{i-2}}^{y_{i-1}} \sum_{n_i=n_{i-1}}^{y_i} \sum_{n_{i+1}=n_i}^{y_{i+1}} \sum_{n_{i+2}=n_{i+1}}^{y_{i+2}-1} \cdots \sum_{n_{Q-1}=n_{Q-2}}^{y_{Q-1}-1} 1 \\ &\quad - \sum_{n_0=0}^{y_0} \sum_{n_1=n_0}^{y_1} \cdots \sum_{n_{i-1}=n_{i-2}}^{y_{i-1}} \left( \sum_{n_{i+1}=n_i}^{y_{i+1}-1} \sum_{n_{i+2}=n_{i+1}}^{y_{i+2}-1} \cdots \sum_{n_{Q-1}=n_{Q-2}}^{y_{Q-1}-1} 1 \right) \\ &\quad - \sum_{n_0=0}^{y_0} \sum_{n_1=n_0}^{y_1} \cdots \sum_{n_{i-1}=n_{i-2}}^{y_{i-1}} \left( \sum_{n_{i+2}=n_{i+1}}^{y_{i+2}-1} \cdots \sum_{n_{Q-1}=n_{Q-2}}^{y_{Q-1}-1} 1 \right) \end{aligned} \quad (\text{A.4})$$

$$\begin{aligned} &= \sum_{n_0=0}^{y_0} \sum_{n_1=n_0}^{y_1} \cdots \sum_{n_{i-1}=n_{i-2}}^{y_{i-1}} \sum_{n_i=n_{i-1}}^{y_i} \sum_{n_{i+1}=n_i}^{y_{i+1}} \sum_{n_{i+2}=n_{i+1}}^{y_{i+2}} \cdots \sum_{n_{Q-1}=n_{Q-2}}^{y_{Q-1}} 1 \\ &\quad - \sum_{n_0=0}^{y_0} \sum_{n_1=n_0}^{y_1} \cdots \sum_{n_{i-1}=n_{i-2}}^{y_{i-1}} \left( \sum_{n_{i+1}=n_i}^{y_{i+1}-1} \sum_{n_{i+2}=n_{i+1}}^{y_{i+2}-1} \cdots \sum_{n_{Q-1}=n_{Q-2}}^{y_{Q-1}-1} 1 \right) \\ &\quad - \sum_{n_0=0}^{y_0} \sum_{n_1=n_0}^{y_1} \cdots \sum_{n_{i-1}=n_{i-2}}^{y_{i-1}} \left( \sum_{n_{i+2}=n_{i+1}}^{y_{i+2}-1} \cdots \sum_{n_{Q-1}=n_{Q-2}}^{y_{Q-1}-1} 1 \right) \\ &\quad \vdots \\ &\quad - \sum_{n_0=0}^{y_0} \sum_{n_1=n_0}^{y_1} \cdots \sum_{n_{i-1}=n_{i-2}}^{y_{i-1}} \left( \sum_{n_{Q-1}=n_{Q-2}}^{y_{Q-1}-1} 1 \right) \\ &\quad - \sum_{n_0=0}^{y_0} \sum_{n_1=n_0}^{y_1} \cdots \sum_{n_{i-1}=n_{i-2}}^{y_{i-1}} (1) . \end{aligned} \quad (\text{A.5})$$

This nested expression then telescopes down to two sums, which can be identified as

$$\begin{aligned}
\mathcal{W}(\mathcal{T}_{(1)}, \rightarrow, \mathcal{T}_{(2)}) &= \sum_{n_0=0}^{y_0} \sum_{n_1=n_0}^{y_1} \cdots \sum_{n_{i-1}=n_{i-2}}^{y_{i-1}} \sum_{n_i=n_{i-1}}^{y_i} \sum_{n_{i+1}=n_i}^{y_{i+1}} \sum_{n_{i+2}=n_{i+1}}^{y_{i+2}} \cdots \sum_{n_{Q-1}=n_{Q-2}}^{y_{Q-1}} 1 \\
&\quad - \sum_{n_0=0}^{y_0} \sum_{n_1=n_0}^{y_1} \cdots \sum_{n_{i-1}=n_{i-2}}^{y_{i-1}} \sum_{n_{i+1}=n_i}^{y_{i+1}} \sum_{n_{i+2}=n_{i+1}}^{y_{i+2}} \cdots \sum_{n_{Q-1}=n_{Q-2}}^{y_{Q-1}} 1 \\
& \tag{A.6}
\end{aligned}$$

$$= \mathcal{W}(\mathcal{T}) - \mathcal{W}(\mathcal{T}_{(1)}, \uparrow, \mathcal{T}_{(2)}) \tag{A.7}$$

which is the desired result, Eq. (2.13).



## Appendix B

### Details of $\mathcal{Q}(z; \alpha, \beta)$

#### B.1 Extraction of coefficients for obtaining $\mathcal{R}(t; a, a, b, b)$

In this section we present the full calculation of extracting coefficients to obtain, from the recursion relation in Eq. (3.40), a closed-form expression for the generating function  $\mathcal{R}(t; a, a, b, b)$ , for the number of walks beginning and terminating at points on the diagonal. We return to Eq. (3.87), which we restate for convenience:

$$\begin{aligned} & xy\mathcal{R}(x, y) + \bar{y}\mathcal{R}(x, \bar{x}\bar{y}) - \bar{x}\mathcal{R}(\bar{x}\bar{y}, y) \\ &= \frac{1}{\sqrt{\Delta(x)}} \left[ \frac{1}{1 - \bar{y}Y_-(x)} + \frac{1}{1 - y\bar{Y}_+(x)} - 1 \right] \left[ \frac{xy}{(1 - bx)(1 - by)} \right. \\ &\quad \left. + \frac{\bar{y}}{(1 - bx)(1 - b\bar{x}\bar{y})} - \frac{\bar{x}}{(1 - b\bar{x}\bar{y})(1 - by)} + t\mathcal{R}(0, 0) - 2t(1 + x)\mathcal{R}(x, 0) \right]. \end{aligned}$$

### B.1.1 $y^0$ coefficient extraction

Extraction of the  $y^0$  component is this time more involved. If we take a cross term of Eq. (3.87) as an example, we obtain the  $y^0$  coefficient with an explicit series expansion

$$\begin{aligned} & \left[ \frac{1}{1 - \bar{y}Y_-(x)} + \frac{1}{1 - y\bar{Y}_+(x)} - 1 \right] \left[ \frac{xy}{(1 - bx)(1 - by)} \right] \\ &= \frac{x}{1 - bx} \left[ \sum_{n \geq 0} (\bar{y}Y_-)^n + \sum_{m \geq 0} (y\bar{Y}_+)^m - 1 \right] \left[ y \sum_{p \geq 0} (by)^p \right] \end{aligned} \quad (\text{B.1})$$

$$= \frac{x}{1 - bx} \sum_{n \geq 1} \sum_{p \geq 0} y^{1+p-n} Y_-^n b^p + \mathcal{O}(y) \quad (\text{B.2})$$

$$= \frac{x}{1 - bx} \sum_{n \geq 1} Y_-^n b^{n-1} + \mathcal{O}(y) + \mathcal{O}(\bar{y}) \quad (\text{B.3})$$

$$= \frac{xY_-(x)}{(1 - bx)(1 - bY_-(x))} + \mathcal{O}(y) + \mathcal{O}(\bar{y}) . \quad (\text{B.4})$$

Applying this same method throughout, the  $y^0$  component of Eq. (3.87) is

$$\begin{aligned} -\bar{x}R^{(d)}(\bar{x}) &= \frac{1}{\sqrt{\Delta(x)}} \left[ t\mathcal{R}(0) - 2t(1+x)\mathcal{R}(x) + \frac{2xY_-(x)}{(1 - bx)(1 - bY_-(x))} \right. \\ &\quad \left. - \frac{2b\bar{x}Y_-(x)}{(1 - b^2\bar{x})(1 - bY_-(x))} - \frac{\bar{x}}{1 - b^2\bar{x}} \right] \end{aligned} \quad (\text{B.5})$$

where we have further condensed the notation and introduced  $\mathcal{R}(x) \equiv \mathcal{R}(x, 0)$ ,  $\mathcal{R}(0) \equiv \mathcal{R}(0, 0)$  and

$$R^{(d)}(x) \equiv \sum_{N \geq 0} \sum_{i \geq 0} \sum_{k \geq 0} \sum_{l \geq 0} t^N x^i b^{k+l} \langle i | \langle i | \mathcal{V}^N | k \rangle | l \rangle . \quad (\text{B.6})$$

Considering the explicit form of  $Y_-(x)$  in Eq. (3.44), one can rearrange the term

$$\frac{Y_-(x)}{1 - bY_-(x)} = -\frac{1}{2} \frac{t(2b + 1 + 2bx + x^2) - x + x\sqrt{\Delta(x)}}{(1 + b)tx^2 + (t + b(bt - 1))x + b(1 + b)t} \quad (\text{B.7})$$

whereby the quadratic in the denominator factorises in a way similar to the kernel

$$(1 + b)tx^2 + (t + b(bt - 1))x + b(1 + b)t = (1 + b)t(x - bY_-(b, t))(x - bY_+(b, t)) . \quad (\text{B.8})$$

Using this, the full equation may be rearranged into the form

$$\begin{aligned}
& \sqrt{\Delta_+(\bar{x})} \left[ -(1 - bY_-(b)\bar{x})R^{(d)}(\bar{x}) + \frac{x}{(1+b)t(x - bY_+(b))} \left( \frac{x}{1-bx} - \frac{b\bar{x}}{1-b^2\bar{x}} \right) \right] \\
&= \frac{1}{\sqrt{\Delta_0\Delta_+(x)}} \left[ (x - bY_-(b)) (t\mathcal{R}(0) - 2t(1+x)\mathcal{R}(x)) \right. \\
&\quad \left. - \frac{t(2b+1+2bx+x^2) - x}{(1+b)t(x - bY_+(b))} \left( \frac{x}{1-bx} - \frac{b\bar{x}}{1-b^2\bar{x}} \right) - \frac{1 - bY_-(b)\bar{x}}{1-b^2\bar{x}} \right] \quad (\text{B.9})
\end{aligned}$$

where we have also multiplied through by a factor  $(x - bY_-(b))$ . At this point we note the impact of introducing the additional factors of  $b$  into this calculation. Comparing Eq. (B.9) to the  $\beta = 1$  case in Eq. (3.66), we encounter a significantly more involved expression for this case, which we aim to extract the positive powers of  $x$  from.

### B.1.2 $x^+$ coefficient extraction

We now find the  $x^+$  coefficient from Eq. (B.9). This is algebraically complicated, so we first split the expression into six terms (suppressing the explicit dependence of  $(b, t)$  in  $Y_+(b, t)$ ,  $Y_-(b, t)$ )

$$(B.9) : \quad T_1 + T_2 = T_3 + T_4 + T_5 + T_6 , \quad (\text{B.10})$$

$$T_1 = -\sqrt{\Delta_+(\bar{x})}(1 - bY_-(b)\bar{x})R^{(d)}(\bar{x}) , \quad (\text{B.11})$$

$$T_2 = \frac{\sqrt{\Delta_+(\bar{x})}}{(1+b)t} \frac{x}{x - bY_+(b)} \left( \frac{x}{1-bx} - \frac{b\bar{x}}{1-b^2\bar{x}} \right) , \quad (\text{B.12})$$

$$T_3 = \frac{1}{\sqrt{\Delta_0\Delta_+(x)}} (x - bY_-(b)) (t\mathcal{R}(0) - 2t(1+x)\mathcal{R}(x)) , \quad (\text{B.13})$$

$$T_4 = -\frac{1}{\sqrt{\Delta_0\Delta_+(x)}} \left( \frac{t(2b+1+2bx+x^2) - x}{(1+b)t(x - bY_+(b))} \left[ \frac{x}{1-bx} \right] \right) , \quad (\text{B.14})$$

$$T_5 = \frac{1}{\sqrt{\Delta_0\Delta_+(x)}} \left( \frac{t(2b+1+2bx+x^2) - x}{(1+b)t(x - bY_+(b))} \left[ \frac{b\bar{x}}{1-b^2\bar{x}} \right] \right) , \quad (\text{B.15})$$

$$T_6 = -\frac{1}{\sqrt{\Delta_0\Delta_+(x)}} \frac{1 - bY_-(b)\bar{x}}{1-b^2\bar{x}} . \quad (\text{B.16})$$

We now extract coefficients term by term. In this we use a number of identities involving the discriminant, found by considering formal power series, that we quote here:

$$\{x^+\} \frac{\bar{x}^2}{\sqrt{\Delta_+(x)}(1-c\bar{x})} \quad (\text{B.17})$$

$$= \frac{1}{1-c\bar{x}} \left( \frac{\bar{x}^2}{\sqrt{\Delta_+(x)}} - \frac{\bar{c}^2}{\sqrt{\Delta_+(c)}} - (\bar{x}^2 - \bar{c}^2) - \frac{1}{2}(X_- + X_+)(\bar{x} - \bar{c}) \right),$$

$$\{x^+\} \frac{\bar{x}}{\sqrt{\Delta_+(x)}(1-c\bar{x})} = \frac{1}{1-c\bar{x}} \left( \frac{\bar{x}}{\sqrt{\Delta_+(x)}} - \frac{\bar{c}}{\sqrt{\Delta_+(c)}} - (\bar{x} - \bar{c}) \right) \quad (\text{B.18})$$

$$\{x^+\} \frac{1}{\sqrt{\Delta_+(x)}(1-c\bar{x})} = \frac{1}{1-c\bar{x}} \left( \frac{1}{\sqrt{\Delta_+(x)}} - \frac{1}{\sqrt{\Delta_+(c)}} \right), \quad (\text{B.19})$$

$$\{x^+\} \frac{x}{\sqrt{\Delta_+(x)}(1-c\bar{x})} = \frac{1}{1-c\bar{x}} \left( \frac{x}{\sqrt{\Delta_+(x)}} - \frac{c}{\sqrt{\Delta_+(c)}} \right), \quad (\text{B.20})$$

$$\{x^+\} \frac{x^2}{\sqrt{\Delta_+(x)}(1-c\bar{x})} = \frac{1}{1-c\bar{x}} \left( \frac{x^2}{\sqrt{\Delta_+(x)}} - \frac{c^2}{\sqrt{\Delta_+(c)}} \right), \quad (\text{B.21})$$

$$\{x^+\} \frac{x\sqrt{\Delta_+(\bar{x})}}{1-cx} = \frac{x\sqrt{\Delta_+(c)}}{1-cx}. \quad (\text{B.22})$$

Again,  $\{x^+\}$  denotes ‘the positive powers in  $x$  within’. Here,  $c$  may be any constant independent of  $x$ . Applying these, we now find the  $\{x^+\}$  component of each term.

$$\{x_+\} T_1 = 0, \quad (\text{B.23})$$

$$\{x^+\} T_2 = \frac{x\sqrt{\Delta_+(b)}}{t(1+b)(1-b^2Y_+)(1-bx)}, \quad (\text{B.24})$$

$$\{x^+\} T_3 = \left( \frac{x-bY_-}{\sqrt{\Delta_0\Delta_+(x)}} - \frac{bY_-}{\sqrt{\Delta_0}} \right) t\mathcal{R}(0) - \left( \frac{2t(1+x)(x-bY_-)}{\sqrt{\Delta_0\Delta_+(x)}} \right) \mathcal{R}(x), \quad (\text{B.25})$$

$$\begin{aligned}
\{x^+\} T_4 = & -\frac{1}{\sqrt{\Delta_0}(1+b)(1-b^2Y_+)t} \left\{ \left[ (2b+1)t \left( \frac{1}{(1-bx)\sqrt{\Delta_+(x)}} - 1 \right) \right] \right. \\
& + \left[ \frac{(2bt-1)x}{(1-bx)\sqrt{\Delta_+(x)}} \right] + \left[ \frac{tx^2}{(1-bx)\sqrt{\Delta_+(x)}} \right] + \left[ \frac{(2b+1)t}{1-bY_+\bar{x}} \left( \frac{1}{\sqrt{\Delta_+(x)}} - \frac{1}{\sqrt{\Delta_+(bY_+)}} \right) \right] \\
& + \left[ \frac{2bt-1}{1-bY_+\bar{x}} \left( \frac{x}{\sqrt{\Delta_+(x)}} - \frac{bY_+}{\sqrt{\Delta_+(bY_+)}} \right) \right] + \left[ \frac{t}{1-bY_+\bar{x}} \left( \frac{x^2}{\sqrt{\Delta_+(x)}} - \frac{b^2Y_+^2}{\sqrt{\Delta_+(bY_+)}} \right) \right] \\
& \left. - \left[ (2b+1)t \left( \frac{1}{\sqrt{\Delta_+(x)}} - 1 \right) \right] - \left[ \frac{(2bt-1)x}{\sqrt{\Delta_+(x)}} \right] - \left[ \frac{tx^2}{\sqrt{\Delta_+(x)}} \right] \right\}, \quad (\text{B.26})
\end{aligned}$$

$$\begin{aligned}
\{x^+\} T_5 = & \frac{1}{\sqrt{\Delta_0}(1+b)(Y_+-b)t} \left\{ bY_+ \left[ \frac{(2b+1)t}{1-bY_+\bar{x}} \left( \frac{\bar{x}^2}{\sqrt{\Delta_+(x)}} - \frac{Y_-^2}{\sqrt{\Delta_+(bY_+)}} \right) \right. \right. \\
& - (\bar{x}^2 - Y_-^2) - \frac{1}{2}(\bar{x} - Y_-)(X_- + X_+) \left. \right] + \frac{2bt-1}{1-bY_+\bar{x}} \left( \frac{\bar{x}}{\sqrt{\Delta_+(x)}} - \frac{Y_-}{\sqrt{\Delta_+(bY_+)}} \right. \\
& \left. \left. - (\bar{x} - Y_-) \right) + \frac{t}{1-bY_+\bar{x}} \left( \frac{1}{\sqrt{\Delta_+(x)}} - \frac{1}{\sqrt{\Delta_+(bY_+)}} \right) \right] - b^2 \left[ \frac{(2b+1)t}{1-b^2\bar{x}} \left( \frac{\bar{x}^2}{\sqrt{\Delta_+(x)}} \right. \right. \\
& - \frac{\bar{b}^4}{\sqrt{\Delta_+(b^2)}} - (\bar{x}^2 - \bar{b}^4) - \frac{1}{2}(\bar{x} - \bar{b}^2)(X_- + X_+) \left. \right] + \frac{2bt-1}{1-b^2\bar{x}} \left( \frac{\bar{x}}{\sqrt{\Delta_+(x)}} - \frac{\bar{b}^2}{\sqrt{\Delta_+(b^2)}} \right. \\
& \left. \left. - (\bar{x} - \bar{b}^2) \right) + \frac{t}{1-b^2\bar{x}} \left( \frac{1}{\sqrt{\Delta_+(x)}} - \frac{1}{\sqrt{\Delta_+(b^2)}} \right) \right] \right\}, \quad (\text{B.27})
\end{aligned}$$

$$\{x^+\} T_6 = -\frac{1}{\sqrt{\Delta_0}(1-b^2\bar{x})} \left( \frac{1-bY_-\bar{x}}{\sqrt{\Delta_+(x)}} - \frac{1-\bar{b}Y_-}{\sqrt{\Delta_+(b^2)}} + bY_-(\bar{x} - \bar{b}^2) \right). \quad (\text{B.28})$$

With Eqs. (B.23)–(B.28), an explicit expression for  $\mathcal{R}(x) = \mathcal{R}(t; x, 0, b, b)$  is found with a rearrangement of terms. Using the recursion relation in Eq. (3.41), and putting in an

explicit form for  $\mathcal{R}(t; a, 0, b, b)$ , we acquire a preliminary expression for  $\mathcal{R}(t; a, a, b, b)$

$$\begin{aligned}
& \frac{(a - bY_-)a^2 K_{aa}}{\sqrt{\Delta_0 \Delta_+(a)}} R(t; a, a, b, b) = \frac{a^2(a - bY_-)}{(1 - ab)^2 \sqrt{\Delta_0 \Delta_+(a)}} + \frac{bY_- t R(t; 0, 0, b, b)}{\sqrt{\Delta_0}} \\
& + \frac{1}{\sqrt{\Delta_0}(1 + b)(1 - b^2 Y_+) t} \left\{ \frac{a \sqrt{\Delta_0 \Delta_+(b)}}{1 - ab} + (2b + 1)t \left( \frac{1}{(1 - ab)\sqrt{\Delta_+(a)}} - 1 \right) \right. \\
& + \frac{(2bt - 1)a}{(1 - ab)\sqrt{\Delta_+(a)}} + \frac{ta^2}{(1 - ab)\sqrt{\Delta_+(a)}} + \frac{(2b + 1)t}{1 - \bar{a}bY_+} \left( \frac{1}{\sqrt{\Delta_+(a)}} - \frac{1}{\sqrt{\Delta_+(bY_+)}} \right) \\
& + \frac{(2bt - 1)}{1 - \bar{a}bY_+} \left( \frac{a}{\sqrt{\Delta_+(a)}} - \frac{bY_+}{\sqrt{\Delta_+(bY_+)}} \right) + \frac{t}{1 - \bar{a}bY_+} \left( \frac{a^2}{\sqrt{\Delta_+(a)}} - \frac{(bY_+)^2}{\sqrt{\Delta_+(bY_+)}} \right) \\
& - (2b + 1)t \left( \frac{1}{\sqrt{\Delta_+(a)}} - 1 \right) - \frac{(2bt - 1)a}{\sqrt{\Delta_+(a)}} - \frac{ta^2}{\sqrt{\Delta_+(a)}} \Big\} \\
& - \frac{bY_+}{\sqrt{\Delta_0}(1 + b)(Y_+ - b)t} \left\{ \frac{(2b + 1)t}{1 - \bar{a}bY_+} \left[ \frac{\bar{a}^2}{\sqrt{\Delta_+(a)}} - \frac{Y_-^2}{\sqrt{\Delta_+(bY_+)}} - (\bar{a}^2 - Y_-^2) \right. \right. \\
& - \frac{1}{2} (\bar{a} - Y_-) (X_- + X_+) \Big] + \frac{(2bt - 1)}{1 - \bar{a}bY_+} \left[ \frac{\bar{a}}{\sqrt{\Delta_+(a)}} - \frac{Y_-}{\sqrt{\Delta_+(bY_+)}} - (\bar{a} - Y_-) \right] \\
& + \frac{t}{1 - \bar{a}bY_+} \left[ \frac{1}{\sqrt{\Delta_+(a)}} - \frac{1}{\sqrt{\Delta_+(bY_+)}} \right] \Big\} \\
& + \frac{b^2}{\sqrt{\Delta_0}(1 + b)(Y_+ - b)t} \left\{ \frac{(2b + 1)t}{1 - \bar{a}b^2} \left[ \frac{\bar{a}^2}{\sqrt{\Delta_+(a)}} - \frac{\bar{b}^4}{\sqrt{\Delta_+(b^2)}} - (\bar{a}^2 - \bar{b}^4) \right. \right. \\
& - \frac{1}{2} (\bar{a} - \bar{b}^2) (X_- + X_+) \Big] + \frac{(2bt - 1)}{1 - \bar{a}b^2} \left( \frac{\bar{a}}{\sqrt{\Delta_+(a)}} - \frac{\bar{b}^2}{\sqrt{\Delta_+(b^2)}} - (\bar{a} - \bar{b}^2) \right) \\
& + \frac{t}{1 - \bar{a}b^2} \left( \frac{1}{\sqrt{\Delta_+(a)}} - \frac{1}{\sqrt{\Delta_+(b^2)}} \right) \Big\} \\
& + \frac{1}{\sqrt{\Delta_0}(1 - \bar{a}b^2)} \left( \frac{1 - \bar{a}bY_-}{\sqrt{\Delta_+(a)}} - \frac{1 - \bar{b}Y_-}{\sqrt{\Delta_+(b^2)}} + bY_- (\bar{a} - \bar{b}^2) \right). \quad (\text{B.29})
\end{aligned}$$

This is highly nested. By using the form of the factorised kernel in Eq. (3.52), however, with extensive algebra we can rewrite Eq. (B.29) more concisely as

$$\begin{aligned}
& a^2 b^2 K_{\bar{a}b} K_{aa} \mathcal{R}(t; a, a, b, b) \\
& = \frac{ab K_{aa}}{(1 - ab)^2} - \frac{\sqrt{\Delta_0 \Delta_+(a) \Delta_+(b)} (\bar{a} - Y_-) ab}{(1 - ab)(b - Y_-)} \\
& - \frac{\sqrt{\Delta_+(a) \Delta(b)} [b^2 - (1 + 2b - b^2)t - (1 + b)^2 t b Y_+]}{\sqrt{\Delta_+(bY_+)}(1 + b)b K_{bb}} \\
& + \frac{\sqrt{\Delta_+(a) \Delta_+(b)} t (\bar{a} - Y_-) \left( b^2 \sqrt{\Delta_0} - t \frac{t - (2b + 1)\sqrt{\Delta_0}}{t - \sqrt{\Delta_0}} \right)}{b K_{bb}}. \quad (\text{B.30})
\end{aligned}$$

We now use a symmetry property: reversing the start and end points of our six-path walk does not change the number of paths between them. This is seen in the TASEP weights as an invariance on exchanging  $\alpha, \beta$ . We then know that  $\mathcal{R}(t; a, a, b, b)$  and  $\mathcal{R}(t; b, b, a, a)$  must be equivalent. Exploiting this, and simplifying a number of the nested square root expressions by the denesting formula in Eq. (3.75) we make Eq. (B.30) manifestly symmetric in  $a, b$ :

$$\begin{aligned} & \mathcal{R}(t; a, a, b, b) \\ &= \frac{1}{(1-ab)^2 ab K_{\bar{a}b}} - \frac{\sqrt{\Delta_+(a)\Delta_+(b)}(1+ab)t^2}{a^3 b^3 K_{aa} K_{bb} K_{\bar{a}b}} - \frac{\sqrt{\Delta_+(a)\Delta_+(b)}t}{(1-ab)a^2 b^2 K_{aa} K_{bb} \sqrt{X_- X_+}} \\ &+ \frac{\sqrt{\Delta_+(a)\Delta_+(b)}t}{a^3 b^3 K_{aa} K_{bb} K_{\bar{a}b} \sqrt{X_- X_+}} \left[ (a+b)t \frac{\sqrt{X_- X_+} + 1}{\sqrt{X_- X_+} - 1} + \frac{ab}{2} \left( 1 + 2t + \sqrt{1 - 4t - 12t^2} \right) \right]. \end{aligned} \quad (\text{B.31})$$

## B.2 Residues of $Q(z; \alpha, \beta)$

In this section we quote results for the residues of the generating function  $Q(z; \alpha, \beta)$ , which we obtain with a series expansion about the relevant singularity. To begin, expanding about the pole  $z_0(\alpha) = \alpha^2(1-\alpha)^2/(\alpha^2 + (1-\alpha)^2)$  strictly within the low density phase  $\alpha < \beta$ ,  $\alpha < 1/2$  as per Eq. (1.113) (elsewhere, either the generating function is analytic at  $z_0(\alpha)$ , or the pole is subdominant) we find a residue

$$\begin{aligned} g_{-1} = & - \left( \frac{1-2\alpha}{1-\alpha} \right)^{3/2} \frac{\beta^2}{\sqrt{\beta(\alpha^2 + (1-\alpha)^2) - \alpha^2}} \times \\ & \left[ \frac{2(1-\alpha)\alpha^2(1-\alpha-\beta) + (2\alpha^2\beta + \beta - \alpha\beta - \alpha^2 - 1) \left( 1 + \sqrt{1 - 4(1-\alpha)^2\alpha^2} \right)}{4\sqrt{\alpha}(\alpha-\beta) [(1-\alpha)\alpha + (\alpha^2 + (1-\alpha)^2)(1-\beta)\beta] (\alpha^2 + (1-\alpha)^2)} \right] \times \\ & \sqrt{2(1-\alpha)^2\alpha^2 + (1-\beta) \left( \sqrt{1 - 4(1-\alpha)^2\alpha^2} - 1 \right)} \times \\ & \sqrt{2(1-\alpha)^2\alpha^2 + (1-\alpha) \left( \sqrt{1 - 4(1-\alpha)^2\alpha^2} - 1 \right)}. \end{aligned} \quad (\text{B.32})$$

About the branch point at  $z_1 = 1/8$ , within the maximal current phase  $\alpha > 1/2$ ,  $\beta > 1/2$  we expand the generating function as per Eq. (1.115) to find the residue

$$h_{\frac{3}{2}} = \left[ \frac{512\sqrt{2}\alpha^2\beta^2(1-\alpha-\beta)^2}{9(1+2\beta-2\beta^2)(1+2\alpha-2\alpha^2)((1-2\alpha)(1-2\beta))^{7/2}} \right] \times$$

$$\left[ \frac{1}{\sqrt{(112-64\sqrt{3})\alpha\beta + (60\sqrt{3}-104)(\alpha+\beta) - 56\sqrt{3} + 97}} \right] \times$$

$$\left[ \begin{aligned} & \left( (64\sqrt{3}-96)\alpha^2\beta^2 + (28\sqrt{3}-18)\alpha\beta + (36-20\sqrt{3})(\alpha^2+\beta^2) \right. \\ & \left. + (48-40\sqrt{3})(\alpha^2\beta+\alpha\beta^2) + (11\sqrt{3}-21)(\alpha+\beta) + 7\sqrt{3}-12 \right) \end{aligned} \right]. \quad (\text{B.33})$$

We quote the factor  $F(\alpha, \beta)$  that we obtain when considering the effective number  $e^{H_2}$  (Eq. (3.100)) in the maximal current phase

$$\frac{1}{F(\alpha, \beta)} = \frac{\sqrt{(1-2\alpha)(1-2\beta)}}{3\sqrt{2}(1+2\alpha-2\alpha^2)(1+2\beta-2\beta^2)} \times$$

$$\left[ \frac{1}{\sqrt{(112-64\sqrt{3})\alpha\beta + (60\sqrt{3}-104)(\alpha+\beta) - 56\sqrt{3} + 97}} \right] \times$$

$$\left[ \begin{aligned} & \left( (64\sqrt{3}-96)\alpha^2\beta^2 + (28\sqrt{3}-18)\alpha\beta + (36-20\sqrt{3})(\alpha^2+\beta^2) \right. \\ & \left. + (48-40\sqrt{3})(\alpha^2\beta+\alpha\beta^2) + (11\sqrt{3}-21)(\alpha+\beta) + 7\sqrt{3}-12 \right) \end{aligned} \right]. \quad (\text{B.34})$$

This function is shown in Figure 3.6.



# Bibliography

- [1] A. J. Wood, R. A. Blythe, and M. R. Evans, “Rényi entropy of the totally asymmetric exclusion process,” *J. Phys. A: Math. Theor.*, vol. 50, no. 47, p. 475005, 2017.
- [2] A. J. Wood, R. A. Blythe, and M. R. Evans, “Solvable model of a many-filament Brownian ratchet,” *Physical Review E*, vol. 100, no. 4, p. 042122, 2019.
- [3] A. J. Wood, R. A. Blythe, and M. R. Evans, “Combinatorial mappings of exclusion processes,” *arXiv preprint arXiv:1908.00942*, 2019.
- [4] R. Bowley and M. Sanchez, *Introductory statistical mechanics*. Clarendon Press Oxford, 1999.
- [5] E. T. Jaynes, “Gibbs vs Boltzmann entropies,” *American Journal of Physics*, vol. 33, no. 5, pp. 391–398, 1965.
- [6] T. Chou, K. Mallick, and R. K. P. Zia, “Non-equilibrium statistical mechanics: from a paradigmatic model to biological transport,” *Reports Prog. Phys.*, vol. 74, no. 11, p. 116601, 2011.
- [7] R. A. Blythe and M. R. Evans, “Nonequilibrium steady states of matrix-product form: a solver’s guide,” *Journal of Physics A: Mathematical and Theoretical*, vol. 40, no. 46, p. R333, 2007.
- [8] A. Rényi *et al.*, “On measures of entropy and information,” in *Proceedings of the Fourth Berkeley Symposium on Mathematical Statistics and Probability, Volume 1: Contributions to the Theory of Statistics*, The Regents of the University of California, 1961.
- [9] C. S. Peskin, G. M. Odell, and G. F. Oster, “Cellular motions and thermal fluctuations: the Brownian ratchet,” *Biophys. J.*, vol. 65, no. 1, pp. 316–324, 1993.

- [10] H. S. Wilf, *Generatingfunctionology*. A K Peters, 3 ed., 2006.
- [11] A. Kolmogoroff, “Über die analytischen Methoden in der Wahrscheinlichkeitsrechnung,” *Mathematische Annalen*, vol. 104, no. 1, pp. 415–458, 1931.
- [12] A. D. Fokker, “Die mittlere Energie rotierender elektrischer Dipole im Strahlungsfeld,” *Annalen der Physik*, vol. 348, no. 5, pp. 810–820, 1914.
- [13] V. Planck, “Über einen Satz der statistischen Dynamik und seine Erweiterung in der Quantentheorie,” *Sitzungsberichte der*, 1917.
- [14] C. T. MacDonald, J. H. Gibbs, and A. C. Pipkin, “Kinetics of biopolymerization on nucleic acid templates,” *Biopolymers: Original Research on Biomolecules*, vol. 6, no. 1, pp. 1–25, 1968.
- [15] C. T. MacDonald and J. H. Gibbs, “Concerning the kinetics of polypeptide synthesis on polyribosomes,” *Biopolymers: Original Research on Biomolecules*, vol. 7, no. 5, pp. 707–725, 1969.
- [16] T. M. Liggett, “Ergodic theorems for the asymmetric simple exclusion process,” *Transactions of the American Mathematical Society*, vol. 213, pp. 237–261, 1975.
- [17] M. Kardar, G. Parisi, and Y.-C. Zhang, “Dynamic scaling of growing interfaces,” *Physical Review Letters*, vol. 56, no. 9, p. 889, 1986.
- [18] J. Krug, “Origins of scale invariance in growth processes,” *Advances in Physics*, vol. 46, no. 2, pp. 139–282, 1997.
- [19] D. Chowdhury, A. Schadschneider, and K. Nishinari, “Physics of transport and traffic phenomena in biology: from molecular motors and cells to organisms,” *Physics of Life reviews*, vol. 2, no. 4, pp. 318–352, 2005.
- [20] E. R. Speer, “The two species totally asymmetric simple exclusion process,” in *On Three Levels*, pp. 91–102, Springer, 1994.
- [21] V. Karimipour, “A multi-species asymmetric exclusion process, steady state and correlation functions on a periodic lattice,” *EPL (Europhysics Letters)*, vol. 47, no. 3, p. 304, 1999.
- [22] M. R. Evans, P. A. Ferrari, and K. Mallick, “Matrix representation of the stationary measure for the multispecies TASEP,” *Journal of Statistical Physics*, vol. 135, no. 2, pp. 217–239, 2009.

- [23] S. Prolhac, M. R. Evans, and K. Mallick, “The matrix product solution of the multispecies partially asymmetric exclusion process,” *Journal of Physics A: Mathematical and Theoretical*, vol. 42, no. 16, p. 165004, 2009.
- [24] C. Arita and K. Mallick, “Matrix product solution of an inhomogeneous multi-species TASEP,” *Journal of Physics A: Mathematical and Theoretical*, vol. 46, no. 8, p. 085002, 2013.
- [25] C. Arita, A. Kuniba, K. Sakai, and T. Sawabe, “Spectrum of a multi-species asymmetric simple exclusion process on a ring,” *Journal of Physics A: Mathematical and Theoretical*, vol. 42, no. 34, p. 345002, 2009.
- [26] T. Sasamoto, “One-dimensional partially asymmetric simple exclusion process on a ring with a defect particle,” *Physical Review E*, vol. 61, no. 5, p. 4980, 2000.
- [27] H. Hinrichsen and S. Sandow, “Deterministic exclusion process with a stochastic defect: matrix-product ground states,” *Journal of Physics A: Mathematical and General*, vol. 30, no. 8, p. 2745, 1997.
- [28] B. Derrida and M. Evans, “Bethe ansatz solution for a defect particle in the asymmetric exclusion process,” *Journal of Physics A: Mathematical and General*, vol. 32, no. 26, p. 4833, 1999.
- [29] J. Dong, B. Schmittmann, and R. Zia, “Inhomogeneous exclusion processes with extended objects: The effect of defect locations,” *Physical Review E*, vol. 76, no. 5, p. 051113, 2007.
- [30] J. de Gier and B. Nienhuis, “Exact stationary state for an asymmetric exclusion process with fully parallel dynamics,” *Physical Review E*, vol. 59, no. 5, p. 4899, 1999.
- [31] A. Povolotsky and V. Priezzhev, “Determinant solution for the totally asymmetric exclusion process with parallel update,” *Journal of Statistical Mechanics: Theory and Experiment*, vol. 2006, no. 07, p. P07002, 2006.
- [32] N. Rajewsky, L. Santen, A. Schadschneider, and M. Schreckenberg, “The asymmetric exclusion process: Comparison of update procedures,” *Journal of statistical physics*, vol. 92, no. 1-2, pp. 151–194, 1998.
- [33] M. Alimohammadi, V. Karimipour, and M. Khorrami, “Exact solution of a one-parameter family of asymmetric exclusion processes,” *Physical Review E*, vol. 57, no. 6, p. 6370, 1998.

- [34] A. Schadschneider and M. Schreckenberg, “Cellular automation models and traffic flow,” *Journal of Physics A: Mathematical and General*, vol. 26, no. 15, p. L679, 1993.
- [35] E. Duchi and G. Schaeffer, “A combinatorial approach to jumping particles: the parallel TASEP,” *Random Structures & Algorithms*, vol. 33, no. 4, pp. 434–451, 2008.
- [36] B. Derrida, M. R. Evans, V. Hakim, and V. Pasquier, “Exact solution of a 1D asymmetric exclusion model using a matrix formulation,” *J. Phys. A Math. Theor.*, vol. 26, pp. 1493–1517, 1993.
- [37] K. Mallick and S. Sandow, “Finite-dimensional representations of the quadratic algebra: applications to the exclusion process,” *Journal of Physics A: Mathematical and General*, vol. 30, no. 13, p. 4513, 1997.
- [38] J. J. Sakurai and E. D. Commins, “Modern quantum mechanics, revised edition,” 1995.
- [39] B. Derrida and M. R. Evans, “Exact correlation functions in an asymmetric exclusion model with open boundaries,” *Journal de Physique I*, vol. 3, no. 2, pp. 311–322, 1993.
- [40] B. Derrida, E. Domany, and D. Mukamel, “An exact solution of a one-dimensional asymmetric exclusion model with open boundaries,” *J. Stat. Phys.*, vol. 69, p. 667, 1992.
- [41] C. Walck, “Hand-book on statistical distributions for experimentalists,” tech. rep., 1996.
- [42] R. Blythe, M. Evans, F. Colaiori, and F. Essler, “Exact solution of a partially asymmetric exclusion model using a deformed oscillator algebra,” *Journal of Physics A: Mathematical and General*, vol. 33, no. 12, p. 2313, 2000.
- [43] R. Brak, S. Corteel, J. Essam, R. Parviainen, and A. Rechnitzer, “A combinatorial derivation of the PASEP stationary state,” *The Electronic Journal of Combinatorics*, vol. 13, no. 1, p. 108, 2006.
- [44] M. Josuat-Vergès, “Combinatorics of the three-parameter PASEP partition function,” *The Electronic Journal of Combinatorics*, vol. 18, no. 1, p. 22, 2011.
- [45] T. Sasamoto, “One-dimensional partially asymmetric simple exclusion process with open boundaries: orthogonal polynomials approach,” *J. Phys. A.: Math. Gen.*, vol. 32, p. 7109, 1999.

- [46] B. Derrida, J. Lebowitz, and E. Speer, “Large deviation of the density profile in the steady state of the open symmetric simple exclusion process,” *Journal of statistical physics*, vol. 107, no. 3-4, pp. 599–634, 2002.
- [47] M. Vanicat, “Exact solution to integrable open multi-species SSEP and macroscopic fluctuation theory,” *Journal of Statistical Physics*, vol. 166, no. 5, pp. 1129–1150, 2017.
- [48] T. Sasamoto, S. Mori, and M. Wadati, “One-dimensional asymmetric exclusion model with open boundaries,” *Journal of the Physical Society of Japan*, vol. 65, no. 7, pp. 2000–2008, 1996.
- [49] J. Sethna, *Statistical mechanics: entropy, order parameters, and complexity*, vol. 14. Oxford University Press, 2006.
- [50] D. Fadeev, “Zum Begriff der Entropie einer endlichen Wahrscheinlichkeitsschemas,” *Arbeiten zur Informationstheorie I. Deutscher Verlag der Wissenschaften*, pp. 85–90, 1957.
- [51] A. Feinstein, *Foundations of information theory*. McGraw-Hill, 1958.
- [52] I. Csiszár, “Axiomatic characterizations of information measures,” *Entropy*, vol. 10, no. 3, pp. 261–273, 2008.
- [53] A. Y. Khinchin, *Mathematical foundations of information theory*. Courier Corporation, 2013.
- [54] P. Erdos, “On the distribution function of additive functions,” *Annals of Mathematics*, pp. 1–20, 1946.
- [55] D. Xu and D. Erdogmuns, *Rényi’s Entropy, Divergence and Their Nonparametric Estimators*, pp. 47–102. New York, NY: Springer New York, 2010.
- [56] K. Życzkowski, “Rényi extrapolation of Shannon entropy,” *Open Systems & Information Dynamics*, vol. 10, no. 03, pp. 297–310, 2003.
- [57] M. O. Hill, “Diversity and evenness: a unifying notation and its consequences,” *Ecology*, vol. 54, no. 2, pp. 427–432, 1973.
- [58] T. Leinster and C. A. Cobbold, “Measuring diversity: the importance of species similarity,” *Ecology*, vol. 93, no. 3, pp. 477–489, 2012.
- [59] A. Chao, C. H. Chiu, T. C. Hsieh, and B. D. Inouye, “Proposing a resolution to debates on diversity partitioning,” *Ecology*, vol. 93, no. 9, pp. 2037–2051, 2012.

- [60] S. Wehner and A. Winter, “Entropic uncertainty relations—a survey,” *New Journal of Physics*, vol. 12, no. 2, p. 025009, 2010.
- [61] S. Bera, H. Schomerus, F. Heidrich-Meisner, and J. H. Bardarson, “Many-Body Localization Characterized from a One-Particle Perspective,” *Physical Review Letters*, vol. 115, p. 046603, 2015.
- [62] A. Ishizaki and G. R. Fleming, “Quantum superpositions in photosynthetic light harvesting: delocalization and entanglement,” *New Journal of Physics*, vol. 12, no. 12, 2010.
- [63] E. H. Simpson, “Measurement of diversity,” *Nature*, vol. 163, no. 4148, p. 688, 1949.
- [64] F. Evers and A. D. Mirlin, “Fluctuations of the inverse participation ratio at the Anderson transition,” *Physical Review Letters*, vol. 84, no. 16, p. 3690, 2000.
- [65] B. Georgeot and D. L. Shepelyansky, “Breit-Wigner width and participation ratio in finite interacting Fermi systems,” *Physical Review Letters*, vol. 79, no. 22, p. 4365, 1997.
- [66] J. C. Baez, “Renyi Entropy and Free Energy,” 2011. arXiv:1102.2098.
- [67] O. C. Ibe, *Elements of random walk and diffusion processes*. John Wiley & Sons, 2013.
- [68] E. Ben-Naim, P. L. Krapivsky, and S. Redner, “Fundamental kinetic processes,” *Boston University, Boston, MA*, 2008.
- [69] R. Ghez, *A primer of diffusion problems*. Wiley, 1988.
- [70] S. Redner, *A guide to first-passage processes*. Cambridge University Press, 2001.
- [71] C. W. Gardiner *et al.*, *Handbook of stochastic methods*, vol. 3. Springer Berlin, 1985.
- [72] M. Bousquet-Mélou, “Walks in the quarter plane: Kreweras’ algebraic model,” *The Annals of Applied Probability*, vol. 15, no. 2, pp. 1451–1491, 2005.
- [73] J. M. Harrison, M. I. Reiman, *et al.*, “Reflected Brownian motion on an orthant,” *The Annals of Probability*, vol. 9, no. 2, pp. 302–308, 1981.
- [74] F. Baccelli and G. Fayolle, “Analysis of models reducible to a class of diffusion processes in the positive quarter plane,” *SIAM Journal on Applied Mathematics*, vol. 47, no. 6, pp. 1367–1385, 1987.

- [75] S. Franceschi and K. Raschel, “Explicit expression for the stationary distribution of reflected Brownian motion in a wedge,” *arXiv Prepr. arXiv1703.09433*, 2017.
- [76] G. Fayolle, V. Malyshev, R. Iasnogorodski, and G. Fayolle, *Random walks in the quarter-plane*, vol. 40. Springer, 1999.
- [77] M. Aigner, “Catalan and other numbers: a recurrent theme,” in *Algebraic combinatorics and computer science*, pp. 347–390, Springer, 2001.
- [78] M. Depken, *Models of non-equilibrium systems*. PhD thesis, University of Oxford, 2003.
- [79] R. Blythe, W. Janke, D. Johnston, and R. Kenna, “The grand-canonical asymmetric exclusion process and the one-transit walk,” *Journal of Statistical Mechanics: Theory and Experiment*, vol. 2004, no. 06, p. P06001, 2004.
- [80] H. W. Gould, “Some generalizations of Vandermonde’s convolution,” *The American Mathematical Monthly*, vol. 63, no. 2, pp. 84–91, 1956.
- [81] R. P. Stanley and S. Fomin, *Enumerative Combinatorics*, vol. 2 of *Cambridge Studies in Advanced Mathematics*. Cambridge University Press, 1999.
- [82] R. Brak, J. de Gier, and V. Rittenberg, “Nonequilibrium stationary states and equilibrium models with long range interactions,” *J. Phys. A.: Math. Gen.*, vol. 37, p. 4303, 2004.
- [83] R. Blythe, W. Janke, D. A. Johnston, and R. Kenna, “Dyck paths, Motzkin paths and traffic jams,” *Journal of Statistical Mechanics: Theory and Experiment*, vol. 2004, no. 10, p. P10007, 2004.
- [84] E. Deutsch, “Dyck path enumeration,” *Discrete Mathematics*, vol. 204, no. 1-3, pp. 167–202, 1999.
- [85] L. Comtet, *Advanced Combinatorics: The art of finite and infinite expansions*. Springer Science & Business Media, 2012.
- [86] R. Brak and J. W. Essam, “Return polynomials for non-intersecting paths above a surface on the directed square lattice,” *Journal of Physics A: Mathematical and General*, vol. 34, pp. 10763–10782, dec 2001.
- [87] T. K. Petersen, “Eulerian numbers,” in *Eulerian Numbers*, pp. 3–18, Springer, 2015.

- [88] T. Narayana, “A combinatorial problem and its application to probability theory,” *Journal of the Indian Society of Agricultural Statistics*, vol. 5, pp. 169–178, 1955.
- [89] G. Kreweras and H. Niederhausen, “Solution of an enumerative problem connected with lattice paths,” *Eur. J. Comb.*, vol. 2, no. 1, pp. 55–60, 1981.
- [90] G. Kreweras, “Sur une classe de problemes de dénombrement liés au treillis des partitions des entiers,” *Cahiers du Bureau universitaire de recherche opérationnelle Série Recherche*, vol. 6, pp. 9–107, 1965.
- [91] H. Niederhausen, “An enumeration problem and some consequences,” *Congr. Numer.*, vol. 33, pp. 261–273, 1981.
- [92] N. J. A. Sloane, “The on-line encyclopedia of integer sequences, sequence A001263,” 1996.
- [93] B. Derrida, M. Evans, and D. Mukamel, “Exact diffusion constant for one-dimensional asymmetric exclusion models,” *Journal of Physics A: Mathematical and General*, vol. 26, no. 19, p. 4911, 1993.
- [94] R. Askey, *Orthogonal polynomials and special functions*, vol. 21. Siam, 1975.
- [95] L. W. Shapiro and D. Zeilberger, “A Markov chain occurring in enzyme kinetics,” *Journal of mathematical biology*, vol. 15, no. 3, pp. 351–357, 1982.
- [96] R. A. Horn and C. R. Johnson, *Matrix analysis*. Cambridge university press, 2012.
- [97] K. Kaygisiz and A. Sahin, “Determinants and permanents of Hessenberg matrices and generalized Lucas polynomials,” *Bulletin of the Iranian Mathematical Society*, vol. 39, no. 6, pp. 1065–1078, 2013.
- [98] O. Mandelshtam, “A determinantal formula for Catalan tableaux and TASEP probabilities,” *Journal of Combinatorial Theory, Series A*, vol. 132, pp. 120–141, 2015.
- [99] R. Brak and J. Essam, “Asymmetric exclusion model and weighted lattice paths,” *Journal of Physics A: Mathematical and General*, vol. 37, no. 14, p. 4183, 2004.
- [100] E. Duchi and G. Schaeffer, “A combinatorial approach to jumping particles,” *Journal of Combinatorial Theory, Series A*, vol. 110, no. 1, pp. 1–29, 2005.



- [101] S. Corteel and L. K. Williams, “A markov chain on permutations which projects to the PASEP,” *International mathematics research notices*, vol. 2007, no. 9, pp. rnm055–rnm055, 2007.
- [102] H. Spohn, “Long range correlations for stochastic lattice gases in a non-equilibrium steady state,” *Journal of Physics A: Mathematical and General*, vol. 16, no. 18, p. 4275, 1983.
- [103] B. Derrida, B. Douçot, and P.-E. Roche, “Current fluctuations in the one-dimensional symmetric exclusion process with open boundaries,” *Journal of Statistical physics*, vol. 115, no. 3-4, pp. 717–748, 2004.
- [104] J. Worpitzky, “Studien über die Bernoullischen und Eulerschen Zahlen.,” *Journal für die reine und angewandte Mathematik*, vol. 94, pp. 203–232, 1883.
- [105] L. Carlitz, “Eulerian numbers and polynomials,” *Mathematics Magazine*, vol. 32, no. 5, pp. 247–260, 1959.
- [106] N. J. A. Sloane, “The on-line encyclopedia of integer sequences, sequence A008292,” 1996.
- [107] L. Carlitz, “q-Bernoulli and Eulerian numbers,” *Transactions of the American Mathematical Society*, vol. 76, no. 2, pp. 332–350, 1954.
- [108] S. Corteel and L. K. Williams, “Tableaux combinatorics for the asymmetric exclusion process,” *Advances in applied mathematics*, vol. 39, no. 3, pp. 293–310, 2007.
- [109] L. K. Williams, “Enumeration of totally positive Grassmann cells,” *Advances in Mathematics*, vol. 190, no. 2, pp. 319–342, 2005.
- [110] R. A. Blythe, W. Janke, D. A. Johnston, and R. Kenna, “Continued fractions and the partially asymmetric exclusion process,” *J. Phys. A: Math. Theor.*, vol. 42, p. 325002, 2009.
- [111] S. Corteel and L. K. Williams, “Tableaux combinatorics for the asymmetric exclusion process and Askey-Wilson polynomials,” *Duke Mathematical Journal*, vol. 159, no. 3, pp. 385–415, 2011.
- [112] S. Corteel, R. Stanley, D. Stanton, and L. Williams, “Formulae for Askey-Wilson moments and enumeration of staircase tableaux,” *Transactions of the American Mathematical Society*, vol. 364, no. 11, pp. 6009–6037, 2012.

- [113] G. Schütz and E. Domany, “Phase transitions in an exactly soluble one-dimensional exclusion process,” *J. Stat. Phys.*, vol. 72, no. 277, 1993.
- [114] M. Bousquet-Mélou and M. Mishna, “Walks with small steps in the quarter plane,” *Contemp. Math*, vol. 520, pp. 1–40, 2010.
- [115] H. Prodinger, “The kernel method: A collection of examples,” *Séminaire Lotharingien de Combinatoire*, vol. 50, p. 19, 2004.
- [116] M. Bousquet-Mélou, “Counting walks in the quarter plane,” in *Mathematics and Computer Science II*, pp. 49–67, Springer, 2002.
- [117] N. J. A. Sloane, “The on-line encyclopedia of integer sequences, sequence A196148,” 1996.
- [118] A. Bostan, M. Bousquet-Mélou, M. Kauers, and S. Melczer, “On 3-dimensional lattice walks confined to the positive octant,” *Annals of Combinatorics*, vol. 20, no. 4, pp. 661–704, 2016.
- [119] J. L. Schiff, *The Laplace transform: theory and applications*. Springer Science & Business Media, 2013.
- [120] H. S. Carslaw and J. C. Jaeger, “Conduction of heat in solids,” *Oxford: Clarendon Press, 1959, 2nd ed.*, 1959.
- [121] J. Beirlant, E. J. Dudewicz, L. Györfi, and E. C. Van der Meulen, “Nonparametric entropy estimation: An overview,” *International Journal of Mathematical and Statistical Sciences*, vol. 6, no. 1, pp. 17–39, 1997.
- [122] T. M. Cover and J. A. Thomas, “Information theory and statistics,” *Elem. Inf. Theory*, pp. 279–335, 1991.
- [123] L. Zhang, Q. Cao, and J. Lee, “A novel ant-based clustering algorithm using Rényi entropy,” *Applied Soft Computing*, vol. 13, no. 5, pp. 2643–2657, 2013.
- [124] T. Van Erven and P. Harremos, “Rényi divergence and Kullback-Leibler divergence,” *IEEE Transactions on Information Theory*, vol. 60, no. 7, pp. 3797–3820, 2014.
- [125] O. Bernardi, M. Bousquet-Mélou, and K. Raschel, “Counting quadrant walks via Tutte’s invariant method,” 2017. arXiv:1708.08215.
- [126] A. Bacher, M. Kauers, and R. Yatchak, “Continued classification of 3D lattice walks in the positive octant,” *arXiv preprint arXiv:1511.05763*, 2015.

- [127] M. v. Smoluchowski, “Experimentell nachweisbare, der Ublichen Thermodynamik widersprechende Molekularphenomene,” *Phys. Zeitschrift*, vol. 13, pp. 1069–1080, 1912.
- [128] R. P. Feynman, R. B. Leighton, and M. Sands, *The Feynman lectures on physics, Vol. I: The new millennium edition: mainly mechanics, radiation, and heat*, vol. 1. Basic books, 2011.
- [129] M. O. Magnasco, “Forced thermal ratchets,” *Phys. Rev. Lett.*, vol. 71, no. 10, p. 1477, 1993.
- [130] J. Bang, R. Pan, T. M. Hoang, J. Ahn, C. Jarzynski, H. T. Quan, and T. Li, “Experimental realization of Feynman’s ratchet,” *New J. Phys.*, vol. 20, no. 10, p. 103032, 2018.
- [131] C. L. Cole and H. Qian, “The Brownian ratchet revisited: Diffusion formalism, polymer-barrier attractions, and multiple filamentous bundle growth,” *Biophys. Rev. Lett.*, vol. 6, no. 01n02, pp. 59–79, 2011.
- [132] A. Perilli, C. Pierleoni, G. Ciccotti, and J.-P. Ryckaert, “On the force–velocity relationship of a bundle of rigid bio-filaments,” *J. Chem. Phys.*, vol. 148, no. 9, p. 95101, 2018.
- [133] J. Valiyakath and M. Gopalakrishnan, “Polymerisation force of a rigid filament bundle: diffusive interaction leads to sublinear force-number scaling,” *Sci. Rep.*, vol. 8, no. 1, p. 2526, 2018.
- [134] J. Whitehouse, R. A. Blythe, M. R. Evans, and D. Mukamel, “Width Scaling of an Interface Constrained by a Membrane,” *Phys. Rev. Lett.*, vol. 121, p. 58102, aug 2018.
- [135] A. Mogilner and G. Oster, “Force generation by actin polymerization II: the elastic ratchet and tethered filaments,” *Biophys. J.*, vol. 84, no. 3, pp. 1591–1605, 2003.
- [136] A. E. Carlsson, “Growth of branched actin networks against obstacles,” *Biophys. J.*, vol. 81, no. 4, pp. 1907–1923, 2001.
- [137] A. E. Carlsson and D. Sept, “Mathematical modeling of cell migration,” *Methods Cell Biol.*, vol. 84, pp. 911–937, 2008.
- [138] R. K. Sadhu and S. Chatterjee, “Actin filaments growing against an elastic membrane: Effect of membrane tension,” *Phys. Rev. E*, vol. 97, no. 3, p. 32408, 2018.

- [139] R. K. Sadhu and S. Chatterjee, “Actin filaments pushing against a barrier: Comparison between two force generation mechanisms,” *Eur. Phys. J. E*, vol. 42, no. 2, p. 15, 2019.
- [140] D. K. Hansda, S. Sen, and R. Padinhateeri, “Branching influences force-velocity curves and length fluctuations in actin networks,” *Phys. Rev. E*, vol. 90, no. 6, p. 62718, 2014.
- [141] R. Wang and A. E. Carlsson, “Load sharing in the growth of bundled biopolymers,” *New J. Phys.*, vol. 16, no. 11, p. 113047, 2014.
- [142] D. Das, D. Das, and R. Padinhateeri, “Collective force generated by multiple biofilaments can exceed the sum of forces due to individual ones,” *New J. Phys.*, vol. 16, no. 6, p. 63032, 2014.
- [143] K. Tsekouras, D. Lacoste, K. Mallick, and J.-F. Joanny, “Condensation of actin filaments pushing against a barrier,” *New J. Phys.*, vol. 13, no. 10, p. 103032, 2011.
- [144] D. A. Lauffenburger and A. F. Horwitz, “Cell migration: a physically integrated molecular process,” *Cell*, vol. 84, no. 3, pp. 359–369, 1996.
- [145] T. Svitkina, “The actin cytoskeleton and actin-based motility,” *Cold Spring Harb. Perspect. Biol.*, vol. 10, no. 1, p. a018267, 2018.
- [146] R. Andorfer and J. D. Alper, “From isolated structures to continuous networks: A categorization of cytoskeleton-based motile engineered biological microstructures,” *Wiley Interdiscip. Rev. Nanomedicine Nanobiotechnology*, p. e1553, 2019.
- [147] R. H. Insall and L. M. Machesky, “Actin dynamics at the leading edge: from simple machinery to complex networks,” *Dev. Cell*, vol. 17, no. 3, pp. 310–322, 2009.
- [148] T. Pujol, O. du Roure, M. Fermigier, and J. Heuvingh, “Impact of branching on the elasticity of actin networks,” *Proc. Natl. Acad. Sci.*, vol. 109, no. 26, pp. 10364–10369, 2012.
- [149] A. Kawska, K. Carvalho, J. Manzi, R. Boujemaa-Paterski, L. Blanchoin, J.-L. Martiel, and C. Sykes, “How actin network dynamics control the onset of actin-based motility,” *Proc. Natl. Acad. Sci.*, 2012.
- [150] T. D. Pollard, “Rate constants for the reactions of ATP-and ADP-actin with the ends of actin filaments,” *J. Cell Biol.*, vol. 103, no. 6, pp. 2747–2754, 1986.

- [151] J. V. Small, G. Isenberg, and J. E. Celis, “Polarity of actin at the leading edge of cultured cells,” *Nature*, vol. 272, no. 5654, p. 638, 1978.
- [152] T. D. Pollard and G. G. Borisy, “Cellular motility driven by assembly and disassembly of actin filaments,” *Cell*, vol. 112, no. 4, pp. 453–465, 2003.
- [153] T. M. Svitkina, A. B. Verkhovsky, K. M. McQuade, and G. G. Borisy, “Analysis of the actin–myosin II system in fish epidermal keratocytes: mechanism of cell body translocation,” *J. Cell Biol.*, vol. 139, no. 2, pp. 397–415, 1997.
- [154] P. Matsudaira, “Actin crosslinking proteins at the leading edge,” in *Seminars in cell biology*, vol. 5, pp. 165–174, Elsevier, 1994.
- [155] T. P. O’Connor and D. Bentley, “Accumulation of actin in subsets of pioneer growth cone filopodia in response to neural and epithelial guidance cues in situ,” *J. Cell Biol.*, vol. 123, no. 4, pp. 935–948, 1993.
- [156] P. K. Mattila and P. Lappalainen, “Filopodia: molecular architecture and cellular functions,” *Nat. Rev. Mol. cell Biol.*, vol. 9, no. 6, p. 446, 2008.
- [157] L. Blanchoin, R. Boujemaa-Paterski, C. Sykes, and J. Plastino, “Actin dynamics, architecture, and mechanics in cell motility,” *Physiol. Rev.*, vol. 94, no. 1, pp. 235–263, 2014.
- [158] M. Gardel, J. H. Shin, F. MacKintosh, L. Mahadevan, P. Matsudaira, and D. Weitz, “Elastic behavior of cross-linked and bundled actin networks,” *Science*, vol. 304, no. 5675, pp. 1301–1305, 2004.
- [159] O. Lieleg, M. M. Claessens, and A. R. Bausch, “Structure and dynamics of cross-linked actin networks,” *Soft Matter*, vol. 6, no. 2, pp. 218–225, 2010.
- [160] M. A. Wear, D. A. Schafer, and J. A. Cooper, “Actin dynamics: assembly and disassembly of actin networks,” *Current Biology*, vol. 10, no. 24, pp. R891–R895, 2000.
- [161] S. Franceschi and I. Kourkova, “Asymptotic expansion of stationary distribution for reflected Brownian motion in the quarter plane via analytic approach,” *Stoch. Syst.*, vol. 7, no. 1, pp. 32–94, 2017.
- [162] M. Kac, “Random walk and the theory of Brownian motion,” *The American Mathematical Monthly*, vol. 54, no. 7P1, pp. 369–391, 1947.
- [163] K. Schulten and I. Kosztin, “Lectures in theoretical biophysics,” 2000.

- [164] M. S. Bartlett, “An inverse matrix adjustment arising in discriminant analysis,” *Ann. Math. Stat.*, vol. 22, no. 1, pp. 107–111, 1951.
- [165] A. Genz and F. Bretz, *Computation of multivariate normal and t probabilities*, vol. 195. Springer Science & Business Media, 2009.
- [166] E. W. Ng and M. Geller, “A table of integrals of the error functions,” *J. Res. Natl. Bur. Stand. B*, vol. 73, no. 1, pp. 1–20, 1969.
- [167] R. Ananthakrishnan and A. Ehrlicher, “The forces behind cell movement,” *Int. J. Biol. Sci.*, vol. 3, no. 5, p. 303, 2007.
- [168] M. R. Evans and R. A. Blythe, “Nonequilibrium dynamics in low-dimensional systems,” *Physica A: Statistical Mechanics and its Applications*, vol. 313, pp. 110 – 152, 2002.